UNIVERSITY OF NAPLES FEDERICO II

Department of Chemical Sciences

PhD Program in Chemical Sciences

XXXI cycle

2015-2018

TOWARDS DNA-TARGETING MAGIC BULLETS: SEARCHING FOR POTENTIAL CONFORMATION-SELECTIVE G-QUADRUPLEX LIGANDS

PhD student:

Dr. Chiara Platella

Tutor: Prof. Daniela Montesarchio

Supervisor: Prof. Luigi Petraccone

Coordinator: Prof. Luigi Paduano

Contents

Summary 1

CHAPTER 1 – INTRODUCTION 6

1.1 G-quadruplexes: an overview of their structural features 6

1.2 Biologically relevant G-quadruplex structures 14

1.2.1 Telomerase, telomeres and telomeric G-quadruplexes 17

1.2.2 Structural characterization of telomeric G-quadruplexes 21

1.2.3 G-quadruplexes in extra-telomeric regions 28

1.3 G-quadruplex ligands 32

1.4 Aims of the PhD project 39

CHAPTER 2 – PREPARATION OF A NOVEL SUPPORT FOR THE ON-LINE SYNTHESIS OF OLIGONUCLEOTIDES 41

2.1 Introduction 41

2.2 Functionalization of Long Chain AlkylAmine-CPG with 5'-*O*-DMT, 3'-*O*-acetylthymidine through a hexaethylene glycol spacer 43

2.3 Synthesis of oligonucleotide models on the CPG support 46

2.3.1 Assembly and deprotection of a hairpin duplex-forming oligonucleotide covalently attached to the CPG support 46

2.3.2 Assembly and deprotection of G4-forming oligonucleotides covalently attached to the CPG support 50

2.4 Experimental section 51

2.4.1 Synthesis of 4,4'-dimethoxytrityl-hexaethylene glycol-COOH (DMT-HEG-COOH) 51

2.4.2 Functionalization of LCAA-CPG with the hexaethylene glycol spacer DMT-HEG-COOH 51

2.4.3 Synthesis of 5'-*O*-DMT, 3'-*O*-acetyl-thymidine 52

2.4.4 Functionalization of support **1** with 5'-*O*-DMT, 3'-*O*-acetylthymidine 52

2.4.5 Assembly and deprotection of hairpin duplex- and G4-forming oligonucleotides on support **2** 53

CHAPTER 3 – G4-CPG ASSAY: AN AFFINITY CHROMATOGRAPHY-BASED METHOD FOR THE SCREENING OF CONFORMATION SELECTIVE G-QUADRUPLEX LIGANDS 54

3.1 General procedure for the binding assays on the novel functionalized CPG supports .. 54

3.2 Monitoring of possible unspecific binding on the nude CPG support 55

3.3 Optimization and validation of the CPG-based method to identify G4-selective ligands 60
3.4 Characterization of the conformations adopted by the oligonucleotide models linked to the CPG support 67
3.5 Experimental section 75
3.5.1 General procedure adopted for the binding assays 75
3.5.2 Materials and general methods 75
3.5.3 Binding assays on nude CPG and nude OAS 76
3.5.4 Use of G4-and hairpin duplex-functionalized CPG and OAS supports for the binding assays 76
3.5.5 Confocal microscopy analyses 77
CHAPTER 4 – SCREENING AND EVALUATION OF A LIBRARY OF MOLECULES FEATURED BY A FUROBENZOXAZINE NAPHTHOQUINONE CORE 78
4.1 Introduction 78
4.2 Selection of compound **4** analogs 80
4.3 Experimental screenings by the G4-CPG assay 80
4.4 Solution studies on the interaction of the selected ligands with oligonucleotide models 84
4.4.1 CD and CD-melting experiments 84
4.4.2 NMR experiments 89
4.4.3 Microscale thermophoresis (MST) experiments 95
4.5 Molecular docking 96
4.6 Biological assays 98
4.7 Experimental section 102
4.7.1 Chemistry 102
4.7.2 G4-CPG assay 102
4.7.3 CD experiments 103
4.7.4 NMR experiments 103
4.7.5 Microscale thermophoresis (MST) experiments 104
4.7.6 Molecular docking 104
4.7.7 Biological experiments 105
CHAPTER 5 – SCREENING AND EVALUATION OF A LIBRARY OF NAPHTHALENE DIIMIDES 107
5.1 Introduction 107

5.2 Experimental screenings by the G4-CPG assay 111
5.3 Biological assays 119
5.4 Solution studies on the interaction of **NDI-8** with oligonucleotide models by CD and fluorescence experiments 122
5.5 Experimental section 127
5.5.1 Chemistry 127
5.5.2 G4-CPG assay 127
5.5.3 Biological experiments 128
5.5.4 CD experiments 129
5.5.5 Fluorescence experiments 129
CHAPTER 6 - STRUCTURAL STUDIES ON THE INTERACTION OF THE DIMERIC NAPHTHALENE DIIMIDE NDI-8 WITH G-QUADRUPLEX MODELS 131
6.1 Selection of the G-quadruplex-forming oligonucleotide models for NMR studies 131
6.2 NMR structures of the here studied DNA G-quadruplex models 131
6.3 Study on the interaction of **NDI-8** with M2 and m-tel24 G-quadruplexes 135
6.4 PAGE experiments 153
6.5 Materials and methods 155
6.5.1 Sample preparation 155
6.5.2 NMR spectroscopy 155
6.5.3 Native PAGE 156
CHAPTER 7 – CONCLUSIONS AND PERSPECTIVES 157
Abbreviation 161
References 164
List of publications and patents 175
List of oral communications and posters presented to conferences and schools 180

Summary

In the search for effective and minimally toxic anticancer drugs, G-quadruplex (G4) structures emerged as appealing targets for their crucial roles in human telomeres and oncogene promoters. G4s are non-canonical nucleic acid secondary structures exhibiting marked structural polymorphism. To achieve an optimal recognition selectivity, thus reducing drug toxicity, a major challenge is to identify ligands which are not only structure-selective, *i.e.* able to discriminate G4 *vs.* duplex DNA, but also conformation-selective, *i.e.* able to specifically recognize different G4 conformations. Thus, considerable efforts are currently devoted to the design of molecules able to selectively target conformationally different G4s and discriminate duplex DNA. To be effective, the huge impulse to synthesize putative conformation-selective ligands has to be coupled with fast and reliable High Throughput Screening (HTS).

Fully inserted in this context is this PhD project, whose objectives were: i) the design and synthesis of oligonucleotide functionalized-solid supports for affinity chromatography; ii) the development of an affinity chromatography-based method for the screening of potential conformation-selective G4 ligands; iii) the identification of effective ligands from focused libraries by the here developed affinity chromatography-based method; iv) the evaluation of the recognition specificity of the selected ligands using proper controls, *i.e.* duplex structures-functionalized supports; v) the biophysical characterization in solution of the best ligands in their interaction with the target DNA; vi) *in vitro* biological tests to assess the anticancer activity of the selected ligands.

In the search for HTS method enabling a rapid and efficient identification of candidate anticancer drugs, our group recently described an affinity chromatography-based assay, named G-quadruplex on Oligo Affinity Support (G4-OAS), for the screening of libraries of putative G4-binders. It consists in flowing solutions of the potential ligands through a polystyrene resin functionalized with a G4-forming DNA sequence and quantifying the bound ligand by spectrophotometric measurements. Though rapid and simple, using this method we observed some problems with ligands featuring large aromatic cores and low hydrophilicity, which gave unspecific interactions with the polystyrene resin and could not therefore be analyzed.

With the aim of addressing this issue and particularly obtaining universal supports for effective screenings of putative conformation-selective G4-ligands, these studies were extended to Controlled Pore Glass (CPG). CPG is the support of choice for oligonucleotide synthesis; its success is essentially due to its chemical inertness, which in principle renders it more convenient than polystyrene also for affinity chromatography. Crucial in our design was the

choice of the linker, which must attach the first nucleoside to the solid support *via* a covalent bond chemically stable under basic conditions used in the final deprotection step of oligonucleotide synthesis, so to obtain the support-bound, fully deprotected oligonucleotides on which the affinity chromatography binding assays can be performed. Therefore, we designed a novel functionalization for CPG supports, involving a linker – made of a flexible spacer of hexaethylene glycol attached to the first nucleoside monomer (*i.e.*, 5'-*O*-DMT-3'-*O*-acetylthymidine) through the nucleobase – suitable for the oligonucleotide elongation by standard protocols and chemically stable to the final deprotection procedure. Hence, using classical phosphoramidite chemistry, biologically relevant G4-forming DNA sequences, taken from human telomeres (tel26, tel46) and oncogene promoters (cmyc, ckit1, ckit2, hTERT1), were synthesized. Furthermore, to evaluate the G4 *vs.* duplex recognition specificity of the putative ligands, the novel synthesized CPG support was also functionalized with an oligonucleotide able to fold into a stable unimolecular hairpin duplex (ds27). Molecules having good or no affinity for G4s (distamycin, netropsin, resveratrol, RHPS4, TO, TMPyP4, 9-Acr-COOH), as well as molecules taken from a library of G4 ligands (7A, 5B, 10B, 1C, 3C, 7D, 7E, 7F) previously proved to have strong unspecific interactions with OAS, were then exploited to validate and optimize the affinity chromatography-based method with the novel functionalized CPG supports. The general procedure adopted for the binding assays was as follows: a weighed amount of each support was left in contact with a ligand solution in a column equipped with a frit. After incubation on a vibrating shaker, each support was eluted with defined volumes of a washing solution and all the eluted fractions were separately analyzed by spectrophotometric measurements. The composition of the washing solution was optimized so to reach the best compromise in terms of solubility of the tested ligands, minimization of undesired absorption of the tested ligands on the assay equipment and capacity of the oligonucleotide sequences to form stable secondary structures. From spectrophotometric measurements of the fractions eluted from the nude CPG, the amount of ligand unspecifically adsorbed on the support was evaluated. In turn, spectrophotometric analysis of the fractions recovered from G4- and hairpin duplex-functionalized supports allowed estimating the amount of ligand bound to the supports carrying the secondary structure-forming oligonucleotides. In all cases, the amount of bound ligand was calculated by subtracting the ligand eluted upon washing, derived by direct spectrophotometric measurements, from the ligand amount initially loaded on each support.

Moreover, as further control, the direct measurement of the bound ligand was obtained by treating each support with a releasing solution, followed by spectrophotometric analysis of the eluted fractions. The amounts of bound ligands thus measured were in good agreement with

those previously determined as a difference with respect to the unbound amounts. The composition of the releasing solution was optimized on the basis of its ability to obtain a fast and quantitative recovery of the bound ligand. To allow the correct G4s and hairpin duplex refolding after this treatment, and thus reuse the same batch of support for subsequent binding assays, each support was resuspended in the washing solution and then subjected to an annealing procedure. This consisted in taking the functionalized support at 75 °C for 5 min, followed by slow cooling to room temperature. The reversibility of the process of folding/unfolding of the G4s and the hairpin duplex allowed effectively recycling the support; indeed, a large number of binding assays (typically more than 50) could be performed on the same batch of CPG without losing in efficiency and reliability of the experiments.

Notably, experimental results showed that the nude CPG has much lower unspecific interactions with all the tested model ligands than previously used OAS resin, allowing higher recovery of the ligands with smaller volumes of the washing solution. In addition, the affinity trend found for the tested ligands on the G4- and hairpin duplex-functionalized supports well reflects what observed for the same systems in solution, confirming the general reliability of the method.

Additionally, to gain a deeper insight into the conformations effectively adopted by the G4s on the glass beads, we exploited a fluorescent core extended naphthalene diimide (c_{ex}-NDI) recently designed to give different fluorescence responses upon interaction with different secondary structure-forming oligonucleotides, thus discriminating hybrid G4s, parallel G4s and duplex DNA. By confocal microscopy, we proved that the oligonucleotides, when anchored to CPG and left in contact with the selected buffer, adopt the same conformations they typically have in solution. This can be mainly attributed to the long and flexible hexaethylene glycol, chosen as the spacer in our synthetic protocol to guarantee proper flexibility and distance from the CPG support of the oligonucleotides, thus minimizing possible steric effects.

This result provided proof-of concept that our novel approach is a powerful tool to identify not only structure-selective G4-ligands, but even conformation-selective G4-ligands.

After full optimization of the G4-CPG assay, two different libraries of putative G4 selective ligands, based either on furobenzoxazine naphthoquinone or naphthalene diimide scaffold, were evaluated.

As far as the focused library of furobenzoxazine naphthoquinone derivatives is concerned, eleven molecules were selected as analogs of a lead-like G-quadruplex targeting compound (**4**), previously proved to be a strong G4 ligand, differing for the pendant groups on the N-atom of the oxazine ring. These molecules were tested *vs.* topologically different G4s by the G4-CPG

assay. The obtained results showed that all the compounds were able to bind several G4 structures, even though with peculiar preferences, and one of them (**S4-5**) fully discriminated G4 *vs.* duplex DNA. Biological assays proved that almost all the compounds produced effective DNA damage, also at the telomeric level, showing marked antiproliferative effects on tumour cells in the low μM range. Combined analysis of the G4-CPG binding assays and biological data led us to focus on compound **S4-5**, being less cytotoxic than the parent compound **4** on normal cells. An in-depth biophysical characterization of the binding of **S4-5** to different G4s was carried out by CD, NMR and Microscale Thermophoresis, demonstrating that the here identified ligand had higher affinity for parallel-type G4s than hybrid-type G4s and duplex DNA. Molecular docking studies in agreement with the NMR data suggested that **S4-5** interacted with the accessible grooves of the target G4 structures, giving clues for its increased binding selectivity. Considering that targeting the most variable regions of the G4 structures, *i.e.* the grooves and the loops, could be a successful, even though still poorly explored, approach for the specific recognition of different G4 conformations, and that very few G4-groove binders have been thus far characterized, these results are of great relevance to develop novel effective candidate anticancer drugs.

As far as the naphthalene diimides (NDIs) library is concerned, twelve novel functionalized monomeric and dimeric NDIs were designed, synthesized and evaluated by the G4-CPG assay. Overall, all the tested compounds proved to be effective G4 ligands, also more efficiently targeting intramolecular dimeric than monomeric G4s. In detail, **NDI-3**, **NDI-4**, **NDI-6**, **NDI-8** and **NDI-9** emerged as the most promising ligands, due to their high G4s *vs.* duplex DNA selectivity. In addition, G4-CPG assay results provided clear evidence that mitigating the affinity of the NDI binding core for G4s allowed the core selectivity emerging.

In vitro biological assays unambiguously designated, among the five selected NDIs, **NDI-8** as the most promising candidate due to its strong activity against cancer cells (IC_{50} = 6.6 nM) and high selectivity in killing cancer cells *vs.* normal cells. Therefore, **NDI-8** was further investigated by CD, fluorescence, NMR and gel electrophoresis analyses. By combination of CD titrations and CD-melting experiments, **NDI-8** was proved to preferentially affect the structure and thermal stability of G4s rather than duplex DNA. Moreover, the ability of **NDI-8** to induce G4 structures formation in the absence of cations was proved by CD and native PAGE experiments. Furthermore, fluorescence experiments revealed binding stoichiometries of 1:1 and 3:2 for complexes of **NDI-8** with a telomeric G4 monomer, while binding stoichiometries of 1:1 and 5:1 were found for NDI complexes with a telomeric G4 dimer. In-depth NMR analyses – performed during my three months-research stay at the Slovenian NMR Centre of

Ljubljana under the supervision of prof. Janez Plavec – showed the preferential binding of **NDI-8** to the 5'-end spatially close residues, the upper quartet and half of the middle quartet of a modified G4 structure (m-tel24) taken from the human telomeric DNA. Finally, the remarkable ability of **NDI-8** to promote the formation of dimeric G4 species was demonstrated by DOSY experiments.

Overall, the novel developed G4-CPG method based on our newly designed CPG support allowed us selecting two promising candidate drugs for *in vivo* studies, **S4-5** and **NDI-8,** showing respectively binding preferences for parallel G4s and monomeric or higher order telomeric G-quadruplex structures, in addition to their high G4s *vs.* duplex DNA selectivity.

Future work will be directed to extend the G4-CPG assay to biologically relevant human *i*-motif-forming and viral G4-forming DNA sequences, as well as automate our method.

CHAPTER 1 – INTRODUCTION

"DNA comes in many forms". This review, written twenty-five years ago by Alexander Rich, well-summarized 40 years of molecular genetics supporting the polymorphic nature of DNA.[1] Only few years after the discovery of the three-dimensional structure of the DNA double helix in 1953,[2] it was found that polynucleotide strands are able to form also triple- and quadruple-stranded nucleic acids.[3] Nevertheless, only three decades ago, when also the biological relevance of these peculiar structures was recognized, non-canonical DNA architectures started to be the object of dedicated investigations.[4–7] The possibility to control genetic pathways responsible for a plethora of pathologies, especially cancer, is a still open and revolutionary challenge from both a medical and scientific point of view. Indeed, getting a deeper insight into the complex biological functions of peculiar DNA structures, as well as selectively targeting them by proper drugs, are among the hottest issues in the scientific research field, especially for the development of effective and minimally toxic targeted therapies.

Focus of this PhD thesis are the G-quadruplex (G4) structures of DNA, proved to have crucial roles in telomeres, replication origins and gene promoters, with G4-forming sequences found in regulatory regions of humans, as well as in virus genomes.[8–15]

1.1 G-quadruplexes: an overview of their structural features

A quadruple-stranded nucleic acid was first observed in 1958 when a fiber of polyinosinic acid was studied by X-ray diffraction.[3] Two different structures were proposed, a three- and a four-stranded one,[3] but only in 1974 the actual structure was determined to be quadruple-stranded.[16] Few years before, in 1962, Gellert and co-workers – likely inspired by Bang's observations on the ability of guanylic acid to form gels, dated back to the beginning of 19th century[17] – characterized the first guanine quartet from a gelatinous substance formed by guanosine monophosphates (Figure 1).[18]

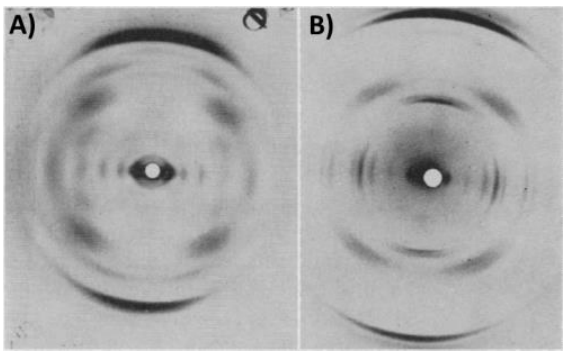

Figure 1. A) X-ray diffraction pattern of 5'-GMP; B) X-ray diffraction pattern of 3'-GMP. (Adapted from Gellert *et al.*[18])

They suggested that four guanines formed a cyclic system and were bound through four pairs of hydrogen bonds. In detail, we know today that each G-quartet (also defined as G-tetrad) is stabilized by eight Hoogsteen-type hydrogen bonds involving, for each guanine, the N1 and the exocyclic NH_2 on C2 as H-bond donors, and the O6 and N7 as H-bond acceptors (Figure 2).[15]

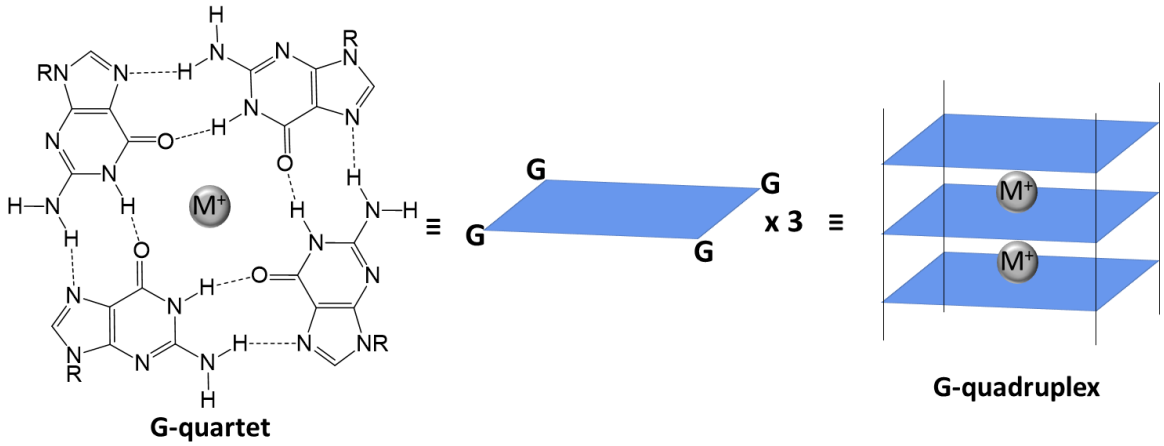

Figure 2. Structure of a G-quartet and a G-quadruplex.

Guanine arrangement in a G-tetrad determines the formation of a cavity in the centre of the planar structure, delimited by guanine carbonyl oxygens, which represents a specific binding site for metal ions, typically K^+ or Na^+.[15,19]

Two or more parallel planes of G-quartets can stack on each other resulting in a G-quadruplex structure (Figure 2), normally featured by a right-handed helical motif with a rise of 3.13-3.30 Å, right-handed twist of 30°, and a diameter of 25 Å.[15]

Moreover, G-quadruplexes exhibit a marked structural polymorphism,[15] which depends on:

- the number of strands involved in the structure;
- the type of linking loops;
- the relative strands orientation;
- the *syn*/*anti* conformation of the guanine residues;
- the nature of the associated metal cations.

G-quadruplexes can be formed from one (unimolecular), two (bimolecular) or four (tetramolecular) polynucleotide strands (Figure 3).

Three different types of loops can be found in G-quadruplex structures: propeller loops, linking adjacent parallel strands on opposite G-quadruplex surfaces; lateral loops, linking adjacent antiparallel strands on the same G-quadruplex surface; and diagonal loops, linking opposite antiparallel strands on the same surface (Figure 4).[15]

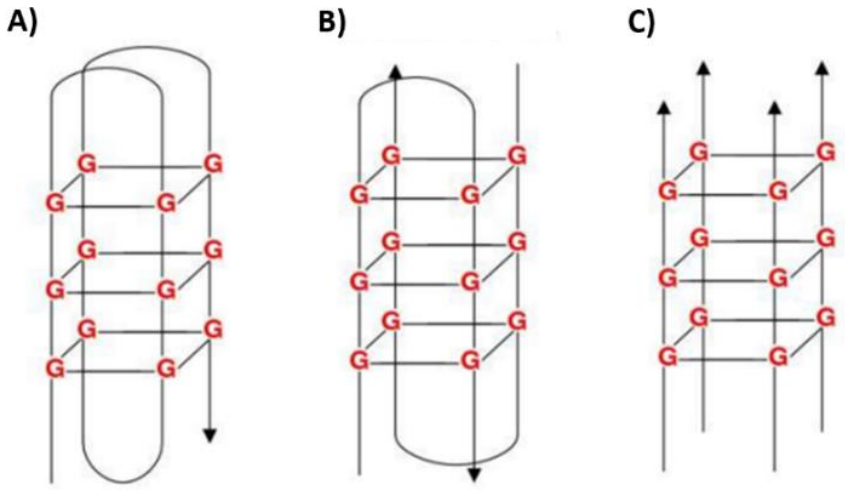

Figure 3. A) Unimolecular, B) bimolecular and C) tetramolecular G-quadruplex structures.

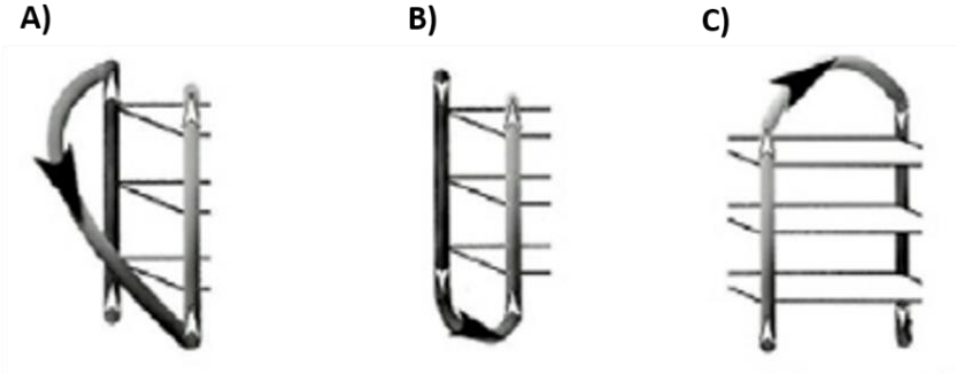

Figure 4. Different types of linking loops in G-quadruplex structures: A) propeller, B) lateral and C) diagonal. (Adapted from Musumeci *et al.*[20])

Moreover, based on the orientation of the four strands, G-quadruplexes are classified in the following topologies: i) parallel (all parallel strands), ii) antiparallel (all antiparallel) or iii) hybrid (3 parallel and 1 antiparallel) (Figure 5).[15,21–24] In particular, two different antiparallel-type topologies can be observed: i) chair-type, in which all the three loops are lateral, and ii) basket-type, with two lateral loops and one diagonal (Figures 5C and 5D).[21,23]

The G-quadruplexes can also be classified according to the conformation adopted by the guanines, which can be *syn* or *anti* along the *N*-glycosidic bond (Figure 6).[15,25] Interestingly, while in B-DNA nucleobases adopt only the *anti* conformation, in G-quadruplex structures guanines can adopt either *syn* or *anti* conformation, thus giving rise to a variety of different arrangements within the G-tetrads, which sensibly contribute to increase the topological diversity of G-quadruplexes.[26]

Differently from B-DNA, in which there are only two different grooves, a major and a minor one, the sugar-phosphate backbone of a G-quadruplex generates four grooves that can accommodate a well-defined network of ordered water molecules.[15] Groove dimension is a consequence of the variation in the glycosidic torsion angles (Figure 7).[27,28]

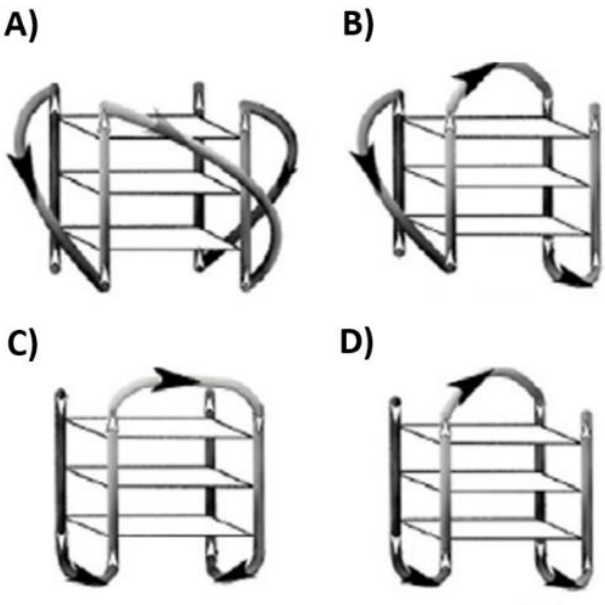

Figure 5. Different G-quadruplex topologies classified on the basis of strands orientation: A) parallel, B) hybrid, C) antiparallel (chair-type), D) antiparallel (basket-type). (Adapted from Musumeci *et al.*[20])

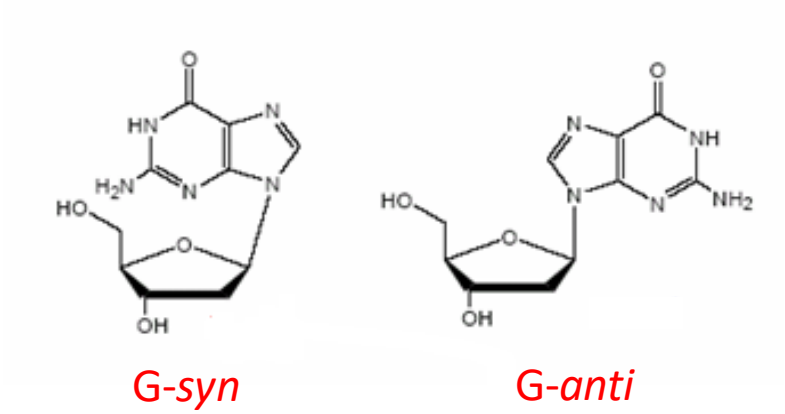

Figure 6. *Syn* and *anti* conformations of the guanines along the *N*-glycosidic bond.

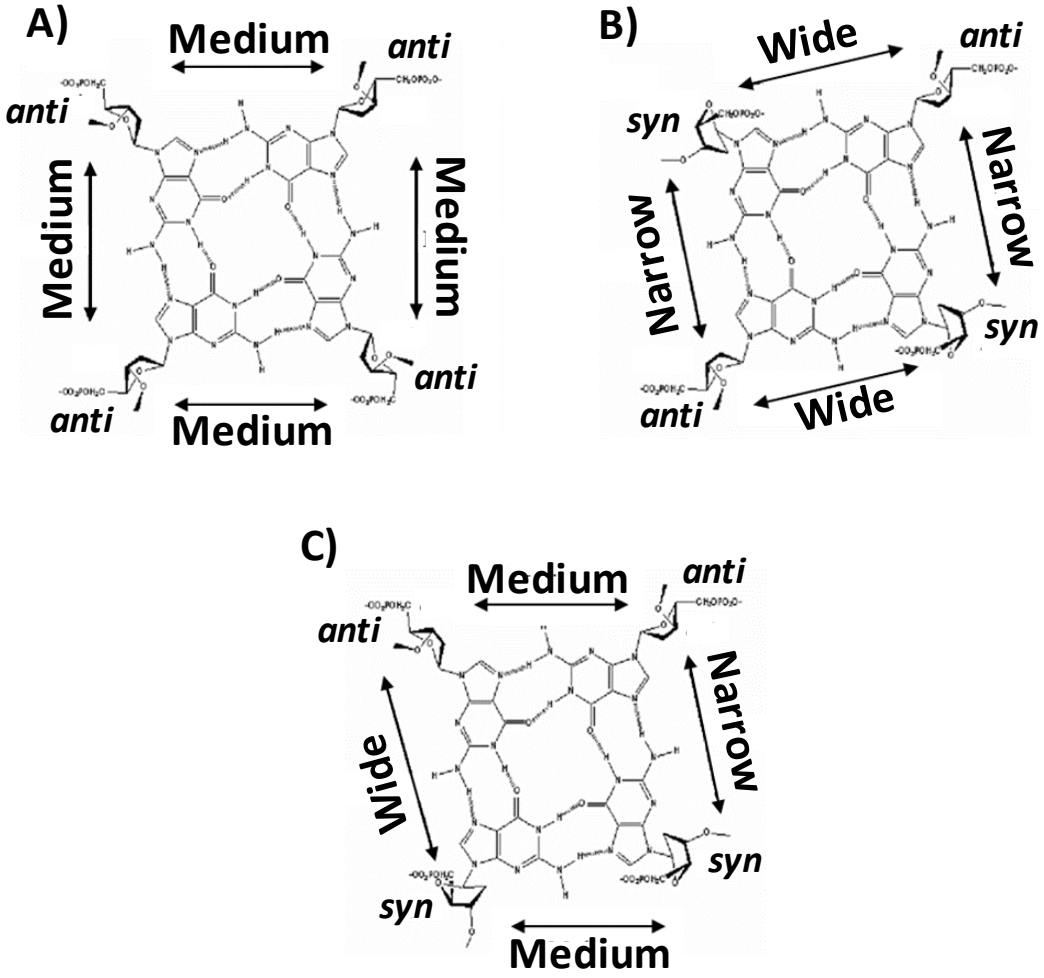

Figure 7. G-quadruplex groove dimensions as a consequence of the different glycosidic torsion angles.

Indeed, if a guanosine in the *syn* conformation points its H-bond donor groups towards a guanosine in the *anti* conformation, the groove formed between them is narrow.[27,28] Conversely, if a guanosine in the *anti* conformation directs the N1 and the exocyclic NH_2 towards a guanosine in the *syn* conformation, the groove is wide.[27,28] Finally, if neighbouring guanosines in the G-tetrad adopt the same glycosidic conformation, the groove is medium.[27,28] In particular, in a parallel four-stranded G-quadruplex, where all the guanosines adopt the *anti* conformation, all the four grooves are of medium width (Figure 7A). Different groove widths alter the hydration network of the resulting structure and determine a different accessibility to hydrogen-bond donors and acceptors of proteins, nucleic acids and small ligands.[27,28]

Intrinsically related to glycosidic conformation of the bases are also the different stacking geometries that two adjacent tetrads can adopt.[29] Considering that, within a G-tetrad, the hydrogen bonds polarity is defined in the direction of hydrogen bond donor to acceptor, from

NH_2 on C2 to N7 and from N1 to O6 (Figure 8), three different stacking geometries in a single G-quadruplex have been experimentally found: i) “partial 5/6-ring” stacking of the *anti*/*anti* step, formed by same-polarity stacked tetrads with a partial overlap of the 5-membered ring of one guanine with the 6-membered ring of another; ii) “5-ring” stacking of the *syn*/*anti* step, formed by opposite-polarity stacked tetrads with an overlap of the 5-membered rings of stacked guanines; iii) “partial 6-ring” stacking of the *anti*/*syn* step, formed by opposite-polarity stacked tetrads with a partial overlap of the 6-membered rings of stacked guanines (Figure 9).[29]

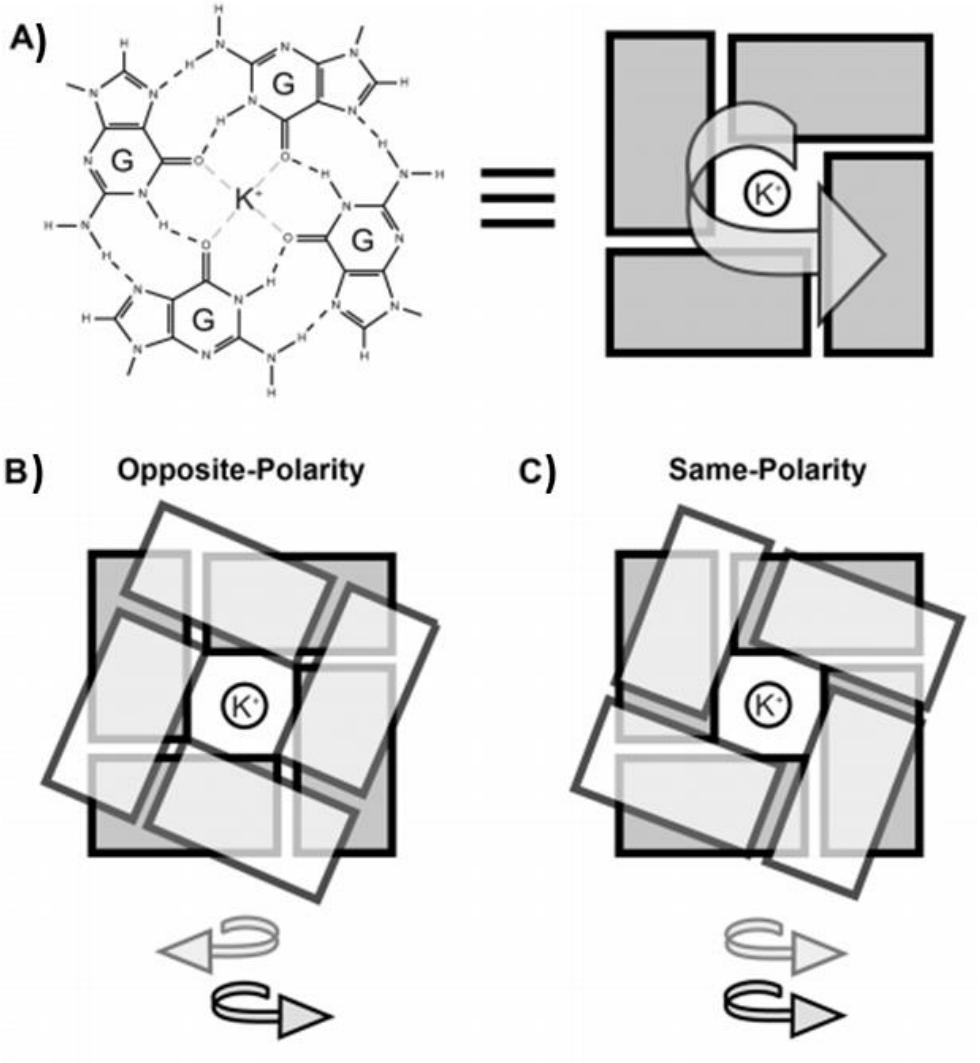

Figure 8. A) Hydrogen bonds polarity is defined in the direction of hydrogen bond donor to acceptor; B) Stacking between two tetrads with opposite polarities; C) Stacking between two tetrads with the same polarity. (Adapted from Lech *et al.*[29])

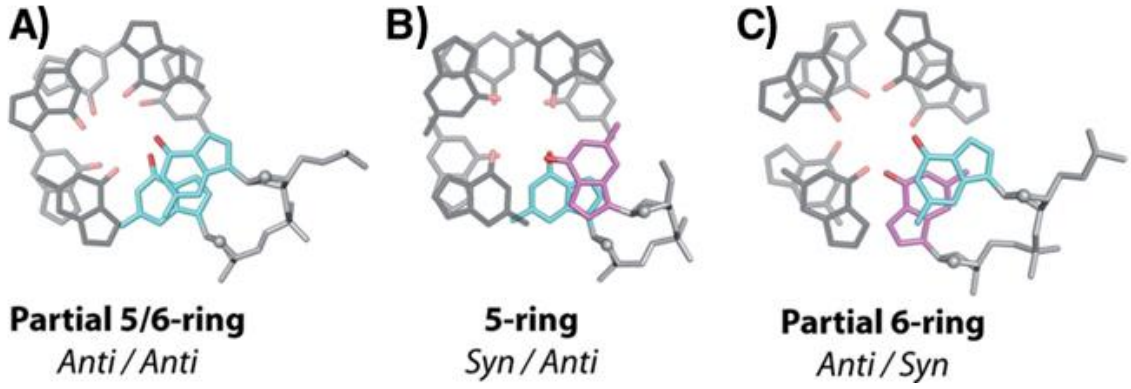

Figure 9. Different stacking geometries experimentally found for two adjacent tetrads in a single G-quadruplex. (Adapted from Lech *et al.*[29])

Furthermore, two or more G-quadruplexes can stack on each other forming dimeric and higher-order structures. By analysing all the NMR and crystallographic dimeric G-quadruplex structures in the Protein Data Bank archive, the following stacking geometries were found at the interface of stacked G-quadruplexes: "partial 6-ring", "6-ring", "5/6-ring" and "5-ring" (Figure 10).[29]

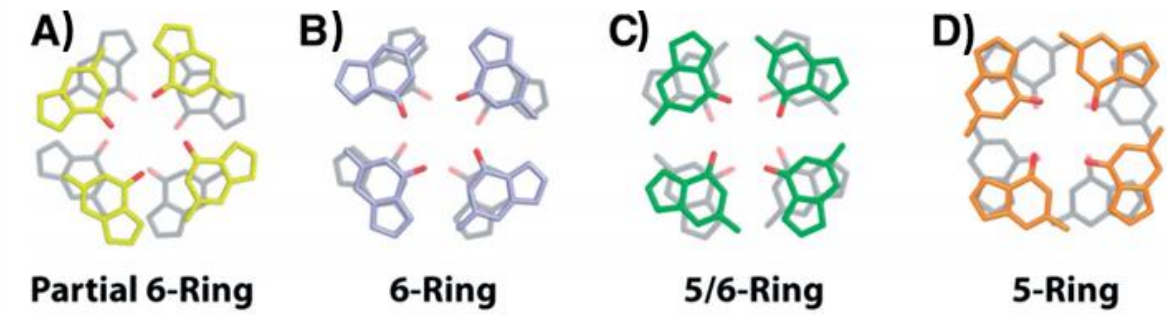

Figure 10. Different stacking geometries experimentally found at the interface of two stacked G-quadruplexes. (Adapted from Lech *et al.*[29])

By computational studies, tetrad stacking energies for experimental geometries were calculated and ranked as follows, core stacking modes: partial 5/6-ring < 5-ring < partial 6-ring, interface stacking modes: 5/6-ring < 6-ring < 5-ring < partial 6-ring.

Finally, investigation of PDB structures and computational studies suggested that 5'-5' ends stacking with 5/6-ring geometry is the favourite arrangement for two stacked G-quadruplexes and probably is a good model also for higher-order structures.[29]

Additional key elements in the modulation of G-quadruplex topology and stability are the associated metal cations. Several metal cations with different radii can be hosted in the central cavity of a G-quadruplex. Circular dichroism (CD) studies revealed that cations with ionic radii between 1.3 and 1.5 Å, such as K^+, Rb^+, NH_4^+, Sr^{2+} and Ba^{2+}, stabilize the G-quadruplex better

than other ions, such as Li^+, Na^+, Cs^+, Mg^{2+} and Ca^{2+}, due to their optimal fit between two adjacent G-tetrads coordinating eight guanines carbonyl oxygens.[30] Smaller cations, such as Li^+, or larger cations, such as Cs^+, do not fit well within two consecutive G-tetrads.[30] The general ranking of G4 stabilization by cations is $Sr^{2+} > Ba^{2+} > K^+ > Ca^{2+} > Na^+$, NH_4^+, $Rb^+ > Mg^{2+} > Li^+ \geq Cs^+$.[31] Notably, if G-quadruplex and monovalent cation concentrations are low enough, some divalent cations, such as Ca^{2+}, Co^{2+}, Mn^{2+}, Zn^{2+}, Ni^{2+} and Mg^{2+} can instead induce G4 instability and dissociation.[32] Presumably, the divalent ions interact with the G-quadruplex structures in two different ways: they can bind to the phosphate groups, reducing the charge repulsion, and, at higher concentrations, also coordinate in a bidentate manner the 6-keto and 7-imine groups of guanines involved in hydrogen bonding, thus disrupting the G-quadruplex structure.[33] Therefore, even cations with similar ionic radii, *e.g.* Ca^{2+} (0.99 Å) and Na^+ (0.97 Å), can have different effects on G-quadruplex stability.[34] Indeed, not only the ionic radius but also other properties of the cations, including the dehydration energy and the coordination number, are essential to determine their overall effect on folding and stability of G-quadruplex structures.[34,35]

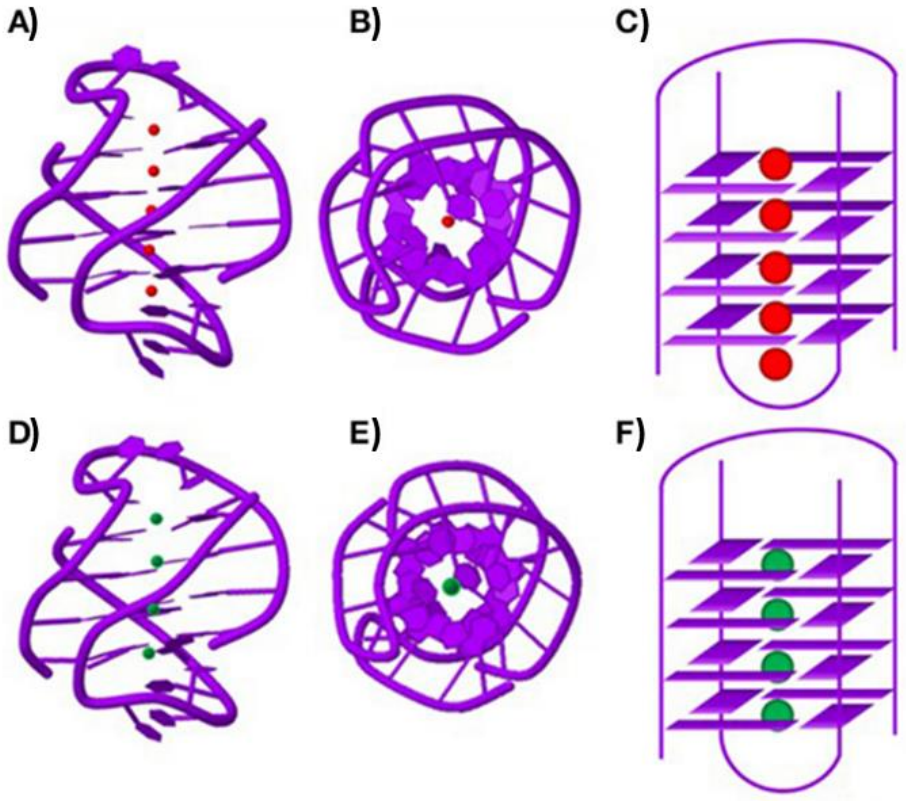

Figure 11. Side view (A, D), top view (B, E) and schematic representations (C, F) of G4 structures obtained from *Oxytricha nova* telomeric DNA d(GGGGTTTTGGGG) in the presence of K^+ (A, B, C) or Na^+ (D, E, F). K^+ ions are located between two adjacent G-tetrads (PDB entry: 1JPQ), while Na^+ ions are in the G-tetrads planes (PDB entry: 1JB7). (Adapted from Bhattacharyya *et al.*[36])

Finally, the precise location of the cations in the G-quadruplex structures is dependent on the nature of the ion: Na^+ ions can be located between two G-tetrads in some structures, whereas they lie within the G-tetrad planes in others; K^+ ions always form sandwich complexes between two adjacent G-tetrads, coordinating eight carbonyl oxygen atoms (Figure 11).[36]
Structural polymorphism of G-quadruplexes, just outlined, is probably the main reason why nature chose them as key elements for the fine regulation of specific biological mechanisms.

1.2 Biologically relevant G-quadruplex structures

By sequencing many genomes it readily came out that they are rich in sequence motifs containing more consecutive guanines. In particular, bioinformatic analyses, exploiting the Quadparser algorithm based on the consensus sequence $d(G_{3+}N_{1-7}G_{3+}N_{1-7}G_{3+}N_{1-7}G_{3+})$, suggested that there could potentially be about 376,000 sequences in the human genome able to fold into G-quadruplex structures.[37] Besides, the above algorithm represents a simplification significantly underestimating the actual number of G4-forming sequences in the genome for several reasons.[37] First of all, since G4s composed of two stacked tetrads are generally less stable than single-stranded or duplex DNA, only sequences able to form three or more G-tetrads are considered physiologically relevant; secondly, loops with lengths from 1 to 7 bases were found to form G4s, with stability decreasing on length increasing; finally, sequences with discontinuities in the G-tracts are not very stable.[37] Indeed, many experimental studies proved that Quadparser algorithm generates both false positives and negatives. To overcome these limitations, Mergny and co-workers recently developed a different algorithm called G4Hunter.[38] It considers the G-richness of a sequence, as well as the C-richness of its complementary strand able to form a stable duplex competing with the potential G-quadruplex structure, and, on this basis, gives a quadruplex propensity score as the output. After validation of the model by analysis of a large dataset of sequences, it was applied to the human genome proving that the number of sequences able to fold into G-quadruplex structures is higher than what previously estimated by a factor of 2-10.[38] Moreover, high-resolution sequencing-based methods to detect G4s in the human genome also confirmed the higher number of G4s that can be formed in the genome (> 700,000) than previously predicted by computational methods.[39]
Notably, G4 location is non-random, with putative G4-forming sequences found in functional and highly conserved human, as well as viral, genomic regions. Indeed, G4-forming sequences

have been found in telomeres, oncogene promoters, around transcription start sites regions, introns, immunoglobulin switch regions and 5' untranslated regions.[9,10,14]

This PhD thesis will focus on DNA G-quadruplex structures found in oncogene promoters and telomeres.[40]

A proto-oncogene is a normal gene coding for a protein responsible for cell growth and division.[41] If a mutation occurs in this gene, it can turn into an oncogene.[41] An oncogene is a gene that encodes for a protein capable of transforming normal cells and inducing cancer.[41] The formation of G-quadruplex structures in oncogene promoters is one of the regulation systems of their transcription.[13] In this context, ligands able to interact with oncogene promoter G-quadruplexes can inhibit a specific mutated proto-oncogene (Figure 12, left).[9]

Telomeres are the ends of eukaryotic chromosomes protecting chromosomal termini from unwanted recombination and degradation, thus guaranteeing proper replication.[42,43] They are made up of double-stranded DNA of 2-20 kb, and of a 3′ single-stranded overhang of approximately 200 nucleotides containing repetitive nucleotide sequences.[44,45]

Telomerase is the enzyme that adds copies of these repetitive sequences to the end of the single-stranded overhang, providing the main mechanism of telomere length maintenance.[46] This enzyme is transcriptionally repressed in human somatic cells, while it is overexpressed in about 85% of cancer cells. In the remaining 15% of human tumours, telomere lengthening is provided by a different mechanism, known as alternative lengthening of telomere (ALT), based on homologous recombination between telomeric sequences.[44,47]

Thus, while in normal cells telomeres get shorter and shorter over time, leading to irreversible cell growth arrest, also known as cellular senescence, in cancer cells telomeres are maintained to a stable length, making cancer cells immortal.[40] Based on this mechanism, it is now widely accepted that telomere maintenance has a key role in the development of tumours.[42] Hence, interfering with telomere homeostasis is an attractive strategy in the search of new anticancer therapies. The 3′ single-stranded overhang of the telomeric DNA, being a G-rich region with repetitive sequences, can fold into G-quadruplex structures.[48] Ligands able to stabilize these peculiar conformations can alter the single-stranded overhang structure, which consequently is no more recognized and elongated by telomerase or by ALT, thus inducing cancer cells senescence and apoptosis (Figure 12, right).[14,47]

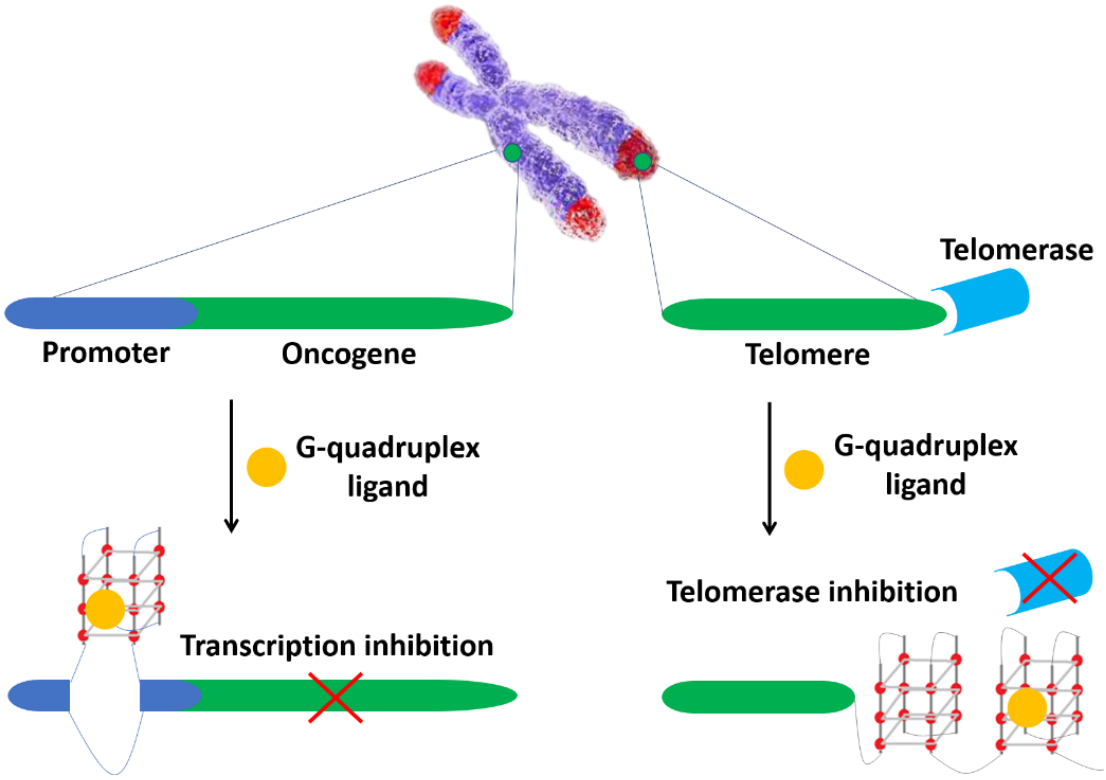

Figure 12. Inhibition of oncogene transcription and telomerase activity through G-quadruplexes formation mediated by ligands.

Hence, there are many advantages in using telomerase activity inhibition mediated by G4 ligands as anticancer therapeutic strategy.[47,49] First of all, telomerase is a specific enzyme for most cancer cells and the most widely expressed tumour marker. Secondly, the risk for development of therapy resistance is very limited because telomeres elongation is the most efficient mechanism for cell immortalization. Thirdly, the very low expression of telomerase in normal cells, along with the longer telomeres in normal stem and germ cells than cancer cells, in principle guarantee specificity towards cancer cells, low toxicity in normal cells, and limited risks in stem and germ cells if the treatment is restricted in time.[47]

The presence of G-quadruplex structures has been proved in the genetic material of human cells by using specific antibodies,[50–52] thus validating both their biological relevance and their role as targets for anticancer strategies (Figure 13).[53–56] In addition, several experiments have fully ascertained that G-quadruplex formation in DNA is modulated during the cell cycle (Figure 13B) and that DNA G-quadruplex structures can be stabilized by small molecule ligands (Figure 13C).[51]

These findings account for the growing interest in the synthesis of small organic molecules as G4 ligands able to interfere with the G-quadruplex functions, essentially aimed at the development of antitumor targeted therapies.

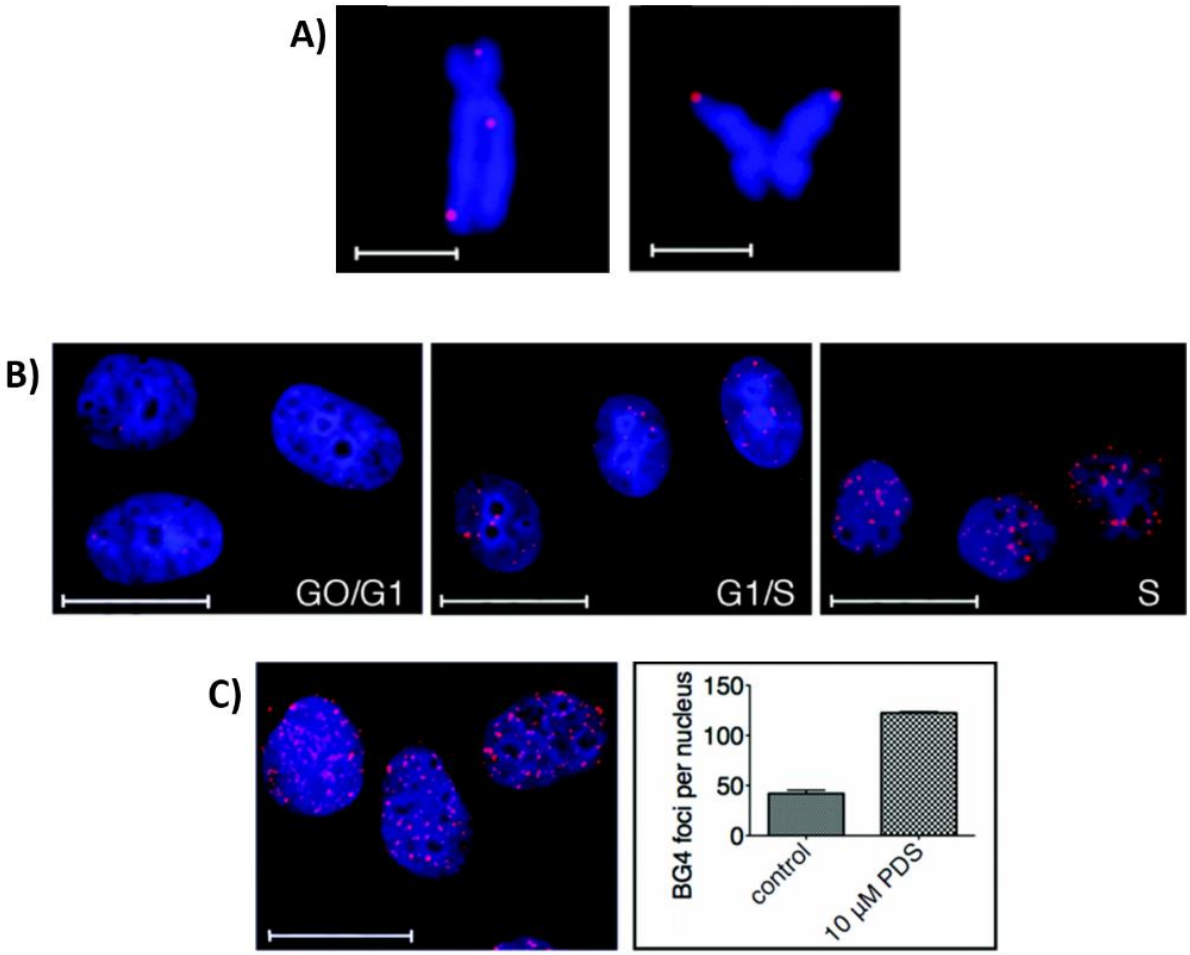

Figure 13. A) Visualization of G-quadruplex structures in telomeres and extra-telomeric regions of metaphase chromosomes by BG4 specific antibody; B) Increase in BG4 foci number during cell cycle, from G0/G1 to S phase; C) Increase in BG4 foci number after treatment with G4 ligand pyridostatin (PDS). Chromosomes and nuclei are counterstained with DAPI (blue). Scale bars correspond to 2.5 μm in A) and 20 μm in B) and C). (Adapted from Biffi *et al.*[51])

1.2.1 Telomerase, telomeres and telomeric G-quadruplexes

The DNA polymerase is not able to replicate the chromosome up to its termination. This problem is referred to as "end replication problem".[57] In the absence of an effective mechanism to solve it, at each cell duplication, a stretch of DNA is not replicated, thus resulting into a loss of genetic information. The solution to this problem is provided by telomerase.[57]

Telomerase is an RNA-dependent ribonucleoprotein consisting of two subunits:

- hTERT (Telomerase Reverse Transcriptase), which has reverse transcriptase enzymatic activity;
- hTR (Telomerase RNA Component), the RNA template used for the synthesis of new telomeric repeats.[58,59]

Telomerase adds repetitive units of oligonucleotide sequences to the 3' end of the chromosomes (Figure 14).[58,59]

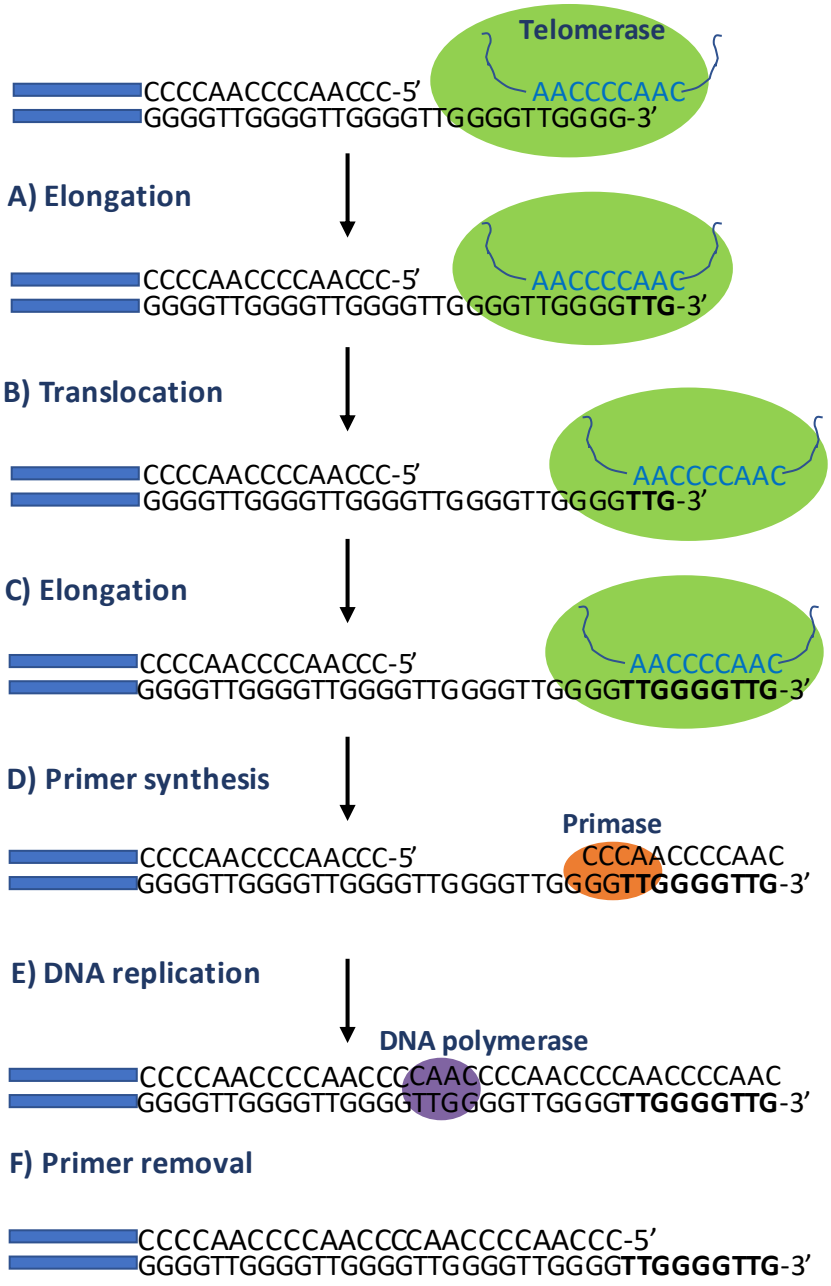

Figure 14. Mechanism of action of telomerase.

The RNA template hybridizes to the strand at the 3' end of the target DNA; the nucleotides not complementary to this strand are used as a template for the addition of a defined number of nucleotides; the telomerase moves to the new 3'-end and the elongation step is repeated. When the telomerase has added a high number of repetitions, a primase synthesizes RNA primers and DNA polymerase copies the second strand of the telomere. The primer is then removed, leaving the 3' end as a single strand (Figure 14).[60]

Telomeric repeat sequence is species-specific, but in general is a guanine-rich oligonucleotide. In particular, human telomeres comprise tandem repeats of the short DNA motif d(TTAGGG).[58,59,61]

Electron microscopy studies proved that the 3'-overhang of the telomere invades the double stranded region of telomeric DNA, making a structure defined displacement loop or D-loop.[62] Probably, the G-rich 3'-overhang interacts with the double stranded telomeric region by base pairing with the C-rich strand. Consequence of strand invasion is the formation of a duplex lariat structure, defined t-loop (Figure 15A).[45] Recently, a structural study suggested that the stabilization of the t-loop is mediated by the formation of G-quadruplexes at the level of the D-loop (Figure 15B).[63]

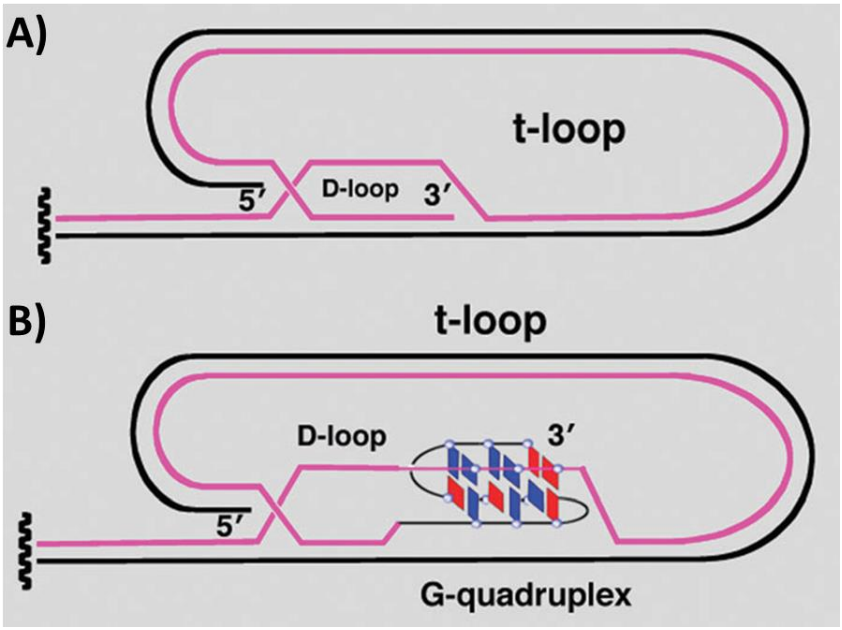

Figure 15. Structure of the 3' telomeric overhang: A) D- and t-loop; B) stabilization of D-loop mediated by a G-quadruplex structure. (Adapted from Xu *et al.*[62])

Moreover, a six-protein complex, called shelterin, is associated to the human telomere (Figure 16).[62] Three shelterin proteins, TRF1, TRF2, and POT1, directly recognize telomere DNA sequences: TRF1 and TRF2 bind the double-stranded telomeric DNA while POT1 binds the 3'-single stranded overhanging of the chromosome end.[64,65] POT1 is involved in the telomerase maintenance mechanism since it disrupts telomeric G-quadruplexes.[66] Conversely, another shelterin protein, Rap1, interacts with TRF2 and promote G-quadruplex formation.[67] The other two shelterin proteins are TIN2 and TPP1. TIN2 interconnects TRF1 and TRF2 with the TPP1-POT1 heterodimer, while TPP1 interacts with POT1 and TIN2 and has the fundamental role of recruiting POT1 at the level of telomeres.[64,65] In conclusion, the shelterin proteins have the complex role of protecting telomeres and regulating their length together with telomerase.[62]

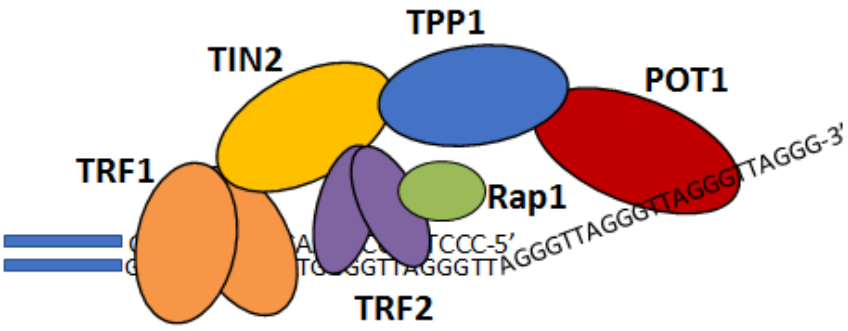

Figure 16. Six protein-complex shelterin.

As mentioned above, telomerase is transcriptionally repressed in healthy somatic cells, therefore telomeres get shorter and shorter over time, and when their length is about 4-6 kb, replicative senescence, also known as mortality stage 1 (M1), is triggered.[68] Hence, normal cells have a defined number of possible cell divisions, the so-called Hayflick limit; once reached this limit, cells undergo to apoptosis. However, some cells can escape M1 and continue to shorten their telomeres, eventually entering mortality stage 2 (M2), featured by genomic instability, fusion/breakage mutagenic events and huge cell death.[68] Furthermore, some cells can reactivate and overexpress telomerase during M1 or M2, leading to immortalization. Even if immortalization is not enough to induce malignant transformation, immortalization acquired from reactivated telomerase in combination with genome instability and mutation from telomere shortening promote cancer onset.[68]

Small molecules, able to stabilize telomeric single strand into G-quadruplex structures can interfere with telomere lengthening by telomerase, leading to cancer cell death.

Two mechanisms of action have been proposed for telomeric G4 binding ligands as anticancer agents:[11,14] i) the classical, slow one, according to which inhibition of telomerase activity due

to ligand-G4 interaction results in telomere shortening, and, after a defined number of cell divisions, cancer cells enter in senescence and finally in apoptosis (Figure 17A); and ii) the fast one, according to which telomeric G4 binding ligands compete with POT1 protein; loss of POT1 deprotects telomeres, and initiates DNA damage-response mediated cancer cell death (Figure 17B).[11,14]

If G4 ligands followed the slow mechanism, senescence would be reached in about 40-50 days after first treatment with drug. Contrarily, experimental evidence proved that several G4 ligands induce senescence after few days of exposure, validating the fast mechanism as the effective one.[11]

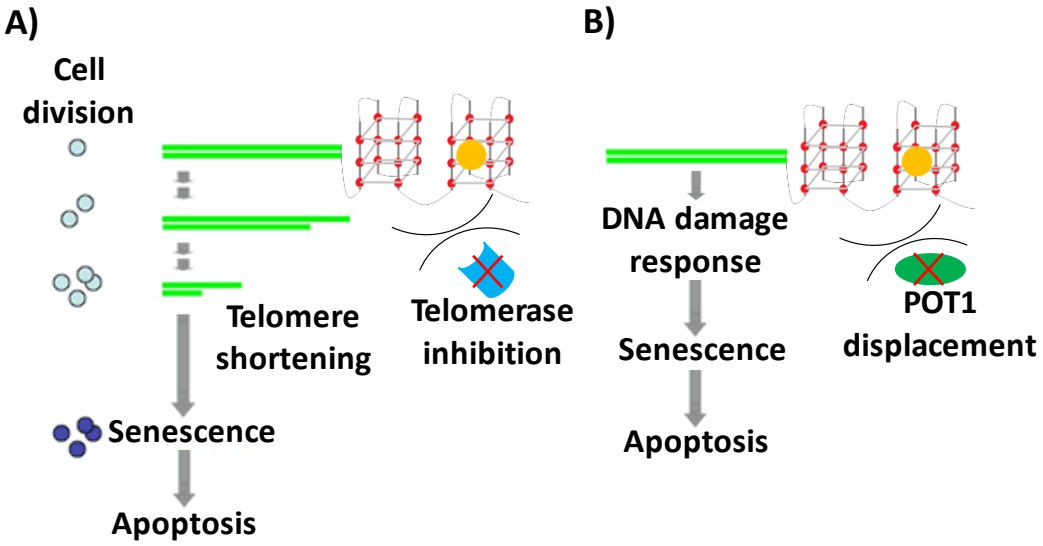

Figure 17. Two different mechanisms of action proposed for telomeric G4 binding ligands as anticancer agents: A) slowly triggered apoptosis by telomere shortening after several cell divisions; B) fast triggered apoptosis by immediate DNA damage response after POT1 protein displacement. G4 ligands are represented as yellow circles.

1.2.2 Structural characterization of telomeric G-quadruplexes

G-quadruplexes formed at telomeric level have been characterized in detail by NMR spectroscopy, X-ray crystallography and circular dichroism.

By NMR studies, the structure of the G-quadruplex telomeric sequence d[AGGG(TTAGGG)$_3$] (tel22) has been obtained in solution containing Na^+ ions (Figure 18A).[27,69] In these conditions, the oligonucleotide tel22 adopts a basket-type topology formed by three planes of G-tetrads connected through three TTA loops, one diagonal and two lateral ones, and featured by the following *N*-glycosidic conformations: *syn*:*syn*:*anti*:*anti* in the upper and lower tetrads, and *anti*:*syn*:*syn*:*anti* in the middle one.[27,70] On the other hand, crystallographic studies have revealed a different conformation for tel22 in the presence of K^+ ions (Figure 18B).[71] Indeed,

in the solid state it adopts a parallel G-quadruplex structure with three propeller loops TTA, with the adenine intercalating between the two thymines in each loop, and all the guanosines in *anti* conformation.[70,71]

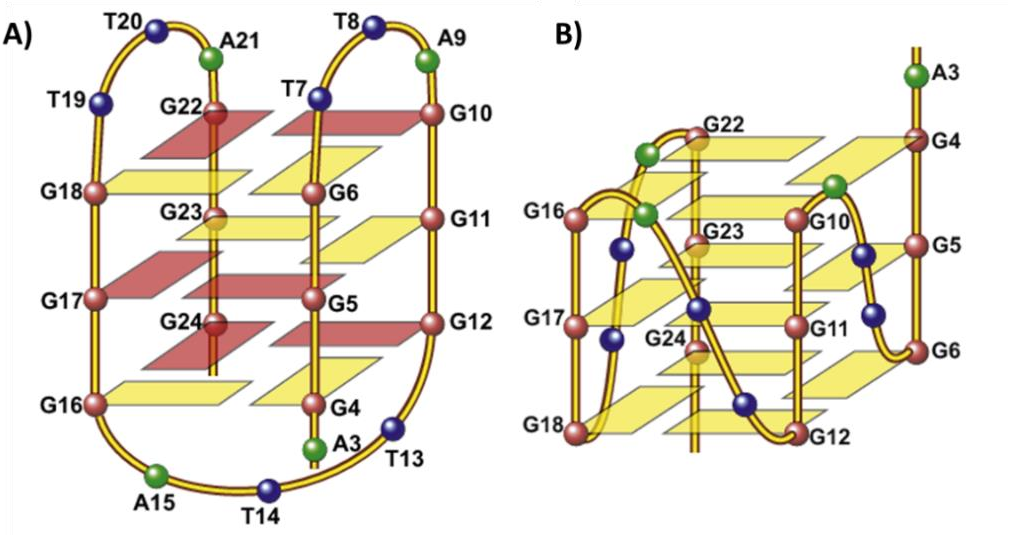

Figure 18. Schematic drawings of the folding topologies of G-quadruplex telomeric sequence d[AGGG(TTAGGG)$_3$] (tel22): A) Basket-type unimolecular G-quadruplex in Na^+ solution, as determined by NMR studies; B) Propeller-type parallel-stranded unimolecular G-quadruplex in the presence of K^+, obtained by X-ray crystallography. Yellow box = (*anti*) guanine, red box = (*syn*) guanine. (Adapted from Dai *et al.*[70])

More recent studies, carried out by NMR and CD, have shown that in solutions containing K^+ ions, telomeric sequences do not adopt a single G-quadruplex conformation, but present multiple conformations.[72] In particular, two are the major ones. These structures, indicated as hybrid 1 and hybrid 2 (Figure 19), differ significantly from the basket-type or parallel conformations, respectively adopted by telomeric DNA in Na^+ solutions or found in the presence of K^+ in crystals.

Hybrid structures, both constituted by three planes of G-tetrads, differ in the arrangement of the loops, in the relative orientation of the strands and in the conformation of the *N*-glycosidic bonds.[72,73] In both structures, there are three parallel strands and one antiparallel, and for this reason they are also known as (3 + 1) structures: the antiparallel strand is the third in hybrid 1, while the second in hybrid 2.[72,73] As far as the conformation of the *N*-glycosidic bonds is concerned, for hybrid 1 the upper tetrad is *syn*:*syn*:*anti*:*syn*, and the other two are *anti*:*anti*:*syn*:*anti*, while for hybrid 2 the upper tetrad is *syn*:*syn*:*syn*:*anti* and the lower ones are

anti:*syn*:*anti*:*anti*.[72,73] Another feature that distinguishes the two hybrid conformations is the size of the grooves, which is obviously different for the two structures.[72,73]

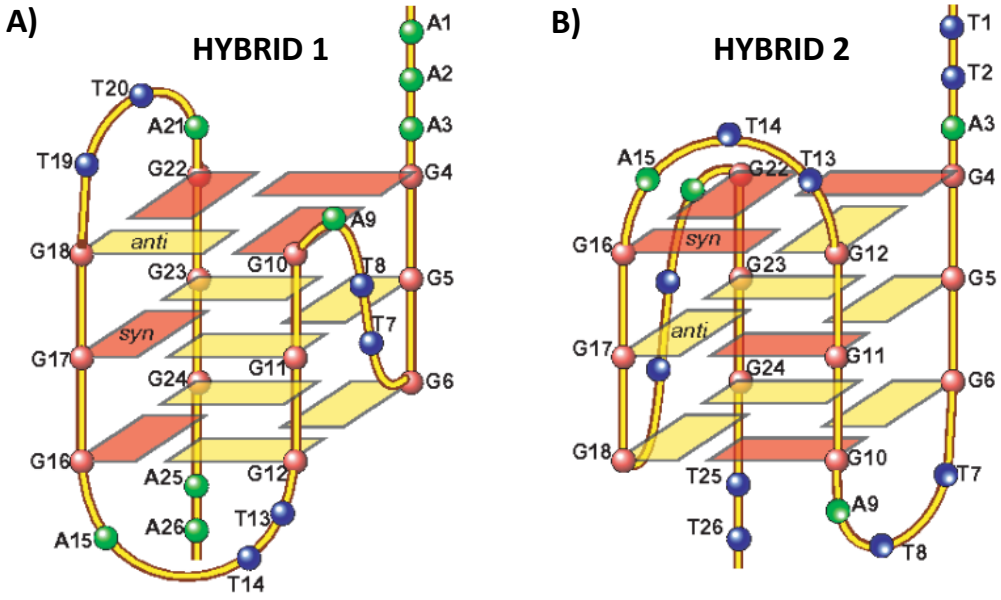

Figure 19. Schematic drawings of: A) hybrid 1 and B) hybrid 2 folding topologies of unimolecular telomeric G-quadruplexes in K^+ solution, determined by NMR using the following sequences: A) d[AAA(GGGTTA)$_3$GGGAA] and B) d[(TTAGGG)$_4$TT]. Yellow box = (*anti*) guanine, red box = (*syn*) guanine. (Adapted from Dai *et al.*[72])

It was also demonstrated that the folding of telomeric sequences in one of two possible hybrid conformations is sensibly affected by the flanking sequences.[74] Indeed, while the hybrid 2 conformation seems to be the predominant form in the case of sequences with TT stretches at the 3' end (for example, the 26-mer native sequence d[(TTAGGG)$_4$TT], tel26), hybrid 1 is the conformation adopted by telomeric sequences which lack the 3'-flanking segment, as in the case of the 24-mer d[(TTAGGG)$_4$] (tel24).[72,75]

This is explained considering that the 3'-flanking TT nucleotides are important for the formation of a stable T:A:T triple capping structure below the lower quartet, that selectively stabilizes the hybrid-2 topology (Figure 20A).[72] Instead, an adenine triple capping structure above the upper quartet was found to form in the hybrid-1 structure, which provides additional stabilization specific to the hybrid-1 topology (Figure 20B).[75]

Another technique extremely useful in structural studies in solution of nucleic acids, and, in particular, for the characterization of the conformations adopted by G-quadruplex-forming oligonucleotides, is circular dichroism spectroscopy.[15,76]

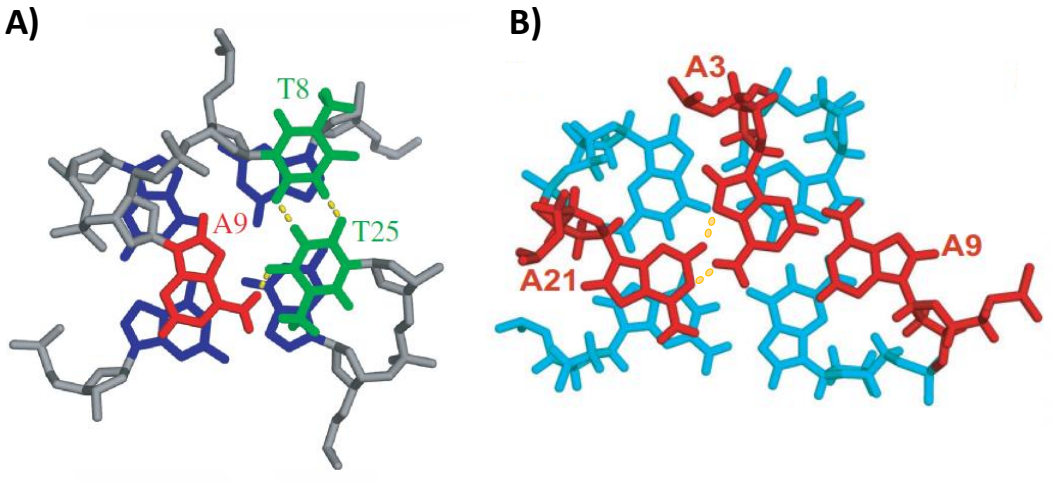

Figure 20. A) Bottom view of the T:A:T triple structure capping the bottom G-tetrad (blue) of hybrid 2 structure (Adapted from Dai *et al.*[72]); B) Top view of the adenine triple structure capping the top G-tetrad (light blue) of hybrid 1 structure. The potential hydrogen bonds are depicted with yellow dash lines. (Adapted from Dai *et al.*[75])

CD spectral signature of G-quadruplex structures is mainly affected by the relative strands orientation and G-tetrads stacking geometries.[77,78] Parallel-stranded G-quadruplexes, in which all guanines have the *anti* glycosidic conformation, are characterized by CD spectra with a positive peak at ~265 nm and a small negative peak at 240 nm (Figure 21A).[21] Antiparallel-stranded G-quadruplexes, in which guanines have alternating *anti* and *syn* glycosidic conformations along each DNA strand, have CD spectra exhibiting a positive peak at 295 nm, a small negative peak at 265 nm, and a small positive peak at 245 nm (Figure 21B).[21] Conversely, the CD spectrum of a hybrid-type G-quadruplex shows a strong positive peak around 290 nm with a shoulder peak around 270 nm, and a small negative peak at 240 nm (Figure 21C). The positive peak around 290 nm is due to the alternating *anti* and *syn* glycosidic conformations along the G-strands between the top and middle G-tetrads, and its shifting from 295 nm is probably due to the presence of the positive peak at 260 nm. The positive peak around 270 nm and the small negative peak around 240 nm are due to the non-alternating *anti* and *syn* glycosidic conformations between the middle and bottom G-tetrads, as elucidated by Ambrus *et al.*[21]

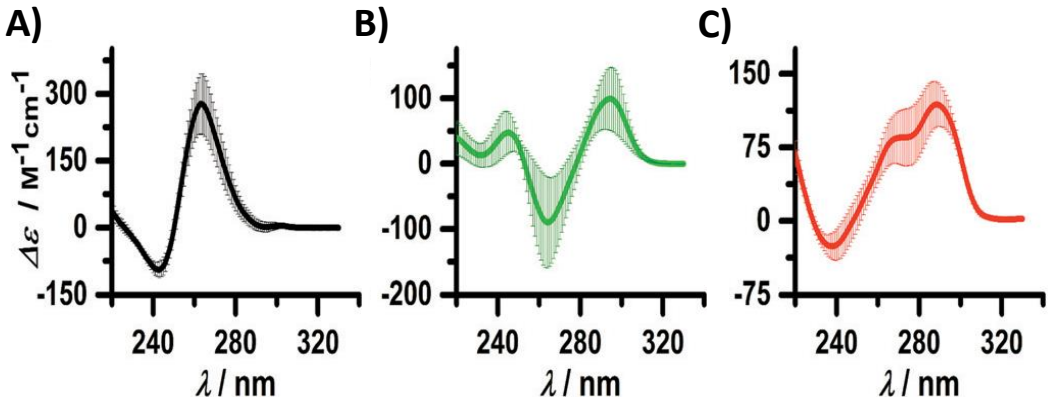

Figure 21. Average CD spectra, obtained from analysis of several G4-forming oligonucleotide sequences, showing CD spectral features for: A) parallel-type G-quadruplex, B) antiparallel, C) hybrid. (Adapted from del Villar-Guerra *et al.*[79])

Using CD spectroscopy, the ability of telomeric sequences to interconvert among different G-quadruplex conformations in the presence of different cations has been investigated by means of titration experiments.[21] Stepwise additions of K^+ ions to preformed tel26 G-quadruplex in Na^+ produces clear spectral changes (Figure 22A), indicating the conversion from a basket-type to a hybrid-type topology. The inverse titration, *i.e.* adding Na^+ ions to preformed tel26 G-quadruplex in K^+, does not induce changes in the CD spectrum (Figure 22B), indicating that the presence of Na^+, even in large excess, does not affect the conformation induced by K^+.[21] These results indicate that the hybrid-type telomeric G-quadruplex is the predominant form in the presence of K^+. The lower stability of the basket-type conformation is generally attributed to the steric interference of the flanking sequences with the diagonal loop, both positioned on the same side of the structure.[21]

Furthermore, considering that the intracellular environment is featured by higher concentrations of K^+ ions than Na^+,[80] the above study also suggests that hybrid-type is the predominant conformation adopted by telomeric G-quadruplexes *in cellulo*.

In addition, a peculiar structural feature of human telomeric DNA is the ability of forming higher-order structures, known as multimers.[70,78] Indeed, since telomeric DNA is *ca.* 100-200 nucleotides long, it can potentially fold into about 8 consecutive G-quadruplexes.[81,82] However, unfavourable coupling free energies could limit complete folding of the 3'-overhang.[83]

An elongated telomeric sequence, depicted in Figure 23A, has been visualized by atomic force microscopy (AFM).[84] The AFM image clearly shows that the higher-order G-quadruplex

consists of blob-shaped protrusions arranged end-to-end and formed by adjacent G-quadruplex units (Figures 23B, 23C and 23D).

Further studies proved that higher-order telomeric G-quadruplexes preferentially adopt structures in which two adjacent quadruplex units have different folding motifs, thus forming a characteristic hybrid1-hybrid2 interface stabilized by stacking interactions (Figure 24).[85,86] Therefore, it can be concluded that monomeric and multimeric G-quadruplexes folded into hybrid topologies can be considered as biologically relevant targets with unique binding sites for ligands,[87,88] and used for the design of novel classes of telomeric-specific DNA drugs.

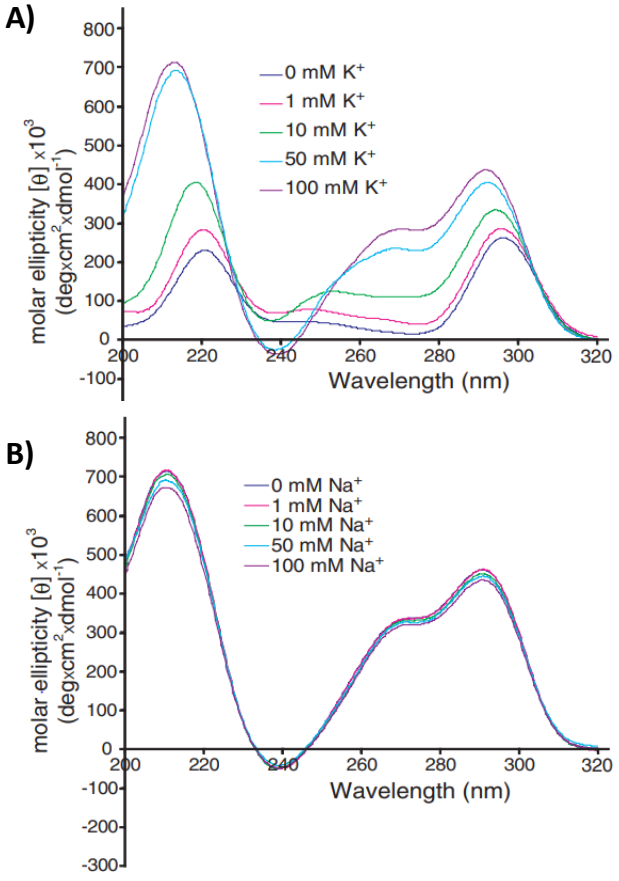

Figure 22. A) CD titration experiments of tel26 by adding K^+ in the presence of 150 mM Na^+; B) CD titration experiments of tel26 by adding Na^+ in the presence of 100 mM K^+. (Adapted from Ambrus *et al.*[21])

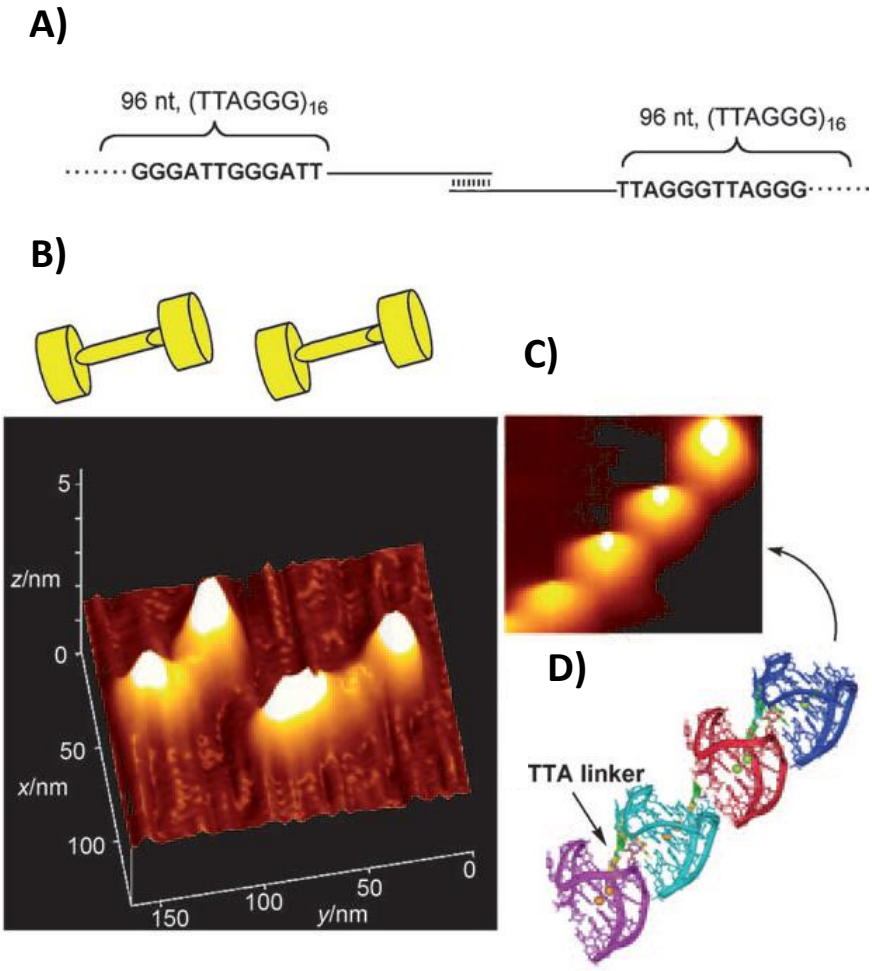

Figure 23. A) Schematic drawing of a DNA model used for AFM visualization. The model has a TTAGGG repeat sequence (96 nt) at both ends and a single-stranded DNA segment (240 nt) linked by a 15 nt duplex; B) AFM image of a DNA model and schematic drawing of its dumbbell-shaped structure; C) High resolution AFM image of higher-order telomeric DNA structures; D) Putative model for the higher-order telomeric DNA structure: four G-quadruplex units linked by TTA linkers. (Adapted from Xu *et al.*[84])

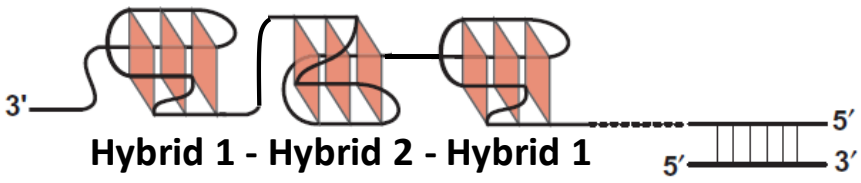

Figure 24. Schematic model of G-quadruplex multimers in human telomeres alternating hybrid 1 and 2 topologies. (Adapted from Dai *et al.*[70])

1.2.3 G-quadruplexes in extra-telomeric regions

Interestingly, even if the highest abundance of G-rich sequences is at telomeres, the majority (~75%) of G4s are found in extra-telomeric regions, such as in the tumour-related gene promoters c-myc, c-kit and hTERT.[9]

c-Myc oncoprotein regulates the expression of 15% of all human genes and its main roles are to promote cell proliferation and arrest cell differentiation.[89] Regarding the c-myc oncogene, many studies have proved that its dysregulation is closely related with tumour initiation and progression. Indeed, 20% of human cancers can be associated with the overexpression of c-myc.[90] Furthermore, c-myc activation increases the expression of hTERT, the gene coding for the telomerase catalytic subunit, therefore involved in cell immortalization.[91] Noteworthy, the first G4 ligand which entered phase II clinical trials is quarfloxin (ClinicalTrials.gov Identifier: NCT00780663), selectively targeting the c-myc G4.[92] Overall, these findings validate c-myc G4 as an attractive anticancer target. Although the c-myc transcription is regulated by multiple promoters, the nuclease hypersensitivity element III1 (NHE III1), consisting of 33 nucleotides, controls 80-90% of the transcriptional activity of c-myc.[93–96] The 33-mer sequence d(TGGGGAGGGTGGGGAGGGTGGGGAAGGTGGGGA) (cmyc) in NHE III1 contains six G-tracts of unequal length and is potentially able to fold into different G4 conformations, involving different guanine runs.[6,97,98] Shorter sequences extracted from the 33-mer involving, respectively, the G-tracts 2, 3, 4, and 5 (Myc2345, Figure 25A) and 1, 2, 4 and 5 (Myc1245, Figure 25B) have been investigated by NMR and proved to fold into parallel-type topologies, with Myc2345 G4 resulting as the most stable one.[22,97,99,100] Interestingly, in contrast to stability data obtained by melting experiments, only Myc1234 G-quadruplex (Figure 25C) was observed in supercoiled plasmid models, thus pointing out the importance of supercoiling in G-quadruplex formation and re-evaluating Myc1234 as the potential biologically relevant G-quadruplex in the c-myc promoter.[101]

The c-kit protein regulates several signal transduction cascades important for the control of cell growth and proliferation.[102–104] Mutations and overexpression of the c-kit oncogene play central roles in oncogenic transformation and are especially related to gastrointestinal stromal tumours (GIST).[105] Despite c-kit kinase inhibitors have been recently approved for clinical use in the treatment of GIST, resistance related to protein mutations remains to be overcome.[106–108] Therefore, the development of small molecules effective as c-kit G-quadruplex ligands can be an alternative and promising strategy.

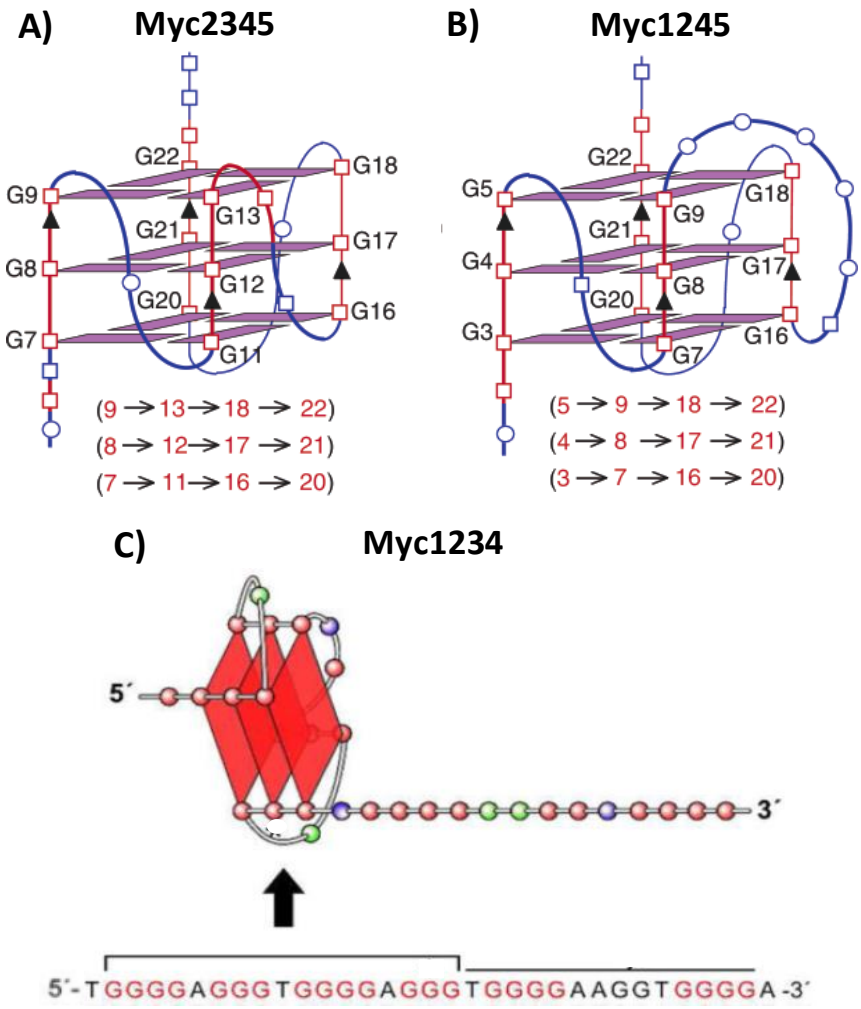

Figure 25. Schematic drawings of: A) Myc2345 d(TGAGGGTGGGGAGGGTGGGGAA) structure in K^+ solution, obtained by NMR; B) Myc1245 d(TGGGGAGGGTTTTTAGGGTGGGGA) structure in K^+ solution, determined by NMR; C) Myc1234 structure proposed by *in vitro* plasmid footprinting experiments. (Adapted from Phan *et al.*[97] and Sun *et al.*[101])

c-kit promoter contains two different G-quadruplexes (ckit1 and ckit2) separated by about three turns of DNA.[109] In detail, one is located between -87 and -109 bp and the other between -140 and -160 bp upstream of the transcription initiation site.[109] The molecular structure of the 22-mer d(AGGGAGGGCGCTGGGAGGAGGG) ckit1 G4 has been determined by NMR (Figure 26A).[110] Having a unique topology with respect to the other known G4s, it results a specific target for drug design.[110,111] In addition, the crystal structure determined for ckit1 G4 is in good agreement with the one solved by NMR.[112] ckit1 G4 adopts a parallel conformation with two single-nucleotide propeller loops and a long five-nucleotide lateral stem loop; moreover, one non-G-tract guanine is involved in the core of the G-quartets (Figure 26A).[110,112,113] On the other hand, the 21-mer ckit2 of sequence d(CGGGCGGGCGCGAGGGAGGGG), depending

on the K^+ concentration in solution, adopts two distinct parallel conformations in slow exchange: i) a monomeric one with two single-nucleotide and a long five-nucleotide propeller loops (Figure 26B) and ii) an unusual dimeric structure, in which stacking interactions between the two G-quadruplexes are mediated by a sandwiched A-A non-canonical pair (Figure 26C).[114]

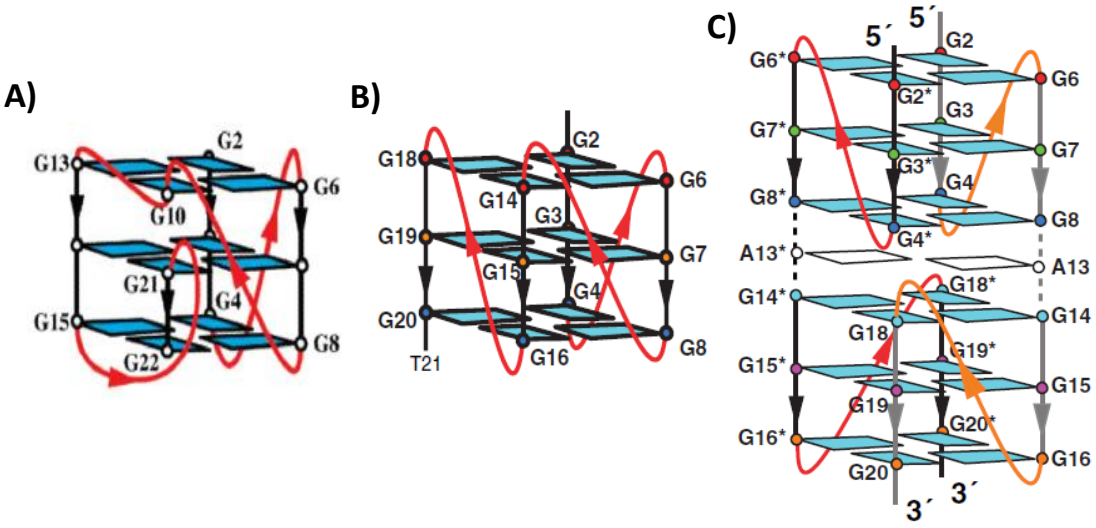

Figure 26. Schematic drawings of: A) ckit1, B) ckit2 monomeric form and C) ckit2 dimeric form determined by NMR respectively in 70 mM KCl, 20 mM potassium phosphate buffer, 20 mM KCl, 5 mM potassium phosphate buffer and 100 mM KCl, 5 mM potassium phosphate buffer. (Adapted from Phan *et al.*[110] and Kuryavyi *et al.*[114])

hTERT is the gene coding for the catalytic subunit of telomerase.[43,115] Its overexpression is associated with over 85% of human cancers, and its transcriptional repression accounts for the lack of telomerase activity in normal somatic cells.[43,115,116] Expression of hTERT is mainly regulated by the core promoter containing five Sp1 (Specificity protein 1) binding sites and one c-Myc protein binding site.[91,115] In particular, the middle three Sp1 binding sites (-167÷-100) have proved to be crucial for hTERT overexpression.[91] There are two different structural models for this G-rich 68-mer sequence, both obtained by low resolution techniques: one consisting of a hairpin structure, a hybrid G-quadruplex and a parallel one (Figure 27A),[117] and the other consisting of three contiguous stacked parallel G4s (Figure 27B).[118] A detailed NMR study was performed for the shorter sequence d(AGGGGAGGGGCTGGGAGGGC) taken from hTERT core promoter, proving the coexistence of a hybrid (> 40%) and a propeller-type parallel-stranded (< 40%) G-quadruplexes in equilibrium (Figure 27C).[119]

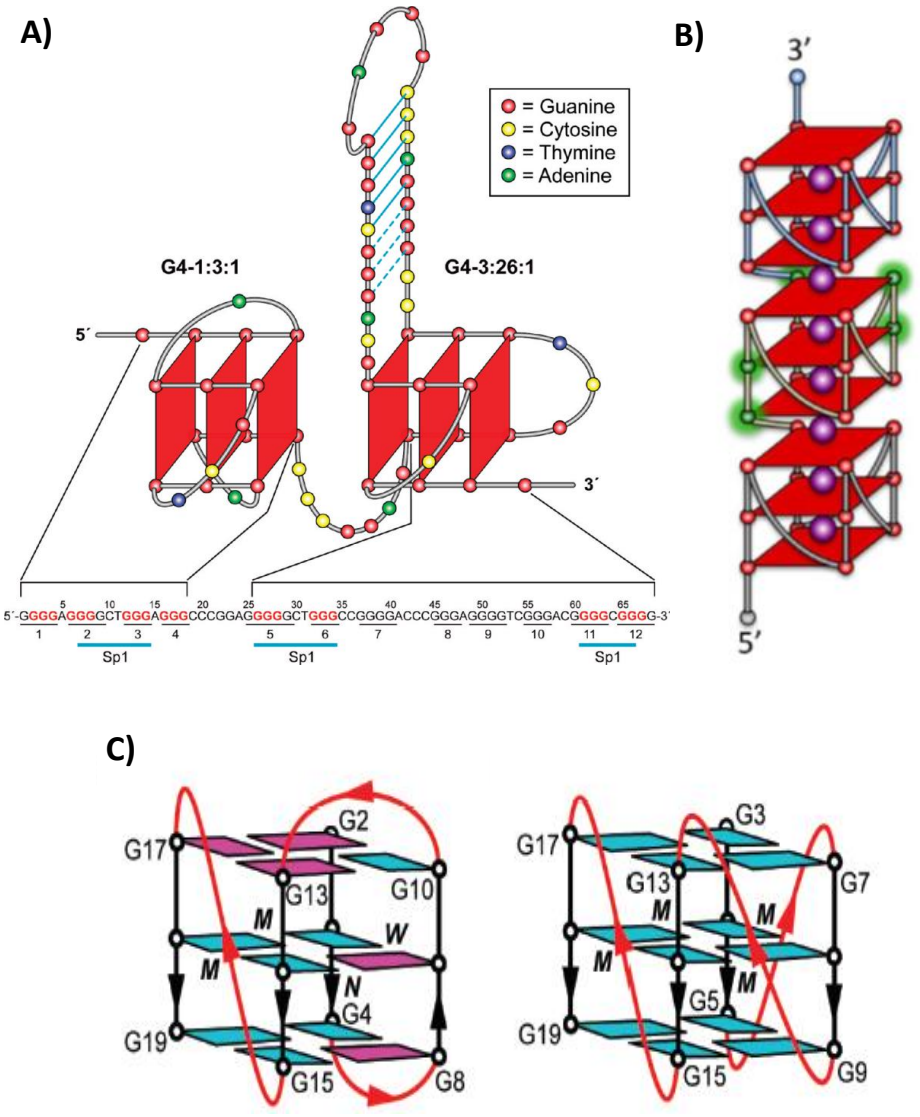

Figure 27. Schematic drawing of two different structural models for the hTERT 68-mer sequence obtained by low resolution techniques: A) model consisting of a hairpin structure, a hybrid G-quadruplex and a parallel one, and B) model consisting of three contiguous stacked parallel G4s. C) Schematic drawing of the structural models obtained by NMR for the shorter sequence taken from hTERT d(AGGGGAGGGGCTGGGAGGGC) in K^+ solutions: on the left, the hybrid one, on the right the parallel one. Light blue box = (*anti*) guanine, violet box = (*syn*) guanine. (Adapted from Palumbo *et al.*[117], Chaires *et al.*[118] and Lim *et al.*[119])

1.3 G-quadruplex ligands

Small organic molecules can interact with G-quadruplex structures through non-covalent interactions, *i.e.*: i) stacking with terminal G-tetrads and/or nucleobases in loops or in the flanking segments, and/or ii) hydrogen bonds or electrostatic interactions with the grooves or loops (Figure 28).[120]

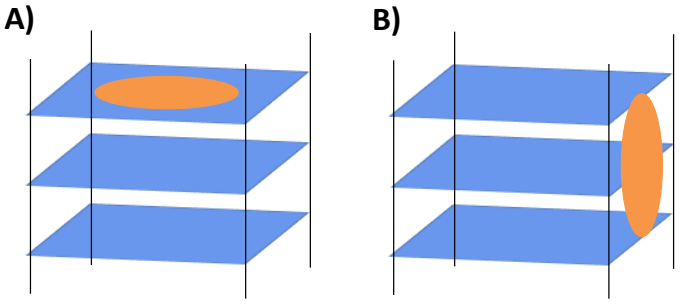

Figure 28. Different binding modes for G-quadruplex ligands: A) stacking with terminal G-tetrads; B) hydrogen bonds or electrostatic interactions with grooves.

Therefore, in order to bind with high affinity G-quadruplex structures, in the design of potential small molecule-based ligands three common features are required:[15]

- a large aromatic core, to realize π-stacking interactions with the G-quartet surface;
- H-bond donors and/or acceptors, to respectively bind acceptors and donors of the oligonucleotide;
- positive charges, to interact with the negative phosphate groups of the DNA backbone through electrostatic interactions.

Since G-quadruplex binding ligands features are also those generally required to interact with duplex DNA, typically ligands recognizing G-quadruplexes are able to interact also with double-stranded DNA.[48] Furthermore, considering that DNA in duplex form is present in the chromosomes in large excess with respect to G-quadruplex structures, a significant increase in selective recognition of G-quadruplexes *vs.* duplex DNA is one of the main requirements to allow the use of G4 ligands as potential anticancer drugs.[48] Essentially, the structural requirements to guarantee G-quadruplex/duplex selectivity involve steric features of ligands and ability to discriminate between quadruplex and duplex grooves, representing the main diversity elements between the two structures.

Several small molecules were extensively studied by NMR and X-rays to obtain detailed information on their interaction with G-quadruplex DNA.

For the pentacyclic acridinium RHPS4, G-quartets end-stacking binding mode was observed in the NMR structure of the complex between the ligand and the parallel human telomere d[(TTAGGGT)]$_4$ G-quadruplex (Figure 29).[121] Several studies showed that the ligand inhibits telomerase and induces telomere uncapping and damage. Furthermore, *in vivo* anticancer activity of RHPS4 proved to be very rapid in xenograft models and well-correlated with its telomerase-inhibitory properties.[122]

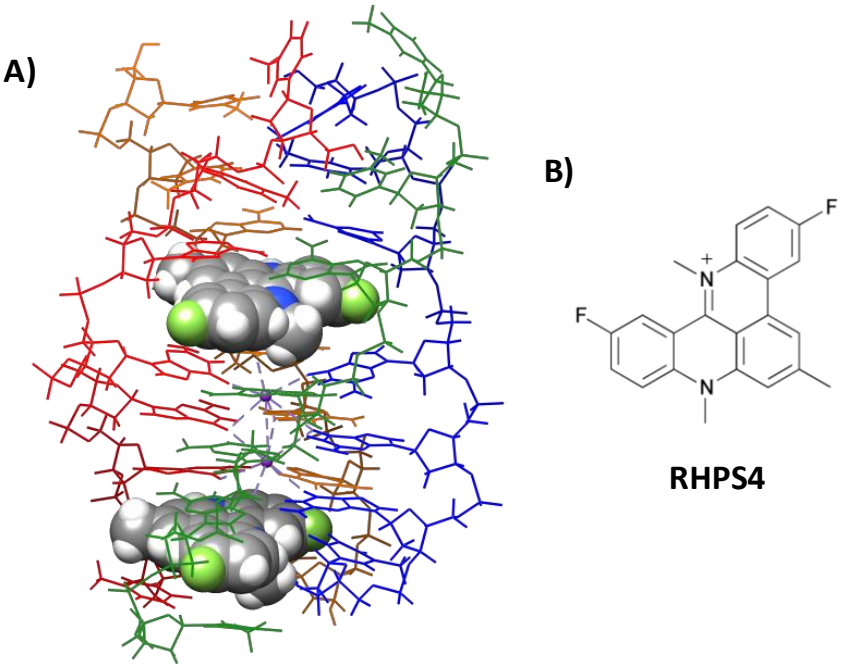

Figure 29. A) NMR structure of the parallel-stranded DNA quadruplex d[(TTAGGGT)$_4$] complexed with RHPS4 (PDB entry: 1NZM). RHPS4 is shown as a space-filled model coloured by atom type, the two potassium ions as violet balls and the four strands in different colours. B) Chemical structure of RHPS4.

For the 3,6,9-trisubstituted acridine BRACO-19 (Figure 30), a crystal structure of its complex with two bimolecular human telomeric G-quadruplexes of sequence d(TAGGGTTAGGGT), arranged in a 5'-3' stacking, was reported.[123] This ligand showed satisfactory G-quadruplex/duplex selectivity and antitelomerase activity (IC_{50} = 115 nM).[124] *In vivo* anticancer activity reported for BRACO-19 in xenograft models is consistent with its ability of inhibiting the capping and catalytic functions of telomerase.[125]

For the tetra-*N*-methyl-4-pyridyl porphyrin TMPyP4 (Figure 30), high affinity for G-quadruplex structures and ability to inhibit telomerase activity (IC_{50} = 6 μM) were proved.[126] By X-ray crystallography studies, the structure of TMPyP4 bound to the bimolecular human telomere G-quadruplex d(TAGGGTTAGGG) was determined.[127] The observed binding mode indicated that two porphyrin molecules stack on the TTA nucleotide tract, either of the external

loop or at the 5' region, without direct contacts with the G-quartets.[127] Contrarily to what observed for the telomeric sequence, TMPyP4 in the complex with a modified sequence taken from c-myc promoter d(TGAGGGTGGIGAGGGTGGGGAAGG) directly stacks on the upper quartet, as determined by NMR.[128] Interestingly, TMPyP4 showed promising anticancer activities *in vivo*, down-regulating the transcription of both c-myc oncogene and human telomerase reverse transcriptase.[129]

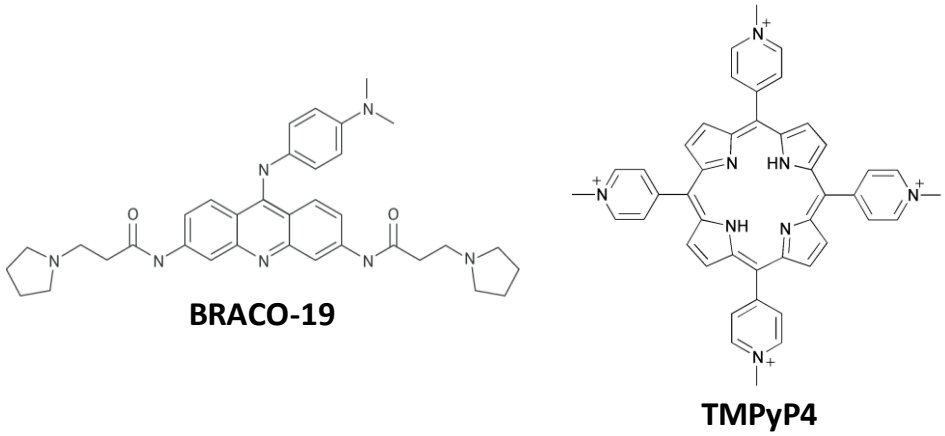

Figure 30. Chemical structures of BRACO-19 and TMPyP4.

Telomestatin is a natural metabolite extracted from *Streptomyces anulatus* bacteria.[130] It showed a high level of G-quadruplex stabilization, quadruplex/duplex selectivity and antitelomerase activity (IC_{50} = 5 nM).[131,132] Even if it is one of the most promising G-quadruplex ligands as anticancer drug candidate, no structure has been solved yet for G4 complexes with telomestatin. However, a high-resolution structure of the complex between the telomestatin derivative and the intramolecular human telomeric G-quadruplex d(TTGGGTTAGGGTTAGGGTTAGGGA) was recently determined by NMR (Figure 31).[133] This compound interacts with the upper quartet through π-stacking and with the loops by electrostatic interactions. Moreover, telomestatin anticancer activity was proved in xenograft mouse model, without displaying any relevant toxicity.[134]

Quinacridine-based molecules also proved to be effective G-quadruplex stabilizing ligands (Figure 32).[135] They interact with the tetramolecular telomeric G4 d[$(TTAGGGT)_4$] by stacking with two G-quartets and by electrostatic interactions with the grooves.[135] These compounds showed remarkable *in vitro* anticancer activity with IC_{50} values in the 100-500 nM range.[135]

Perylene diimides are characterized by a broad hydrophobic core with two external amine pendant groups. This family of compounds was shown to be active as telomerase inhibitors (IC_{50} = 20 μM).[136] In particular, the perylene derivative PIPER (Figure 32) proved to induce

G-quadruplex formation *in vitro* from both telomeric DNA and the hTERT promoter region and inhibit telomerase in a dose-dependent manner.[137,138] In these experiments, the telomerase activity well-correlated with the level of hTERT mRNA, suggesting that the reduction in telomerase activity by PIPER is due to the down-regulation of hTERT expression.[137]

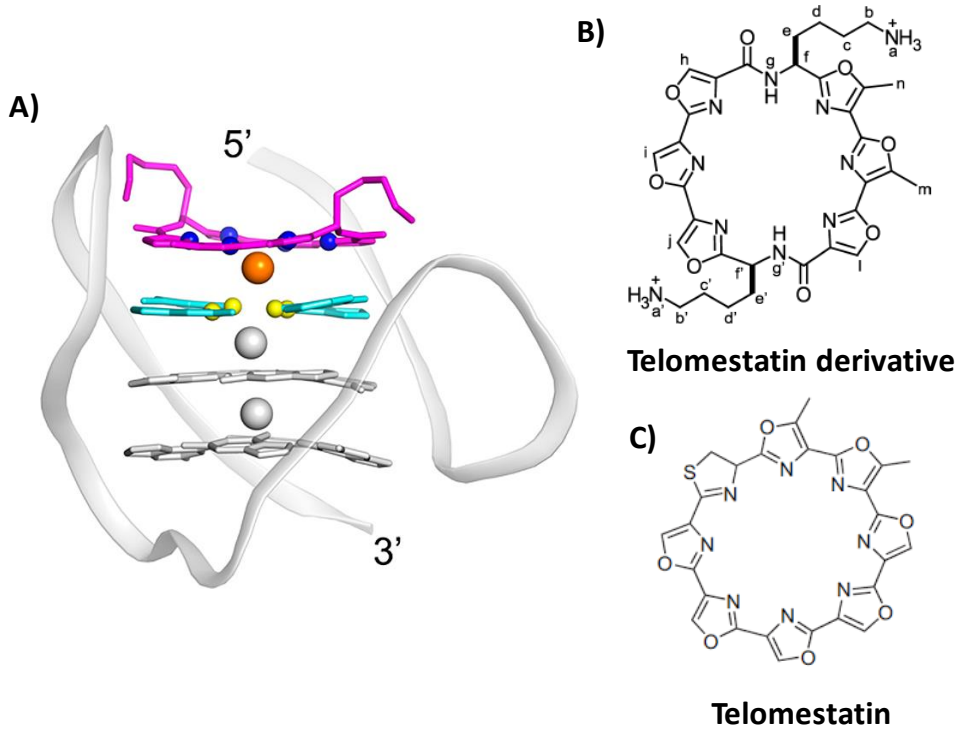

Figure 31. A) NMR structure of the unimolecular DNA quadruplex d(TTGGGTTAGGGTTAGGGTTAGGGA) complexed with the telomestatin derivative here depicted (PDB entry: 2MB3). The backbone is represented as a ribbon. The top G-tetrad and the ligand are highlighted: the potassium ion is coloured in orange, the nitrogen atoms are coloured in blue, the oxygen atoms are coloured in yellow, the ligand is coloured in magenta and the guanine residues are coloured in cyan. B) Chemical structure of the telomestatin derivative used in NMR study. C) Chemical structure of telomestatin. (Adapted from *Chung et al.*[133])

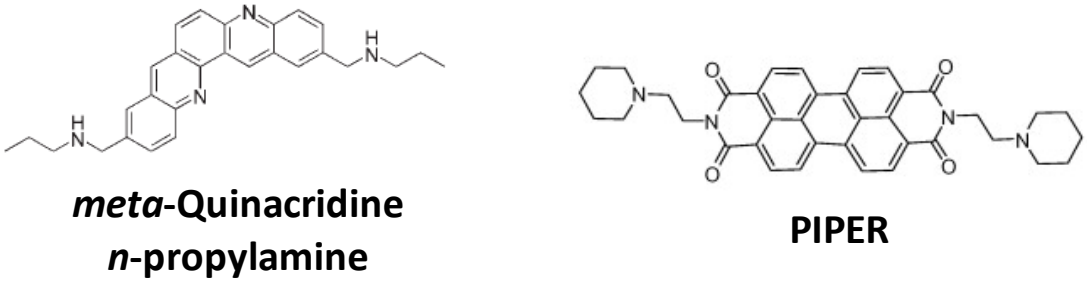

Figure 32. Chemical structures of a quinacridine-based molecules and PIPER.

Other interesting molecules as high affinity G-quadruplex ligands are naphthalene diimides (NDIs).[139,140] It has been shown that the substitution pattern of the NDI core as well as the chemical nature of the substituents play a crucial role in the G4 binding and selectivity toward G4 rather than duplex DNA.[141,142] Neidle *et al.* have shown that in a crystal structure π-π stacking of the NDI naphthalene core with the G-tetrad of telomeric G4 d[AGGG(TTAGGG)$_3$] occurs at the 3'-end, while the 5'-end is stacked on the 5'-end of a second G4, resulting in the formation of a 5'-5' dimer (Figure 33).[143] In addition, the NDI positively charged substituents protrude into the G4 grooves and interact with the phosphates of the DNA backbone (Figure 33).[143] Recently, some NDIs have been shown to be very cytotoxic on selected cancer cell lines,[144] and proved to have antitumor activity *in vivo* in human pancreatic ductal adenocarcinoma (PDAC) animal models.[145]

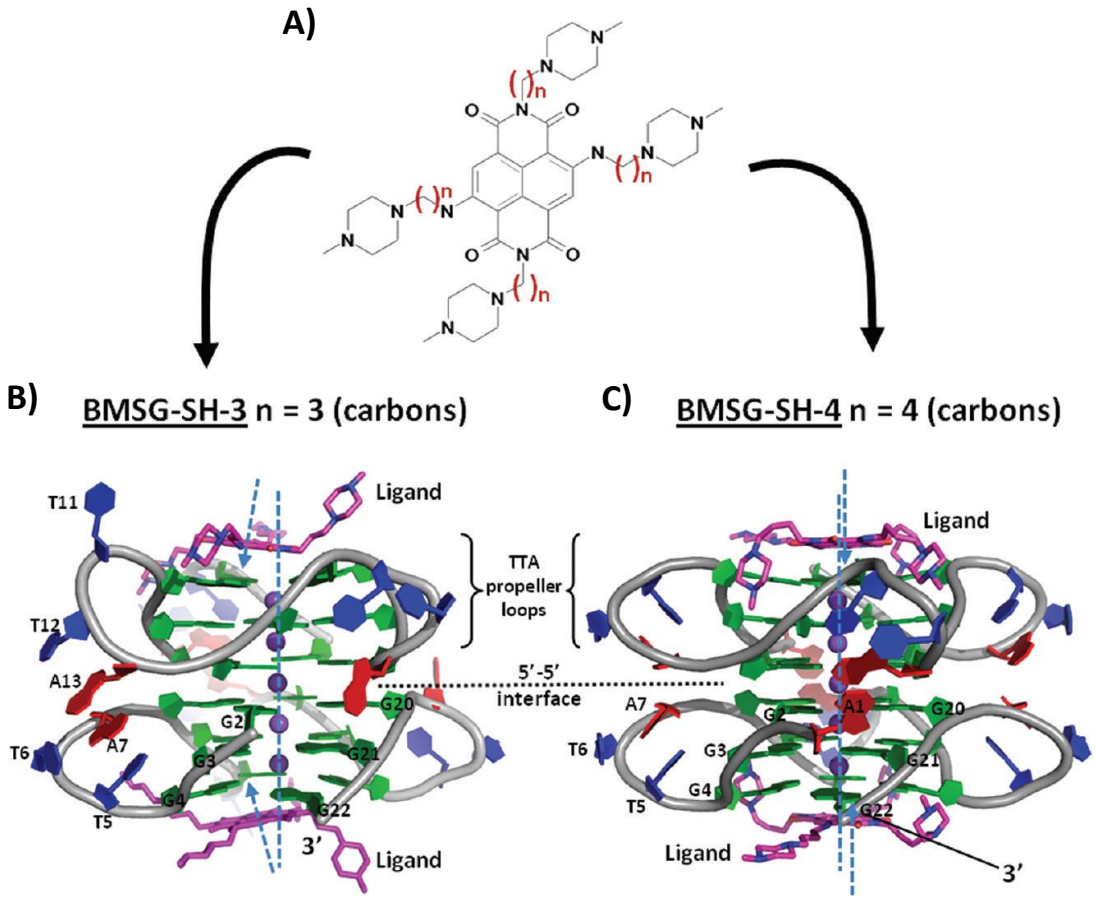

Figure 33. A) Chemical structures of naphthalene diimide based molecules. B) and C) Cartoon representations of the naphthalene diimide-based molecules complexed with telomeric G4 d[AGGG(TTAGGG)$_3$]. The end-to-end quadruplex dimers are shown, highlighting packing, topology and ligand binding orientation. The potassium ions are shown as blue spheres. (Adapted from Collie *et al.*[143])

Contrarily to the plethora of end-stacker ligands, few groove binder ligands are known and only two were well-characterized: distamycin and netropsin (Figure 34).[146,147] Known as minor groove binders of duplex DNA, specifically recognizing AT-rich sequences by electrostatic interactions and hydrogen bonds,[148,149] they have been recently recognized also as G-quadruplex groove binders.[150] By NMR studies on the tetramolecular G-quadruplex d[(TGGGGT)$_4$], distamycin proved to bind in dimeric form the target G-quadruplex in two opposite grooves, thus forming a 4:1 complex.[151] Conversely, netropsin forms a 2:1 complex, probably because its doubly charged nature prevents the formation of dimers.[152] Both ligands expand the grooves to which they are bound, reducing the size of the opposite grooves and thus hampering interactions with other ligands.

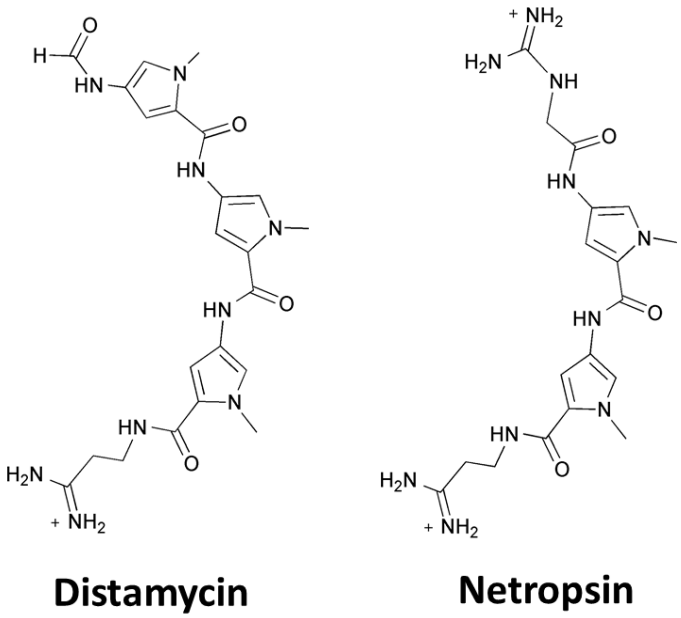

Figure 34. Chemical structures of netropsin and distamycin.

Unfortunately, none of the above molecules has progressed to clinical trials because of unfavourable pharmacokinetics or severe off-target toxicity.[153]

The only G-quadruplex ligands that reached advanced clinical trials are quarfloxin and CX-5461 (Figure 35). Quarfloxin has progressed to Phase II for the treatment of neuroendocrine/carcinoid tumours (ClinicalTrials.gov Identifier: NCT00780663).[154] Several studies suggested that its mechanism of action involves disruption of the interactions between ribosomal DNA G-quadruplexes and the abundant protein nucleolin.[92] It is relocated to the nucleoplasm, where it binds the c-myc G-quadruplex, thus inhibiting c-myc expression and leading to cancer cells apoptosis.[92] Moreover, docking studies showed quarfloxin ability to

directly interact with the c-myc G4.[155] Indeed, using the sequence d(TGAGGGTGGGTAGGGTGGGTAA), taken from c-myc promoter, quarfloxin proved to intercalate between the top tetrad and the 5'-end flanking bases and direct its side chains into the two single-base loops (Figure 35A).[155]

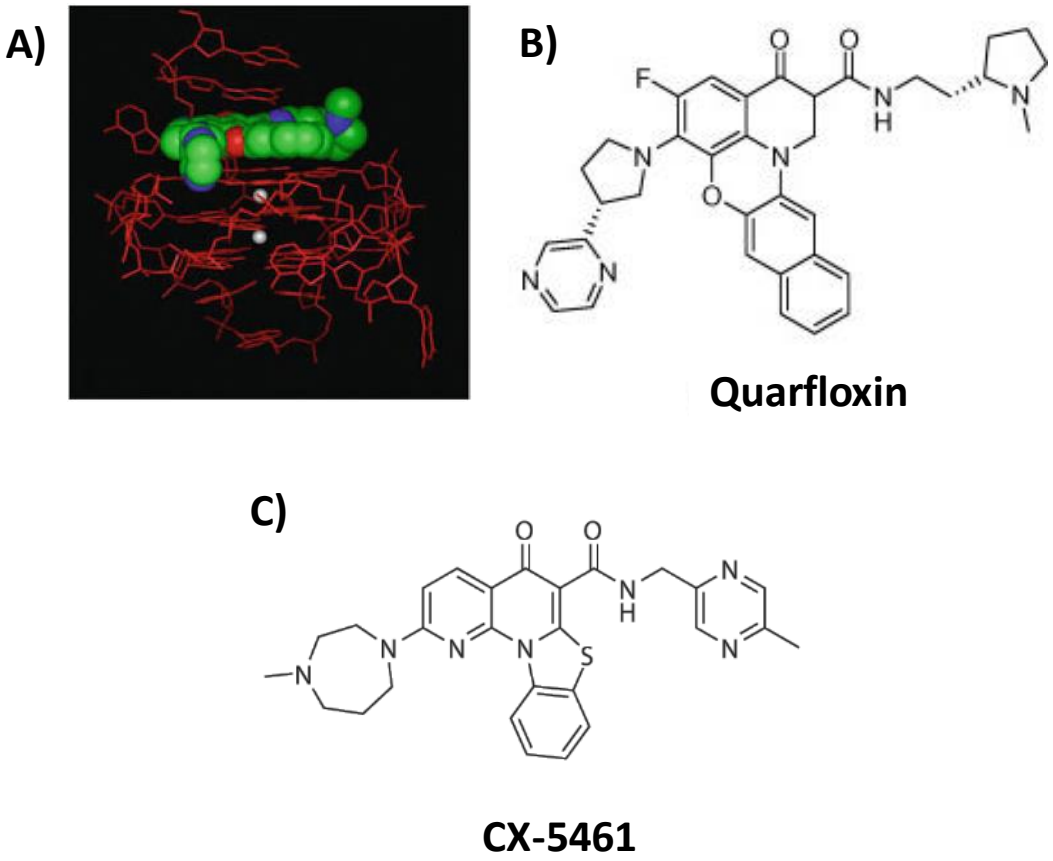

Figure 35. A) Molecular model of quarfloxin with c-myc G4 d(TGAGGGTGGGTAGGGTGGGTAA). Quarfloxin is shown as a space-filled model coloured by atom type and the two potassium ions as white balls. (Adapted from Kaiser *et al.*[155]) B) Chemical structure of quarfloxin. C) Chemical structure of CX-5461.

Quarfloxin did not proceed past Phase II trials because of bioavailability issues, but its toxicity profile is very encouraging and suggests that successive optimizations could improve its pharmacological properties.[156]

On the other hand, CX-5461 is currently in advanced phase I clinical trial for the treatment of patients with BRCA1/2 deficient tumours (ClinicalTrials.gov Identifier: NCT02719977).[157,158] Treatment with CX-5461 induces G4 structures formation and DNA damage *in vitro*. BRCA1 and BRCA2 deficient cells, *i.e.* lacking essential proteins in the process of DNA damage repair,

are less competent to bypass drug stabilized G4 structure during DNA replication and less efficient to repair G4 associated DNA damage. As a consequence, the accumulated DNA damage in BRCA deficient cells leads to apoptosis. Furthermore, CX-5461 is also effective in tumours resistant to poly(ADP-ribose) polymerase (PARP) inhibition and/or platinum complexes.[157]

All these findings prove the complete feasibility and high promise of a general therapeutic approach based on the use of G-quadruplex binders as anticancer drugs. However, notwithstanding the remarkable and conspicuous achievements in this field, no G-quadruplex binder has been approved as a drug yet. Therefore, for a real progress of this anticancer strategy, two actions are urgently required: a huge synthetic effort for the production of large libraries of novel classes of putative G4 ligands, associated with the development of efficient screening methods to quickly identify novel G4 selective ligands as optimized candidates for *in vivo* studies.

1.4 Aims of the PhD project

The final aim of this PhD project is the discovery and evaluation of novel ligands specifically binding to peculiar non-canonical G-quadruplex DNA structures, recognized to play crucial roles in regulatory regions of human genome associated with cancer.[13,156] To achieve an optimal recognition selectivity, which is the prerequisite to avoid off-target drug toxicity, most research efforts have been directed to identify structure-selective ligands, *i.e.* small molecules able to discriminate G4 *vs.* duplex DNA. One additional, major challenge is the discovery of conformation-selective ligands, *i.e.* able to selectively recognize specific G4 conformations over others.

To this purpose, design and synthesis of a novel universal solid support for affinity chromatography-based High Throughput Screening (HTS) of conformation-selective G-quadruplex ligands is here presented. The support is unique as it allows performing the on-line synthesis of the oligonucleotides, as well as the successive binding assays. In addition, the novel affinity chromatography-based methodology enabling a fast, simple and reliable screening of focused libraries of ligands, recently developed in our laboratories,[159,160] will be here used and implemented. It consists in flowing the tested compounds through the novel derivatized glass supports functionalized with oligonucleotides able to form conformationally different G4 structures under proper conditions. The molecules with high affinity for the G4s are retained by the solid supports, while those with low affinity are eluted with a washing solution. The

specific interaction with a G4 structure is confirmed by inducing its denaturation, resulting in full release in solution of the captured ligand. All the here described steps can be quantitatively monitored by simple and fast UV measurements.

Immobilization on the solid support of DNA single strands able to fold into stable hairpin duplex structures provides proper controls to evaluate the G4 *vs.* duplex DNA recognition specificity of the ligands.

Conformational properties of the oligonucleotides linked to the support are also investigated to provide a proof-of-concept that our novel approach is a powerful tool to identify not only structure-selective G4-ligands, but even conformation-selective G4-ligands, thus assuring higher selectivity and lower toxicity of the selected molecules in view of *in vivo* applications.

Validation and optimization of the affinity chromatography-based method is achieved by exploiting known G4 ligands, and after this step, novel focused libraries of potential conformation-selective G4 ligands are analyzed.

Detailed biophysical characterization in solution of the interactions between the target DNA and the best ligands in terms of recognition affinity and specificity is carried out involving several spectroscopic techniques in a combined approach.

Finally, *in vitro* tests, carried out in collaboration with specialized laboratories to assess the anticancer activity of the selected ligands, are also described.

CHAPTER 2 – PREPARATION OF A NOVEL SUPPORT FOR THE ON-LINE SYNTHESIS OF OLIGONUCLEOTIDES

2.1 Introduction

The identification of selective G-quadruplex ligands, able to discriminate *in vivo* different nucleic acids conformations having crucial roles in tumours, is of paramount importance for the development of effective and minimally toxic anticancer drugs. Thus, considerable efforts are currently devoted to the design and synthesis of molecules able to selectively target G4 structures and discriminate duplex DNA. To be effective, this huge impulse to synthesize new potential ligands has to be coupled with fast and reliable High Throughput Screening methods. In this context, a highly reproducible affinity chromatography-based method for the identification of putative G4-ligands has been recently described by our research group.[159,160] Affinity chromatography is a powerful methodology for probing small molecule-biomolecule interactions; it consists of simple and efficient assays based on the immobilization of the target molecule or, more frequently, biomolecule on a solid support, thus allowing screenings of large libraries in a short time.

In a first design, the Oligo Affinity Support (OAS), a commercially available polystyrene/polyethylene glycol copolymer (Glen Research Corporation, Sterling, VA, USA),[161] functionalized with a protected adenosine monomer through the adenine exocyclic amino group *via* a stable covalent linkage, was selected to realize the binding assays (Figure 36A).[161] The OAS resin was hence used for the assembly of the 26-mer d[(TTAGGG)$_4$TT] sequence (tel26), a truncation of human telomeric DNA, able to fold, under proper conditions, into a unimolecular G4 (Figure 36B).[159] Due to its peculiar functionalization, the final aq. ammonia treatment, after the oligonucleotide solid phase synthesis, fully deprotected the oligomer without detaching it from the support. The above method was optimized on known G4 and non-G4 ligands.[159] After the optimization, the binding assay, named G4-OAS (G4 on Oligo Affinity Support), was applied to the screening of a focused library of 60 small organic molecules, selected as potential G4 groove binders by virtual screening.[160] For each of the 60 selected molecules, the absence of unspecific binding on the nude OAS support was verified first, and, subsequently, the ability to interact with the G4-functionalized support. Thus, the binding assay allowed the identification of 7 telomeric G4 good binders out of the 60 compounds (Figure 37).[160] Furthermore, biological assays on human tumour cells

demonstrated that 3 out of the 7 tested compounds were able to effectively induce a DNA damage response at telomeres, even at 1 μM concentration.[160]

Though rapid, simple and effective, a major limitation emerged on using the G4-OAS assay, resulting from the chemical nature of the OAS support. Indeed, about one third of the 60 small molecules showed strong unspecific binding on the polystyrene nude OAS resin, due to stacking interactions between the polystyrenic resin and the aromatic cores of the ligands, making therefore impossible to acquire information on their binding to the G4-functionalized support.[160] Hence, taking into account that most known binders of G-quadruplexes share a common planar aromatic core, necessary to realize π-π stacking interactions with the nucleobases, there is a felt need to provide supports being chemically inert, differently from the commercially available OAS, and properly functionalized to elongate secondary structure-forming oligonucleotides for affinity chromatography-based binding assays.

With the aim of addressing this issue and realizing a universal support for effective screenings of putative conformation-selective G4 ligands, we have conceived a novel functionalization for Controlled Pore Glass (CPG) allowing both the on-line synthesis of fully deprotected support-bound oligonucleotides and subsequent affinity chromatography-based binding assays.[162,163] For its intrinsic chemical inertness and peculiar structure, not producing stacking interactions with aromatic putative ligands, this solid support is expected to overcome the drawbacks (essentially, unspecific ligand binding) associated with the use of polystyrenic Oligo Affinity Support.

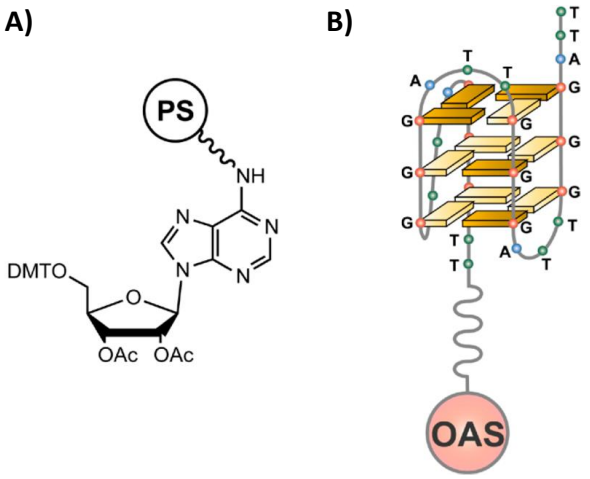

Figure 36. A) Schematic representation of the commercially available polystyrene/polyethylene glycol (PS)-based Oligo Affinity Support (OAS) resin; B) OAS resin functionalized with the 26-mer d[(TTAGGG)$_4$TT] sequence (tel26), a truncation of human telomeric DNA, folded into a G4 structure in a K^+-containing solution. DMT = 4,4'-dimethoxytrityl; Ac = acetyl. (Adapted from Musumeci *et al.*[159])

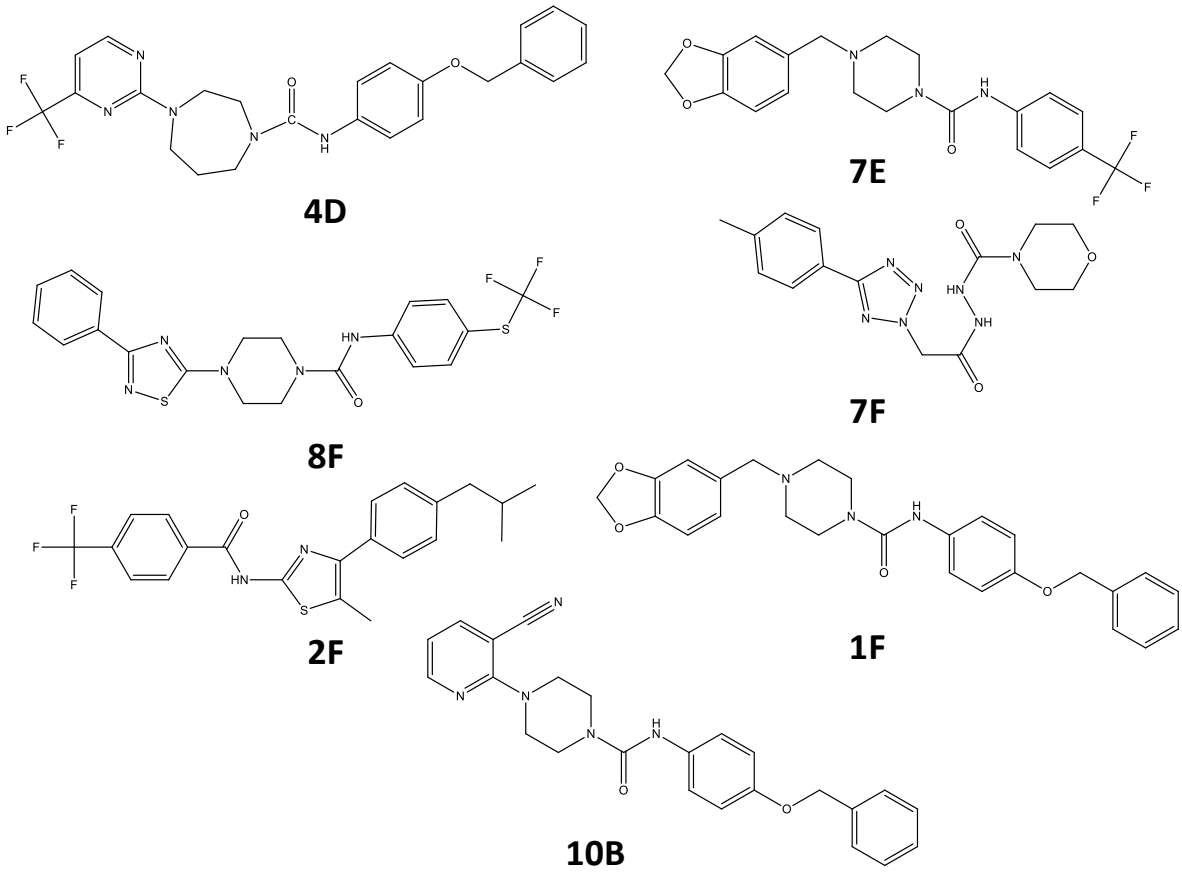

Figure 37. Chemical structures of the 7 telomeric G4 ligands identified by G4-OAS assay.[160]

2.2 Functionalization of Long Chain AlkylAmine-CPG with 5'-*O*-DMT, 3'-*O*-acetylthymidine through a hexaethylene glycol spacer

In order to prepare the novel functionalized CPG support, a hexaethylene glycol derivative (DMT-HEG-COOH) has been selected as the spacer and *ad hoc* synthesized.[162,163] To prepare DMT-HEG-COOH, hexaethylene glycol has been first protected at one end with the DMT group using standard procedures (Scheme 1A), and the resulting product 4,4'-dimethoxytrityl-hexaethylene glycol (DMT-HEG-OH) then oxidized exploiting 2,2,6,6-tetramethyl-1-piperidinyloxy (TEMPO) as catalyst, finally obtaining the DMT-HEG-COOH (Scheme 1B).

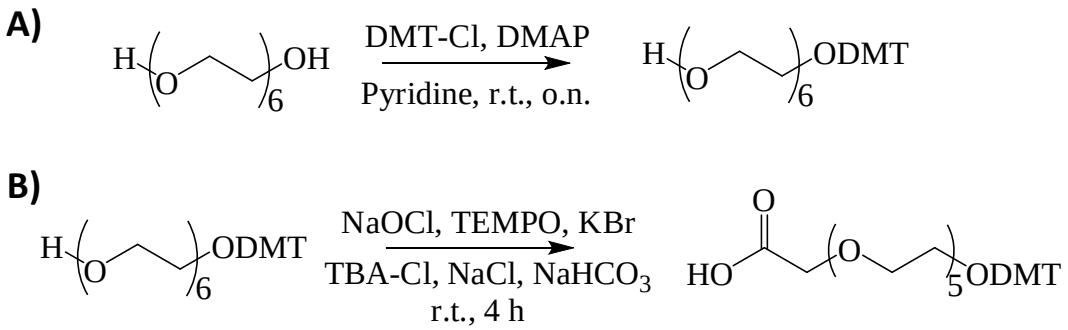

Scheme 1. Synthesis of 4,4'-dimethoxytrityl-hexaethylene glycol-COOH (DMT-HEG-COOH). A) Dimethoxytritylation of hexaethylene glycol to obtain its mono 4,4'-dimethoxytritylether DMT-HEG-OH; B) Oxidation of DMT-HEG-OH to DMT-HEG-COOH. DMT-Cl = 4,4′-dimethoxytrityl chloride; DMAP = 4-dimethylaminopyridine; TBA-Cl = tetrabutylammonium chloride; TEMPO = 2,2,6,6-tetramethyl-1-piperidinyloxy.

Successively, the commercially available Long Chain AlkylAmine-CPG (LCAA-CPG) solid support (Figure 38)[164] has been reacted with DMT-HEG-COOH, in the presence of the activators of the carboxylic functional group *N*,*N*'-dicyclohexylcarbodiimide (DCC) and 1-hydroxybenzotriazole (HOBt) (Scheme 2).[162,163]

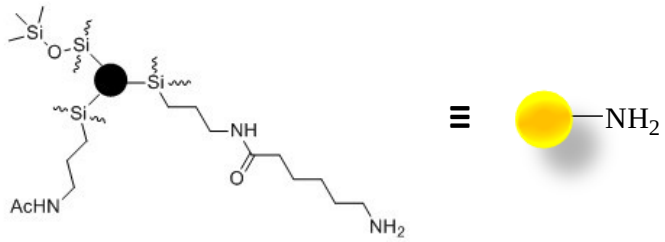

Figure 38. Commercially available Long Chain AlkylAmine-CPG (LCAA-CPG) solid support.[164]

Thus, the CPG solid support has been functionalized with the hexaethylene glycol spacer bound through an aliphatic amide function and protected at the terminal hydroxyl moiety with the 4,4'-dimethoxytrityl (DMT) protecting group.

In the synthetic protocol, hexaethylene glycol has been chosen as the spacer because of its good solubility properties in both apolar and polar solvents, which make it suitable for both oligonucleotide synthesis, carried out in organic solvents, and affinity chromatography-based assays, carried out in aqueous solutions. Indeed, its length and flexibility guarantee minimization of possible steric effects with the solid matrix during both the oligonucleotide elongation and binding assays.[165] Remarkably, the spacer also ensures that, once assembled, the linked oligonucleotide is kept at an appropriate distance from the solid support, so that in

principle it has sufficient conformational freedom to adopt its preferred secondary structure, as if in solution.

After CPG derivatization with the spacer, the DMT group has been removed by acidic treatment and the resulting support **1** has been functionalized with 5'-*O*-DMT, 3'-*O*-acetyl-thymidine – synthesized by standard acetylation of commercially available 5'-*O*-DMT-thymidine – through a Mitsunobu reaction, using triphenylphosphine and diethyl azodicarboxylate (DEAD) as activators (Scheme 2).[162,163,166]

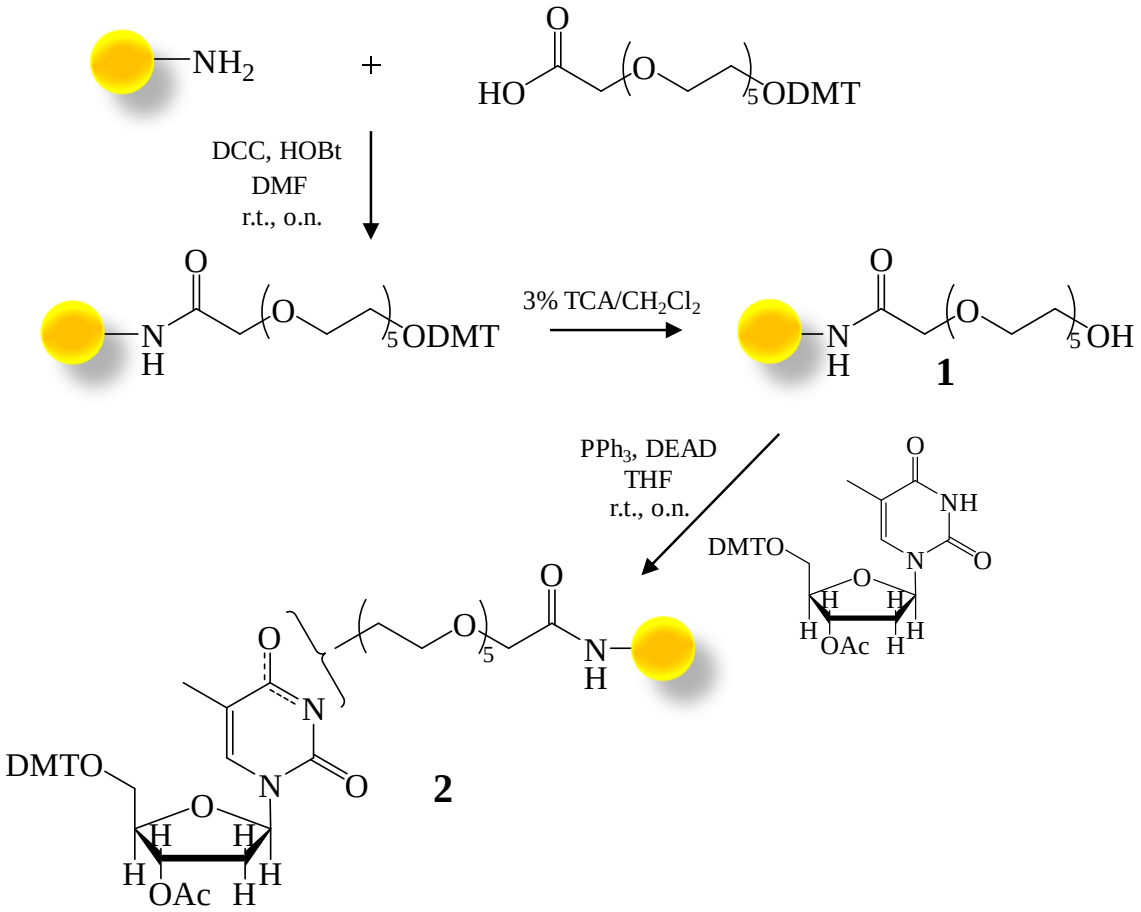

Scheme 2. Functionalization of LCAA-CPG with 5'-*O*-DMT, 3'-*O*-acetyl-thymidine through a hexaethylene glycol spacer. Ac = acetyl; DCC = *N*,*N'*-dicyclohexylcarbodiimide; DEAD = diethyl azodicarboxylate; DMF = *N*,*N*-dimethylformamide; DMT = 4,4'-dimethoxytrityl; HOBt = 1-hydroxybenzotriazole; TCA = trichloroacetic acid; THF = tetrahydrofuran.

In particular, we have incorporated as first monomer on the support a pyrimidine nucleoside, and not a purine, as in functionalized OAS resin, to avoid undesired, unspecific interactions in the successive binding assays. Indeed, we reasoned that purines should be discarded in the first functionalization step since they might generate additional stacking interactions with both the

tested ligands and the oligonucleotide sequence of interest, somehow affecting its conformation and thus the binding assays. Following this procedure, we obtained a CPG solid support functionalized with a DMT-protected nucleoside attached through the nucleobase (support **2**) so that, after acidic treatment allowing the DMT removal, the 5'-position is available for oligonucleotide elongation. Moreover, the chemically stable bond between the spacer and the first nucleoside guarantees, once the oligonucleotide chain elongation is completed, that the oligonucleotides can be fully deprotected without detaching them from the solid support.[162,163] Standard capping treatments with acetic anhydride in pyridine have been introduced in the synthetic protocol to block both the unreacted amino groups on the support after DMT-HEG-COOH incorporation and the unreacted hydroxyl groups on **1** after the Mitsunobu reaction. Spectrophotometric DMT tests, quantifying the DMT cation released upon acidic treatment of weighed samples of CPG, allowed monitoring the yield of each reaction step. Overall, this synthetic route provided solid support **2** with an average DMT functionalization of 0.023 meq/g.[162,163]

2.3 Synthesis of oligonucleotide models on the CPG support

2.3.1 Assembly and deprotection of a hairpin duplex-forming oligonucleotide covalently attached to the CPG support

The main requirement for a G4 ligand to be a potential anticancer drug in targeted therapies is the ability to strongly discriminate G4 *vs.* duplex DNA. Thus, we have here synthesized a duplex-functionalized solid support, as a negative control allowing assessing the ability of putative ligands to discriminate non-canonical DNA conformations *vs.* duplex DNA.

Bimolecular duplex systems obtained by elongation of a single strand on the support, followed by hybridization to its complementary strand – used in the first design of this assay (G4-OAS) – proved to be not completely stable in the conditions used for the binding assays, partially releasing the complementary strand in solution at each assay and thus providing not fully reliable results.[160] To overcome this limitation, we have here chosen, for the elongation on support **2**, the sequence d(CGCGAATTCGCGTTTCGCGAATTCGCG) (ds27) as the model, because of its ability to fold into a stable hairpin unimolecular duplex under proper conditions, well-mimicking a double-stranded DNA. Indeed, it consists of two Dickerson dodecamer tracts – a very well-known model for B-DNA duplex[167–169] – connected by a TTT loop.

The length and base composition of the loop have been selected on the basis of the following observations:

- loops longer than 3 residues can promote the formation of Z-DNA unimolecular duplex structures;[170]
- among the loops containing 1, 2 and 3 residues, the highest thermal stability is observed in the case of a 3 residues loop;[170,171]
- the nucleobases present in the loop should minimally affect the binding of the putative ligands to the duplex; thus, pyrimidine nucleosides are preferred since purines can produce additional stacking interactions;
- the nucleobases not requiring protecting groups (as is the case of thymines) make easier and speed up the final deprotection step in solid phase oligonucleotide syntheses.

The hairpin duplex-forming oligonucleotide has been assembled on support **2** using standard phosphoramidite chemistry (Scheme 3), including the following steps:

- deprotection of the 5'-OH group by removal of the DMT protecting group of the nucleoside anchored to the solid support by treatment with 2% trichloroacetic acid (TCA) solution;
- coupling of the 5'-OH position available for oligonucleotide elongation with a nucleoside 3'-*O*-(2-cyanoethyl)-*N*,*N*-diisopropyl phosphoramidite monomer in the presence of the standard phosphoramidite activator 5-ethylthio-1H-tetrazole (ETT) to obtain a phosphite triester linkage;
- capping of the unreacted 5'-OH groups on the solid support by using a mixture of acetic anhydride and *N*-methylimidazole in pyridine;
- oxidation of the phosphite triester linkage to phosphate triester moiety by using a solution of I_2/H_2O/pyridine in THF;
- repetition of the coupling, capping and oxidation steps for a number of times corresponding to the number of nucleotides contained in the target oligonucleotide sequence.

The coupling efficiency was monitored after each synthetic cycle by spectrophotometric measurements of the DMT cation, removed before each coupling step by standard acidic treatment. Considering the number of couplings (27 bases) and the average yield per cycle of 99.2%, the overall yield was determined to be 80%, corresponding to a final functionalization of 0.018 meq/g.[162,163]

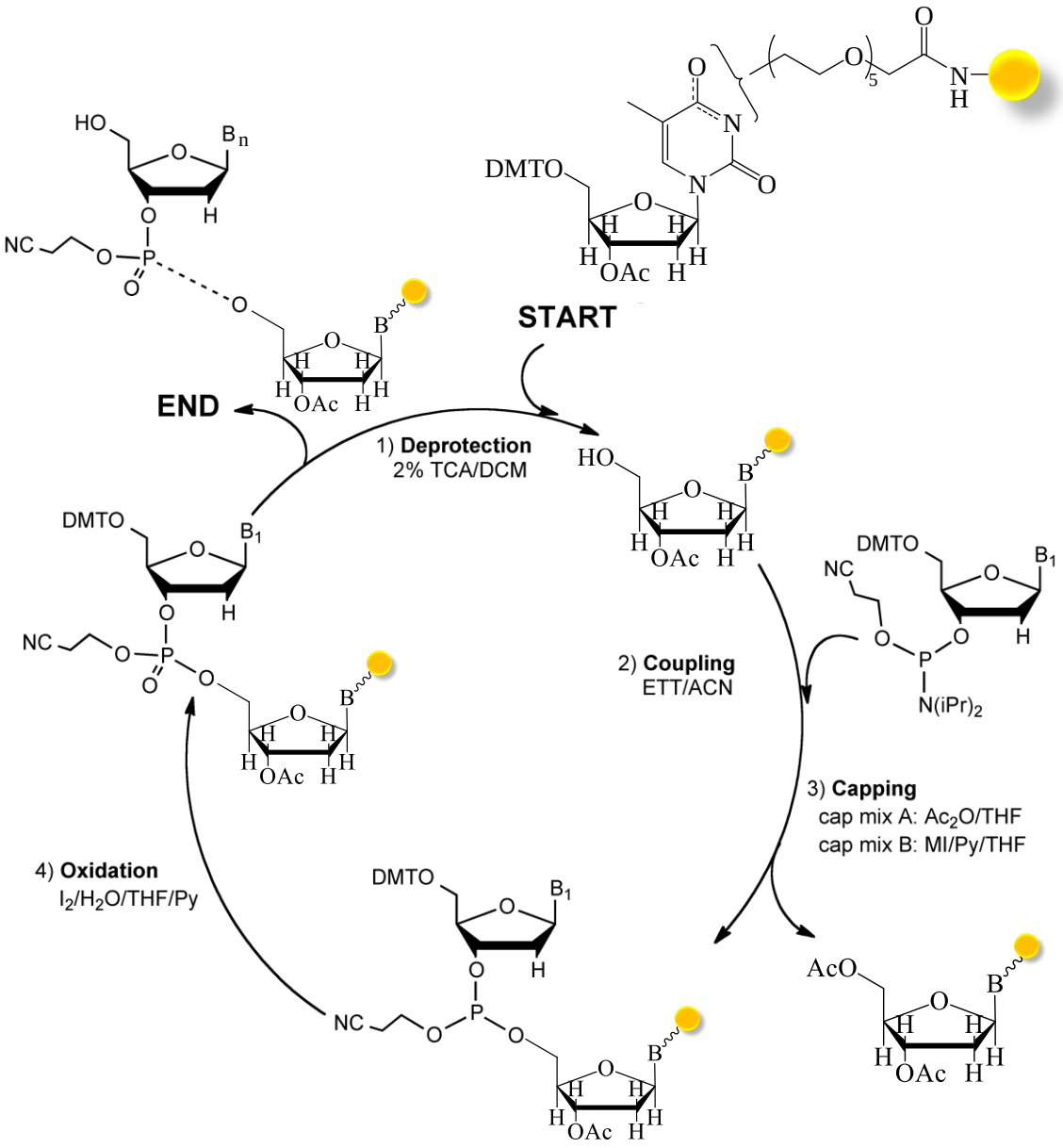

Scheme 3. Schematic illustration of the synthesis cycle of oligodeoxyribonucleotides on novel derivatized CPG support. Ac = acetyl; ACN = acetonitrile; DCM = dichloromethane; DMT = 4,4'-dimethoxytrityl; ETT = 5-ethylthio-1H-tetrazole; MI = *N*-methylimidazole; TCA = trichloroacetic acid; THF = tetrahydrofuran.

Aiming at completely deprotecting the oligonucleotide without detaching it from the solid support, two different deprotection protocols have been tested. Two batches of oligonucleotide-bound support – still bearing the terminal 5' DMT group – were treated in parallel with 30% ammonium hydroxide (NH_4OH) at r.t. for 24 h, and with 30% ammonium hydroxide/40% methylamine 1:1, v/v (AMA) at r.t. for 2 h, respectively. The resulting supports were then washed several times with water until neutralization. To verify if the final basic treatment promoted even partial detachment of the oligonucleotide from the solid supports, the eluates relative to NH_4OH and AMA deprotection were collected, taken to dryness, redissolved in H_2O and analyzed by UV spectroscopy. In both cases, the presence of nucleotidic material was observed. This is probably due to silica instability under basic solutions: indeed, pure silica partially dissolves under these conditions.[172] The DMT test was then performed on dried and weighed samples of the two CPG batches, allowing the determination of the final functionalization for hairpin duplex-bound supports, which resulted to be 0.005 meq/g (30% oligonucleotide attached to the support) and 0.011 meq/g (60% oligonucleotide attached to the support) after the NH_4OH and AMA deprotection treatment, respectively.[162] Taking for granted that the NH_4OH treatment, carried out under standard conditions, resulted in the full deprotection of the oligonucleotide bound to the support,[173] with the aim of evaluating if also the AMA deprotection treatment went to completeness, we analyzed the eluate relative to AMA deprotection by HPLC. As shown in figure 38, upon AMA deprotection, only two major species were present in the eluate: one peak at 10.9 min retention time, *i.e.* the full-length oligonucleotide detached, which had accidentally lost its 5'-DMT protecting group; and one peak at 14.0 min, identified as the DMT-ON, full-length oligonucleotide detached. Indeed, upon detritylation of the latter species, only one peak, with the same retention time of the first product, appeared in the HPLC chromatogram. Furthermore, we compared the experimental data for known duplex ligands obtained from our affinity chromatography-based binding assay on two oligonucleotide-bound supports previously treated using the mentioned different deprotection methods. For all the tested ligands, the results were always in good agreement within the experimental error. Overall, these results – even if indirectly – proved that the 2 h AMA treatment guarantees complete deprotection for the oligonucleotide bound to support **2**, in accordance with current protocols of oligonucleotide synthesis, sensibly reducing the detachment of the synthesized oligonucleotide from the CPG support compared to the NH_4OH treatment.[163]

Considering that the amount of oligonucleotide bound to the support cannot be too low, thus allowing the use of small amounts of support for each binding test, nor too high, to avoid steric

hindrance due to high functionalization density in the binding assays, the final functionalization obtained by our optimized protocol for the on-line oligonucleotide synthesis and deprotection proved to be fully suitable for the successive binding assays.

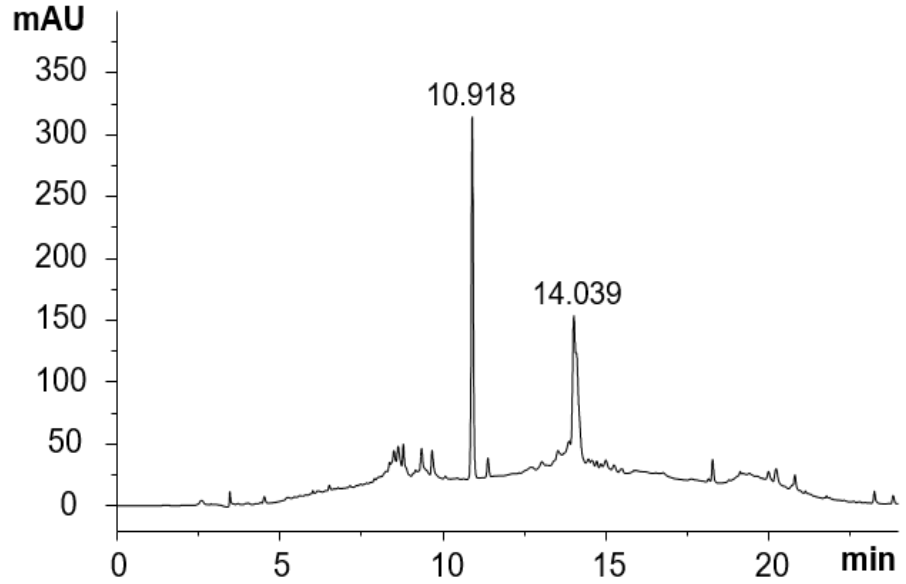

Figure 38. HPLC profile of the eluate relative to ammonium hydroxide/methylamine (AMA) deprotection of the hairpin duplex-bound support.

2.3.2 Assembly and deprotection of G4-forming oligonucleotides covalently attached to the CPG support

Following the same protocol adopted for the hairpin duplex-forming oligonucleotide, a truncation of human telomeric DNA of sequence d[(TTAGGG)$_4$TT] (tel26)[21] and the 22-mer d(AGGGAGGGCGCTGGGAGGAGGG) (ckit1)[110,112] taken from the c-kit oncogene promoter, able to fold in proper conditions into unimolecular G4s, have been assembled on support **2**.[162,163] The coupling efficiency was monitored after each synthetic cycle by spectrophotometric measurements of the DMT cation, removed before each coupling step by standard acidic treatment. Considering the number of couplings and the average yields per cycle of 99.4% and 99.9% for tel26 and ckit1 respectively, the overall yields were determined to be 86% and 98%, corresponding to a final functionalization of 0.020 meq/g and 0.022 meq/g, respectively. After the coupling cycles, aiming at fully deprotecting the oligonucleotides, the solid supports were treated with 30% ammonium hydroxide/40% methylamine 1:1, v/v (AMA) at r.t. for 2 h. The resulting supports were then washed with water until neutralization. DMT tests, performed on dried and weighed samples of the supports, allowed determining the final

functionalization for the support-bound G-quadruplex-forming oligonucleotides, which was 0.012 meq/g and 0.013 meq/g, respectively for tel26 and ckit1, after the AMA deprotection treatment.

2.4 Experimental section

2.4.1 Synthesis of 4,4'-dimethoxytrityl-hexaethylene glycol-COOH (DMT-HEG-COOH)

Hexaethylene glycol (887 µL, 3.54 mmol, commercially available from Sigma-Aldrich) was reacted with a mixture of 4,4′-dimethoxytrityl chloride (DMT-Cl, 718 mg, 2.12 mmol) and 4-dimethylaminopyridine (DMAP, 26 mg, 0.212 mmol) in anhydrous pyridine (3 mL) at r.t. overnight. The resulting product (DMT-HEG-OH) was purified by flash chromatography on a silica gel column eluted with increasing amounts of CH_3OH in CH_2Cl_2, from 0% to 2%, containing 1% of triethylamine (recovered yield = 72%). The identity of the purified product was confirmed by ^1H NMR (C_6D_6, 400 MHz): δ 7.77 (d, 2H, DMT H2"), 7.55 (d, 4H, DMT H2 and H2'), 7.19 (t, 2H, DMT H3"), 7.07 (t, 1H, DMT H4"), 6.78 (d, 4H, DMT H3 and H3'), 3.64 (t, 2H, HOCH_2), 3.59-3.28 (complex signals, 22H, 5 x OCH_2CH_2 and $HOCH_2CH_2$), 3.32 (s, 6H, 2 x OCH_3), 2.67 (br, 1H, OH).

DMT-HEG-OH (450 mg, 0.77 mmol) was then reacted with a mixture of 2,2,6,6-tetramethyl-1-piperidinyloxy (TEMPO, 19 mg, 0.12 mmol), KBr (20 mg, 0.17 mmol), tetrabutylammonium chloride (TBA-Cl, 46 mg, 0.17 mmol), $NaHCO_3$ (1.0 mL of an aq. satd. solution), NaClO (2.5 mL) and NaCl (1.0 mL of an aq. satd. solution) at r.t. for 4 h. The resulting product (DMT-HEG-COOH) was purified by flash chromatography on a silica gel column eluted with increasing amounts of CH_3OH in CH_2Cl_2, from 5% to 10%, containing 1% of triethylamine (recovered yield = 62%). The identity of the purified product was confirmed by ^1H NMR (C_6D_6, 400 MHz): δ 8.11 (br, 1H, COOH), 7.71 (d, 2H, DMT H2"), 7.69 (d, 4H, DMT H2 and H2'), 7.54 (t, 2H, DMT H3"), 7.52 (t, 1H, DMT H4"), 7.22 (d, 4H, DMT H3 and H3'), 3.88 (s, 2H, CH_2CO), 3.34-3.06 (complex signals, 20H, 5 x OCH_2CH_2), 3.21 (s, 6H, 2 x OCH_3).

2.4.2 Functionalization of LCAA-CPG with the hexaethylene glycol spacer DMT-HEG-COOH

LCAA-CPG 1000 Å (155 mg, 0.069 meq/g, 10.7 mmol; Link Technologies, Bellshill, UK)[164] was left in contact with a mixture of DMT-HEG-COOH (64 mg, 107 mmol), *N,N'*-dicyclohexylcarbodiimide (DCC, 22 mg, 107 mmol) and 1-hydroxybenzotriazole (HOBt, 14.5 mg, 107 mmol) in anhydrous DMF (500 µL) at r.t. overnight. After removing the excess of the

reactants from the resin by exhaustive washings with DMF, CH_3OH, AcOEt, *n*-hexane and CH_2Cl_2, the support was taken to dryness under reduced pressure. DMT tests performed on dried and weighed samples of the resulting support allowed determining the incorporation yield of DMT-HEG-COOH onto the CPG support, which resulted to be 74% (0.051 meq/g). The solid support was then treated with a capping solution, consisting of a mixture of acetic anhydride/pyridine (1:1, v/v), at r.t. for 4 h to block the unreacted amino groups, followed by exhaustive washings with CH_2Cl_2, CH_3OH, and again CH_2Cl_2. Finally, the DMT protecting group was removed by treatment with 3% trichloroacetic acid (TCA) in CH_2Cl_2 giving support **1.** The DMT cation collected after this acidic treatment and quantified by UV measurements gave a functionalization of 0.051 meq/g, in agreement with the previous value.

2.4.3 Synthesis of 5'-*O*-DMT, 3'-*O*-acetyl-thymidine

5'-*O*-DMT-thymidine (94 mg, 0.17 mmol, Sigma-Aldrich) was reacted with 1 mL of a mixture of acetic anhydride/pyridine (1:1, v/v) at r.t. for 2 h. The resulting product was taken to dryness under reduced pressure, dissolved in CH_2Cl_2 and purified by water/CH_2Cl_2 extraction, finally giving pure 5'-*O*-DMT, 3'-*O*-acetyl-thymidine (87 mg, 0.15 mmol). The identity of the purified product was confirmed by ^1H NMR (C_6D_6, 400 MHz): δ 8.81 (br, 1H, NH thymine residue), 7.62-6.82 (complex signals, 13H, DMT aromatic protons), 7.51 (s, 1H, H6 thymine residue), 6.64 (t, 1H, H1'), 5.42 (s, 1H, H4'), 4.01 (s, 1H, H3'), 3.54 (s, 2H, H5'), 3.36 (s, 6H, 2 x OCH_3), 2.18 (d, 2H, H2'), 1.59 (s, 6H, thymine CH_3 and CH_3COO).

2.4.4 Functionalization of support 1 with 5'-*O*-DMT, 3'-*O*-acetylthymidine

Diethyl azodicarboxylate (DEAD, 118 µL, 0.75 mmol) was added to a mixture of support **1** (145 mg, 0.051 meq/g, 7.4 mmol), 5'-*O*-DMT, 3'-*O*-acetyl-thymidine (87 mg, 0.15 mmol) and triphenylphosphine (PPh_3, 122 mg, 0.47 mmol) in THF (1.5 mL) and left at r.t. overnight. After exhaustive washings with CH_2Cl_2, CH_3OH, CH_3CN and again with CH_2Cl_2, the resulting support **2** was dried under reduced pressure. Incorporation yield of 5'-*O*-DMT, 3'-*O*-acetylthymidine was 45% (0.023 meq/g), as determined by DMT tests performed on dried and weighed samples of support **2**. Reiteration of this reaction did not allow increasing the functionalization. A capping reaction with acetic anhydride in pyridine (1:1, v/v) was then performed at r.t. for 4 h to block unreacted hydroxyl groups on the support. After exhaustive washings with CH_2Cl_2, CH_3OH, and again CH_2Cl_2, the functionalization, as determined by DMT test performed on a dried and weighed sample of the support, proved to be 0.023 meq/g, in agreement with the previous value.

2.4.5 Assembly and deprotection of hairpin duplex- and G4-forming oligonucleotides on support 2

The automated solid phase oligonucleotide synthesis was performed on an Applied Biosystem 3400 DNA/RNA synthesizer, using the following reagents: amidite diluent (anhydrous CH_3CN); deblocking mix (TCA/CH_2Cl_2); activator (ETT/CH_3CN); cap mix A (Ac_2O/THF); cap mix B (MI/Py/THF); oxidizing solution (I_2/H_2O/Py/THF). The oligonucleotides of sequence d(CGCGAATTCGCGTTTCGCGAATTCGCG) (ds27), d[$(TTAGGG)_4$TT] (tel26) and d(AGGGAGGGCGCTGGGAGGAGGG) (ckit1) were assembled on support **2**, using a 1 µmol-scale protocol ("DMT ON"). The coupling efficiency was monitored by spectrophotometric measurements of the DMT cation, removed before each coupling step by acidic treatment with 2% TCA in CH_2Cl_2. Considering the number of couplings and the average yield per cycle of 99.2%, 99.4% and 99.9% respectively for ds27, tel26 and ckit1, the overall yield was determined to be 80%, 86% and 98% respectively, corresponding to a final functionalization of 0.018, 0.020 and 0.022 meq/g. At the end of each synthesis, small samples of each solid support were treated with either 30% ammonium hydroxide (NH_4OH) at r.t. for 24 h or 30% ammonium hydroxide/40% methylamine 1:1, v/v (AMA) at r.t. for 2 h. The resulting supports were then washed several times with water until neutralization. DMT tests, performed on dried and weighed support samples, allowed determining the final functionalizations for the support-bound ds27, tel26 and ckit1 oligonucleotides, which were, respectively, 0.005, 0.006 and 0.007 meq/g, after the NH_4OH deprotection treatment, and 0.011, 0.012 and 0.013 meq/g, after the AMA deprotection treatment. Eluates of both deprotection treatments were analyzed by HPLC on a Phenomenex analytical C18 column (250 x 4 mm) using the gradient: 3-40% solution B in A over 15 min (solution A: 0.1 M triethylammonium acetate, pH = 7.0; solution B: CH_3CN; flow rate: 1 mL/min).

CHAPTER 3 – G4-CPG ASSAY: AN AFFINITY CHROMATOGRAPHY-BASED METHOD FOR THE SCREENING OF CONFORMATION SELECTIVE G-QUADRUPLEX LIGANDS

3.1 General procedure for the binding assays on the novel functionalized CPG supports

The general procedure adopted for the binding assays is as follows: a weighed amount of the oligonucleotide-bound CPG supports, synthesized as described above, is left in contact with a ligand solution of known concentration in a polypropylene column equipped with a polytetrafluoroethylene frit, a stopcock and a cap (Figure 39).

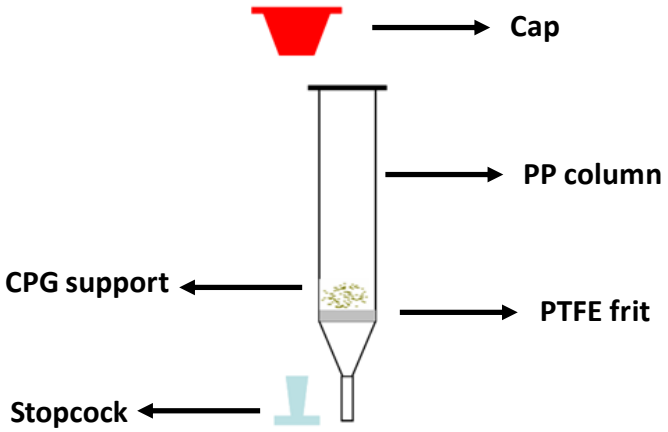

Figure 39. Assay equipment. PP = polypropylene; PTFE = polytetrafluoroethylene.

After incubation on a vibrating shaker, the support is eluted with defined volumes of a washing solution and all the eluted fractions are separately analyzed by UV measurements (Figure 40). From UV measurements of the fractions eluted from the nude CPG −obtained upon detritylation of support **2** (Figure 41A) −the amount of ligand unspecifically adsorbed on the support is evaluated. In turn, UV analysis of the fractions recovered from G4- and hairpin duplex-functionalized supports (Figures 41B, 41C and 41D) allows estimating the amount of ligand bound to the support carrying the secondary structure-forming oligonucleotides (tel26, ckit1 and ds27). In all cases, the amount of bound ligand is calculated by subtracting the ligand eluted upon washing, derived by direct UV measurements, from the ligand amount initially loaded on the support. Moreover, as further control, the direct measurement of the bound ligand is obtained by treating the support with a releasing solution, followed by UV analysis of the eluted fractions (Figure 40). In order to allow the correct G4s and hairpin duplex refolding after this treatment, and thus reuse the same functionalized CPG batch for subsequent binding assays, the

support is resuspended in the washing solution and then subjected to an annealing procedure, by taking it at 75 °C for 5 minutes, followed by slow cooling to room temperature (Figure 40).

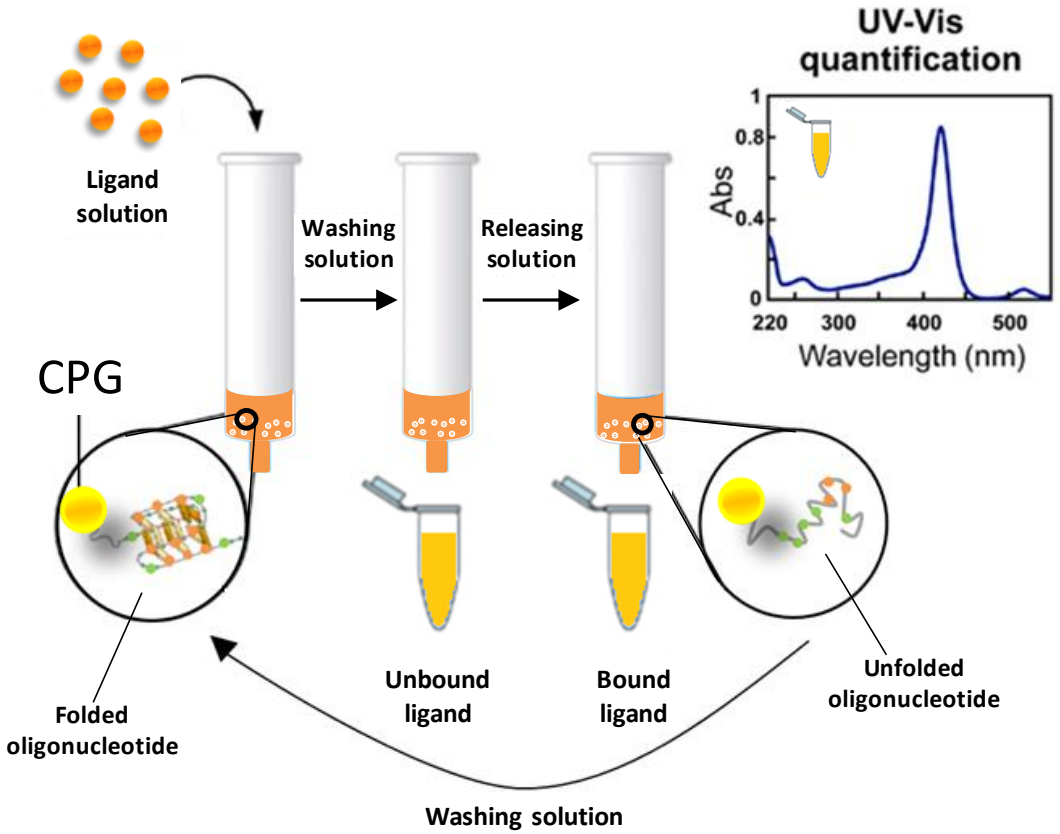

Figure 40. General scheme depicting the overall procedure used in the here described binding assays.[162] CPG = Controlled Pore Glass.

3.2 Monitoring of possible unspecific binding on the nude CPG support

Aiming at checking the absence of possible interferences of our modified CPG support in the successive binding assays, nude CPG was left in contact with known concentration solutions of different molecules, having either good or no affinity for G4 structures. In detail, cationic porphyrin 5,10,15,20-tetrakis(1-methyl-4-pyridinio)porphyrin (TMPyP4),[127] thiazole orange (TO),[174] resveratrol,[175] two acridine derivatives, *i.e.* 3,11-difluoro-6,8,13-trimethyl-8H-quino[4,3,2-kl]acridinium methosulfate (RHPS4)[176] and acridine-9-carboxylic acid (9-Acr-COOH),[177] along with two pyrrole-containing polyamide analogs, *i.e.* netropsin[152] and distamycin,[150] have been used as model ligands in our binding assays (Figure 42). Furthermore, also a diverse set of compounds chosen from a library of virtual screening-selected molecules – previously analyzed on our G4-OAS support and proved to be strongly,

unspecifically retained by the polystyrenic OAS[160] – has been tested on the novel functionalized CPG support (Figure 43).

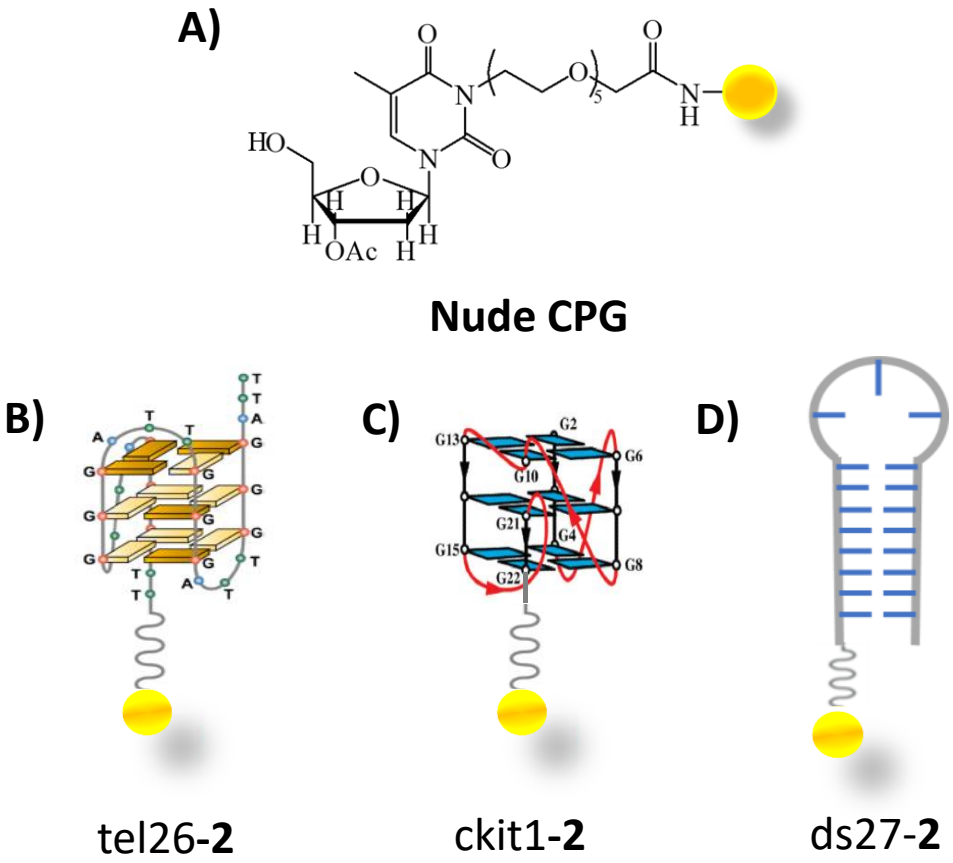

Figure 41. A) Chemical structure of LCAA-CPG functionalized with 3'-*O*-acetyl-thymidine through a hexaethylene glycol spacer, here named nude CPG. B), C) and D) Schematic representations of tel26-, ckit1- and ds27-bound support **2**.

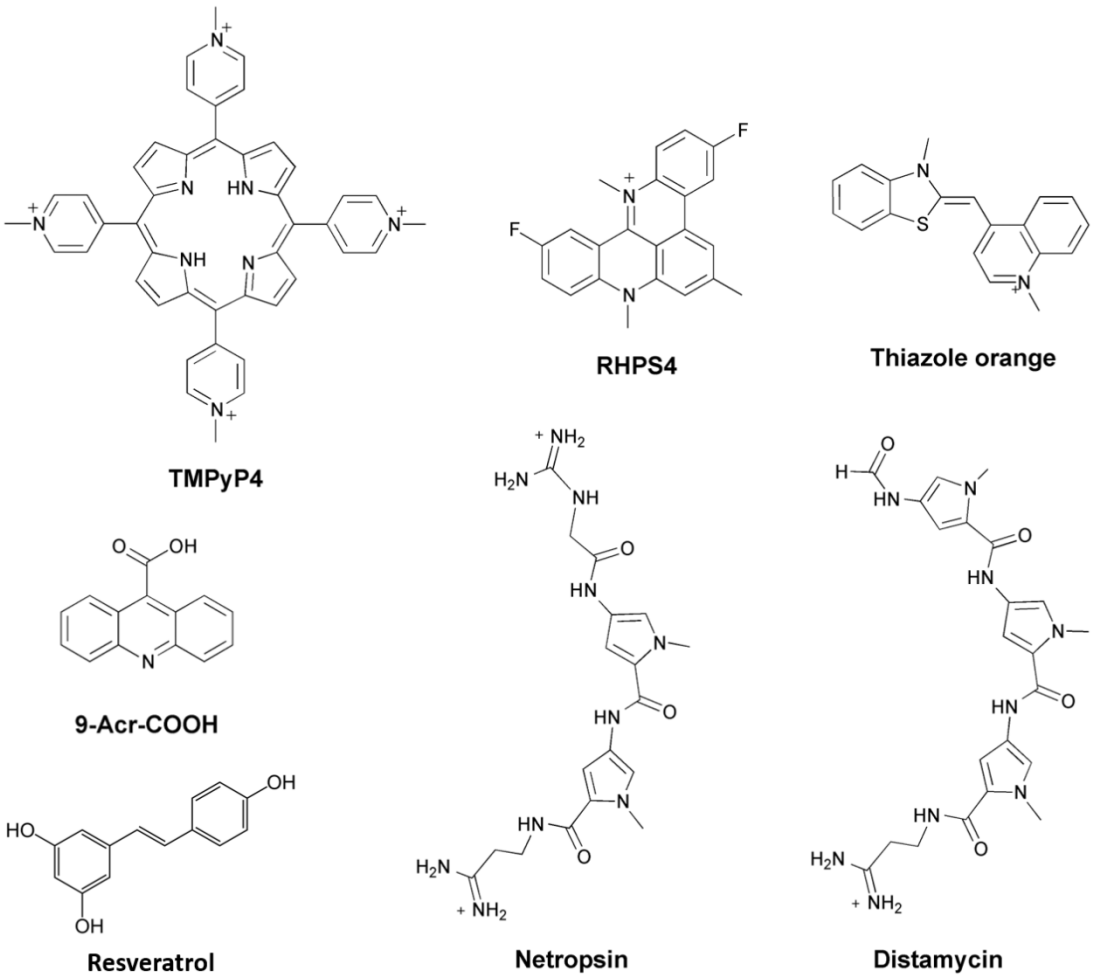

Figure 42. Chemical structure of the molecules here used as models in our binding assays having either good or no affinity for G4 structures.

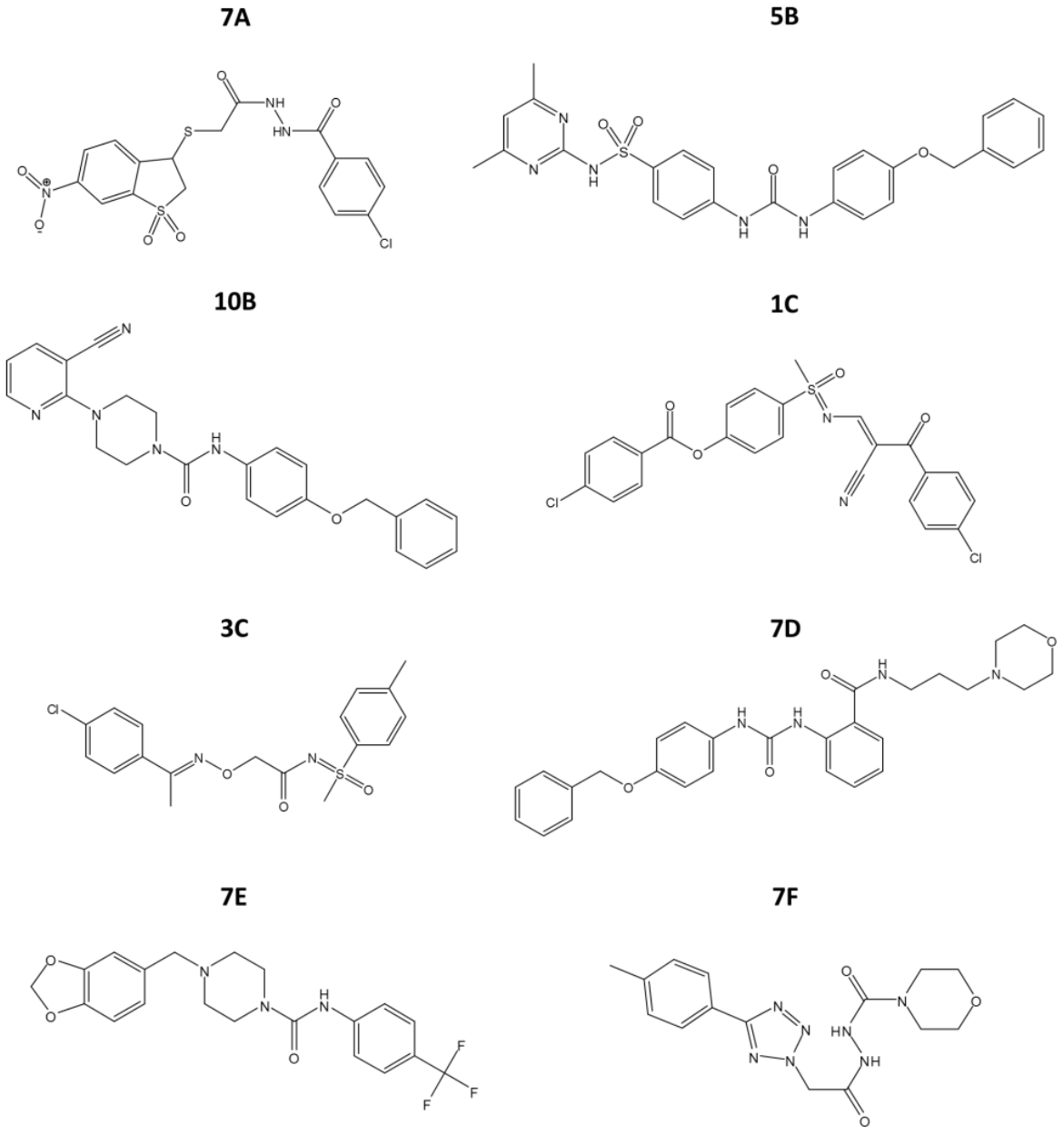

Figure 43. Chemical structure of compounds 7A, 5B, 10B, 1C, 3C, 7D, 7E and 7F, selected from a library of putative ligands previously screened employing the G4-OAS assay.[160]

Using the above protocol, after incubation on a vibrating shaker, the surnatant was allowed flowing through the support and the nude CPG (Figure 41A) was washed with several volumes of the washing solution, *i.e.* 50 mM KCl, 10% DMSO, 10% CH_3CH_2OH in H_2O. The composition of the washing solution was optimized so to achieve the best results in terms of solubility of the tested ligands, minimization of undesired absorption of the ligands on the assay equipment, and capacity of the oligonucleotide sequences to form stable secondary

structures.[162] In detail, K^+ ions are essential for a correct folding and stabilization of the G4 structures bound to the supports, the small percentage of DMSO is made necessary to allow a full solubilization of the tested molecules, and, finally, the small percentage of ethanol to avoid undesired absorption of the tested ligands on the assay equipment, *i.e.* the polypropylene column and the PTFE frit. However, the total percentage of organic solvent was kept within 20% to guarantee the solubility of tested ligands without perturbing the correct folding of the support-bound oligonucleotides.

The results of the binding assays on the ligands tested on the nude CPG are shown in Table 1. These data were compared with those obtained on the nude OAS (detritylated OAS resin, Figure 36A).

Table 1. Summary of the binding assay data obtained for nude CPG and OAS through UV measurements.

Ligand	Recovered ligand from nude CPG (%)[a,b]	Recovered ligand from nude OAS (%)[a,b]
Distamycin	96	93
Netropsin	95	100
Resveratrol	98	74
RHPS4	93	93
TO	92	90
TMPyP4	85	97
9-Acr-COOH	100	95
7A	99	35
5B	97	9
10B	100	79
1C	96	29
3C	100	34
7D	100	27
7E	96	92
7F	100	92

[a]Recovered ligands were obtained using the washing solution: 50 mM KCl, 10% DMSO, 10% CH_3CH_2OH

[b]The amounts of recovered ligands are expressed as percentage of the quantity initially loaded on the support; the errors associated with the reported percentages are within ± 2%

Remarkably, the ligands were generally recovered in higher amounts from nude CPG, requiring smaller volumes of the washing solution for their quantitative recovery compared to nude OAS (Δ_{volume} ~ 3 mL).[162] Noteworthy, a significant reduction of unspecific binding to the solid support was observed for all the compounds taken from the library of 60 virtual screening-selected molecules previously investigated on G4-OAS. Among others, a significant example is compound 5B: contrarily to what observed on nude OAS resin, for which compound 5B had shown high affinity (nude OAS bound ligand = 91%), in the experiments with nude CPG complete absence of binding was found (nude CPG bound ligand = 3%).
Overall, these results proved that the novel support has low-to-null unspecific interactions with the tested model ligands, in contrast to previously used OAS.

3.3 Optimization and validation of the CPG-based method to identify G4-selective ligands

Before performing the binding assays on G4- and hairpin duplex-functionalized supports, we first verified that the model oligonucleotides chosen for the experiments on the CPG supports maintain their preferred conformations in the solution adopted for the binding experiments (50 mM KCl, 10% DMSO, 10% CH_3CH_2OH). Thus, we analyzed in solution the three selected oligonucleotide sequences, *i.e.* tel26, ckit1 and ds27, by UV and CD spectroscopy.
Particularly, Thermal Difference Spectra analysis confirmed that tel26 and ckit1, showing the typical minimum for G-quadruplexes at 295 nm, form G4 structures, while ds27 a duplex structure (Figure 44, left).[178,179] Furthermore, CD spectra showed that tel26 folds into a hybrid-type G4,[21,83] ckit1 forms a parallel G4,[110] and ds27 adopts a B-DNA conformation,[180] also in the here used experimental solution (Figure 44, right). These experiments proved that the addition of small amounts of organic solvents in our binding assays (10% DMSO, 10% CH_3CH_2OH), necessary to ensure optimal ligand solubility, does not affect the overall conformational behaviour of the studied oligonucleotides.
Moreover, in order to verify if the TTT loop in ds27 somehow perturbs the duplex conformation adopted by the Dickerson dodecamer d(CGCGAATTCGCGC), circular dichroism spectra in the here used conditions were recorded also on a sample of this solution. The unimolecular hairpin duplex ds27 showed the same CD features as the bimolecular Dickerson dodecamer, however with an enhanced structuration (Figure 45), proving to be a good B-DNA duplex model.
CD-melting experiments were then performed for all the investigated oligonucleotides (Figure 46). Melting temperatures of 60 °C and 72 °C were found for tel26 G4 and ckit1 G4, respectively, consistently with literature data.

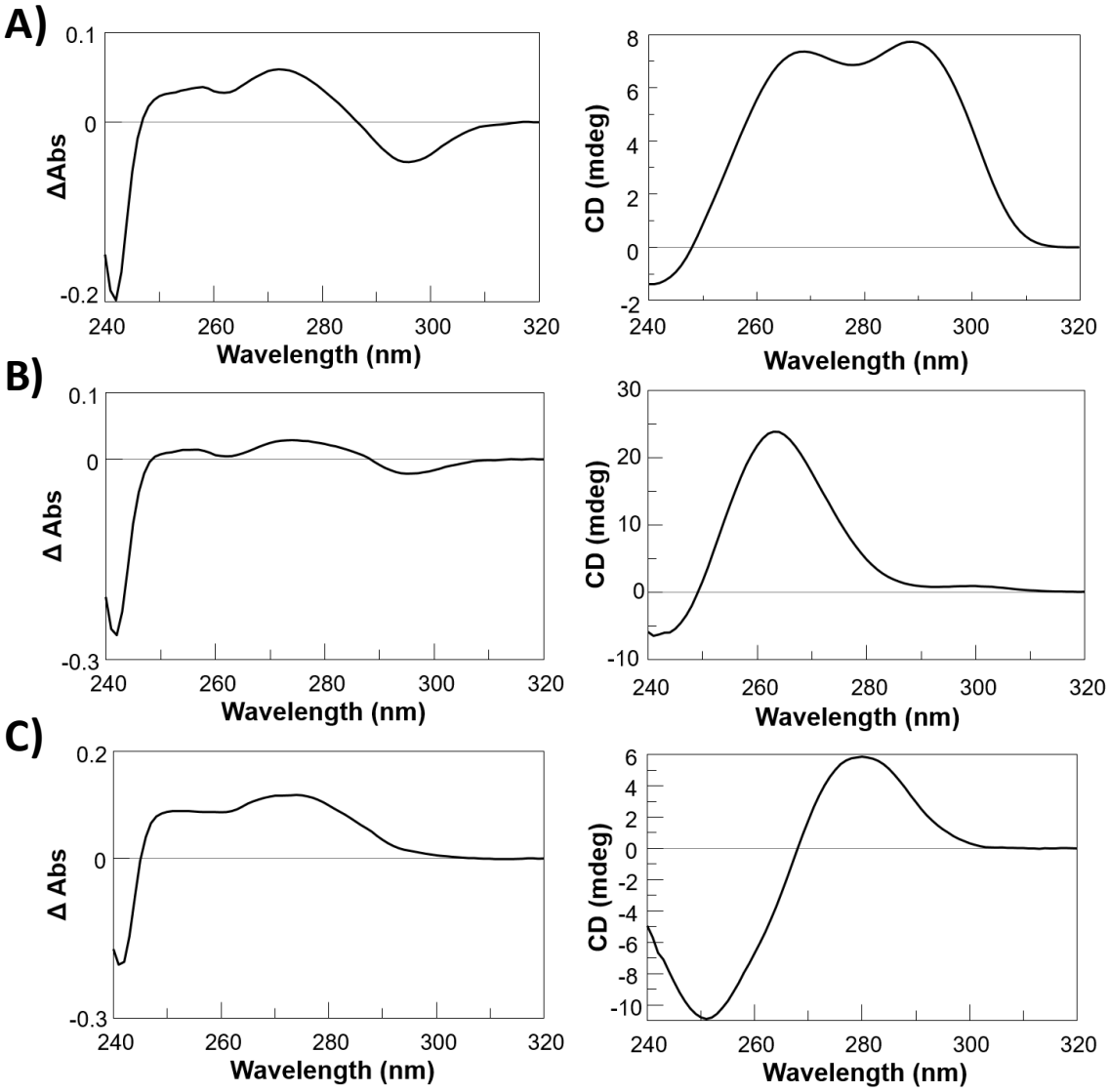

Figure 44. Thermal Difference Spectra (left) for A) tel26, B) ckit1 and C) ds27 sequences dissolved at 2 µM concentration in 50 mM KCl, 10% DMSO, 10% CH_3CH_2OH aq. solutions, and related CD spectra (right).

Remarkably, the hairpin duplex gave a T_m of 73 °C, proving to be more stable than the bimolecular duplex, showing a T_m of 55 °C under the same conditions, with a ΔT_m of 18 °C. These results validate the chosen oligonucleotide sequences as stable G4 and duplex models in solution. All the here collected data showed that the studied oligonucleotides, after annealing, fold into, respectively, stable G-quadruplexes and hairpin-duplex also under the solution conditions used for our binding assays and this – taking into account the presence of a long and flexible hexaethylene glycol spacer keeping apart the biomolecule from the solid support – could be reasonably valid also for the oligonucleotides attached to the CPG .

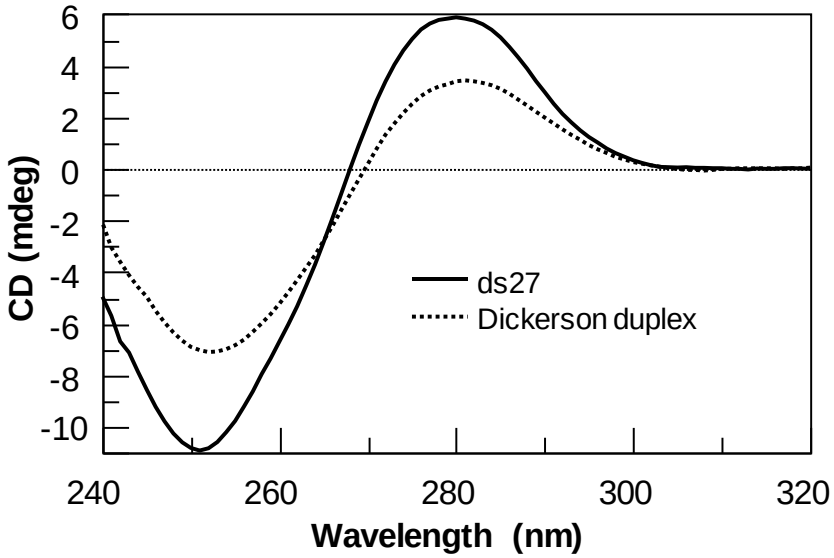

Figure 45. Circular dichroism spectra for 2 μM solutions of unimolecular hairpin duplex ds27 (solid line) and bimolecular duplex formed by Dickerson dodecamer (dotted line) in 50 mM KCl, 10% DMSO, 10% CH_3CH_2OH aq. solutions.

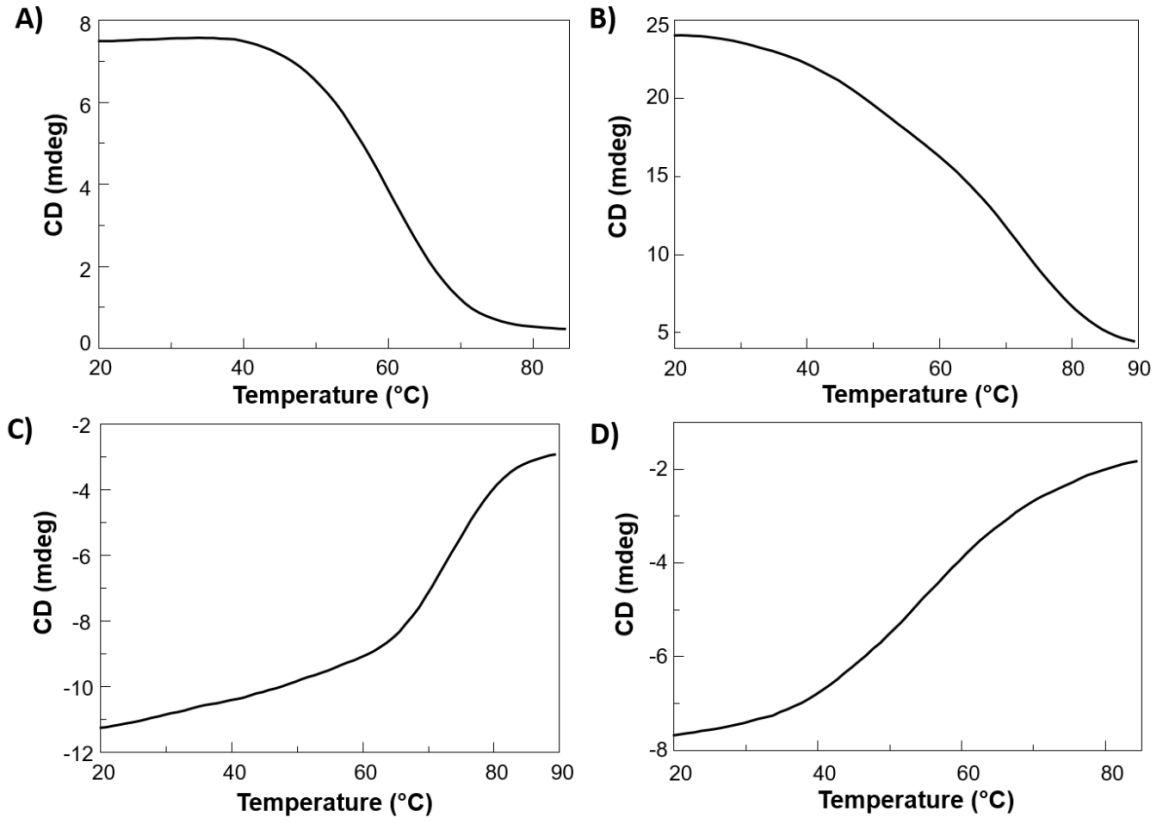

Figure 46. CD melting curves for 2 μM solutions of: A) tel26, B) ckit1, C) ds27 and D) Dickerson duplex in 50 mM KCl, 10% DMSO, 10% CH_3CH_2OH aq. solutions. CD melting curves were recorded at 290 nm (A), 263 nm (B), and 251 nm (C and D).

After these preliminary experiments in solution, the set of compounds here used as models of good or poor G4-binding ligands (TMPyP4, RHPS4, TO, netropsin, distamycin, resveratrol and 9-Acr-COOH) were tested on G4- and hairpin duplex-functionalized supports **2** (Figure 41B, 41C and 41D) and the results compared with those obtained on the OAS support. Before performing the binding assays, oligonucleotide-functionalized supports were subjected to an annealing procedure in the washing solution by taking them at 75 °C for 5 minutes, followed by slow cooling to room temperature (Figure 40). Higher temperatures typically used for annealing procedures in solution, *i.e.* 85-95 °C, were avoided to prevent the detachment of even tiny oligonucleotide amounts from the supports. After 16 h at 4 °C, the supernatants on the supports, collected along with several washings, were checked by UV analysis. The quantification of the detached oligonucleotide amounts was obtained by measuring at 85 °C the absorbance at λ = 260 nm, using the molar extinction coefficients calculated for the unstacked oligonucleotide.[181] From these analyses, we estimated that up to a maximum of 0.1-0.5% of oligonucleotide material was detached from the CPG after each annealing procedure. These results show that this support is particularly more advantageous than polystyrene-based resins for which, after each annealing, detachment of 0.5-1.0% of nucleotide material was always observed. Indeed, less oligonucleotide is detached upon thermal treatments, more binding assays can be performed on the same batch of support.[162]

G4- and hairpin duplex-functionalized supports **2** were then treated, analogously to the control nude CPG, with solutions of the ligands dissolved at known concentration in the washing solution. After incubation, the supports were treated with the washing solution several times and the eluted fractions were collected and analyzed by UV measurements. To allow the complete release in solution of the oligonucleotide-bound ligands, the supports were then eluted with the releasing solution (Figure 40). The amounts of bound ligands directly measured after treatment with the releasing solution were in good agreement with those previously determined as a difference with respect to the unbound amounts recovered by the washing solution. The composition of the releasing solution, *i.e.* 2.5 M $CaCl_2$, 15% DMSO in H_2O, was optimized on the basis of its ability to obtain a fast and quantitative recovery of the bound ligand, as a consequence of the oligonucleotide denaturation induced by high concentration of divalent cations and/or organic solvents.[162] For ligands not fully soluble in the Ca^{2+}-containing solution, pure DMSO was used as alternative, and even stronger, releasing solution.

The amounts of bound ligand measured on the tel26-**2** support were in general agreement with those determined for the tel26-OAS support (Table 2). Moreover, the percentages of bound ligand on the tel26-OAS support were in some cases overestimated, *e.g.* for resveratrol,

accounting for the unspecific interactions of the tested ligands with the nude OAS resin. Thus, the experimental data acquired on tel26-**2** support proved to be much cleaner and more reliable than those obtained on tel26-OAS. Remarkably, as additional evidence that the novel synthesized support has less unspecific interactions with the model ligands than previously used polystyrenic tel26-OAS, we found that the ligands tested on the tel26-**2** and ds27-**2** supports could be recovered in higher amounts (Tables 2 and 3) requiring smaller volumes of releasing solution than in the case of tel26-OAS (Δ_{volume} ~ 3 mL).[162]

Moreover, the retention order observed for both tel26-**2** and ds27-**2** supports (Tables 2 and 3) well reflects the affinity trend of the ligands tested in solution for the human telomeric G4 and the Dickerson duplex,[150,152,174–177,182,183] confirming the general reliability of the support **2**-based method.

Adopting the same protocol used for tel26-**2** and ds27-**2**, ckit1-functionalized support (ckit1-**2**) was also tested in its ability to bind known ligands with different affinity for G4s. In particular, thiazole orange and resveratrol were selected as representative molecules of a strong and a very weak G4 binder,[174,175] respectively. The obtained data, showing high affinity (bound ligand = 97±2%) for TO and low-to-null affinity (bound ligand = 4±2%) for resveratrol, verified the efficacy also of ckit1-**2**.

In order to allow the correct G4s and hairpin duplex refolding after the denaturation induced by the releasing solution, and thus reuse the same batch of support for subsequent binding assays, the supports were resuspended in the washing solution and then left annealing. The reversibility of the process of folding/unfolding of the G4s and hairpin duplex allows effectively recycling the same support for multiple, sequential experiments; indeed, a large number of binding assays could be performed on the same batch of support without losing in efficiency and reliability of the analyses. In detail, for its lower unspecific binding and higher thermal stability, typically the same batch of functionalized CPG could be used to perform more than 50 experiments, *i.e. ca.* three times the number of binding assays generally carried out on the tel26-OAS resin.[162]

Table 2. Summary of the binding assay data obtained for tel26-**2** and tel26-OAS through UV measurements.

	Support **2**		OAS	
Ligand	**tel26-bound ligand (%)[a,c]**	**Recovered ligand from tel26-2 (%)[b,c]**	**tel26-bound ligand (%)[a,c]**	**Recovered ligand from tel26-OAS (%)[b,c]**
TMPyP4	100	98	99	90
RHPS4	99	100	96	93
TO	97	92	98	88
Netropsin	86	67	93	91
Distamycin	22	96	28	89
Resveratrol	4	96	22	96
9-Acr-COOH	0	-	1	-

[a]tel26-bound ligand (%) is calculated as a difference from the unbound ligand, recovered with the washing solution 50 mM KCl, 10% DMSO, 10% CH_3CH_2OH.

[b]Data on % of ligand recovered from tel26-**2** and ligand recovered from tel26-OAS are obtained using as releasing solution either 2.5 M $CaCl_2$, 15% DMSO or 100% DMSO.

[c]The amounts of bound/recovered ligands are expressed as percentage of the quantity initially loaded on the support; the errors associated to the percentages are within ± 2%.

Table 3. Summary of the binding assay data obtained for ds27-**2** through UV measurements.

	Support **2**	
Ligand	**ds27-bound ligand (%)[a,c]**	**Recovered ligand from ds27-2 (%)[b,c]**
Netropsin	52	98
TO	51	96
TMPyP4	50	99
RHPS4	48	100
Distamycin	36	93
Resveratrol	1	99
9-Acr-COOH	0	100

[a]The amount of ds27-bound ligand (%) was calculated as a difference from the unbound ligand recovered with the washing solution 50 mM KCl, 10% DMSO, 10% CH_3CH_2OH.

[b]The ligand recovered from ds27-**2** (%) was obtained using as releasing solution either 2.5 M $CaCl_2$, 15% DMSO or 100% DMSO.

[c]The amounts of bound/recovered ligands are expressed as percentage of the quantity initially loaded on the support; the errors associated to the reported percentages are within ± 2%.

3.4 Characterization of the conformations adopted by the oligonucleotide models linked to the CPG support

Main prerequisite for an affinity chromatography-based screening to be effective is that the oligonucleotide linked to the support must maintain its native conformation, as in solution. To gain a deeper insight into the effective conformations adopted by the G4s on the glass beads, we exploited a fluorescent and water-soluble core-extended naphthalene diimide (c_{ex}-NDI, Figure 47).[184]

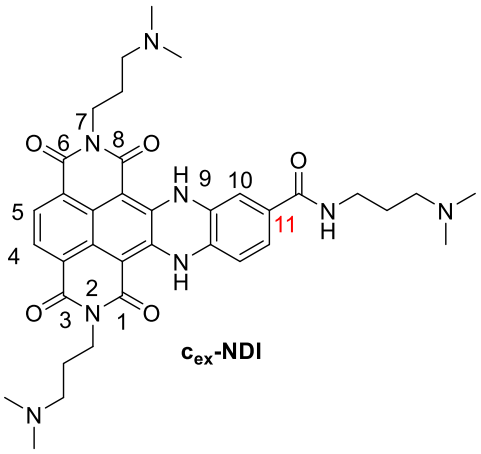

Figure 47. Chemical structure of the core-extended naphthalene diimide (c_{ex}-NDI), here used as fluorescent probe.

This red fluorescent c_{ex}-NDI, carrying a [3-(dimethylamino) propyl]carboxamide moiety at C-11, has been recently designed to give different fluorescence responses upon binding to different secondary structure-forming oligonucleotides.[184] In fact, under physiological conditions it tends to aggregate and, as a result, its intrinsic fluorescence is essentially quenched. Upon interaction with DNA in solution, it disaggregates, producing a dramatic fluorescence enhancement when it binds to hybrid or antiparallel G4s; contrarily, a much weaker emission is observed when it binds to parallel G4s or duplex DNA (Figure 48).[184]
This peculiar behaviour is explained considering the different binding modes of c_{ex}-NDI to different DNA structures: in the former cases, it interacts with the G4s grooves, while for the latter ones an end-stacking (for the parallel G4s) or intercalating (for the duplex) interaction mode occurs.[184] Thus, tel26-, ckit1- and ds27-functionalized supports were left in contact with c_{ex}-NDI, which in all cases bound each support-linked oligonucleotide by 98% (±2%) of the total loaded amount. After incubation with the c_{ex}-NDI, followed by exhaustive washings, the three supports were analyzed by confocal microscopy.

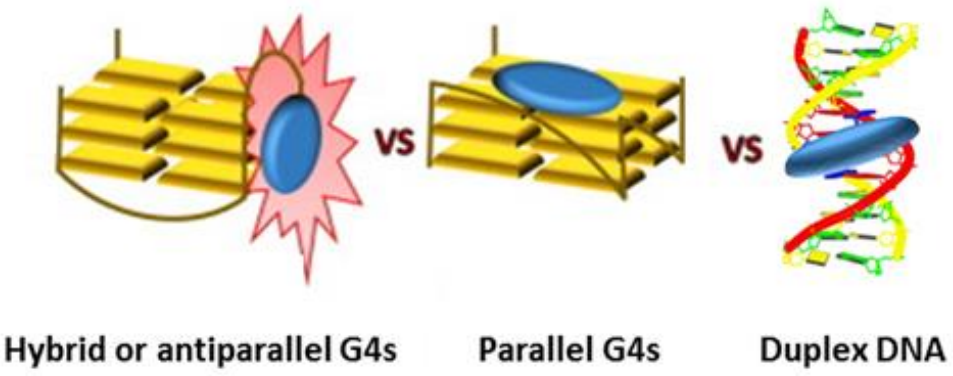

Figure 48. Fluorescent behaviour of c_{ex}-NDI in solution. When bound to hybrid or antiparallel G4s, c_{ex}-NDI produces a dramatic fluorescence enhancement, while a weaker emission is observed when it binds to parallel G4s or duplex DNA. (Adapted from Zuffo *et al.*[184])

Using transmitted light detection, the supports appeared as irregular beads with a mean size of 110 µm (Figure 49, middle), as expected.[164] On the other hand, by confocal fluorescence visualization (Figure 49, left), different fluorescence intensities were observed for the three functionalized glass beads, even if c_{ex}-NDI is able to bind all of them with comparable affinity. In particular, a high fluorescence emission was observed for tel26-functionalized CPG, a medium fluorescence for ckit1-functionalized CPG and a low fluorescence for the ds27-functionalized support. In an effort to implement these analyses, we performed a semi-quantitative determination of the fluorescence emission for all the investigated systems in a comparative manner. For each support, different images were acquired in several fields of view with a 63x magnification (Figures 50-53). Firstly, confocal fluorescence microscopy images were taken for proper controls. No intrinsic fluorescence was observed for the nude CPG or the G4- and hairpin duplex-functionalized CPGs in the absence of the c_{ex}-NDI, when excited at the maximum of absorption of the ligand (555 nm). Moreover, no fluorescence emission was found for the nude CPG or the functionalized CPGs in the presence of the c_{ex}-NDI by exciting outside the ligand absorption wavelengths range. In turn, negligible fluorescence was observed for the nude CPG upon incubation with c_{ex}-NDI (Figure 50), since only a small amount of this fluorescent probe (*ca.* 16% of the total loaded ligand) bound to the nude support. Then, for the three c_{ex}-NDI-linking supports, the average of the mean intensity values taken from different edge glass beads-containing regions of each image was calculated. The highest values of fluorescence intensity were found for the tel26-linking support, the lowest values for the ds27-linking support, while an intermediate value was observed for ckit1-linking support, confirming the qualitative visual analysis (Figure 54). As mentioned above, c_{ex}-NDI interacts with secondary structure-forming oligonucleotides in solution resulting in a high fluorescence

quantum yield with hybrid and antiparallel G4s, in a medium fluorescence quantum yield with parallel G4s and in a low fluorescence quantum yield with duplex DNA.[184] Taking this into account and considering that, in the absence of Na^+ ions, tel26 is not able to adopt antiparallel G4 conformations,[21] our semi-quantitative confocal microscopy analysis confirmed that tel26, ckit1 and ds27 sequences, linked to the CPG supports, were folded into a hybrid G4, a parallel G4 and a hairpin duplex, respectively, under the studied experimental conditions.

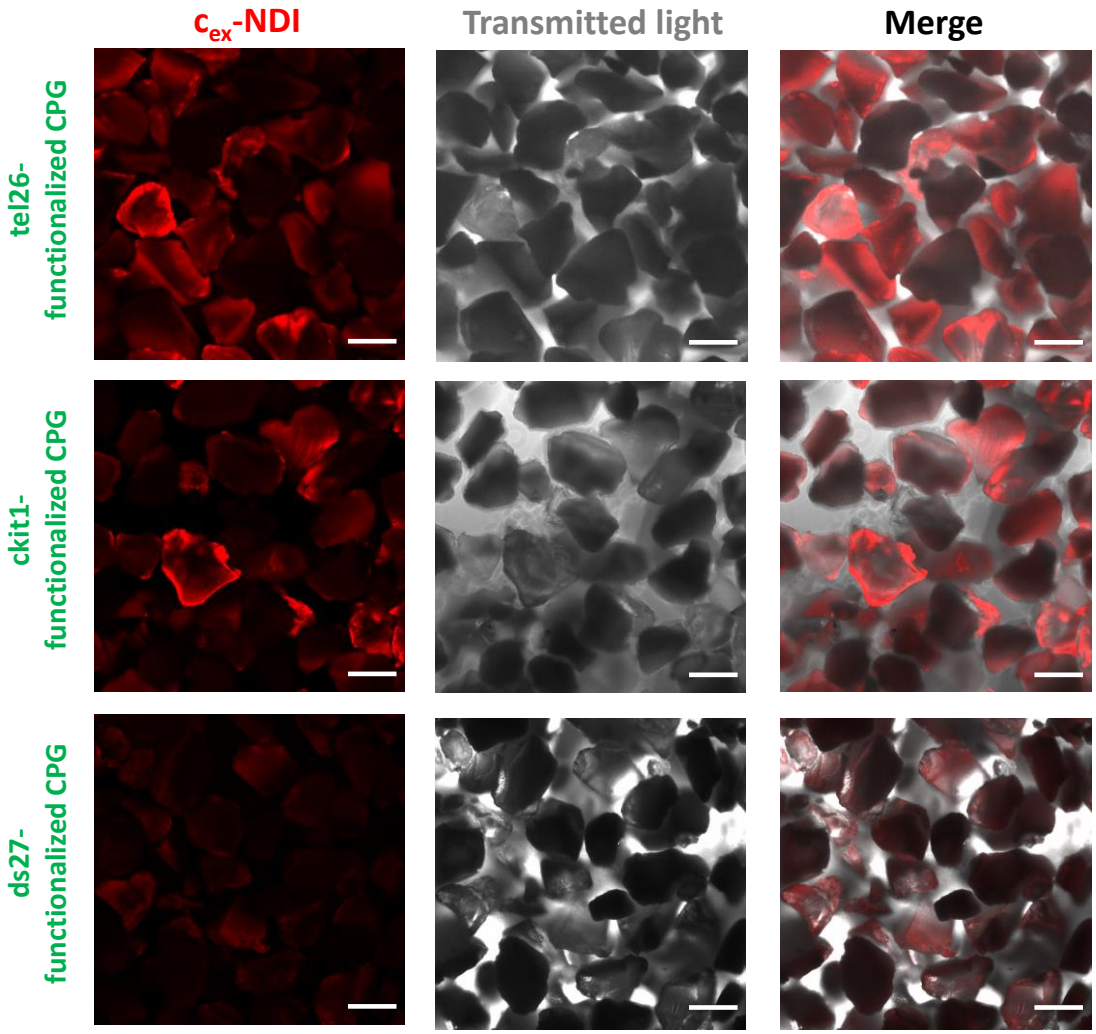

Figure 49. Representative confocal images of G4- and hairpin duplex-functionalized CPG supports after incubation with the c_{ex}-NDI. Images were obtained using a 10x objective, exciting at 555 nm and recording emission in the 578-800 nm range. Left: fluorescence images; middle: transmitted light images; right: merged images. Scale bars correspond to 100 μm.

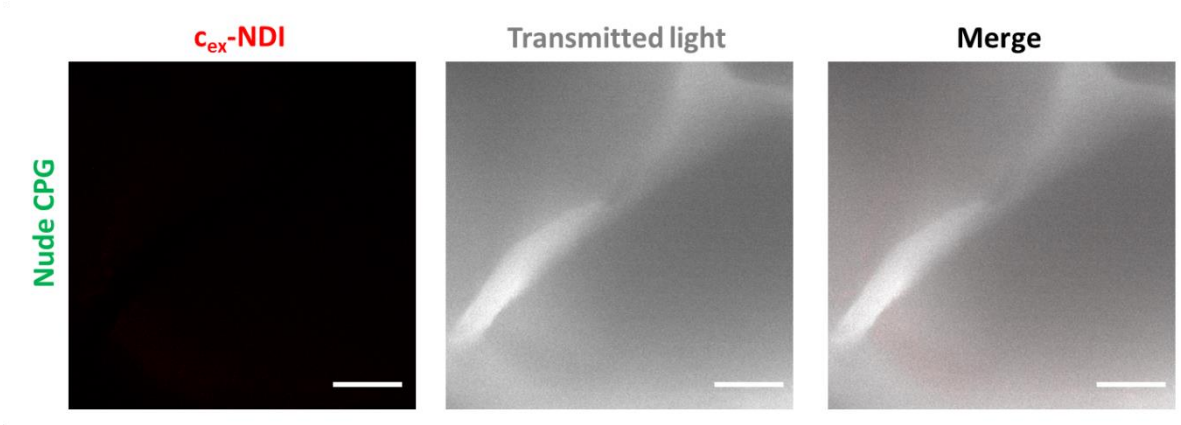

Figure 50. Representative confocal images using a 63x oil immersion objective, exciting at 555 nm and recording emission in the 578-800 nm range of the nude CPG after incubation with c_{ex}-NDI. Left: fluorescence image, middle: transmitted light image, right: merged image. Parameters settings through acquisition were kept identical to those used for tel26-, ckit1- and ds27-functionalized CPG. Scale bars correspond to 20 µm.

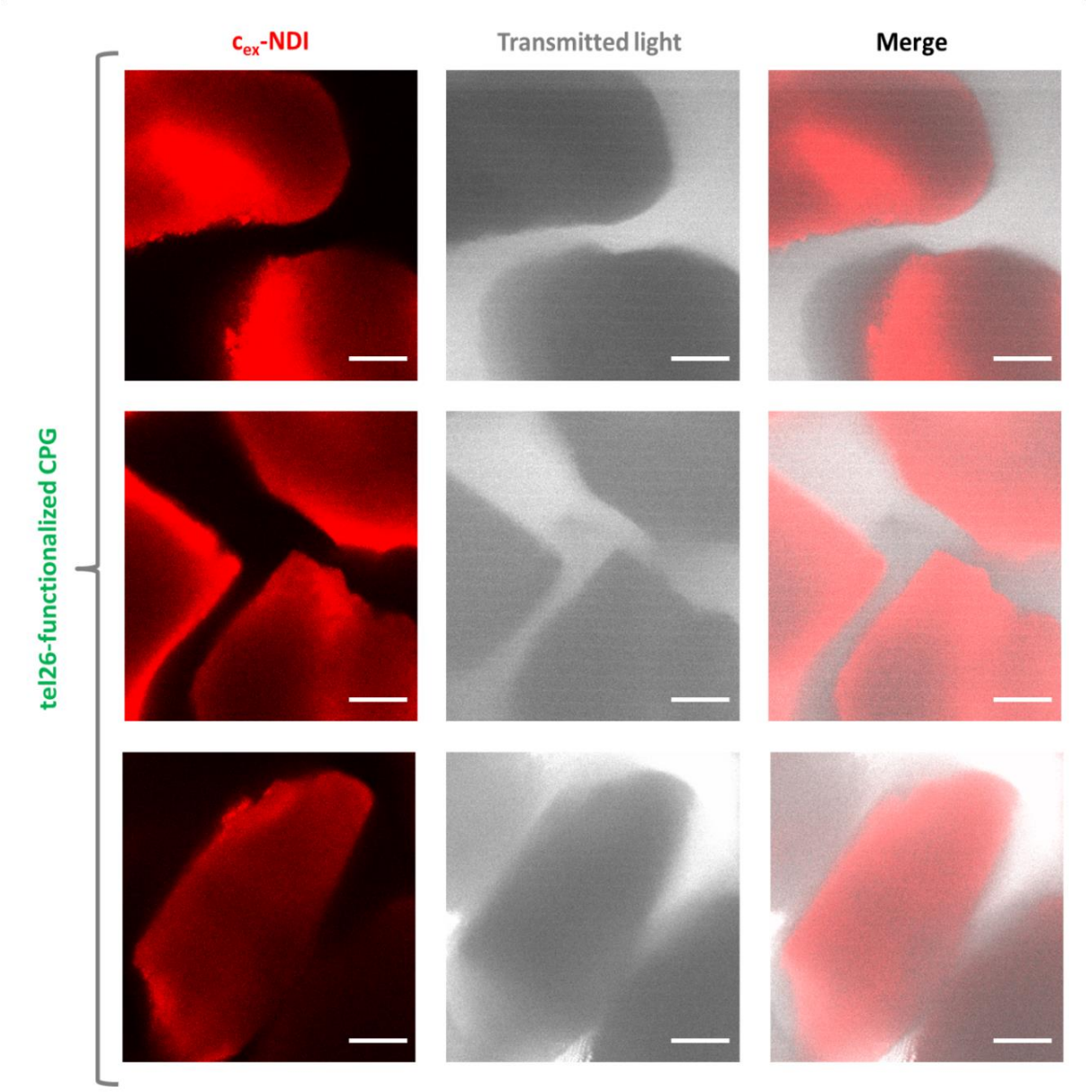

Figure 51. Representative confocal images using a 63x oil immersion objective, exciting at 555 nm and recording emission in the 578-800 nm range of the tel26-functionalized CPG after incubation with c_{ex}-NDI. Left: fluorescence images, middle: transmitted light images, right: merged images. Parameters settings through acquisition were kept identical to those used for nude CPG, ckit1- and ds27-functionalized CPG. Scale bars correspond to 20 µm.

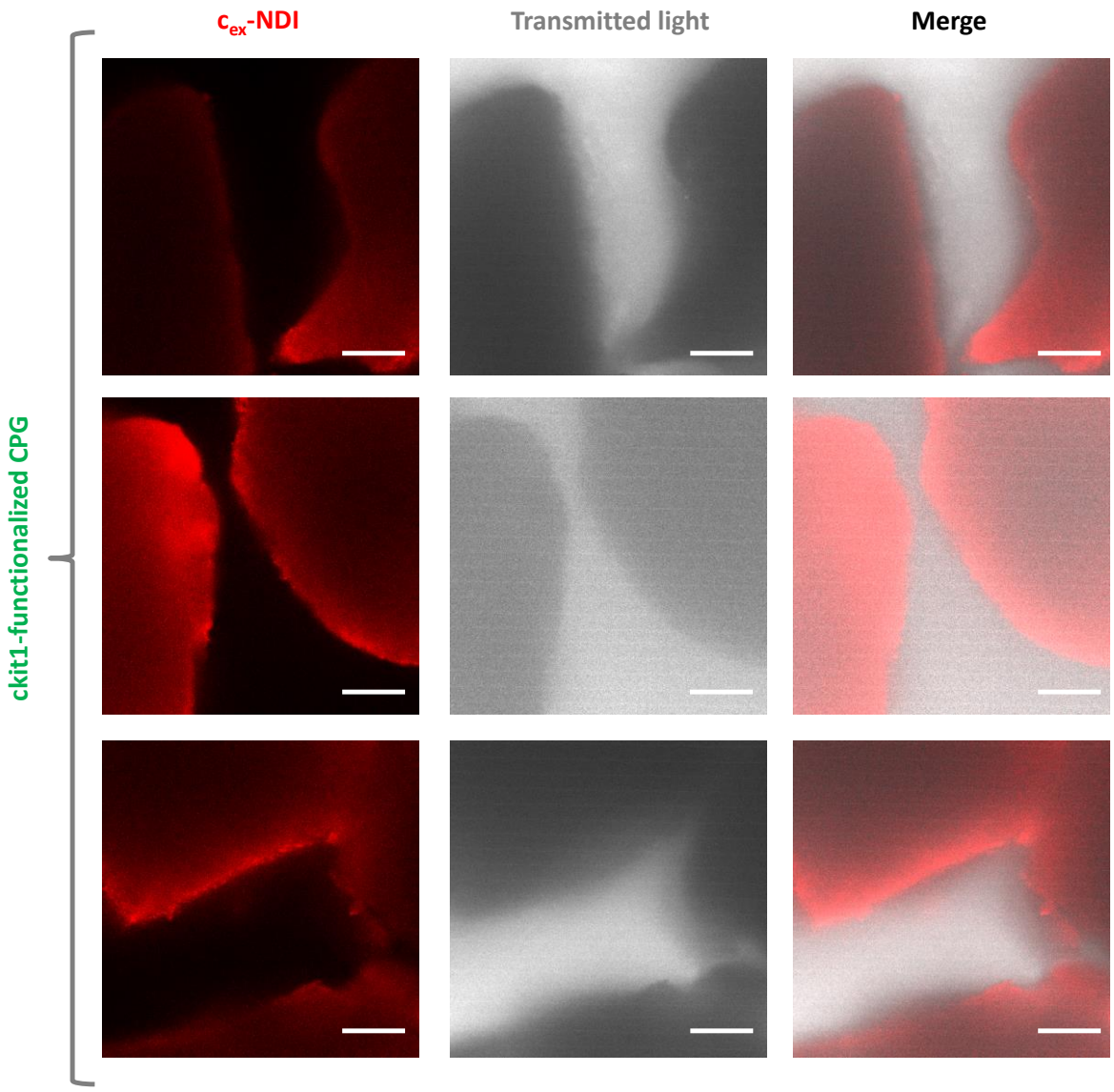

Figure 52. Representative confocal images using a 63x oil immersion objective, exciting at 555 nm and recording emission in the 578-800 nm range of the ckit1-functionalized CPG after incubation with c_{ex}-NDI. Left: fluorescence images, middle: transmitted light images, right: merged images. Parameters settings through acquisition were kept identical to those used for nude CPG, tel26- and ds27-functionalized CPG. Scale bars correspond to 20 µm.

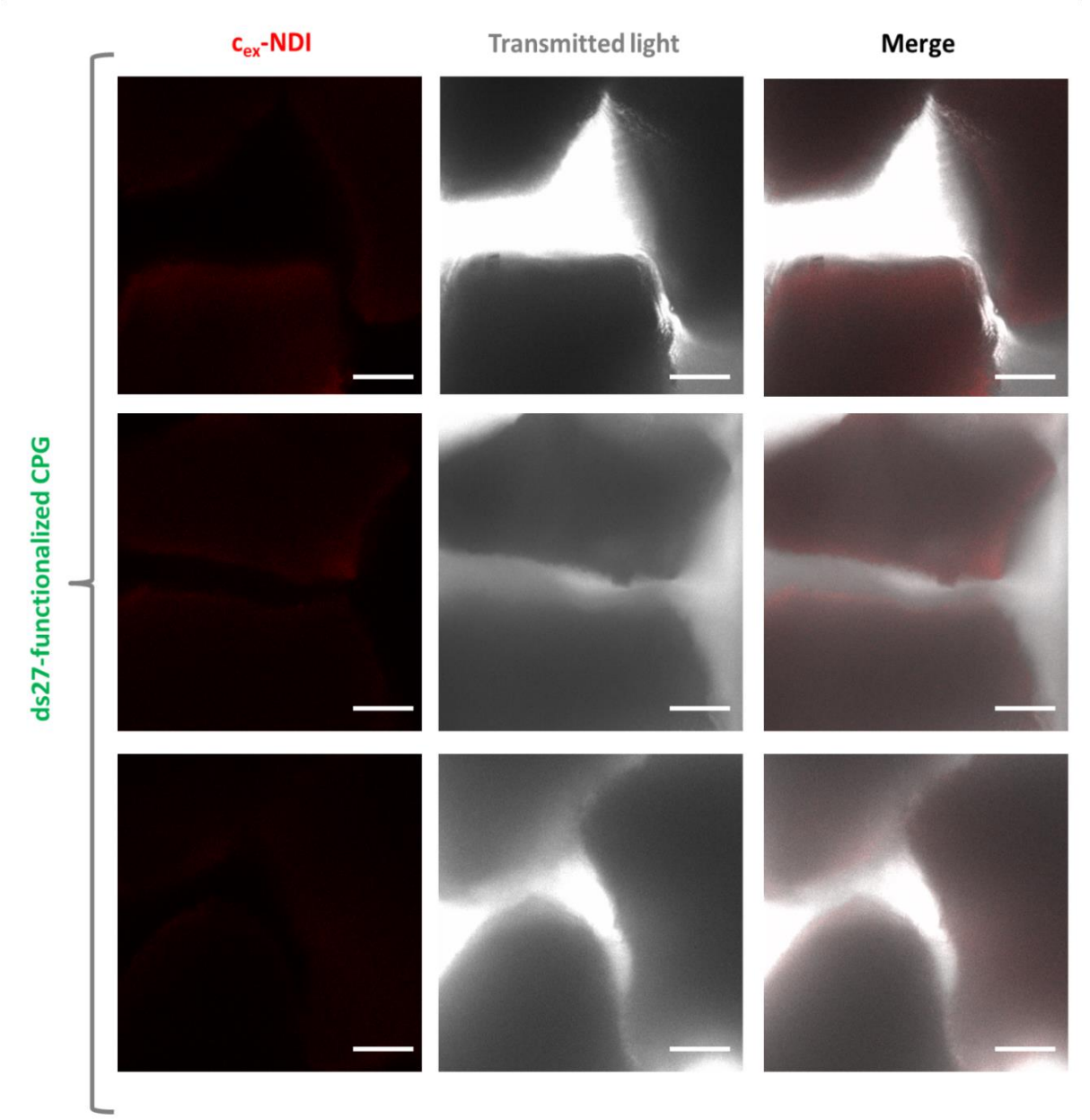

Figure 53. Representative confocal images using a 63x oil immersion objective, exciting at 555 nm and recording emission in the 578-800 nm range of the ds27-functionalized CPG after incubation with c_{ex}-NDI. Left: fluorescence images, middle: transmitted light images, right: merged images. Parameters settings through acquisition were kept identical to those used for nude CPG, tel26- and ckit1-functionalized CPG. Scale bars correspond to 20 µm.

Therefore, it can be concluded that these oligonucleotides, when anchored to CPG and left in contact with the selected buffer, adopt the same conformations they typically have in solution (Figure 44). This result further validates the efficacy and feasibility of our method for the identification of a large variety of effective G4 ligands.

In addition, we have here provided proof-of concept that our novel approach is a powerful tool to identify not only structure-selective G4-ligands, but even conformation-selective G4-ligands, thus assuring higher selectivity and lower toxicity of the selected molecules in view of *in vivo* applications.

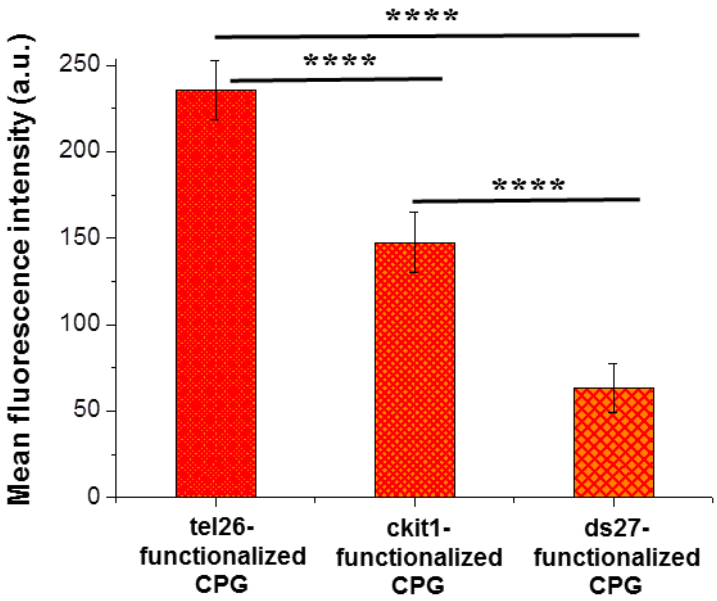

Figure 54. Mean fluorescence intensity values (±S.D.) taken from different edge glass beads-containing regions of each image (63x magnification) acquired for G4-and hairpin duplex-functionalized CPG supports. p-values have been calculated using the Student's t-test (****$p < 0.0001$).

3.5 Experimental section

3.5.1 General procedure adopted for the binding assays

The investigated ligands were purchased from Sigma-Aldrich or Maybridge. Stock solutions for each ligand were prepared by dissolving a known amount of it in pure DMSO or H_2O. A measured volume was taken from the stock solution to obtain a 60 µM ligand solution. All the binding assays were carried out in triplicate, using freshly prepared solutions for each tested ligand. The detailed general procedure adopted for the assays is described as follows: a weighed amount of the CPG supports (5-10 mg) was left in contact with 300 µL of the 60 µM ligand solution in a polypropylene column (4 mL volume, Alltech) equipped with a polytetrafluoroethylene frit (10 µm porosity), a stopcock and a cap. After incubation on a vibrating shaker for 4 min, each support was washed with defined volumes of the washing solution (50 mM KCl, 10% DMSO, 10% CH_3CH_2OH in H_2O) or the releasing solution (2.5 M $CaCl_2$, 15% DMSO in H_2O or pure DMSO) and all the eluted fractions were separately analyzed by UV measurements. After treatment with the releasing solution, inducing G4s and hairpin duplex denaturation, the supports were suspended in the washing solution and then subjected to annealing, by taking them at 75 °C for 5 min and then slowly cooling to room temperature.

3.5.2 Materials and general methods

The sequences d[$(TTAGGG)_4TT$] (tel26), d(AGGGAGGGCGCTGGGAGGAGGG) (ckit1) and d(CGCGAATTCGCGTTTCGCGAATTCGCG) (ds27) selected for the solution studies were synthesized by automated solid phase oligonucleotide synthesis on an Applied Biosystem 3400 DNA/RNA synthesizer. After ammonia deprotection and cleavage from the solid support carried out at 55 °C for 12 h, the crude oligonucleotides were purified by HPLC using a Nucleogel SAX (Macherey-Nagel, 1000-8/46) analytical column and then dialyzed against water using a Float-A-Lyzer G2 dialysis device (MWCO 0.5-1.0 kDa, three H_2O changes over 24 h). Each oligonucleotide was dissolved in pure H_2O and its concentration was determined by measuring the absorbance at 260 nm and 85 °C, using the molar extinction coefficient calculated for the unstacked oligonucleotide.[181] All the studies in solution were carried out in a 50 mM KCl, 10% DMSO, 10% CH_3CH_2OH aq. solution. First, the annealing procedure was performed by dissolving the oligonucleotides at the proper concentration in the K^+-containing solution. The resulting mixture was then heated in a water bath at 95 °C for 5 min, and successively slowly cooled to room temperature in 12 h.

UV spectra were recorded on a JASCO V-550 UV-vis spectrophotometer equipped with a Peltier Thermostat JASCO ETC-505T. The spectra were recorded in the range 240-320 nm, at 20 °C and 85 °C, using a quartz cuvette with a path length of 1 cm, a scanning speed of 100 nm/min and a bandwidth of 2.0 nm, in all cases subtracting the appropriate baseline.
CD spectra were obtained in a quartz cuvette with a path length of 1 cm on a Jasco J-715 spectropolarimeter associated with a Peltier-type temperature control system (model PTC-348WI). The spectra were recorded at room temperature in the 240-320 nm range with 1 s response, 100 nm/min scanning speed and 2.0 nm bandwidth and corrected for the background. All the spectra were averaged over 3 scans.
In both the UV and CD experiments, the oligonucleotides were analyzed at 2 μM concentration.

3.5.3 Binding assays on nude CPG and nude OAS

4.4 mg of support **2** (23 μmol/g loading, 100 nmol) and 3.3 mg of OAS support (30 μmol/g loading, 100 nmol) were treated with 3% TCA in CH_2Cl_2 to remove the DMT protecting group. After exhaustive washings with CH_2Cl_2, CH_3OH, and again CH_2Cl_2, both supports were taken to dryness and then left in contact with 300 μL of a 60 μM solution (18 nmol) of the model ligand under investigation. After incubation on a vibrating shaker for 4 min, the surnatant was allowed flowing through the supports, which were then treated with several volumes of the washing solution. The eluted fractions were collected and analyzed by UV measurements.

3.5.4 Use of G4-and hairpin duplex-functionalized CPG and OAS supports for the binding assays

8.3, 7.7 and 9.1 mg of, respectively, dried tel26-, ckit1- and ds27-functionalized support obtained from **2** (tel26-**2**, ckit1-**2** and ds27-**2**, 100 nmol of oligonucleotide each) and 5.0 mg of dried tel26-OAS (20 μmol/g loading, 100 nmol of oligonucleotide) were left in contact, in different columns, with 300 μL of the washing solution and subjected to the annealing procedure. After removing the surnatant, the supports were treated, analogously to the control nude CPG, with 300 μL of the ligand dissolved at 60 μM concentration (18 nmol) in the washing solution. After 4 min incubation, the supports were treated with several volumes of the washing solution and the eluted fractions were collected and analyzed by UV measurements. Finally, to allow the complete release in solution of the ligands retained by the oligonucleotides on the supports, these were then repeatedly washed with the releasing solution.

3.5.5 Confocal microscopy analyses

To perform confocal microscopy analyses, nude CPG or G4- and hairpin duplex-functionalized supports were seeded on rectangle glass slides and mounted in water by using rectangle glass coverslips. Images were captured by using a confocal laser scanning microscope (Zeiss LSM 710, Zeiss, Germany) and a 63x objective oil immersion system. When necessary, images were taken by using a 10x objective, in order to obtain information about the morphological homogeneity of the samples. For each CPG support, images were taken in at least three independent experiments. For each objective, images were taken under identical conditions. Fluorescence intensity analyses were performed by using the Zen Lite 2.3 software package. For this analysis, areas characterized by high fluorescence intensities were selected for each sample. The fluorescent probe, c_{ex}-NDI (Figure 47), was synthesized and purified according to a published procedure.[184]

CHAPTER 4 – SCREENING AND EVALUATION OF A LIBRARY OF MOLECULES FEATURED BY A FUROBENZOXAZINE NAPHTHOQUINONE CORE

4.1 Introduction

With a view to expanding the repertoire of drug-like G4 binders and speeding up the search for true hits, docking studies can be valid tools, especially to screen large libraries of putative ligands.[185] In this frame, a 6000 compounds library − from the commercially available Life Chemicals database − was recently virtually screened against the tetramolecular and parallel G4 of sequence d[(TGGGGT)$_4$] by exploiting Autodock4.2 software.[186] Among the 6000 compounds, 6 molecules (**1**-**6**, Figure 55) were found to be good G4 binders, as also experimentally confirmed by NMR studies.[186] These compounds were subsequently studied in their interaction with topologically different G-quadruplexes by biophysical techniques.[187]

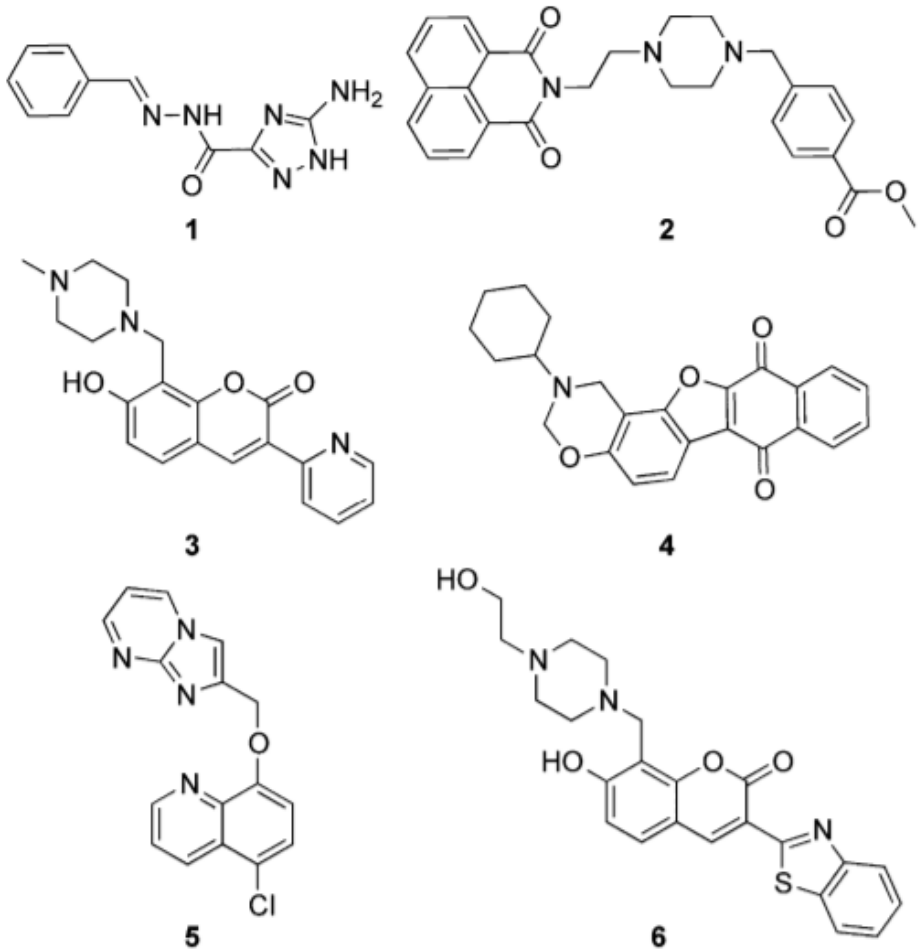

Figure 55. Chemical structures of compound **1-6** previously selected from a commercially available database by virtual screening.[186]

Remarkably, two of the six G4 binders (**2** and **4**, Figure 55) proved to be able to selectively stabilize parallel G4s, discriminating antiparallel or hybrid G4s and duplex DNA and inducing telomere damage in the μM range.[187] In particular, compound **4** proved to be the strongest ligand being able to largely stabilize both telomeric and extra-telomeric parallel G4s, as well as induce G4 formation in some G-rich oligonucleotides also in the absence of cations.[187] Encouraged by its promising activity, we identified and analyzed a focused library of structural analogs of **4**, featured by different pendant groups on the N-atom of the oxazine ring (Table 4), with the aim of developing more potent and selective G4 ligands.[188]

Table 4. Chemical structures of compound **4** and its analogs.

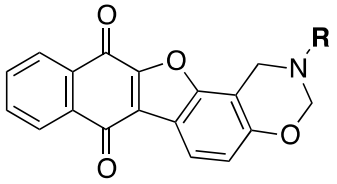

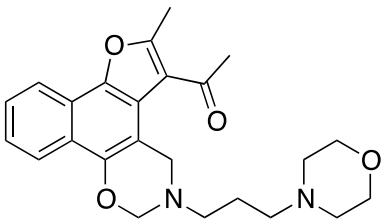

D4

Compound	R	Compound	R
4	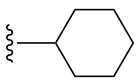	**S4-6**	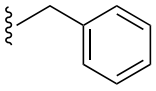
S4-1		**S4-7**	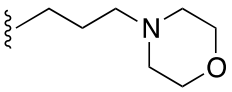
S4-2	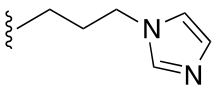	**S4-8**	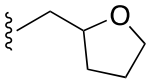
S4-3	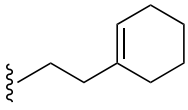	**S4-9**	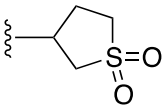
S4-4	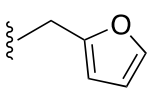	**S4-10**	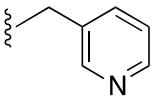
S4-5	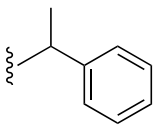		

First, the selected molecules have been screened against topologically different G4s by our affinity chromatography-based method (G4-CPG assay). Then, the best analog, in terms of affinity towards G4s and selectivity over duplex DNA, has been characterized in its interaction with DNA secondary structure-forming oligonucleotide models by biophysical studies and analyzed for its biological activity.[188]

4.2 Selection of compound 4 analogs

Aiming at synthesizing G4-selective ligands with enhanced activity/toxicity ratio, a convenient synthetic strategy can be to start from a known lead compound featured by a suitable aromatic core and then functionalize it with a set of different decorations. In this way, the stabilizing stacking interactions with the target can be preserved, and an improved selectivity achieved, by exploiting additional specific interactions realized by the decorations with the G4 target grooves. In the present case, starting from lead compound **4**, a set of its analogs, featured by the same pentacyclic core and bearing different decorations on the N-atom of the oxazine ring, were selected (Table 4).

Given the relative synthetic accessibility of pentacyclic furobenzoxazine naphthoquinones, analogs of **4** were searched in commercial molecular databases. This approach has the advantage of quickly providing a library of structural analogs of the lead compound and being cost-effective. Therefore, the Dice similarity coefficient was computed between **4** and the compounds present in the ZINC database collection of commercially available compounds (https://zinc15.docking.org) setting the similarity threshold to 70%. This search resulted in 40 compounds that were visually inspected revealing that, as desired, a number of furobenzoxazine-containing naphthoquinone derivatives were identified, as well as some analogs exhibiting different scaffolds. Ten of the furobenzoxazine naphthoquinone derivatives resulting from the filtered database were thus selected (**S4-1**–**S4-10**, Table 4). A furonaphthoxazine analog (**D4**, Table 4) was also included in this study to have a different scaffold as a reference.

4.3 Experimental screenings by the G4-CPG assay

Aiming at expanding the potential of the G4-CPG assay and extending it to a wide variety of topologically different G4 structures, the CPG support was functionalized with a set of biologically relevant G4-forming oligonucleotides. In addition to previously synthesized tel26, ckit1 and ds27, we selected for the elongation on the CPG support the following sequences: the

33-mer d(TGGGGAGGGTGGGGAGGGTGGGGAAGGTGGGGA) (cmyc) from the nuclease hypersensitive element in the human c-myc promoter,[101] the 21-mer d(CGGGCGGGCGCGAGGGAGGGG) (ckit2) from c-kit oncogene promoter[114] and the 24-mer d(AAGGGGAGGGGCTGGGAGGGCCCGGA) (hTERT1) from the G-rich region in the hTERT core promoter, which represents the main regulatory element of the hTERT gene.[119]
The binding assays were performed on the functionalized CPG supports following the procedures described in Chapter 3. All the oligonucleotide-functionalized supports were first tested in their ability to bind known G4 ligands with different affinity for G4 structures. In particular, thiazole orange (TO) and resveratrol (Figure 42) were used as model molecules, being respectively a strong and a very weak G4 binder.[174,175] The obtained data, showing high affinity (bound ligand > 97%) for TO and very low affinity (bound ligand < 4%) for resveratrol on all the tested supports, proved the efficacy of the novel functionalized CPG supports.
Successively, the stock solutions for compound **4** and its analogs were prepared by dissolving a weighed amount of the solid compound in pure DMSO; only compound **S4-1** proved to be not completely soluble in DMSO at the concentration required for the binding assays and was therefore discarded. All the other compounds as well as compound **4** proved to be well soluble in the washing/releasing solutions used in our binding assays and at the concentration chosen for the binding experiments. After solubility checks for all the tested compounds, we verified the absence of unspecific binding on the solid support by incubating them with the nude CPG. Low-to-null unspecific interactions with the solid support have been observed for compound **4** and its analogs (Table 5). These results further prove the inertness of the nude CPG, previously demonstrated for G4 model ligands, also with this novel and chemically different class of compounds, confirming the possibility of expanding the chemical space of potential ligands that can be tested on the support, as well as the general reliability of our method. Then, all the investigated ligands were tested on the G4s- and hairpin duplex-functionalized CPG supports (Table 5 and Figure 56). The obtained results showed that all the analyzed ligands had good affinity for tel26 immobilized on the solid support. However, no marked improvement was found with respect to **4**, still the strongest binder in the series when tested on this G4-forming sequence, with the only exception of **S4-4**, showing comparable results as **4**. In contrast, when tested on cmyc, compounds **S4-2**, **S4-4**, **S4-7**, **S4-8** and **S4-10** displayed higher affinity than **4**. As far as ckit1 is concerned, almost all the tested compounds proved to be stronger binders than compound **4**, with the sole exception of **S4-3**. In the case of ckit2, **S4-2**, **S4-4,** and **S4-10** showed higher binding abilities than **4**. Notably, also in this case compound **S4-3** was the weakest binder

of the series. Finally, for hTERT1 all the tested analogs had comparable or higher affinity than **4**.

Table 5. Summary of the binding assays data for compound **4** and its analogs on nude and functionalized CPG supports.

Compound	Bound ligand (%)[a]						
	Nude CPG	**CPG-tel26**	**CPG-cmyc**	**CPG-ckit1**	**CPG-ckit2**	**CPG-hTERT1**	**CPG-ds27**
4	0	86	86	70	82	74	18
S4-2	0	80	94	85	91	82	46
S4-3	0	73	84	55	67	73	16
S4-4	0	86	93	90	92	91	2
S4-5	0	80	84	78	80	82	0
S4-6	10	80	87	76	83	78	12
S4-7	11	80	89	77	84	92	33
S4-8	0	78	90	88	83	87	20
S4-9	5	75	73	72	68	76	16
S4-10	0	79	94	90	88	89	28
D4	7	76	74	75	70	78	22

[a]Bound ligand is calculated as a difference from the unbound ligand, recovered with 50 mM KCl, 10% DMSO, 10% CH_3CH_2OH washing solution, and expressed as % of the amount initially loaded on the support. The errors associated with the % are within ± 2%.

Overall, all the tested analogs proved to be effective G4 ligands – also when compared with the known G4 binders, tested in previous experiments – typically showing high binding affinities (bound ligand > 80%), in many cases better than compound **4**. Among all the investigated compounds, **D4** was the worst G4 ligand, evidencing that its polycyclic core, different from the other tested molecules, is not suitable for G4 targeting. On the other hand, the best G4 ligand seems to be compound **S4-4** for its ability to tightly interact both with telomeric and extra-telomeric G4s. In addition, the highest percentages of bound ligand were found for the cmyc sequence, probably the preferred target for the here screened chemotypes. In order to evaluate the G4s *vs.* duplex DNA selectivity, all the compounds were also tested in their interaction with the ds27 hairpin duplex-forming oligonucleotide. Overall, all the ligands proved to be able to effectively discriminate G4- *vs.* duplex-forming oligonucleotides. In particular, **S4-4** and **S4-5** had a significantly lower affinity for ds27 than **4**, with **S4-5** showing zero affinity for duplex

DNA. Therefore, considering its good affinity for the G4 sequences and its high G4s *vs.* duplex DNA selectivity degree, **S4-5** emerged as the most promising analog. Thus, we selected **S4-5** to gain a deeper insight, by means of biophysical techniques, into the binding to G4 and duplex models, in comparison with lead compound **4**.

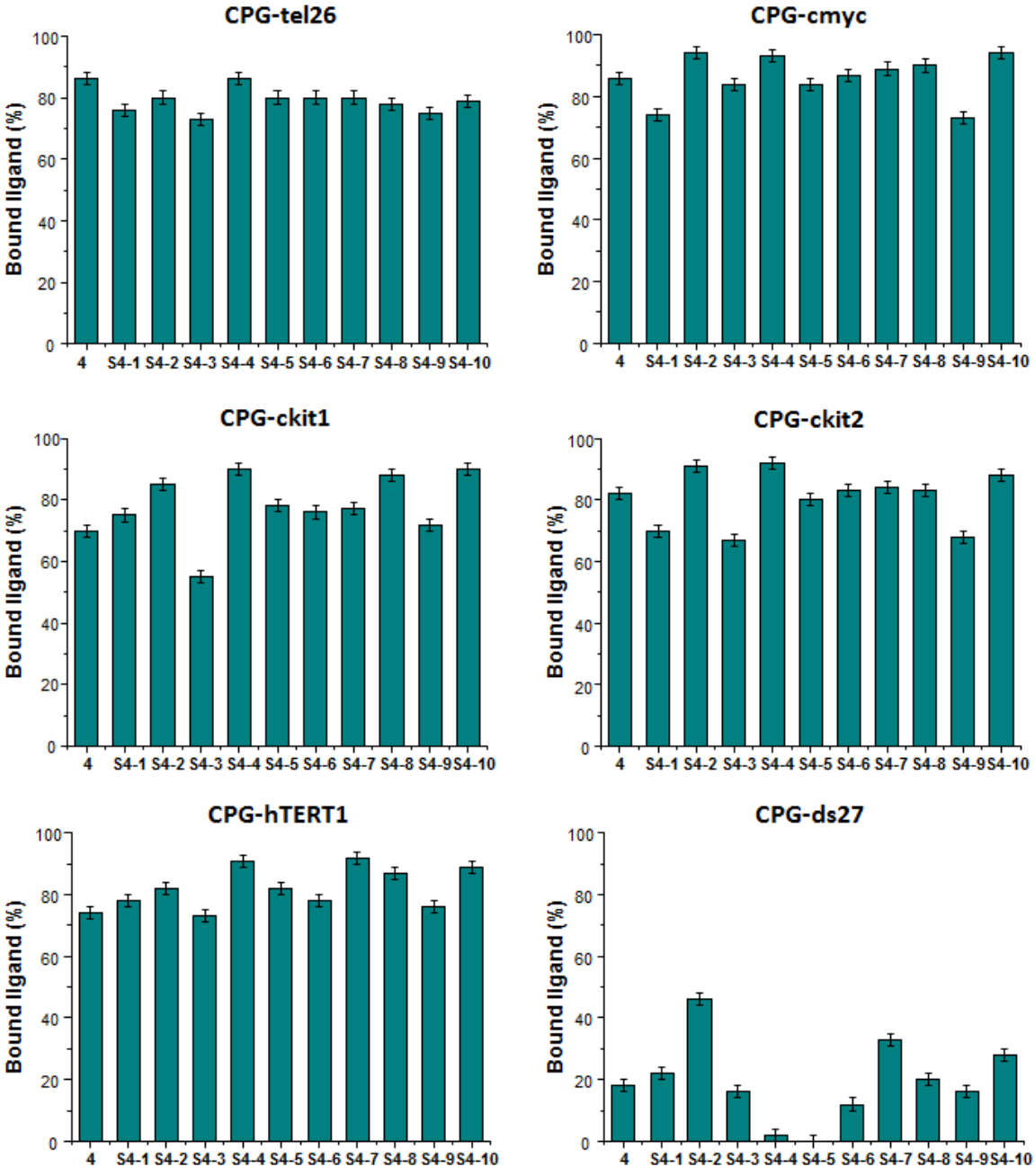

Figure 56. Bound ligand expressed as percentage of the quantity initially loaded on each functionalized CPG support for all the investigated compounds. The errors associated to the percentages are within ± 2%.

4.4 Solution studies on the interaction of the selected ligands with oligonucleotide models

4.4.1 CD and CD-melting experiments

Taking into account the results of the G4-CPG assay, we investigated the ability of compound **S4-5**, in parallel with compound **4**, to interact with a human telomeric G4, an extra-telomeric G4 and a duplex structure by CD experiments. In particular, among the extra-telomeric G4s, we chose c-myc, for which **S4-5**, as well as the other analogs, showed the highest affinity. In addition, the same sequences elongated on the CPG supports (tel26, cmyc and ds27) were used as models. 2 μM solutions of the three secondary structure-forming oligonucleotides in 20 mM KCl, 5 mM KH_2PO_4, 10% DMSO buffer (pH 7) were titrated with increasing amounts of the two compounds, and spectra recorded after each addition.

As expected in the above buffered conditions, tel26 folds into a hybrid II-type G4 featured by maximum at 290 nm and a shoulder at 270 nm,[83] cmyc forms a parallel G4 with a maximum centered at 263 nm,[22,101] while ds27 shows the characteristic positive band at 280 nm with a minimum at 251 nm relative to a B-DNA duplex structure[180] (Figure 57). In the case of tel26 titration with **S4-5**, a dose-dependent increase of the intensity of the 290 nm band and a reduction of the 270 nm shoulder were observed (Figure 57A). In the titration experiments with cmyc, the addition of **S4-5** produced only weak changes, with a slight reduction of the 263 nm band and an increase of the 288 nm band (Figure 57B). In contrast, in the titration of ds27 no detectable change in the CD profile of the duplex was observed, suggesting that this structure was essentially unaffected by the addition of even a large excess of ligand (Figure 57C). A similar behaviour was found for compound **4** towards G4s DNA, while a slight conformational variation was observed for ds27, with a reduction of the minimum at 251 nm. (Figure 58). In all cases, up to 5 equivalents of ligand were added to the oligonucleotide solutions, as the best compromise between the solubility of the analyzed ligands and the saturation of the oligonucleotide CD signals. No induced CD signal was observed for all the investigated systems (Figure 59).

CD-melting experiments were also performed on all the oligonucleotide/ligand mixtures to evaluate if stabilizing or destabilizing effects on the G4s and hairpin duplex structures were obtained upon incubation with the two ligands (Figures 60 and 61). CD-melting curves of tel26, cmyc and ds27 in the absence or presence of each ligand (1:5 oligonucleotide/ligand ratio) were recorded by following the CD changes at the wavelength of intensity maximum (290, 263, and 251 nm for tel26, cmyc and ds27, respectively).

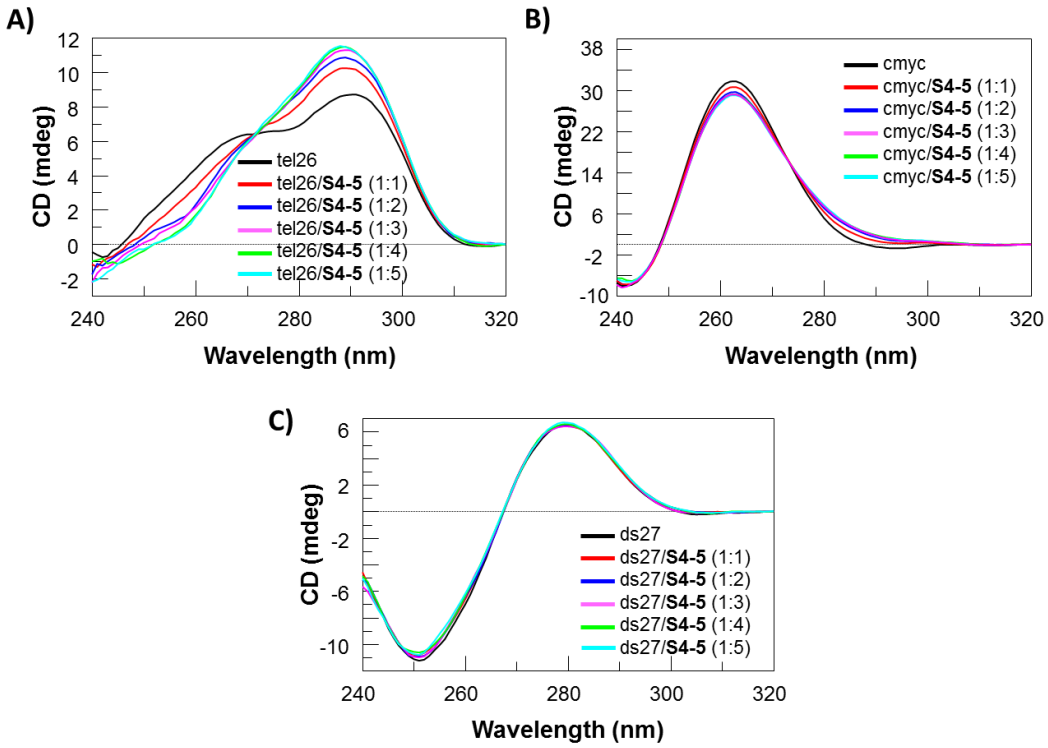

Figure 57. CD spectra of 2 µM solutions of tel26 (A), cmyc (B) and ds27 (C) in 20 mM KCl, 5 mM KH_2PO_4, 10% DMSO buffer (pH 7) in the absence and presence of increasing amounts of **S4-5** (up to 5 equivalents).

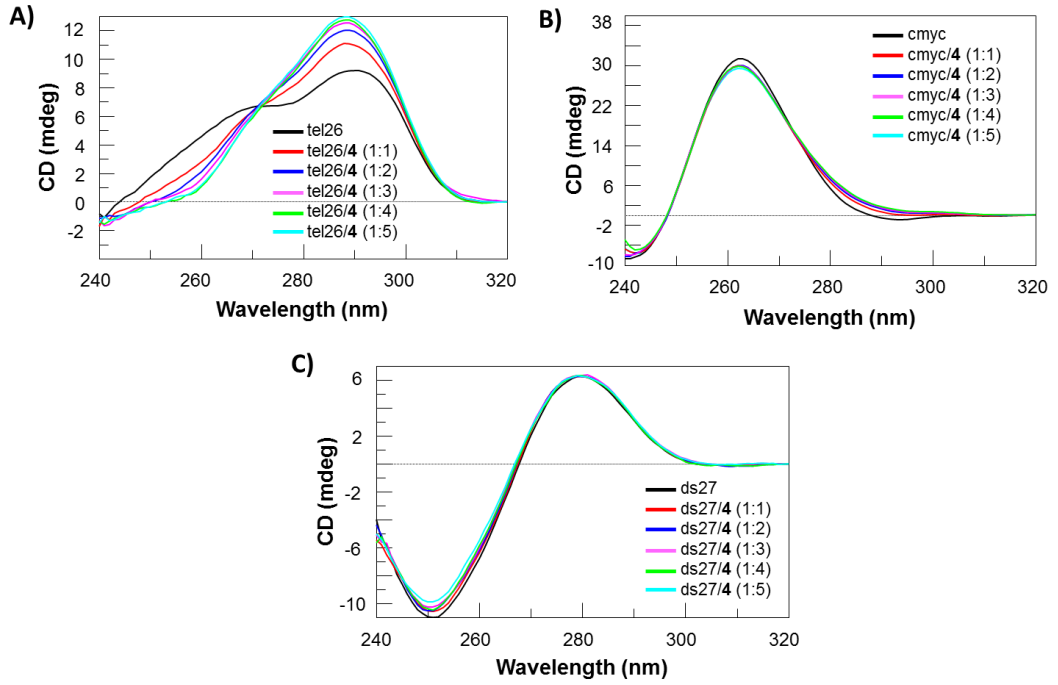

Figure 58. CD spectra of 2 µM solutions of tel26 (A), cmyc (B) and ds27 (C) in 20 mM KCl, 5 mM KH_2PO_4, 10% DMSO buffer (pH 7) in the absence and presence of increasing amounts of **4** (up to 5 equivalents).

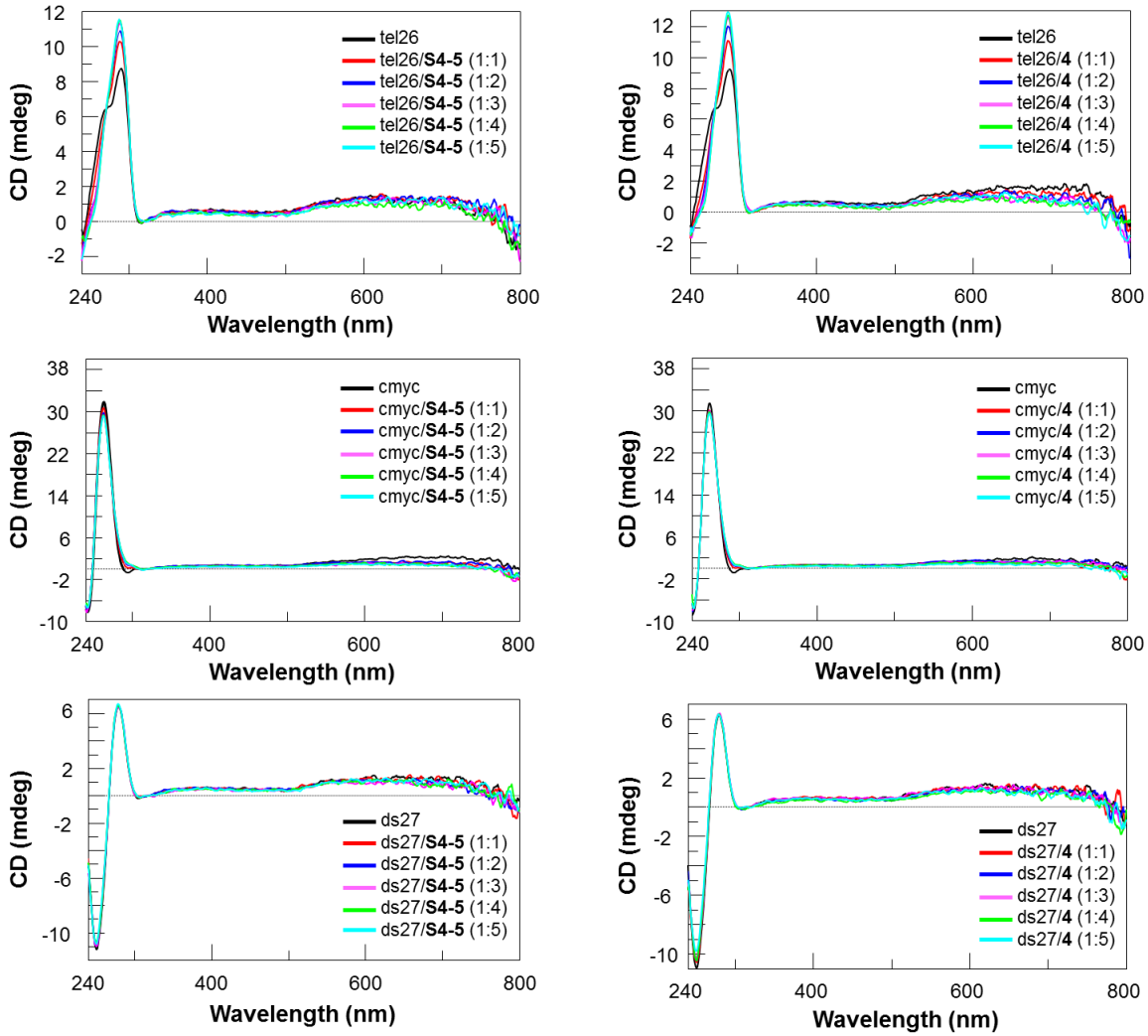

Figure 59. CD titrations of 2 μM solutions of tel26, cmyc and ds27 (top, middle and bottom, respectively) in 20 mM KCl, 5 mM KH_2PO_4, 10% DMSO buffer (pH 7) with **S4-5** (1-5 equivalents) (left panels) and **4** (1-5 equivalents) (right panels).

The results of the CD melting experiments clearly showed that compounds **S4-5** and **4** did not significantly affect the stability of the tel26 and ds27 structures (Table 6). Conversely, both ligands appreciably stabilized the cmyc G4 structure (ΔT_m > 8 °C).

Overall, these results confirmed the ability of the here investigated pentacyclic scaffold to selectively interact with G4 structures discriminating duplex DNA, as proved by CD titrations, and to markedly stabilize parallel G4s, not affecting the stability of other G4 conformations and duplex DNA.

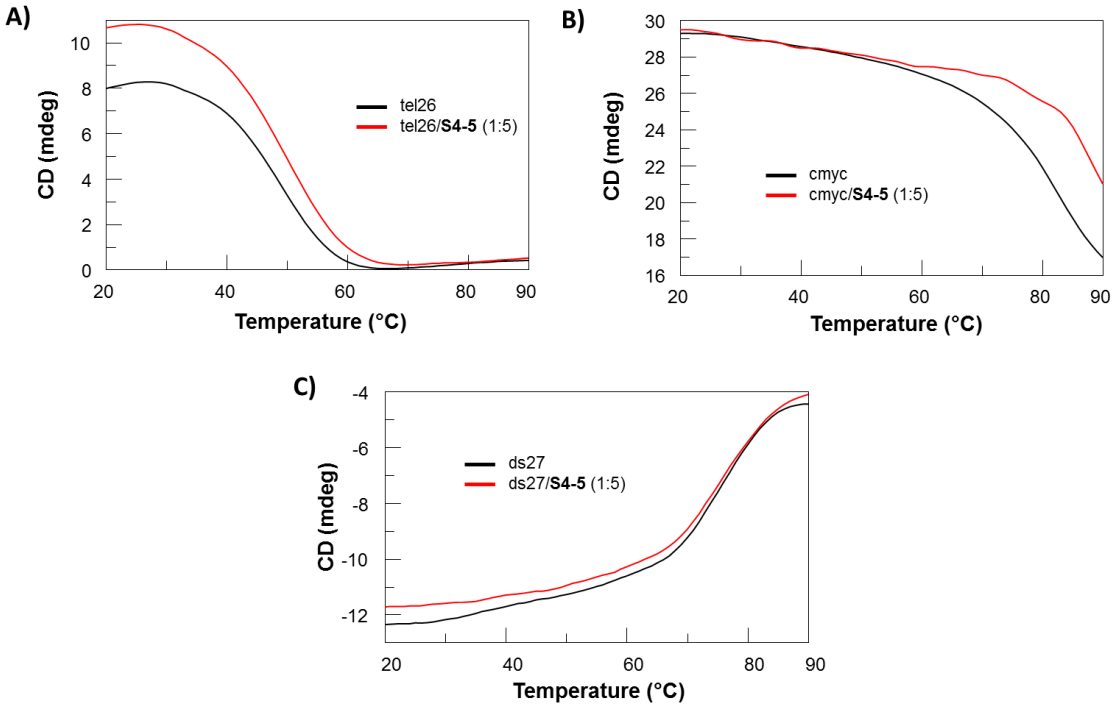

Figure 60. CD melting curves for tel26/**S4-5** (A), cmyc/**S4-5** (B) and ds27/**S4-5** (C) mixtures (1:5) in 20 mM KCl, 5 mM KH_2PO_4, 10% DMSO buffer (pH 7), recorded at 290, 263, and 251 nm, respectively.

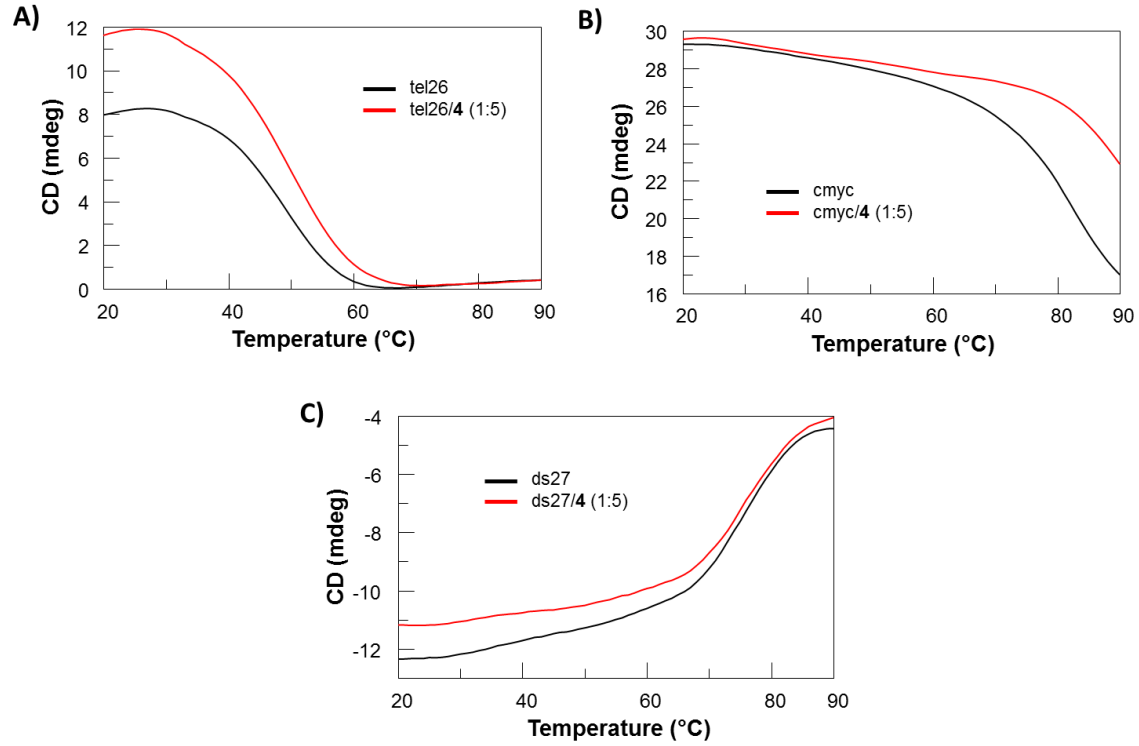

Figure 61. CD melting curves for tel26/**4** (A), cmyc/**4** (B) and ds27/**4** (C) mixtures (1:5) in 20 mM KCl, 5 mM KH_2PO_4, 10% DMSO buffer (pH 7), recorded at 290, 263, and 251 nm, respectively.

Table 6. Melting temperatures (T_m) of tel26, cmyc and ds27 in the absence or presence of the ligands (5 equivalents) as measured by CD melting experiments.

Ligand	**T_m (°C) (±1)**		
	tel26	**cmyc**	**ds27**
No ligand	49	82	75
4	49	> 90	76
S4-5	50	> 90	76

4.4.2 NMR experiments

In order to get information on the binding mode of compounds **4** and **S4-5** to the G4 structures formed by the human telomeric and c-myc promoter DNA sequences, NMR titration experiments were performed in collaboration with the group of prof. Antonio Randazzo of the Department of Pharmacy of University of Naples Federico II.[188] The modified telomeric sequence d[TTGGG(TTAGGG)$_3$A] (m-tel24)[189] and the shortened c-myc sequence d(TGAGGGTGGGTAGGGTGGGTAA) (myc22)[190] were used for this study since they are characterized by a predominant G4 conformation in solution and therefore give higher quality NMR spectra than the wild-type, polymorphic sequences. Twelve well-resolved imino proton peaks were observed in the ^{1}H NMR spectra of m-tel24 and myc22, perfectly matching the NMR data reported in the literature (Figures 62-65).[189,190] The investigated oligonucleotides were then titrated with **4** and **S4-5**, in parallel experiments, up to a 1:4 G4/ligand ratio. Addition of increasing amounts of ligands to the G4 solutions produced considerable proton resonance changes in both imino and aromatic proton regions of the spectra (Figures 62-65), thus suggesting that both **4** and **S4-5** may not have a unique binding site. The relative line broadening observed for all the imino resonances and most of the aromatic ones also suggested that the ligands could explore different poses in fast exchange within the same G4 binding pocket. In detail, imino signals broadening was more prominent at low concentrations both of **4** and **S4-5** (up to 1 ligand equivalent), while at higher concentrations novel imino signals appeared, with the sole exception of m-tel24/**S4-5** system. However, only in the case of myc22/**4** system, twelve well-resolved imino signals were observed, therefore suggesting the formation of a single G4-ligand complex, as well as a peculiar binding stoichiometry of 1:3 myc22/**4**. On the other hand, some distinct aromatic protons of both m-tel24 and myc22 G4s were only weakly affected by the ligands. As far as **4** is concerned, for m-tel24 (Figure 62) this is the case of residues T6-T7-A8, which form the double-chain reversal loop of the G4; for myc22 (Figure 63) this is the case of A6, which stacks on top of the 5' G-tetrad, and of residues T10, T14-A15, and T19 (numbering according to Ambrus *et al.*),[190] which form the three double-chain reversal loops of the G4 structure. The NMR titrations with **S4-5** show that in the interaction with m-tel24 G4 (Figure 64) the ligand does not appreciably affect the aromatic protons of A8, which is in the double-chain reversal loop, and of residues T18-T19-A20, which form a lateral loop close to the external G-tetrad; while in the interaction with myc22 (Figure 65), the least affected ones are the aromatic protons of A6, which stacks on top of the 5' G-tetrad, and of

residues T14-A15 and T19, which form the second and third double-chain reversal loop of G4, respectively.

Overall, these findings suggest that the loops are generally very little or not at all affected by both ligands. Thus, **4** and **S4-5** may bind m-tel24 and myc22 either by interaction with the grooves not masked by the loops, or by stacking on the external G-tetrads.

Aiming at investigating the G4 *vs.* duplex DNA selectivity of **4** and **S4-5**, NMR titrations were also carried out with a model duplex DNA formed by the Dickerson dodecamer d(CGCGAATTCGCG) (ds12). The ^{1}H NMR spectrum of ds12 well matched the one reported in the literature (Figures 66 and 67).[191] Noteworthy, no significant variation of the chemical shift values of ds12 was observed upon treatment with **S4-5** (Figure 66), up to a 1:4 DNA/ligand ratio, thus confirming that it does not bind the investigated duplex DNA. On the other hand, **4** caused a small perturbation of the ds12 spectrum, in terms of both intensity decrease and line broadening of all the ^{1}H NMR signals (Figure 67), suggesting that **4** could somehow interact with duplex DNA in a weak and unspecific way. These results are in full agreement with those obtained from G4-CPG assay.

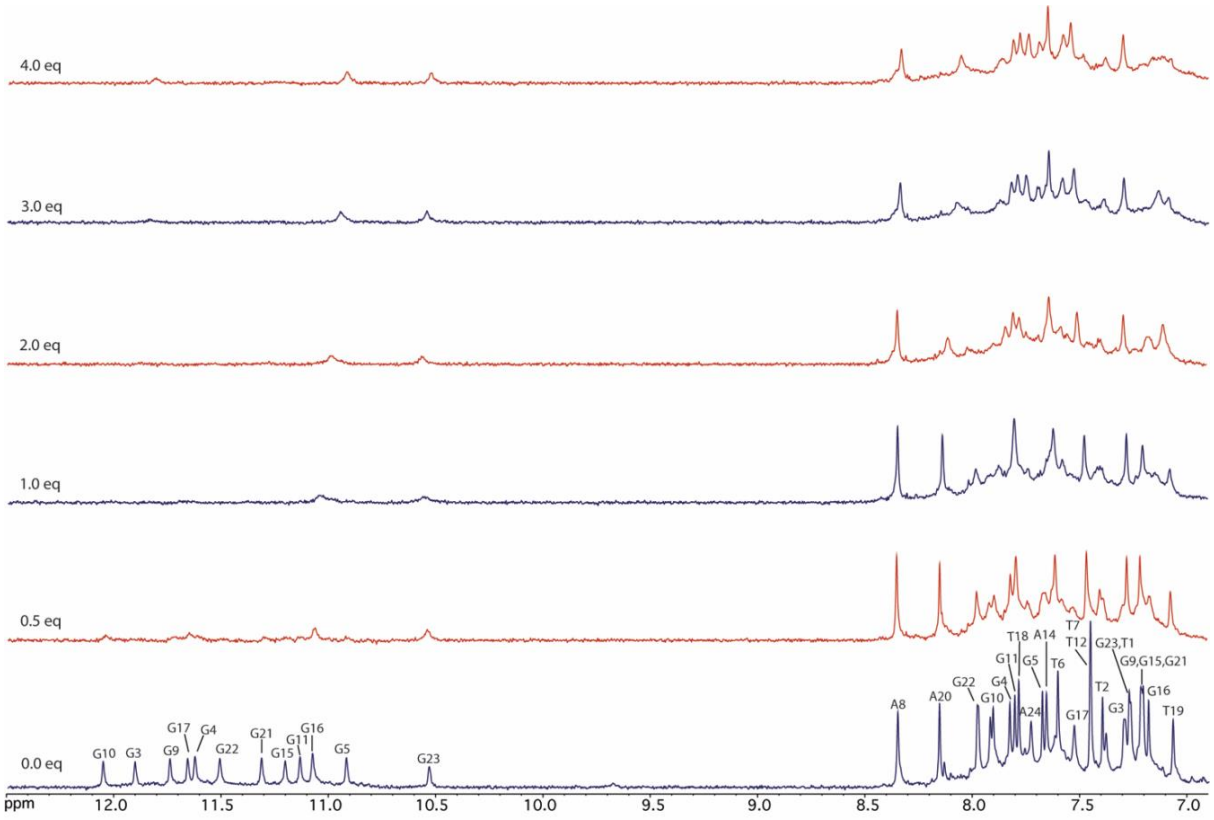

Figure 62. Imino and aromatic regions of the ^{1}H NMR spectra of m-tel24 G4 titrated with **4**. The ligand equivalents are shown on the left of the spectra.

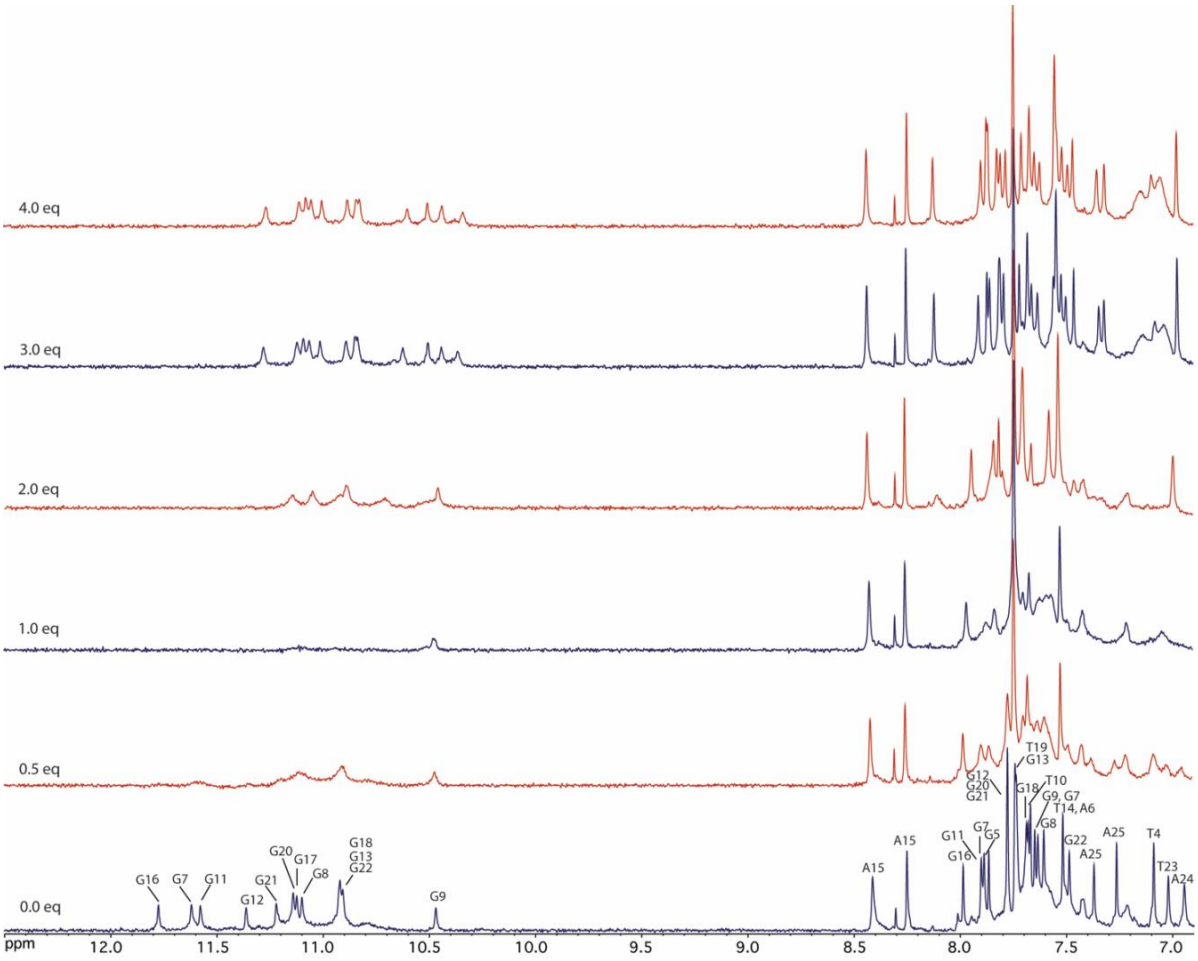

Figure 63. Imino and aromatic regions of the ^{1}H NMR spectra of myc22 G4 titrated with **4**. The ligand equivalents are shown on the left of the spectra.

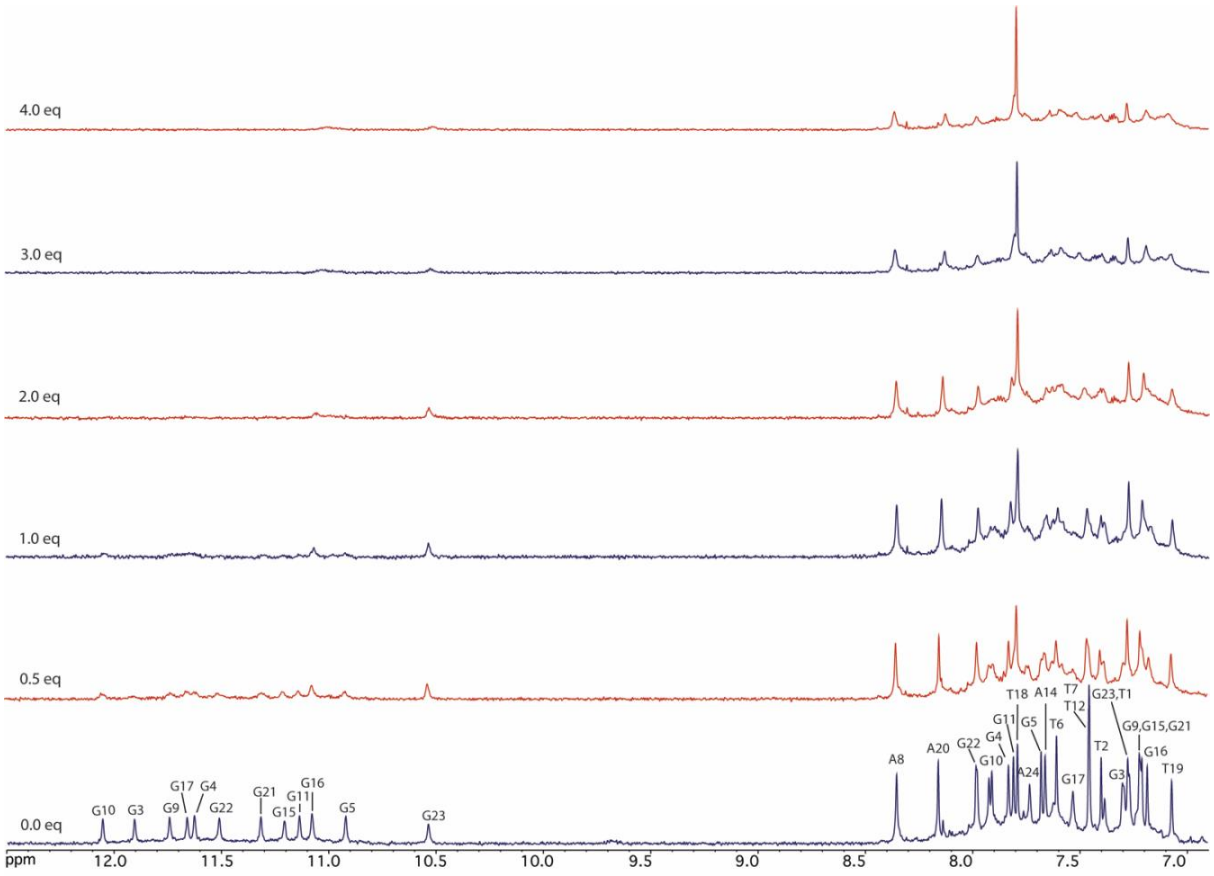

Figure 64. Imino and aromatic regions of the ^{1}H NMR spectra of m-tel24 G4 titrated with **S4-5**. The ligand equivalents are shown on the left of the spectra.

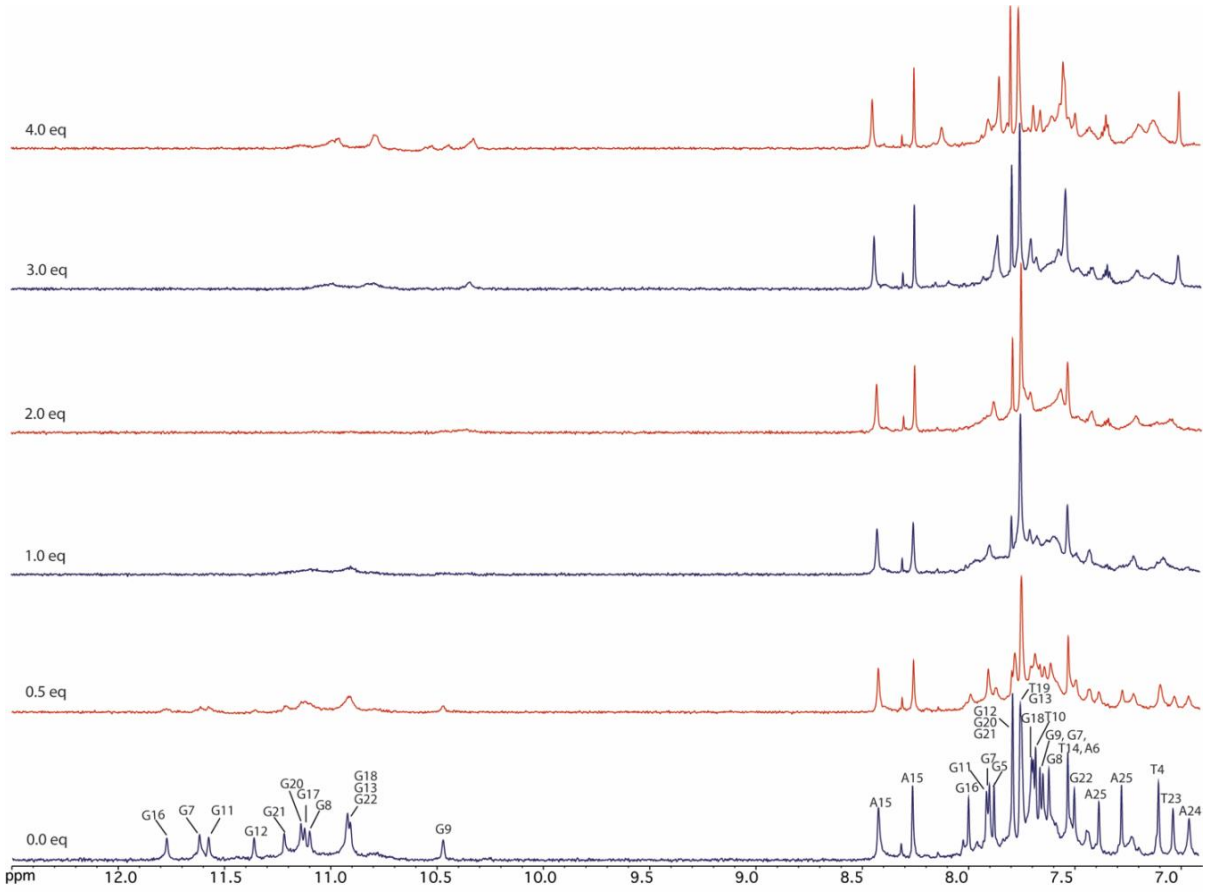

Figure 65. Imino and aromatic regions of the ^{1}H NMR spectra of myc22 G4 titrated with **S4-5**. The ligand equivalents are shown on the left of the spectra.

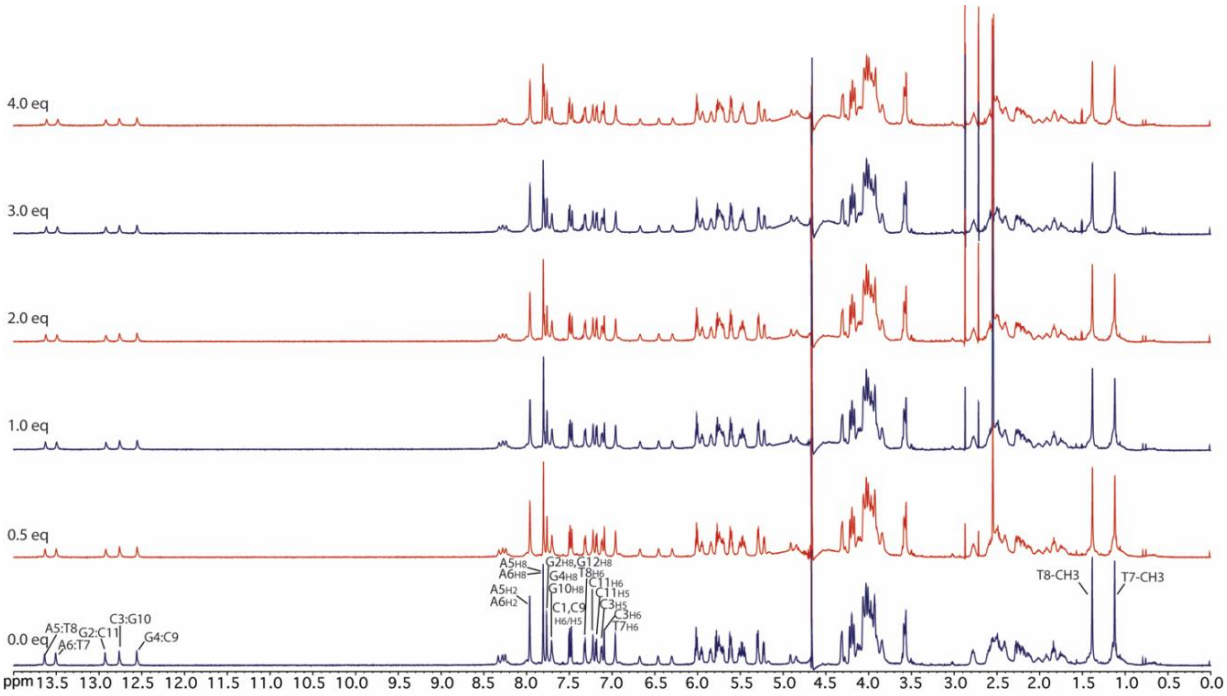

Figure 66. ^{1}H NMR spectra of the ds12 duplex titrated with **S4-5**. The ligand equivalents are shown on the left of the spectra.

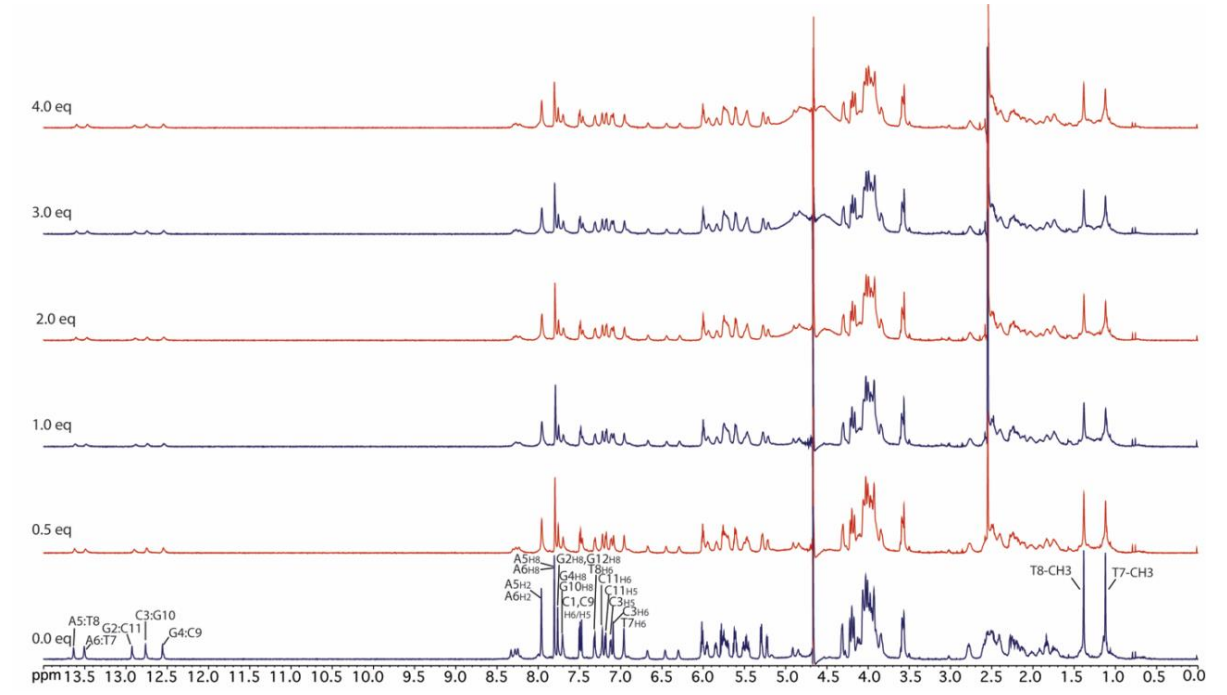

Figure 67. ^{1}H NMR spectra of the ds12 duplex titrated with **4**. The ligand equivalents are shown on the left of the spectra.

4.4.3 Microscale thermophoresis (MST) experiments

To obtain quantitative data about the affinity of **S4-5** for the human telomeric and c-myc promoter G4s, microscale thermophoresis (MST) experiments were performed in collaboration with the group of prof. Antonio Randazzo at the Department of Pharmacy of University of Naples Federico II.[188] MST is a fast and easy technique used to characterize small molecule-nucleic acid interactions in solution, which records the thermophoretic movement of a fluorescently-labeled molecule under microscopic temperature gradients.[192] This molecular motion strongly depends on changes in size, charge, and hydration shell. Since the binding of a small molecule to a given target affects at least one of these parameters, also its thermophoretic behaviour is affected. This effect can be used to determine equilibrium constants, such as the dissociation constant K_d. To this aim, serial dilutions of **S4-5** were prepared, mixed with a constant concentration of Cy5-labeled oligonucleotides (tel26 or myc22), loaded into capillaries and analyzed by MST. MST measurements proved that compound **S4-5** was able to bind both tel26 G4 (K_d = 26 (±4) µM) and myc22 G4 (K_d = 13 (±2) µM), indicating for this ligand twice higher affinity for the parallel than hybrid G4 structure (Figure 68).

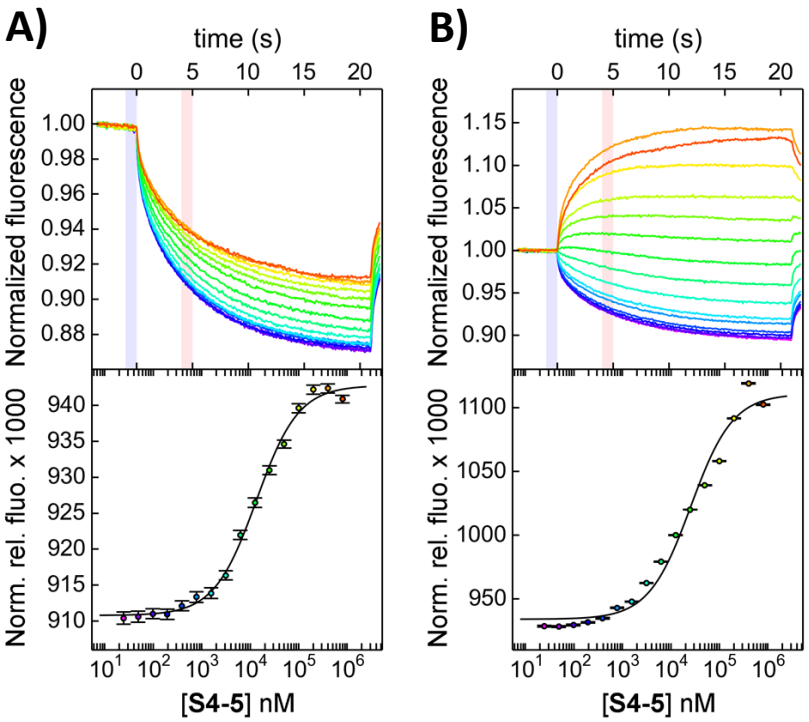

Figure 68. MST measurements for **S4-5** with myc22 (A) and tel26 (B) G4s. (Top) Time traces recorded by incubating increasing concentrations of **S4-5** with the labeled G4s and (bottom) the corresponding binding curves.

4.5 Molecular docking

To get a deeper insight into the binding mode of **S4-5** with human telomeric and c-myc promoter G4s, molecular docking studies were carried out in collaboration with prof. Sandro Cosconati of the Department of Environmental, Biological, and Pharmaceutical Sciences and Technologies (DiSTABiF) of University of Campania "Luigi Vanvitelli".[188] **S4-5** was docked into the solution G4 structure of c-myc (myc22, PDB ID: 1XAV) and into the hybrid-type G4 structure formed in K^+ solution by the 26-mer from the human telomere (tel26, PDB ID: 2JPZ). The software Autodock 4.2,[193] which is the same one previously exploited to identify **4** as a G4 ligand, was here employed.

Analysis of the results obtained when **S4-5** was docked into the myc22 G4 structure showed that the ligand is inserted into the G4 groove not covered by the loop, where it is stabilized by van der Waals interactions with G21, G22, and T23 residues and ionic interactions with the backbone phosphate oxygens of A24 residue through the protonated nitrogen of the oxazine ring (Figure 69). Furthermore, the pendant benzyl group is well positioned to form π-π interactions with the G9 guanine ring. Interestingly, both the (*R*)- and the (*S*)-isomer of **S4-5** were docked but no enantio-discriminating binding was detected. In contrast, the methyl substituent on the benzylic carbon seems to optimally orient the phenyl ring to give the aforementioned stacking interactions. Indeed, the obtained theoretical model was perfectly consistent with the binding mode indicated by NMR studies, proving the general reliability of docking results.

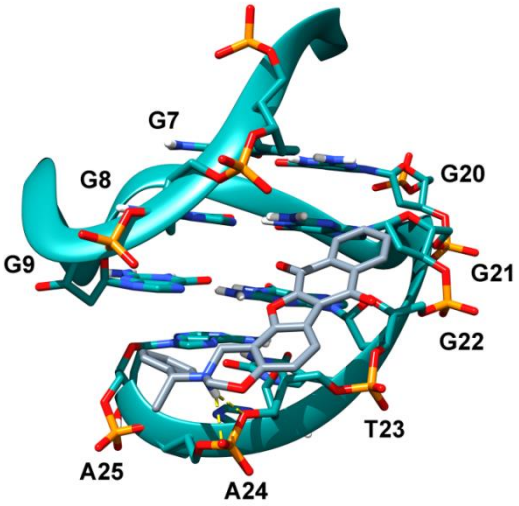

Figure 69. Binding mode of **S4-5** when docked into myc22 G4 solution structure. The ligand is represented as grey sticks while the DNA as dark cyan ribbons and sticks. H-bonds are represented as dashed yellow lines. DNA residues were numbered according to Ambrus *et al.*[190]

As far as tel26 is concerned, the docking software suggested three possible binding poses in which **S4-5** is always inserted in the groove not occupied by the loop, between the first and fourth strand of the G4 structure (Figure 70). Indeed, the ligand adopts the same orientation with respect to the G4 but at different levels of the groove, one towards the 3' end (here referred to as pose A), one in the middle (pose B), and one towards the 5' end (pose C).

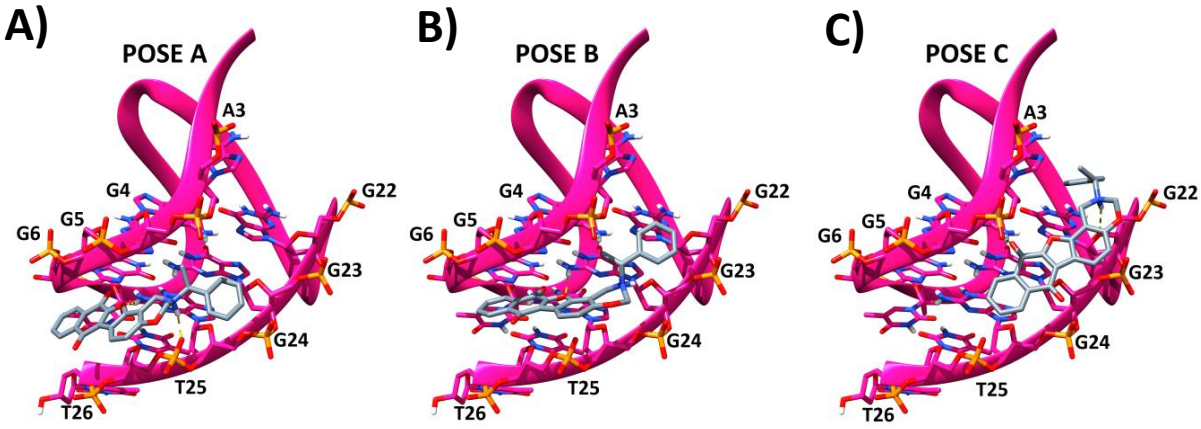

Figure 70. Alternative binding poses predicted for **S4-5** when docked into the tel26 solution structure. The ligand is represented as grey sticks, the DNA as magenta ribbons and sticks. H-bonds are represented by dashed yellow lines.

In pose A the ligand forms an H-bond, through its furan oxygen, with the NH_2 group of G24, and an ionic interaction, through its protonated oxazine nitrogen, with the T25 phosphate group. In pose B, an H-bond is formed between the ligand furan oxygen and the G23 NH_2 group. In pose C, one of the two ligand quinone oxygens forms an H-bond with the NH_2 group of the G4 and a charged, reinforced H-bond through its protonated oxazine nitrogen and the sugar O4' atom of G22. Moreover, the phenyl ring of the ligand benzyl moiety forms π-π interactions with the A3 and G22 aromatic rings. As observed for the myc22 structure, also for tel26 no enantio-discriminating binding was detected. From the above-described docking results, we cannot give a preference for one of the obtained solutions; rather, it is possible to speculate that the ligand is able to slide into the G4 groove adopting almost isoenergetic binding conformations. This hypothesis is corroborated by the results of the NMR titration experiments, which were not helpful in indicating a specific binding region.

4.6 Biological assays

Specific biological experiments were carried out for the here studied ligands, in collaboration with the research group of dr. Annamaria Biroccio at Regina Elena Cancer Research Institute in Rome.[188]

In order to investigate the telomere damage induced by the here tested ligands, immunofluorescence-based assays (IF) were used.[194] In particular, indirect IF is used to identify a cellular antigen by using a primary antibody that recognizes a specific protein. A secondary antibody conjugated with a fluorophore, visible under IF microscope, is used to recognize the immunoglobulins of the primary antibody and amplify its signal. When a DNA damage response is activated, the damage factor H2AX is phosphorylated (γH2AX) in correspondence of the DNA breaks.[195] This antigen can be visualized by indirect IF.[194] Using these experiments, qualitative and quantitative analysis of DNA damage can be performed. In fact, staining homogeneity grade is a qualitative measurement of the progress in cellular arrest growth, while the average number of spots per nucleus is a quantitative measurement of the extension of the damage along the DNA. Moreover, DNA damage can be quantified by evaluating the percentage of γH2AX-positive cells, *i.e.* the percentage of cells showing DNA damage on the total number of cells.[194]

To determine if the damage is localized at the telomeres, it is necessary a co-immunostaining of DNA with both a DNA damage marker (γH2AX) and a telomeric marker (TRF1, one of the shelterin complex proteins); co-localization of these markers is called Telomere-Dysfunction Induced Foci (TIFs).[194,196] Telomere damage can be quantified by evaluating the percentage of TIF-positive cells, *i.e.* cells with more than four co-localizations per nucleus. Furthermore, co-localization analysis provides the main method to determine the ability of ligands to induce specific DNA damage at the telomeres *vs.* other DNA sites; in fact an easy count of the number of co-localizing *vs.* non co-localizing spots can give us the required information. Finally, the mean number of TIFs per cell is indicative of the intensity of telomere damage per single cell.[194]

Thus, BJ-EHLT cells – a human foreskin-derived fibroblast cell line, expressing the human telomerase reverse transcriptase (hTERT) and SV40 early region[197] – were treated for 24 h with 0.5 μM of each compound and the DNA damage was evaluated. To appreciate possible improvements in terms of biological activity of the analogs over lead compound **4**, the time and dose conditions previously optimized for **4** and able to induce a slight DNA damage were used. IF analysis showed relevant amounts of γH2AX, evidencing that all the tested ligands – with

the sole exception of **D4**, **S4-9**, and **S4-10** – induced similar DNA damage extent as the lead compound (Figure 71A).

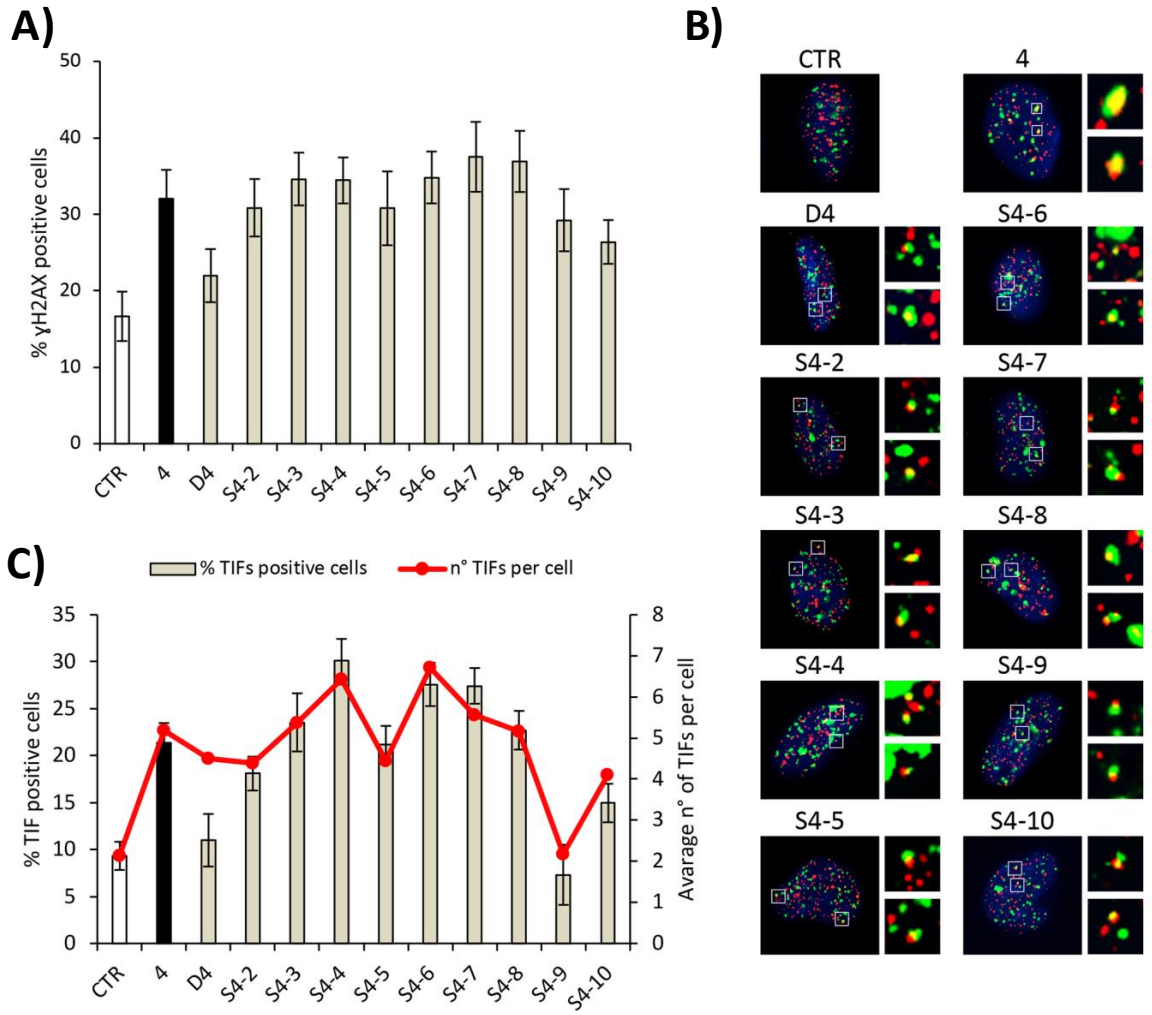

Figure 71. Compound **4** analogs induce telomeric DNA damage. BJ-EHLT fibroblasts were untreated (CTR, white bar) or treated for 24 h with **4** (black bar) and the indicated analogs (light-grey bars) at 0.5 μM concentration. Cells were processed for immunofluorescence (IF) using antibodies against γH2AX and TRF1 to visualize the DNA damage and telomeres, respectively. A) Percentages of γH2AX-positive cells. B) Representative merged images of IF of untreated and treated BJ-EHLT cells; γH2AX spots in green, TRF1 spots in red and nuclei in blue. Enlarged views of Telomere Induced Foci (TIFs) are reported on the right panels of each picture. The images were acquired with a Leica Deconvolution microscope (magnification 63x). C) Quantitative analysis of TIFs. The graph represents the percentages of TIF-positive cells (bars) and the mean number of TIFs for cell (red line) in the indicated samples. Cells with at least four γH2AX/TRF1 foci were scored as TIF positive. Histograms show the mean values ±S.D. of three independent experiments.

In parallel, we also evaluated whether the induced DNA damage was located at the telomeres (Figure 71B). Noteworthy, quantitative analysis confirmed and reinforced the previous observations, evidencing that all the compounds (with the only exception of **D4**, **S4-9**, and **S4-10**) induced a percentage of TIF positive cells and average number of TIFs per cell similar to lead compound **4** (Figure 71C). These data are consistent with those found by the G4-CPG assays, relative to the affinities of compound **4** and its analogs towards the telomeric model sequence, which proved to be in all cases similar.

Successively, to test the antitumor efficacy of compound **4** analogs, the cell colony-forming ability of the human cervical cancer cells, HeLa, untreated or treated with the different compounds, was evaluated. To set up the optimal dose of the drug, first a dose-response experiment was performed by using three different concentrations (0.5, 1 and 2 μM) of **4**: the 2 μM concentration proved to be the minimal effective dose and was thus selected for the successive tests (Figure 72A). Interestingly, cell survival experiments evidenced that derivatives **S4-4**, **S4-6**, **S4-8**, and **S4-10**, despite their high affinity for G4 structures *in vitro* (Table 5), were less effective than **4** in affecting tumour cell viability (Figures 72B and 72C). Compounds **D4** and **S4-3** also showed an antiproliferative activity lower than compound **4** (Figures 72B and 72C), which could be related, in this case, to an overall G4-affinity lower than compound **4** (Table 5). Conversely, the potent cytotoxic activity observed for derivatives **S4-2**, **S4-7** and **S4-9** (Figures 72B and 72C) might be attributed to non-specific, G4-independent, effects since these ligands showed either a good affinity also for duplex DNA (**S4-2** and **S4-7**) or, as in the case of **S4-9**, an affinity towards G4 structures generally lower than other analogs (Table 5). In summary, ligand **S4-5**, despite showing an antitumor activity similar to lead compound **4**, emerged as the most interesting ligand of this series. Indeed, its high affinity for G4 structures associated with null affinity for duplex DNA (Table 5) suggests a promisingly improved target specificity compared to the starting compound.

Finally, in order to evaluate the selectivity of **S4-5** in cell, the effects of this compound were also tested on normal cells. Briefly, human immortalized BJ fibroblasts (BJ-hTERT) were treated with **4** or **S4-5** at 1 and 2 μM concentrations and, after 6 days, the number of viable cells was evaluated. Remarkably, these experiments clearly evidenced that the cytotoxic effects of ligand **S4-5** on normal cells were definitely lower than those produced by compound **4** (Figure 73A). Moreover, IF analysis of γH2AX evidenced that **S4-5**, in contrast to **4**, was unable to induce an appreciable DNA damage in normal cells (Figures 73B and 73C). Overall, these data unambiguously indicated that **S4-5** has a much higher selectivity in killing cancer cells than lead compound **4**, making it a promising candidate drug.

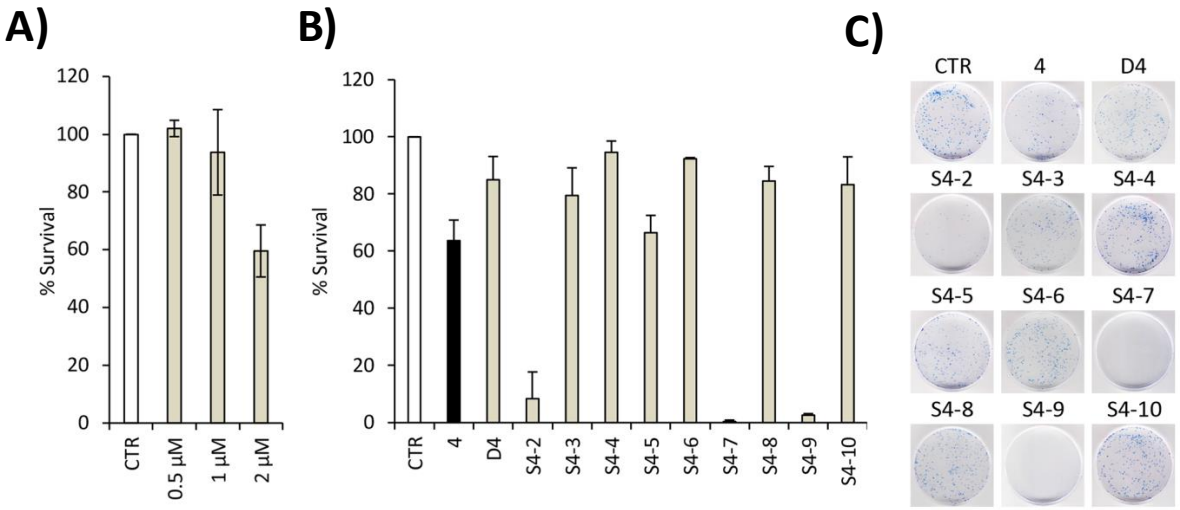

Figure 72. Anti-tumour efficacy of compound **4** analogs. A) Clonogenic activity of human cervical cancer cells, HeLa, untreated (CTR, white bar) or treated with **4** at the indicated doses. Surviving fractions were calculated as the ratio of absolute survival of the treated sample/absolute survival of the untreated sample. B) Clonogenic activity of HeLa cells, untreated (CTR, white bar), treated with **4** (black bar) or the indicated analogs (light-grey bars) at 2 µM dose. Surviving fractions were calculated as reported in A. C) Representative images of the clonogenic assay described in B. Histograms show the mean values ±S.D. of three independent experiments.

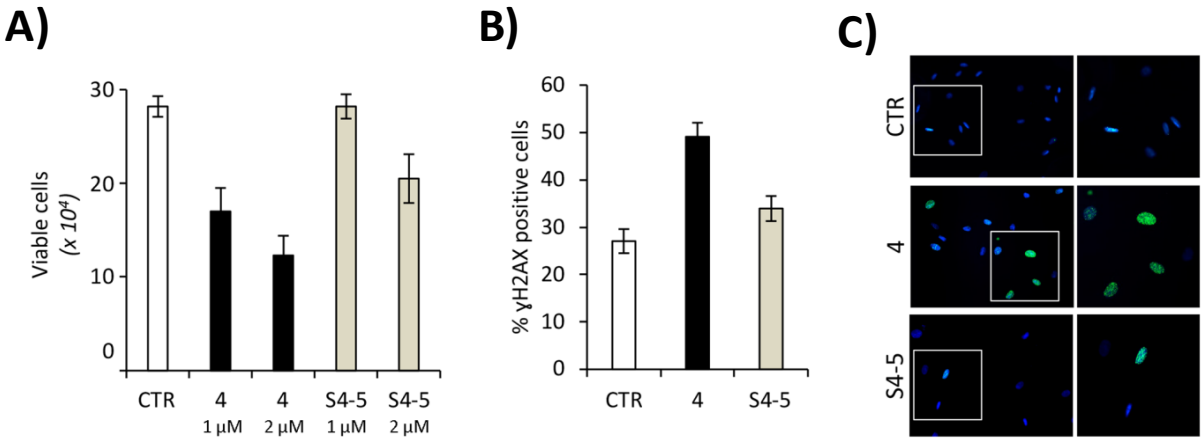

Figure 73. A) Human immortalized fibroblasts (BJ-hTERT) were treated with compound **4** or **S4-5** at the doses of 1 and 2 µM for 6 days. Viable cell number was determined by the Trypan Blue exclusion test. B) BJ-hTERT were treated with **4** or **S4-5** at the 1 µM dose for 24 h and processed for IF using antibodies against γH2AX. The histogram represents the percentages of γH2AX-positive cells. C) Representative merged images of IF: γH2AX spots in green and nuclei in blue. Histograms show the mean values ±S.D. of three independent experiments.

4.7 Experimental section

4.7.1 Chemistry

All commercial reagents and solvents were purchased from Sigma-Aldrich or Link Technologies, unless otherwise stated. The selected compounds were purchased from Life Chemicals Europe (Germany) and used without further purification. Compound supplier codes: F1094-0196 (**4**), F1217-0039 (**S4-1**), F1094-0208 (**S4-2**), F1094-0205 (**S4-3**), F1094-0204 (**S4-4**), F1094-0201 (**S4-5**), F1094-0200 (**S4-6**), F1094-0209 (**S4-7**), F1061-0006 (**S4-8**), F1094-0199 (**S4-9**), F1094-0203 (**S4-10**), F1094-0190 (**D4**).

4.7.2 G4-CPG assay

Long Chain AlkylAmine-CPG 1000 Å was functionalized with 3'-*O*-acetyl-5'-*O*-(4,4'-dimethoxytrityl)thymidine through a hexaethylene glycol spacer as previously described in section 2.4. Standard phosphoramidite chemistry on an automated Applied Biosystem 394 DNA/RNA synthesizer was used to obtain the oligonucleotide-functionalized CPG supports. In particular, using a 1 µmol-scale, "DMT-ON" protocol, the following oligonucleotides were assembled on the CPG supports: d[(TTAGGG)$_4$TT] (tel26), d(TGGGGAGGGTGGGGAGGGTGGGGAAGGTGGGGA) (cmyc), d(AGGGAGGGCGCTGGGAGGAGGG) (ckit1), d(CGGGCGGGCGCGAGGGAGGGG) (ckit2), d(AAGGGGAGGGGCTGGGAGGGCCCGGA) (hTERT1), and d(CGCGAATTCGCGTTTCGCGAATTCGCG) (ds27). The coupling efficiency of each base was monitored by spectrophotometric measurements of the DMT cation, released from the support by acidic treatment with 3% TCA in CH_2Cl_2 before the subsequent coupling step. Considering the number of couplings and the average yield per cycle of 99.8%, 99.7%, 99.9%, 99.7%, 99.9% and 99.2%, respectively for tel26, cmyc, ckit1, ckit2, hTERT1 and ds27, the overall yield was determined to be 95%, 91%, 98%, 94%, 98%, and 80%. Stock solutions of each tested compound were prepared by dissolving a weighed amount of the solid compound in pure DMSO. G4-CPG binding assays were performed as described in section 3.5. The UV measurements were performed on a JASCO V-550 UV-vis spectrophotometer equipped with a Peltier Thermostat JASCO ETC-505T. The UV quantification of the ligands was determined by measuring the absorbance relative to the λ_{max} characteristic of each ligand and referring it to the corresponding calibration curves. A quartz cuvette with a path length of 1 cm was used.

4.7.3 CD experiments

CD spectra were recorded in a quartz cuvette with a path length of 1 cm on a Jasco J-715 spectropolarimeter equipped with a Peltier-type temperature control system (model PTC-348WI). The spectra were recorded at 20 °C in the range 240-800 nm with 2 s response, 200 nm/min scanning speed, 2.0 nm bandwidth, and corrected by subtraction of the background scan with buffer. All the spectra were averaged over 3 scans. The oligonucleotides d[(TTAGGG)$_4$TT] (tel26), d(TGGGGAGGGTGGGGAGGGTGGGGAAGGTGGGGA) (cmyc) and d(CGCGAATTCGCGTTTCGCGAATTCGCG) (ds27) were synthesized by standard automated solid phase oligonucleotide synthesis on an Applied Biosystem 394 DNA/RNA synthesizer. After ammonia treatment (55 °C, 12 h) allowing both deprotection and detachment from the solid support, the crude oligonucleotides were purified by HPLC on a SAX analytical column and then dialyzed against water using a Float-A-Lyzer G2 dialysis device (MWCO 0.5-1.0 kDa, three H_2O changes over 24 h). After lyophilization, the oligonucleotides were dissolved in a 20 mM KCl, 5 mM KH_2PO_4, 10% DMSO buffer (pH 7) to obtain 2 μM solutions, then annealed by heating to 95 °C for 5 min, followed by slow cooling to room temperature. The ligand stock solutions were 4 mM in DMSO. CD titrations were obtained by adding increasing amounts of the ligands (up to 5 molar equivalents, corresponding to a 10 μM solution in ligand) to tel26, cmyc and ds27. After each ligand addition, the system was allowed equilibrating before recording the spectra. For the CD-melting experiments, the ellipticity was recorded at 290, 263 and 251 nm for tel26, cmyc and ds27, respectively, with a temperature scan rate of 0.5 °C/min in the range 20-90 °C.

4.7.4 NMR experiments

NMR experiments were performed on a 700 MHz Varian Unity INOVA spectrometer. One dimensional ^{1}H NMR spectra of the samples in H_2O were recorded at 25 °C using pulsed-field gradient DPFGSE for H_2O suppression. Data were processed on iMAC running iNMR software (www.inmr.net). DNA samples were prepared at 0.2-0.4 mM strand concentration in 0.6 mL of H_2O/D_2O (9:1) buffer solution. The following oligonucleotides were used for the NMR experiments: the truncation of human telomeric sequence d[TTGGG(TTAGGG)$_3$A] (m-tel24), the d(TGAGGGTGGGTAGGGTGGGTAA) sequence from the NHE III element of the c-myc oncogene (myc22), containing two G to T substitutions (G14/T and G23/T, numbering according to Ambrus *et al.*), and the self-complementary duplex-forming dodecamer d(CGCGAATTCGCG) (ds12). In order to avoid different G4 foldings or conformational

heterogeneity in solution, DNA samples were prepared using the appropriate experimental conditions adopted for the determination of their 3D structures. Thus, the following buffers containing 10% D_2O were used: 25 mM KH_2PO_4, 70 mM KCl, 0.2 mM EDTA (pH 7.0) for myc22 and m-tel24; 20 mM NaH_2PO_4, 200 mM NaCl (pH 7.0) for ds12. The samples were heated at 90 °C for 5 min and then slowly cooled to room temperature overnight to achieve the correct folding of the oligonucleotides. Aliquots of **4** and **S4-5** stock solutions in DMSO-d_6 were directly added to the DNA solution inside the NMR tube; the final DMSO concentration was 14%. A control titration was also performed by adding DMSO-d6 alone to the DNA solution.

4.7.5 Microscale thermophoresis (MST) experiments

MST measurements were performed using the Monolith NT.115 (Nanotemper Technologies, Munich, Germany). The Cy5-fluorescently labeled tel26 and myc22 oligonucleotides (Biomers) were prepared in 5 mM potassium phosphate buffer (pH 7.0) containing 20 mM KCl supplemented with 0.1% Tween. The concentration of the labeled oligonucleotide was kept constant at 80 nM, while a serial dilution of the ligand (1:2 from 4 mM ligand stock solution in 100% DMSO) in the same buffer used for DNAs was prepared and mixed with the oligonucleotide solution with a volume ratio of 1:1. All the samples, containing 8% DMSO as the final concentration, were loaded into standard capillaries (NanoTemper Technologies). Measurements were performed at 20 °C, using auto-tune LED power and medium MST power. MST data analysis was performed by employing the MO. software. Affinity Analysis software (v2.3) provided with the instrument. Plots were rendered with GUSSI version 1.2.1 software (http://biophysics.swmed.edu/MBR/software.html).

4.7.6 Molecular docking

The latest version of the docking software AD4 (version 4.2), along with its graphical user interface AutoDockTools (ADT), were employed. The NMR structures used for the docking studies had the following PDB codes: 2JPZ, and 1XAV. The DNA G4s were prepared for the docking using the Maestro suite (Schrödinger Release 2017-2: Maestro, Schrödinger, LLC, New York, NY, 2017), which assigns bond orders, adds hydrogen atoms, deletes water molecules and generates the appropriate protonation states. The 2D Sketcher tool of Maestro was used to build **S4-5**. Of this ligand, the protonation, tautomeric, and isomeric states were calculated through LigPrep, part of the same suite. The ligand and the G4 DNA structures were

converted to the AD4 specific file format (PDBQT) using the python scripts prepare_ligand4.py and prepare_receptor4.py, part of ADT, applying the standard settings. The docking area was centered on the DNA center of mass. For each G4 structure, a set of grids of 60 Å × 60 Å × 60 Å with 0.375 Å spacing was calculated around the docking area for the ligand atom types using AutoGrid4. For each G4, 100 separate docking calculations were performed. Each docking calculation consisted of 10 million energy evaluations using the Lamarckian genetic algorithm local search (GALS) method. The GALS method evaluates a population of possible docking solutions and propagates the most successful individuals from each generation into the subsequent generation of possible solutions. A low-frequency local search according to the method of Solis and Wets is applied to docking trials to ensure that the final solution represents a local minimum. All dockings were performed with a population size of 250, and 300 rounds of Solis and Wets local search were applied with a probability of 0.06. A mutation rate of 0.02 and a crossover rate of 0.8 were used to generate new docking trials for subsequent generations, and the best individual from each generation was propagated over the successive generation. The docking results from each of the 100 calculations were clustered on the basis of root-mean square deviation (rmsd) (solutions differing by less than 2.0 Å) between the Cartesian coordinates of the atoms and were ranked on the basis of the free energy of binding (ΔG_{AD4}). Molecular modeling figures were rendered using the UCSF Chimera software.

4.7.7 Biological experiments

Cells and culture condition. Human fibroblasts (BJ) and human cervical cancer cells (HeLa) were obtained as previously reported. BJ-hTERT cells were obtained infecting primary BJ cells with a retrovirus carrying hTERT (Addgene plasmid #1773); BJ-EHLT derived from the transformation of BJ fibroblasts with hTERT and SV40 early region (BJ-EHLT).[197] BJ-hTERT, BJ-EHLT and HeLa were grown in Dulbecco Modified Eagle Medium (DMEM, Invitrogen Carlsbad, CA, USA) supplemented with 10% Fetal Bovine Serum (FBS), 2 mM L-glutamin and antibiotics at 37°C in a 5% CO_2-95% air atmosphere.

Immunofluorescence. Cells were fixed in 2% formaldehyde and permeabilized in 0.25% Triton X-100 in phosphate buffered saline (PBS) for 5 min at r.t. For immune-labeling, cells were incubated with primary antibody for 2 h at r.t., washed twice in PBS and finally incubated with the secondary antibodies for 1 h. The following primary antibodies were used: Mouse mAb anti-γH2AX (Millipore, Billerica, MA, USA) and Rabbit pAb anti-TRF1 N19 (Santa Cruz Biotechnologies, Santa Cruz, CA, USA). The following secondary antibodies were used: Anti-

Mouse IgG (H+L), F(ab')$_2$ Fragment (Alexa Fluor 488 Conjugate) (Cell Signaling) and Anti-rabbit IgG (H+L), F(ab')$_2$ Fragment (Alexa Fluor 555 Conjugate) (Cell Signaling). Nuclei were stained with 4',6-diamidino-2-phenylindole (DAPI, Sigma). Fluorescence signals were recorded by using a Leica DMIRE2 microscope equipped with a Leica DFC 350FX camera and elaborated by Leica FW4000 deconvolution software (Leica, Solms, Germany). For quantitative analysis of γH2AX positivity, 300 cells on triplicate slices were scored. For TIF analysis, a single plane was analyzed, and 30 γH2AX-positive cells were scored. Cells with at least four co-localizations (γH2AX/TRF1) were considered as TIF-positive.

Clonogenic assay. Human cervical cancer cells, HeLa, were seeded in 60 mm-Petri dishes at the clonogenic density of 500 cells/plate in DMEM medium with 10% FBS. After 24 h, cells were treated with compound **4** or its analogues at 2 μM concentration. After 10 days, the cells were stained with 2% methylene blue in 50% ethanol and the number of colonies was counted. Surviving fractions were calculated as the ratio of absolute survival of the treated sample/absolute survival of the untreated sample.

Cell viability. BJ-hTERT fibroblasts were seeded in 60-mm Petri dishes at a density of 5×10^4 cells/plate. After 24 h from plating, cells were treated with compound **4** or **S4-5** at the doses of 1 and 2 μM. Cell viability (Trypan Blue dye exclusion) was determined after 6 days from treatment.

CHAPTER 5 – SCREENING AND EVALUATION OF A LIBRARY OF NAPHTHALENE DIIMIDES

5.1 Introduction

In the search for G-quadruplex selective ligands, naphthalene diimides (NDIs) emerged as promising compounds for their well-proved ability to interact with G-tetrads, chemical accessibility and possibility to easily functionalize their aromatic cores with multiple, diverse pendant groups, thus allowing a fine modulation of their affinity towards different secondary structure-forming oligonucleotides.[142,198,199] Indeed, it has been shown that the substitution pattern of the NDI core as well as the chemical nature of the substituents play a crucial role in G4 binding and selectivity toward G4 *vs.* duplex DNA.[141,142] For these peculiar features, NDIs have been extensively studied both as fluorescent probes and oligonucleotide-targeting ligands.[200,201]

Recently, a series of monomeric NDIs with alkylamine substituents on the naphthalene core (**1a**-**4a** and **1-Br**, Figure 74) were synthesized by prof. Mauro Freccero's group at the Department of Chemistry of University of Pavia. These compounds proved to have excellent water solubility and cellular entry, thus emerging as promising compounds for both therapeutic and diagnostic applications.[139,202] In particular, the tetra-substituted compound **4a** was able to generate singlet oxygen species, which produced photo-induced cytotoxicity.[202,203] Its efficient nuclear uptake was evidenced by fluorescence confocal imaging exploiting the intrinsic NDI fluorescence.[202]

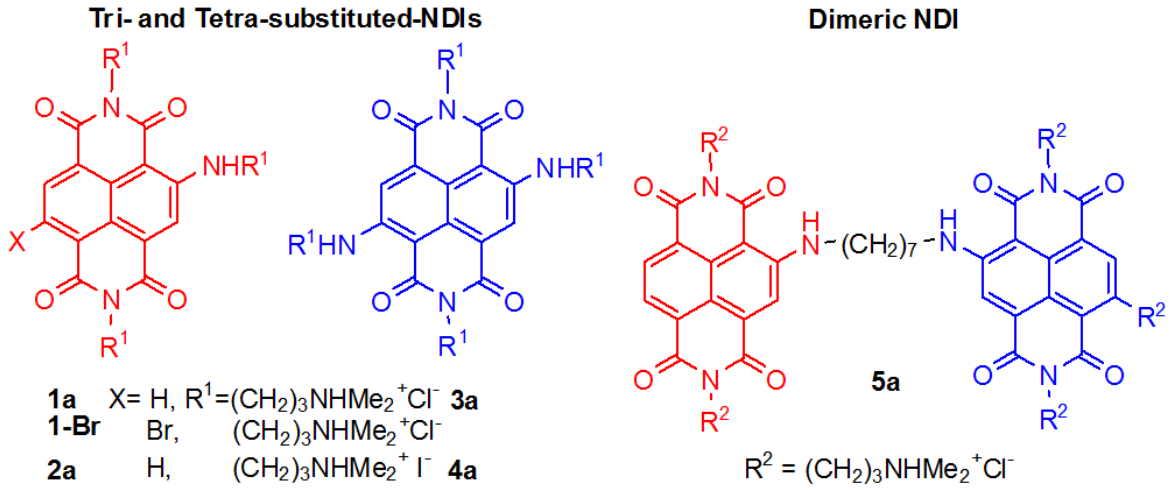

Figure 74. Chemical structures of previously synthesized tri-, tetra-substituted and dimeric naphthalene diimides.[139,204]

The chemical diversity of this class of compounds was further expanded producing the dimeric NDI **5a** (Figure 74), obtained by coupling **1a** with **3a** connected through a $–(CH_2)_7–$ flexible spacer.[204] Remarkably, this NDI has appealing properties for *in vivo* applications aiming at detecting and targeting G4 structures.[204] In fact, the non-fluorescent **5a** compound, containing both a red and a blue NDI dyes, becomes red emitting upon G4 binding. Moreover, its average fluorescence lifetime is significantly different if **5a** interacts with a G4 or with a duplex DNA, and this property can represent a key feature for the development of new rationally engineered G4-based sensors for detection applications.[204] In addition, although compound **5a** did not discriminate between the different G4 structures investigated, it exhibited a good G4 *vs.* duplex DNA selectivity,[204] which made it an interesting lead compound for the design of novel putative G4-selective ligands.

Here we focus on the potential of this class of G-quadruplex targeting NDIs as therapeutic agents. To this purpose, several novel NDI analogs have been synthesized by Freccero's group. In detail, a novel library of derivatized NDIs, including the monomeric **1-4** (Figure 75), used as controls, as well as the dimeric systems **5-12,** (Figure 76) were designed and characterized, aiming at enhancing the G4 *vs.* duplex selectivity of **5a** and testing the ability of novel functionalized dimeric NDIs to discriminate diverse G4 conformations.

The design of these novel putative G4-binders has been conceived following a general strategy recently proposed, counterintuitively based on the reduction of the overall ligand affinity for G4s.[205] The main idea is based on the evidence that the most potent ligands strongly interact with all DNA structures, regardless of their identity and conformation. Therefore, a possible way to potentiate their target selectivity is by reduction of their overall affinity. Most well-studied G4-ligands carry amine moieties,[125,133,135,137,139] which being protonated at physiological pH are strongly attracted by the oligonucleotide backbone negative charges. Within the set of here investigated NDI derivatives, unspecific interactions resulting from electrostatic attractions between the oligonucleotide phosphates and the protonated ammonium groups are removed by making the NDIs intrinsically neutral. In this way, some degrees of affinity are lost, but the core selectivity can emerge.

To this aim, eight new dimeric NDIs (Figure 76) were synthesized by linking one NDI unit displaying dimethyl amine groups, positively charged at physiological pH, with a second NDI unit functionalized with carboxylic groups, which at physiological pH are negatively charged. The here designed molecules should maintain charge neutrality at physiological pH, thus disfavouring the above unspecific electrostatic interactions. The nature of the spacer and the substituents on the aromatic core was also modulated. In detail, the here studied dimeric NDIs

contain –$(CH_2)_7$– or –$(CH_2CH_2O)_2CH_2CH_2$– connecting spacers and bear $(CH_2)_5COOH$, $(CH_2)_5COOMe$ or $(CH_2)_3N(CH_3)_2$ pendant groups on the imide nitrogen atoms, and $NH(CH_2)_3N(CH_3)_2$, Br or no substituent on the naphthalene cores (Figure 76). In parallel, monomeric NDIs (Figure 75) functionalized with similar substituents as in the dimeric structures, *i.e.* $NH(CH_2)_2CH_3$, $NH(CH_2)_3N(CH_3)_2$, $NH(CH_2)_7NH_2$ or $NH(CH_2CH_2O)_2CH_2CH_2NH_2$, and bearing the same pendant groups on the imide nitrogen atoms, *i.e.* $(CH_2)_3N(CH_3)_2$, were also synthesized and characterized. All these derivatives were then evaluated by the G4-CPG assay and successively analyzed by biological and biophysical experiments.

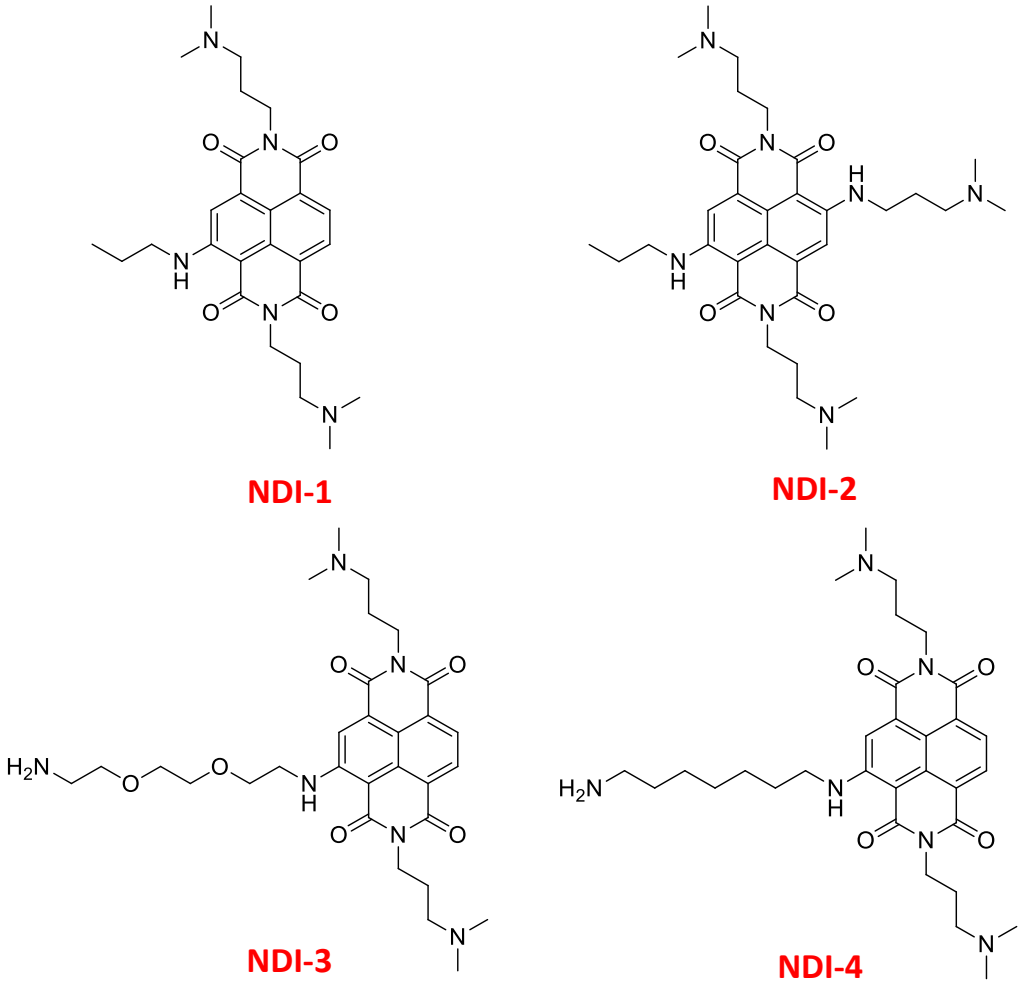

Figure 75. Chemical structures of the monomeric naphthalene diimides here investigated.

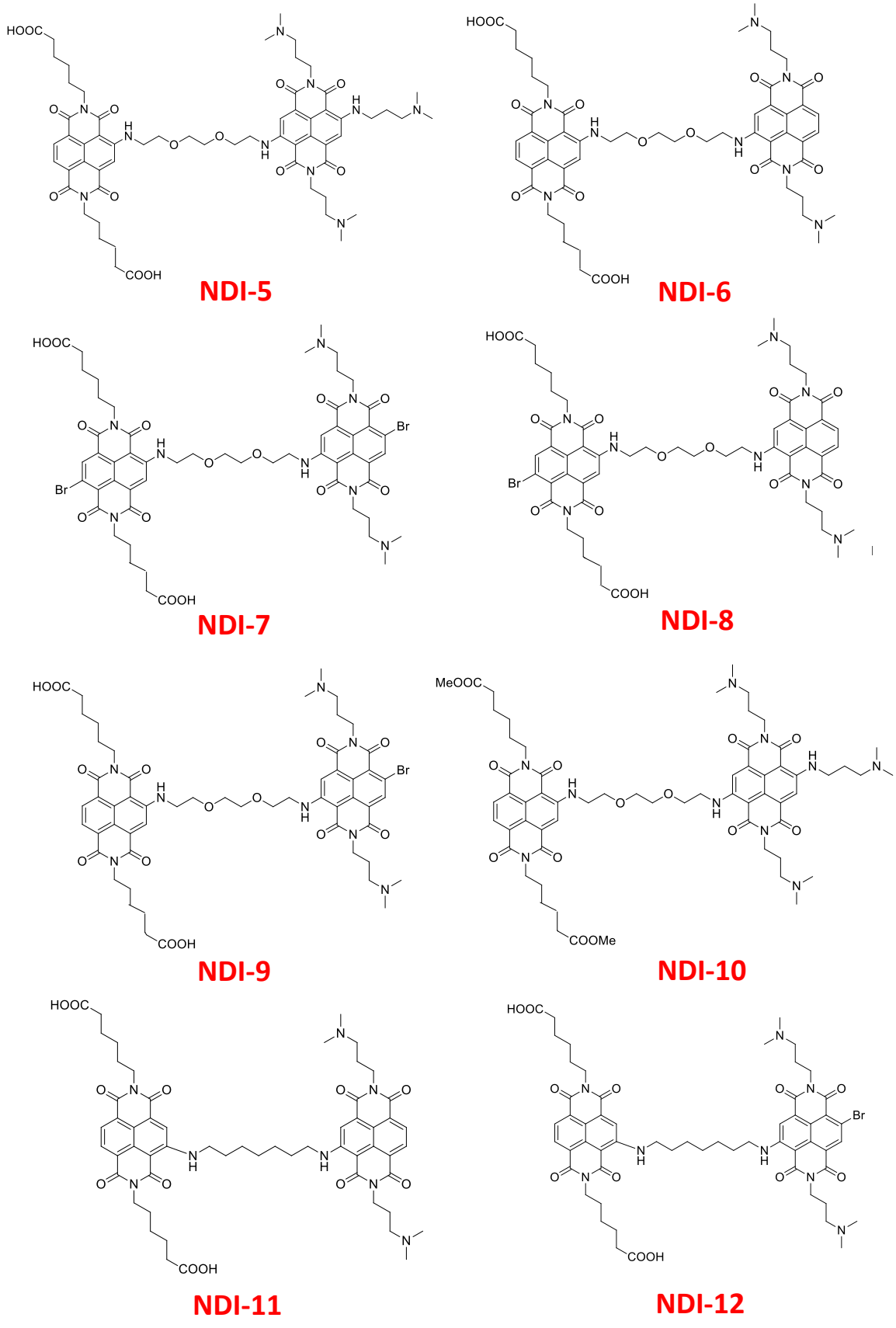

Figure 76. Chemical structures of the dimeric naphthalene diimides here investigated.

5.2 Experimental screenings by the G4-CPG assay

With the aim of further expanding the potential of the G4-CPG assay and extending it to longer sequences able to fold into multiple consecutive G4 structures, better mimicking the multimers formed by telomeric G-quadruplexes,[78,82] the CPG support has been functionalized with the 46-mer oligonucleotide of sequence d[AGGG(TTAGGG)$_7$] (tel46),[206,207] modelling the human telomeric DNA and able to form an intramolecular dimeric G4.[87] Then, we tested the library of the novel naphthalene diimides depicted in Figures 75 and 76 on four CPG supports: two systems functionalized with the telomeric sequences tel26 and tel46,[82] respectively, one with the extra-telomeric sequence cmyc,[101] and one with the control duplex ds27. Before performing the binding assays with the novel compounds, the tel46-functionalized support was first tested in its ability to bind known G4 ligands with different affinity for G4 structures, similarly to what previously carried out with CPG-tel26, CPG-cmyc and CPG-ds27. In detail, BRACO-19 (Figure 30, left), TMPyP4, TO, resveratrol and 9-Acr-COOH (Figure 42) were used as model molecules, known to have very high (BRACO-19, TMPyP4 and TO)[125,174,208] or low-to-null (resveratrol and 9-Acr-COOH)[175,177] affinity for G4 structures. The obtained data (Table 7), showing high affinity (bound ligand > 97%) for BRACO-19, TMPyP4 and TO, and very low affinity for resveratrol and 9-Acr-COOH (bound ligand ≤ 4%), proved the efficacy of the tel46-functionalized CPG support (tel46-**2**).

The binding assays were performed as described in Chapter 3. Ligand stock solutions were prepared by dissolving a weighed amount of the solid compound in H_2O or pure DMSO, respectively for the monomeric and dimeric naphthalene diimides. All the compounds proved to be well soluble in the washing/releasing solutions used in our binding assays and at the concentration chosen for the binding experiments. After solubility checks for all the tested compounds, we first verified the absence of unspecific binding on the solid support by incubating them with the nude CPG (Figure 41A) and then, all the investigated ligands were tested on the G4s- and hairpin duplex-functionalized CPG supports. The results of the binding assays are reported in Table 8 and Figures 77-80, showing no significant unspecific interactions with the solid support for the tested NDIs, as well as the quantitative recovery of the bound ligands by using washings with the releasing solutions.

All the analyzed ligands exhibited good affinity for tel26 and cmyc monomeric G4s immobilized on the solid supports, with monomeric NDIs showing higher affinity than dimeric compounds (Table 8 and Figures 77-80).

Table 7. Summary of the binding assay data obtained for tel46-**2** through UV measurements.

	Support **2**	
Ligand	**tel46-bound ligand (%)[a,c]**	**Recovered ligand from tel46-2 (%)[b,c]**
BRACO-19	100	89
TMPyP4	100	86
TO	97	96
Resveratrol	4	99
9-Acr-COOH	0	-

[a]tel46-bound ligand (%) was calculated as a difference from the unbound ligand recovered with the washing solution 50 mM KCl, 10% DMSO, 10% CH_3CH_2OH

[b]Recovered ligand from tel46-**2** (%) was obtained using as releasing solution either 2.5 M $CaCl_2$,15% DMSO or 100% DMSO

[c]The amounts of bound/recovered ligands are expressed as percentage of the quantity initially loaded on the support; the errors associated to the reported percentages are within ± 2%.

Moreover, the tested compounds proved to be stronger binders for tel46 than tel26 and cmyc G4s (Table 8), however being generally all effective G4 ligands, also in comparison with known G4 binders (Tables 2 and 7). Among all the investigated compounds, **NDI-8** and **NDI-9** showed the lowest affinity for G4s. On the other hand, the best G4 ligands appeared to be **NDI-3** and **NDI-4** for their ability to tightly interact with both telomeric and extra-telomeric G4s (Table 8).

In order to evaluate the G4s *vs.* duplex DNA selectivity, all the compounds were also tested in their interaction with the ds27 hairpin duplex-forming oligonucleotide. Overall, all the ligands proved to be able to effectively discriminate G4- *vs.* duplex-forming oligonucleotides, except **NDI-11** and **NDI-12** (Table 8 and Figures 79-80). In Table 9 selectivity indexes are reported, calculated as the ratio between the percentages of ligand bound to G4s- and hairpin duplex-functionalized supports. In detail, **NDI-3**, **NDI-4** and **NDI-6** recognized both telomeric sequences (tel26 and tel46) and cmyc with a twice-higher affinity than ds27, while **NDI-8** and **NDI-9** bound tel26, tel46 and cmyc more than five times stronger compared to ds27 (Table 9). Overall, the best G4 *vs.* duplex selectivity was found for the weaker G4 binders **NDI-8** and **NDI-9**, corroborating the initial hypothesis that losing some affinity allows the NDI core

selectivity emerging. On the other hand, these ligands showed similar affinity towards the two telomeric sequences, as well as no ability to discriminate between the two monomeric tel26 and cmyc G4s (Table 9).

Therefore, considering their good affinity for the G4 sequences and high G4s *vs.* duplex DNA selectivity, **NDI-3**, **NDI-4**, **NDI-6**, **NDI-8** and **NDI-9** proved to be the most promising ligands. Thus, we decided to further investigate these five compounds and evaluate their cytotoxic activity on both cancer and normal cells.

Table 8. Summary of the binding assays data for monomeric and dimeric naphthalene diimides on nude and functionalized CPG supports.

Compound	**Bound ligand (%)**[a]				
	Nude CPG	**CPG-tel26**	**CPG-tel46**	**CPG-cmyc**	**CPG-ds27**
NDI-1	4	85	98	95	50
NDI-2	0	92	99	98	46
NDI-3	0	100	100	97	48
NDI-4	7	97	100	95	41
NDI-5	5	90	100	87	71
NDI-6	15	85	85	79	34
NDI-7	11	73	82	78	38
NDI-8	5	41	51	26	3
NDI-9	0	67	72	64	12
NDI-10	4	84	100	87	57
NDI-11	14	77	55	75	61
NDI-12	14	75	60	79	71

[a]Bound ligand is calculated as a difference from the unbound ligand, recovered with 50 mM KCl, 10% DMSO, 10% CH_3CH_2OH washing solution, and expressed as % of the amount initially loaded on the support. The errors associated with the % are within ± 2%.

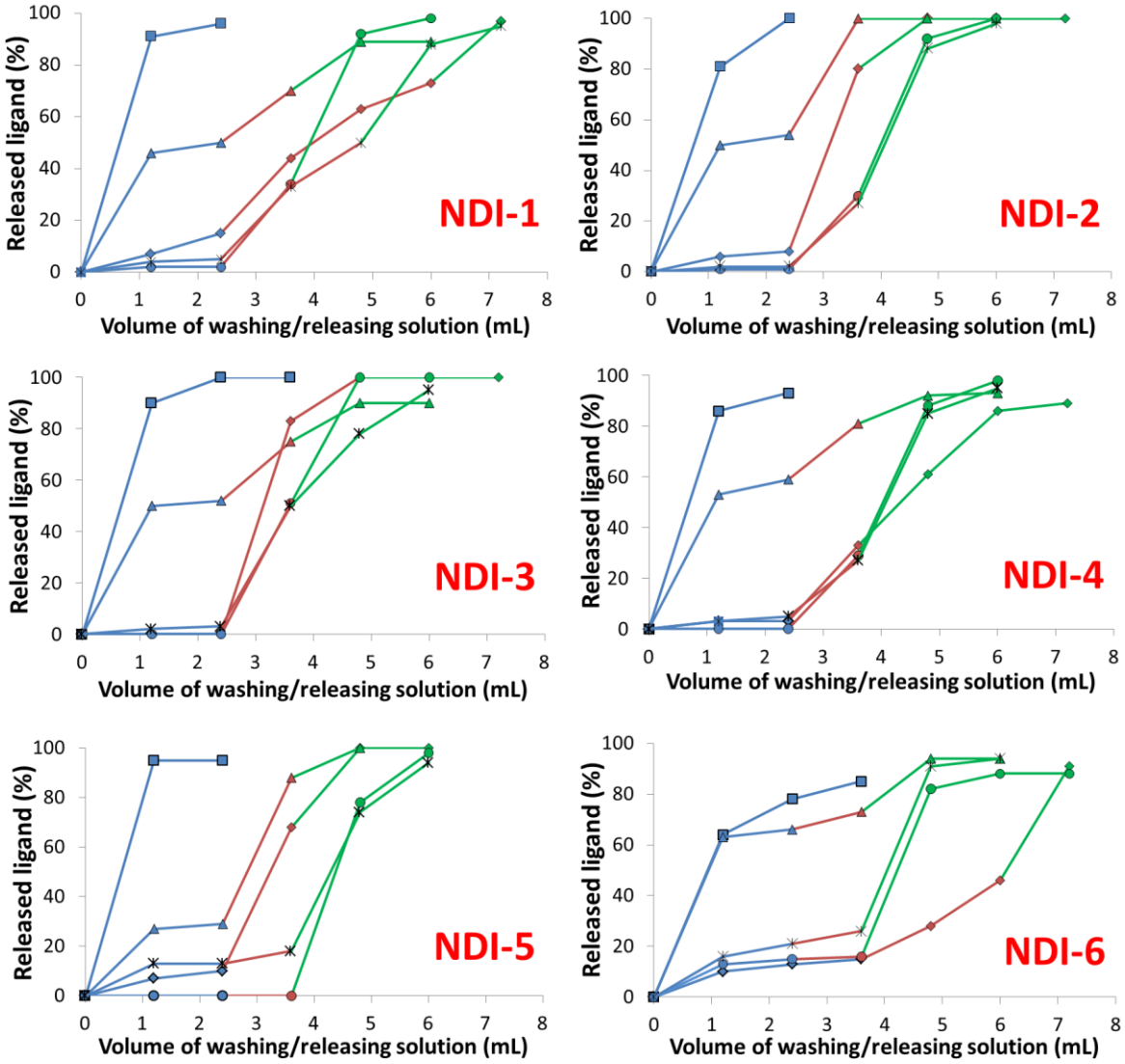

Figure 77. Amount of the released ligands **NDI1-NDI6**, expressed as percentage of the quantity loaded on nude CPG (-■-), CPG-tel26 (-♦-), CPG-tel46 (-●-), CPG-cmyc (-∗-) and CPG-ds27 (-▲-) as a function of the volume of the washing solution 50 mM KCl, 10% DMSO, 10% CH_3CH_2OH (blue line) and the releasing solutions 2.5 M $CaCl_2$, 15% DMSO (red line) or pure DMSO (green line). The errors associated with the % are within ± 2%.

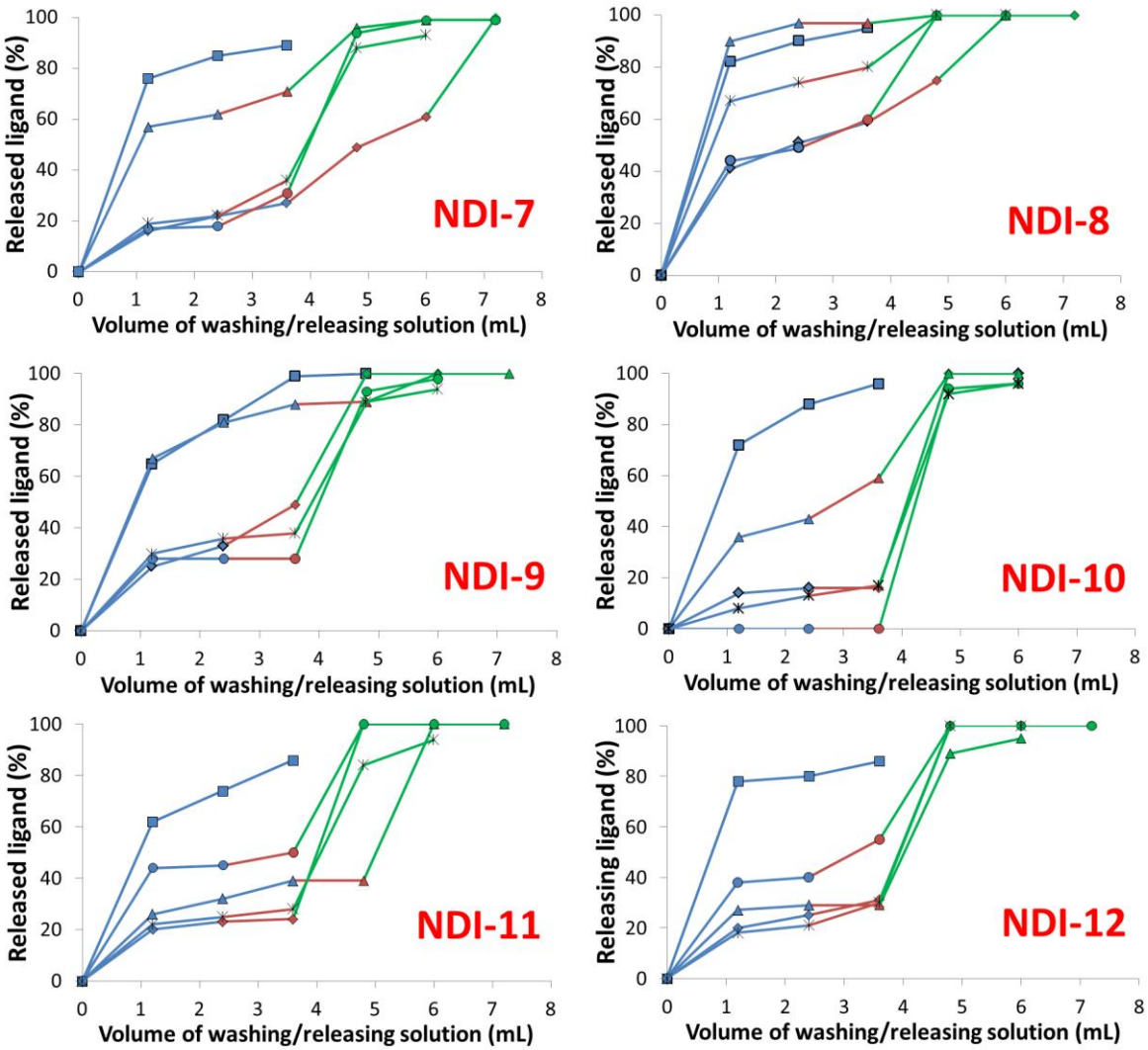

Figure 78. Amount of the released ligands **NDI7**-**NDI12**, expressed as percentage of the quantity loaded on nude CPG (-■-), CPG-tel26 (-♦-), CPG-tel46 (-●-), CPG-cmyc (-∗-) and CPG-ds27 (-▲-) as a function of the volume of the washing solution 50 mM KCl, 10% DMSO, 10% CH_3CH_2OH (blue line) and the releasing solutions 2.5 M $CaCl_2$, 15% DMSO (red line) or pure DMSO (green line). The errors associated with the % are within ± 2%.

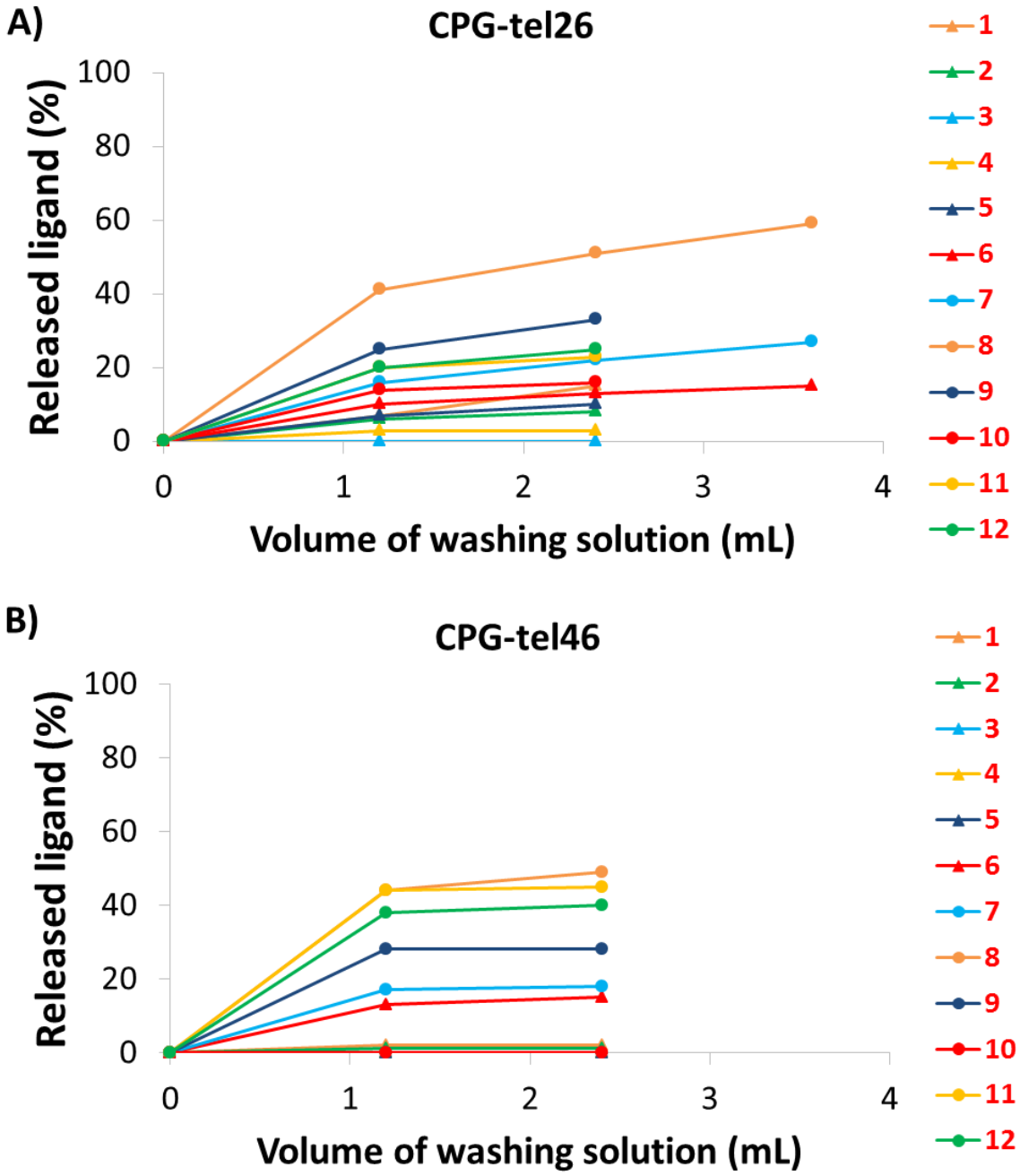

Figure 79. Amount of the released ligands **NDI1**-**NDI12**, expressed as percentage of the quantity loaded on A) CPG-tel26 and B) CPG-tel46 as a function of the volume of the washing solution (50 mM KCl, 10% DMSO, 10% CH_3CH_2OH). The errors associated with the % are within ± 2%.

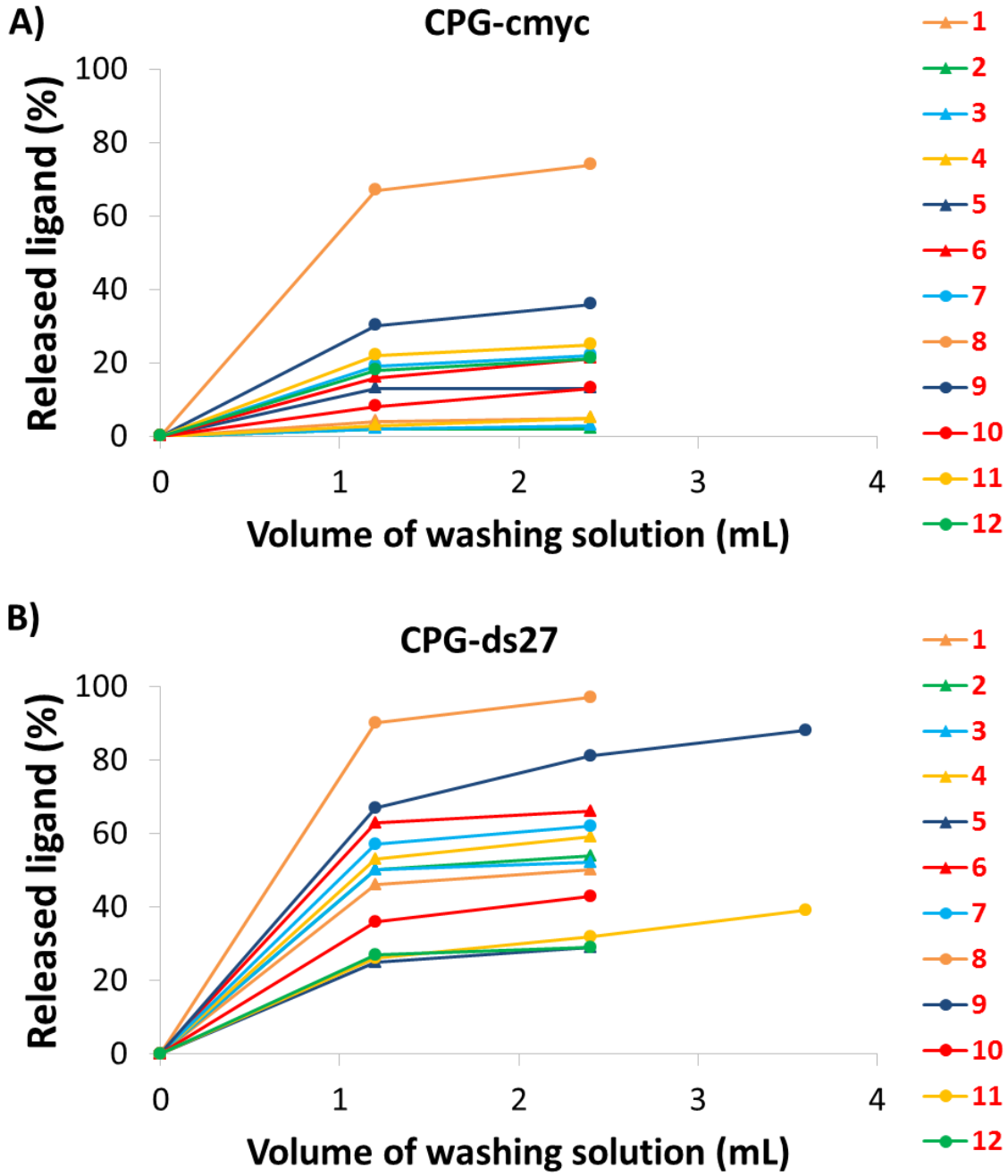

Figure 80. Amount of the released ligands **NDI1-NDI12**, expressed as percentage of the quantity loaded on A) CPG-cmyc and B) CPG-ds27 as a function of the volume of the washing solution (50 mM KCl, 10% DMSO, 10% CH_3CH_2OH). The errors associated with the % are within ± 2%.

Table 9. Selectivity indexes calculated as the ratio between the percentages of ligand bound to the indicated G4s- and hairpin duplex-functionalized supports.

Compound	Selectivity index				
	CPG-tel26/ CPG-ds27	**CPG-tel46/ CPG-ds27**	**CPG-cmyc/ CPG-ds27**	**CPG-tel46/ CPG-tel26**	**CPG-tel26/ CPG-cmyc**
NDI-1	1.7	2.0	1.9	1.2	0.9
NDI-2	2.0	2.2	2.0	1.1	0.9
NDI-3	2.1	2.1	2.0	1.0	1.0
NDI-4	2.4	2.4	2.3	1.0	1.0
NDI-5	1.3	1.4	1.2	1.1	1.0
NDI-6	2.5	2.5	2.3	1.0	1.1
NDI-7	1.9	2.2	2.0	1.1	0.9
NDI-8	13.7	17.0	8.7	1.2	1.6
NDI-9	5.6	6.0	5.3	1.1	1.0
NDI-10	1.5	1.8	1.5	1.2	1.0
NDI-11	1.3	0.9	1.2	0.7	1.0
NDI-12	1.1	0.8	1.1	0.8	0.9

5.3 Biological assays

In order to evaluate the antiproliferative activity of dimeric compounds **NDI-6**, **NDI-8** and **NDI-9** and monomeric compounds **NDI-3**, **NDI-4**, *in vitro* experiments were carried out in collaboration with dr. Annamaria Biroccio's group at Regina Elena Cancer Research Institute in Rome.

Human transformed fibroblasts (BJ-EHLT) were treated for 24 h with five different concentrations of NDIs (from 0.05 to 1 μM) and the DNA damage was evaluated. IF analysis showed relevant amounts of γH2AX, evidencing that the ligands **NDI-8**, **NDI-3** and **NDI-4** were able to induce DNA damage to a greater extent than **NDI-6** and **NDI-9** (Figure 81A). The same assay was also performed on normal human fibroblasts (BJ-hTERT) for **NDI-8**, **NDI-3** and **NDI-4** at the lowest concentration found, for each compound, to induce a DNA damage in more than 50% of the treated cells (Figures 81B and 81C). The effects of these compounds on normal cells proved to be twice less marked than on transformed BJ-EHLT cells (Figure 81C). In parallel, for the three most active compounds tested at the same concentration (0.5 μM), it was also evaluated whether the induced DNA damage was located at the telomeres (Figure 81D). Notably, quantitative analysis showed that **NDI-8** induced significant and higher percentage of TIF positive cells and average number of TIFs per cell than **NDI-3** and **NDI-4** (Figure 81E). These data are consistent with the ones obtained by the G4-CPG assay confirming the ability of **NDI-8** to selectively target telomeric sequences and discriminate duplex DNA better than all the other investigated ligands.

Successively, to test the antitumor efficacy of compounds **NDI-6**, **NDI-8**, **NDI-9**, **NDI-3** and **NDI-4**, the cell colony-forming ability of the human cervical cancer cells, HeLa, untreated or treated with the different compounds, was evaluated (Figure 82). Dose-response experiments were performed by using different concentrations of the tested compounds and IC_{50} values were calculated (Figure 82A). **NDI-8**, **NDI-3** and **NDI-4** proved to be highly cytotoxic, with IC_{50} values in the low nanomolar range (6.6, 52 and 64 nM, respectively). Interestingly, cell survival experiments evidenced a good correlation between the antiproliferative activity and the relative G4s affinities obtained by G4-CPG assay (Table 8). Indeed, compounds **NDI-6** and **NDI-9**, found weaker G4 binders than **NDI-3** and **NDI-4**, proved to be the least active ones, while **NDI-3** and **NDI-4**, which were the strongest G4 ligands, were among the most active ones.

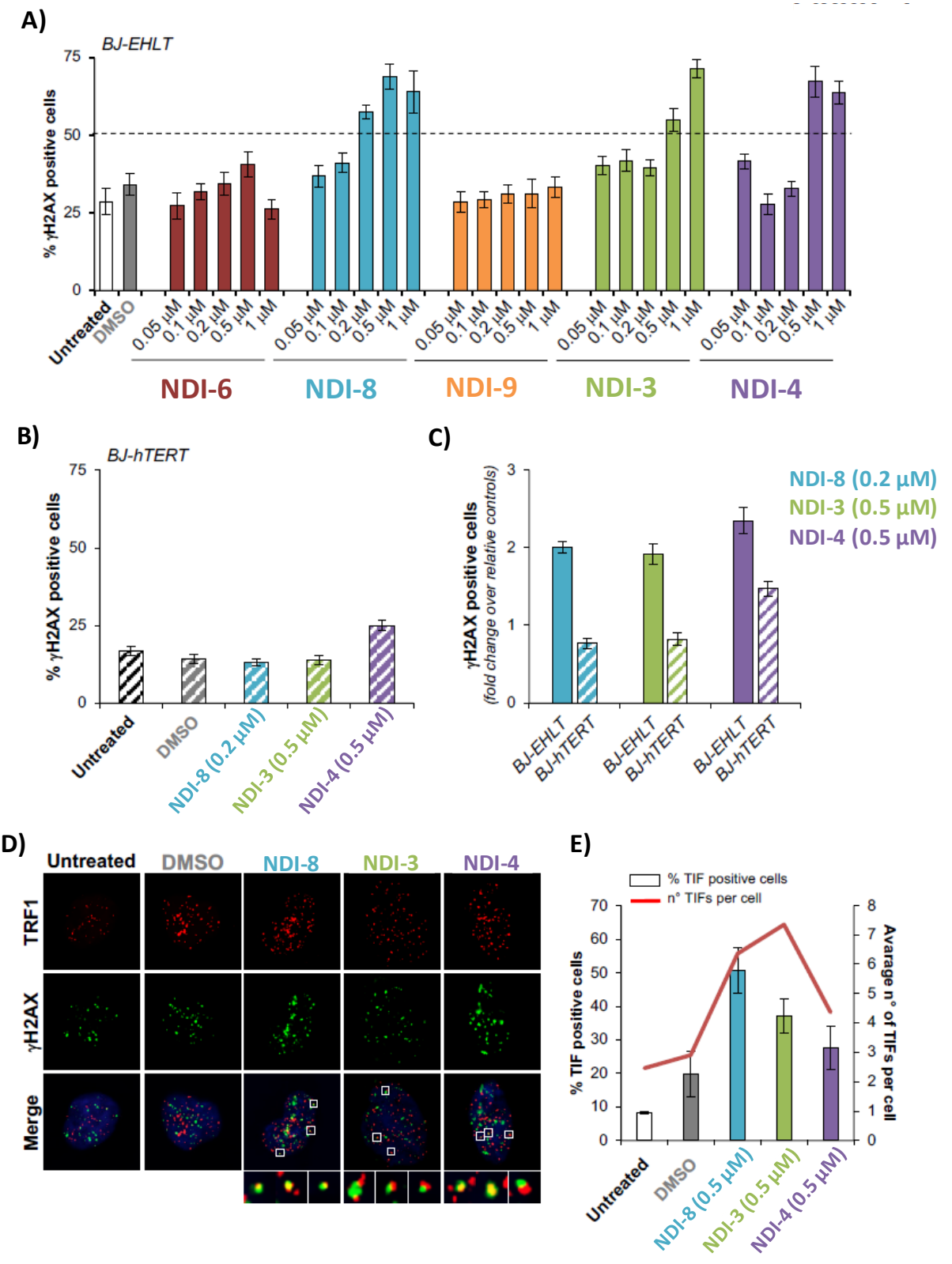

Figure 81. BJ-EHLT and BJ-hTERT fibroblasts were untreated or treated for 24 h with DMSO or the investigated NDIs at the indicated concentrations. Cells were processed for immunofluorescence (IF) using antibodies against γH2AX and TRF1 to visualize the DNA damage and telomeres, respectively. A) Percentages of γH2AX-positive BJ-EHLT cells. B) Percentages of γH2AX-positive BJ-hTERT cells. C) Comparison between the percentages of γH2AX-positive BJ-EHLT and BJ-hTERT cells.

D) Representative merged images of IF of untreated and treated BJ-EHLT cells; γH2AX spots in green, TRF1 spots in red and nuclei in blue. Enlarged views of Telomere Induced Foci (TIFs) are reported on the bottom panels of each picture. The images were acquired with a Leica Deconvolution microscope (magnification 63x). E) Quantitative analysis of TIFs. The graph represents the percentages of TIF-positive cells (bars) and the mean number of TIFs per cell (red line) in the indicated samples. Cells with at least four γH2AX/TRF1 foci were scored as TIF positive. Histograms show the mean values ±S.D. of three independent experiments.

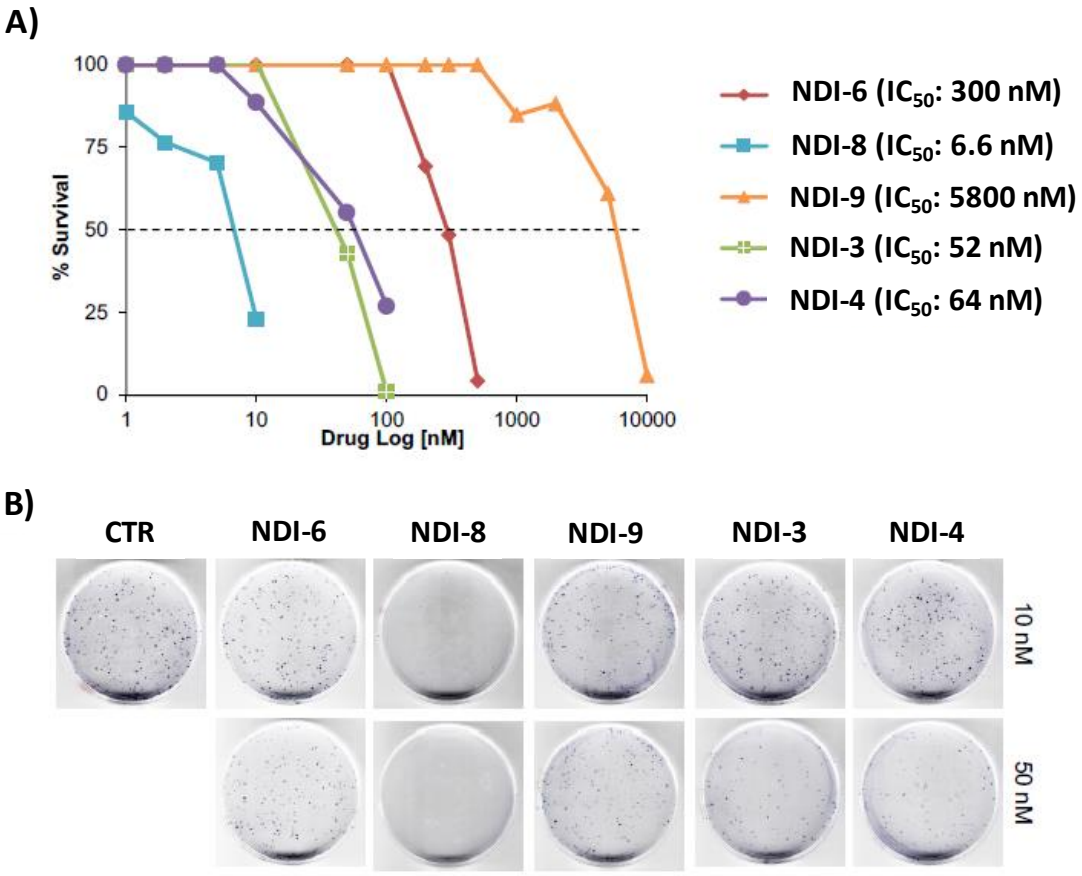

Figure 82. Antitumor efficacy of the tested NDIs. A) Clonogenic activity of human cervical cancer cells, HeLa, treated with the different NDIs at the indicated doses. Surviving fractions were calculated as the ratio of absolute survival of the treated sample/absolute survival of the untreated sample. B) Representative images of the clonogenic assay described in A).

Finally, in order to evaluate the selectivity of NDIs in cell, the effects of these compounds were also tested on normal cells. Briefly, the human immortalized fibroblasts (BJ-hTERT) were treated with the tested NDIs at their lowest effective concentrations and the number of viable cells was evaluated (Figure 83). Remarkably, these experiments clearly evidenced that the cytotoxic effects of ligands on normal cells are lower than those produced on cancer cells.

Overall, these data unambiguously designated **NDI-8** as the most promising candidate drug since it proved to be the most active compound against cancer cells, also having high selectivity in killing cancer cells than normal cells.

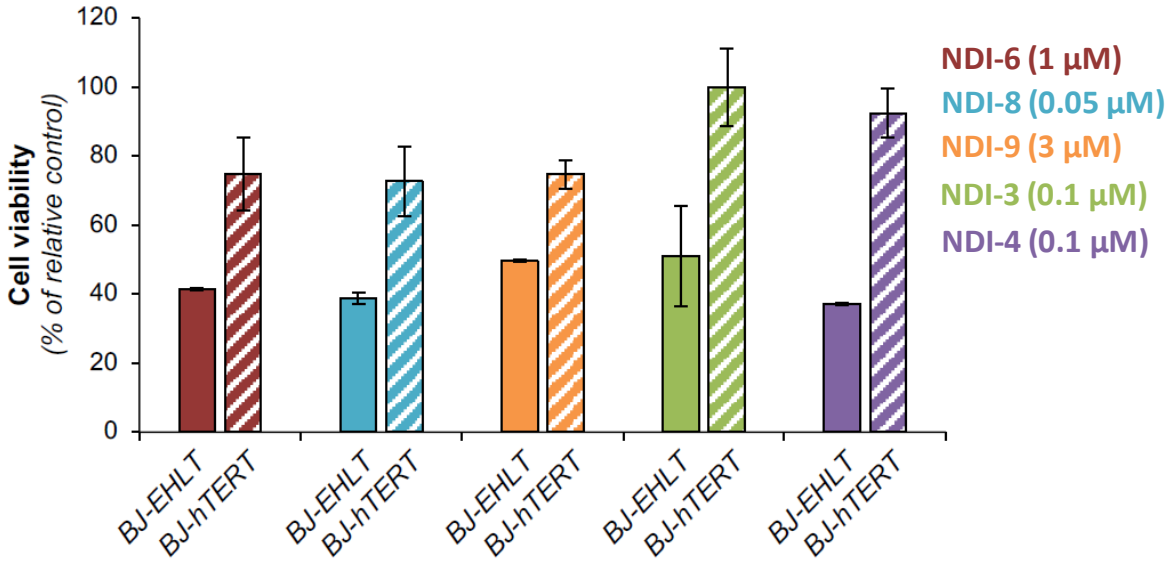

Figure 83. BJ-EHLT and BJ-hTERT cells were treated with compounds **NDI-6**, **NDI-8**, **NDI-9**, **NDI-3** and **NDI-4** at the indicated doses. Viable cell number was determined by the Trypan Blue exclusion test. Histograms show the mean values ±S.D. of three independent experiments.

5.4 Solution studies on the interaction of NDI-8 with oligonucleotide models by CD and fluorescence experiments

Considering the interesting results of the G4-CPG and biological assays, we decided to get a deeper insight into the interaction of compound **NDI-8** with the human telomeric G4s tel26 and tel46, the extra-telomeric G4 cmyc and the duplex structure ds27 by analysing these systems in solution *via* CD experiments. 2 µM solutions of all the investigated oligonucleotides in a 20 mM KCl, 5 mM KH_2PO_4, 10% DMSO buffer (pH 7) were titrated with increasing amounts of **NDI-8**, and spectra recorded after each addition.

As expected in the above buffered conditions, CD spectra showed that tel26 and tel46 respectively folded into hybrid G4 structures, featured by a maximum at 290 nm and a shoulder at 270 nm, cmyc formed a parallel G4 with a maximum centered at 263 nm, while ds27 showed a positive band at 280 nm with a minimum at 251 nm, characteristic of a B-DNA duplex structure (Figure 84). In the case of tel26 and tel46 titrations with **NDI-8**, a dose-dependent increase of the intensity of the 290 nm band and a reduction of the 270 nm shoulder were observed, as well as the presence of an isosbestic point at 277 nm (Figures 84A and 84B). In the titration experiments with cmyc, a slight reduction of the 263 nm band, an increase of the

288 nm band and an isosbestic point at 273 nm were observed (Figure 84C). As far as the titration of ds27 is concerned, the addition of **NDI-8** produced a slight reduction of the 250 nm band and an increase of the 280 nm band (Figure 84D). In all cases, a maximum of 6 equivalents was added to the oligonucleotide solutions, as the best compromise between solubility of the analyzed ligand and saturation of the oligonucleotide CD signals. No induced CD signal was observed for all the investigated systems.

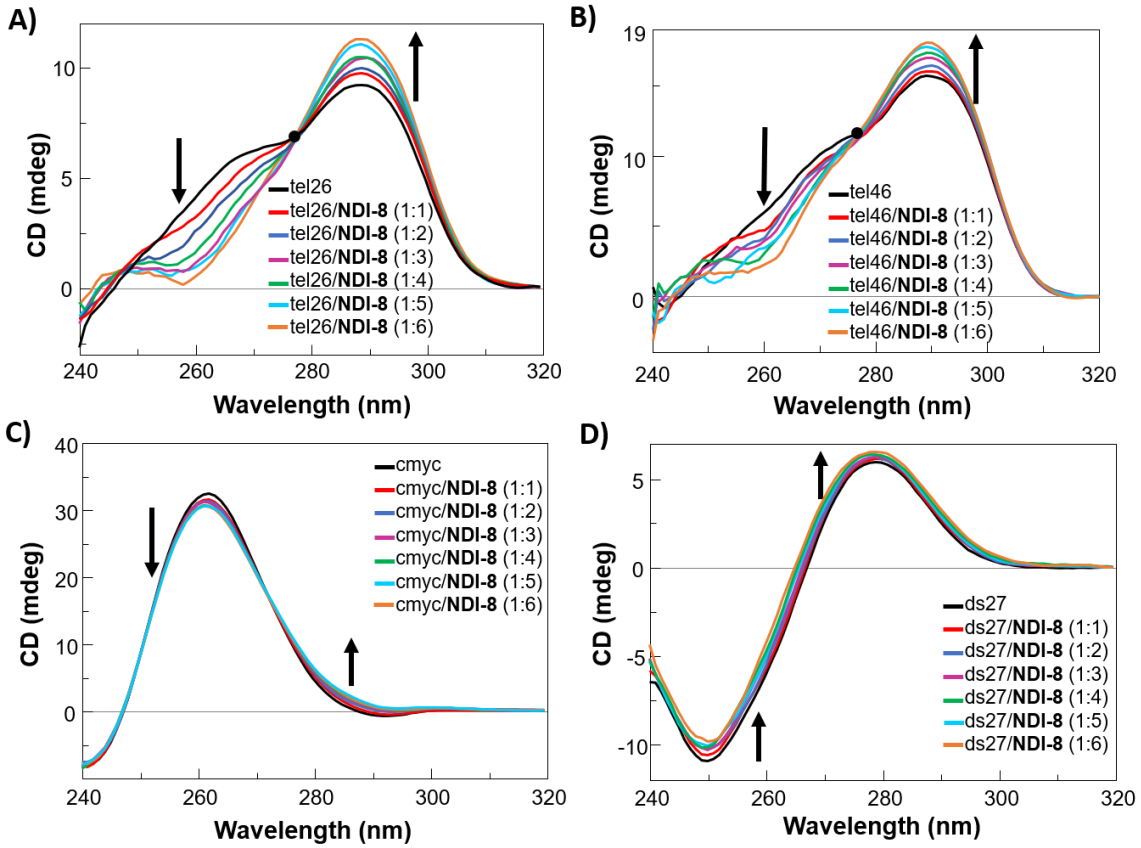

Figure 84. CD spectra of 2 µM solutions of: A) tel26, B) tel46, C) cmyc and D) ds27 in 20 mM KCl, 5 mM KH_2PO_4, 10% DMSO buffer (pH 7) in the absence and presence of increasing amount of **NDI-8** (up to 6 equivalents). Isosbestic points in A), B) and C) are showed as black dots; black arrows indicate intensity variations of the specific bands going from 1:1 to 1:6 oligonucleotide/**NDI-8** ratio.

CD-melting experiments were also performed on all the oligonucleotide/ligand mixtures to evaluate if stabilizing or destabilizing effects on the G4s and hairpin duplex structures were obtained upon incubation with **NDI-8** (Table 10). CD melting curves of tel26, tel46, cmyc and ds27 in the absence or presence of the ligand (1:6 oligonucleotide/**NDI-8** ratio) were recorded by following the CD changes at the wavelength of intensity maximum (290 nm for tel26 and tel46, 263 and 251 nm for cmyc and ds27, respectively). The results of the CD melting experiments showed that compound **NDI-8** preferably stabilized tel26, tel46 and cmyc G4s

structure (ΔT_m > 9 °C), but however produced an appreciable stabilization also of ds27 with ΔT_m of 6 °C (Table 10).

Overall, both CD titrations and CD-melting experiments demonstrated the ability of the here investigated **NDI-8** to affect the structure and stabilization of telomeric G4s and cmyc G4 to a greater extent than duplex DNA.

Table 10. Melting temperatures (T_m) of tel26, tel46, cmyc and ds27 in the absence or presence of **NDI-8** (6 equivalents) measured by CD melting experiments.

Ligand	**T_m (°C) (±1)**			
	tel26	**tel46**	**cmyc**	**ds27**
No ligand	49	49	82	75
NDI-8	58	59	92	81

The capacity of **NDI-8** to induce the formation of G4 structures was also investigated, taking the telomeric sequences as models. Solutions of tel26 and tel46 in 10 mM Tris-HCl, 10% DMSO buffer (pH 7) were titrated with increasing amounts of the NDI, and CD spectra were recorded after each addition (Figure 85). Remarkably, **NDI-8** was able to induce the formation of hybrid-type and antiparallel G4s, respectively starting from unfolded tel26 and tel46, featured by T_m of 37 and 36 °C in 10 mM Tris-HCl, 10% DMSO buffer (pH 7). On the other hand, cmyc and ds27 proved to fold into stable secondary structures, *i.e.* a parallel G4 and a hairpin duplex respectively, even in the absence of cations; it was not therefore possible to gain information about the ability of this NDI to induce G4 formation on cmyc and ds27.

To investigate the binding stoichiometry of the complexes formed between **NDI-8** and the here studied tel26, tel46, cmyc and ds27 secondary structure-forming sequences, fluorescence experiments were carried out. Fluorescence spectra were recorded for different DNA/ligand mixtures, prepared varying the NDI mole fraction from 0 to 1 and keeping constant the total molar concentration ([ligand] + [DNA]) at 2 µM (Figures 86A, 86C, 86E and 86G). The analysis of the Job plot for tel26/NDI mixtures showed changes at NDI mole fractions of 0.48 and 0.63, corresponding to stoichiometry ratios of approximately 1:1 and 2:3 tel26/**NDI-8** (Figure 86B). These stoichiometries of binding suggest the formation of a complex in which first one NDI binds one G4, and then a dimeric G4 structure is formed, with two NDI molecules likely bound by end stacking and an additional NDI inserted at the G4-G4 interface. On the other hand, the analysis of the Job plot for the tel46/NDI mixtures showed slope changes at

NDI mole fractions of 0.54 and 0.84, corresponding to stoichiometry ratios of approximately 1:1 and 1:5 tel46/**NDI-8** (Figure 86D). Taking into account the above suggested model for tel26/**NDI-8**, probably two NDI molecules bind the tel46 dimer at its extremities, a third NDI at the G4-G4 interface and the other two NDIs interact with each of the two G4s forming tel46 dimer at the loops or grooves. For cmyc/NDI mixtures, slope changes were found at NDI mole fraction of 0.68, corresponding to stoichiometry ratio of 1:2 cmyc/**NDI-8** (Figure 86F). Finally, the Job plot analysis for ds27/NDI mixtures allowed separating the total stoichiometry in two binding events at NDI mole fractions of 0.52 and 0.85, corresponding to stoichiometry ratios of approximately 1:1 and 1:6 ds27/**NDI-8** (Figure 86H). In the first binding event one NDI molecule binds to ds27 hairpin duplex, in the second binding event other five NDI molecules bind ds27, suggesting non-specific interactions of **NDI-8** to the duplex structure.

Further studies on the interaction in solution of **NDI-8** with the here investigated G-quadruplex structures have been carried out to better elucidate their binding mode and are discussed in the following chapter.

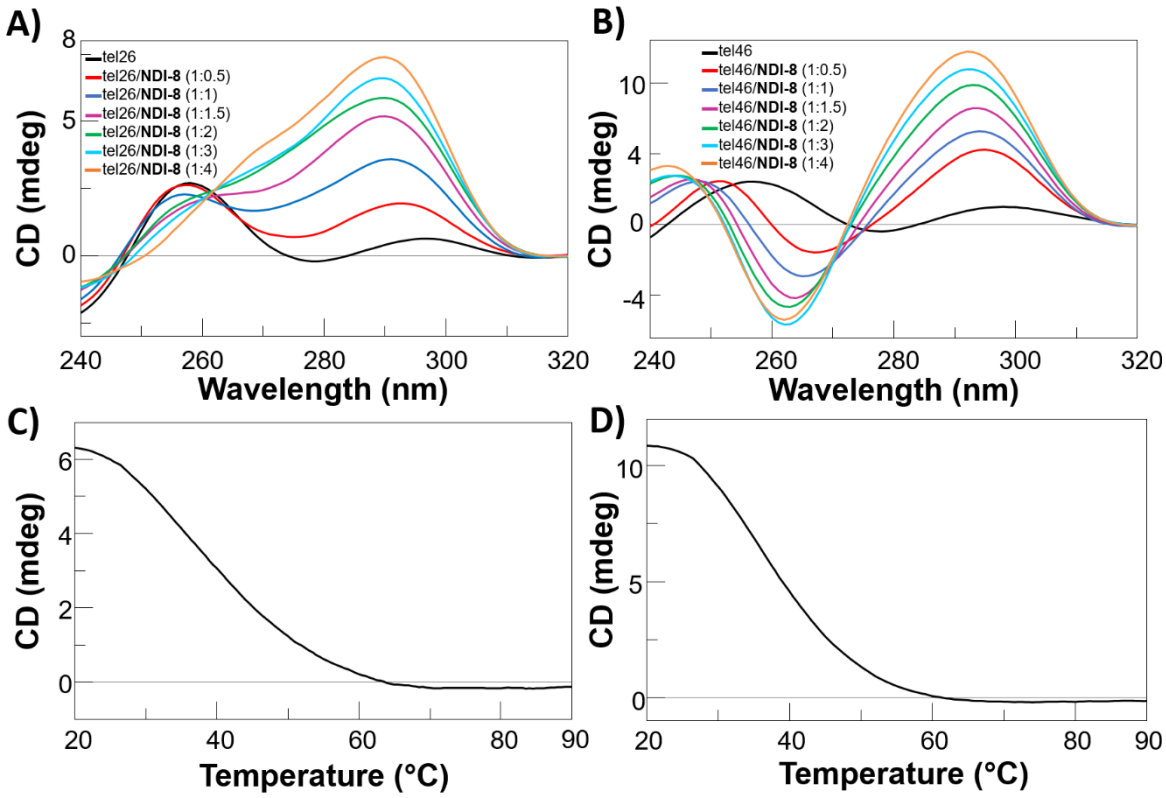

Figure 85. CD spectra of: A) tel26 and B) tel46, each 20 µM solutions in 10 mM Tris-HCl, 10% DMSO buffer (pH 7), in the absence and presence of increasing amounts of **NDI-8** (up to 4 equivalents), and related melting curves for: C) tel26/**NDI-8** and D) tel46/**NDI-8** mixtures (1:4) recorded at 290 and 293 nm, respectively.

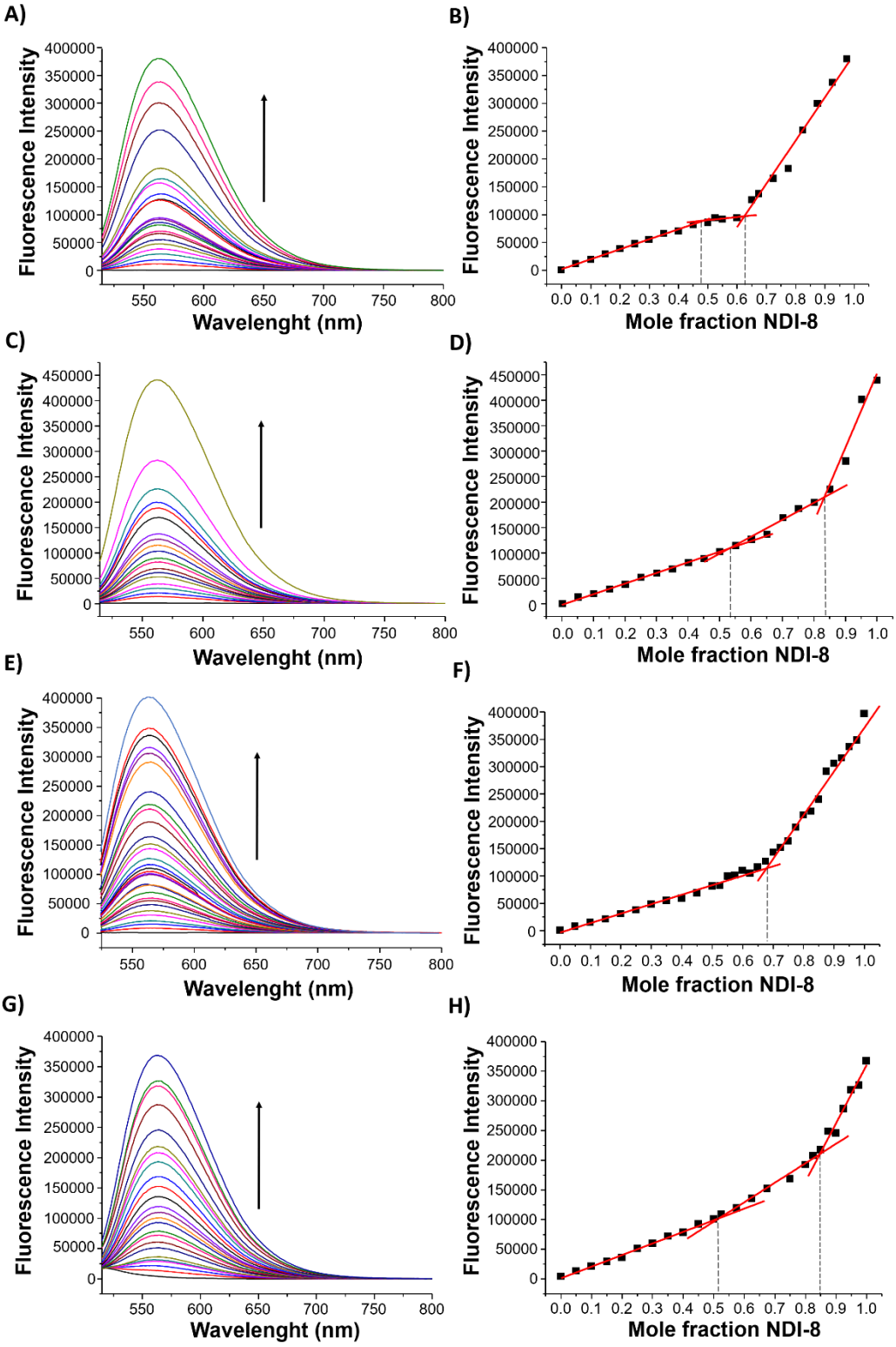

Figure 86. Fluorescence spectra of **NDI-8** in the absence and presence of: A) tel26, C) tel46, E) cmyc and G) ds27 and related Job plot analyses for the binding of **NDI-8** to: B) tel26, D) tel46, F) cmyc and H) ds27. The total molar concentration ([ligand] + [DNA]) was kept constant at 2 μM. The experiments were performed in 20 mM KCl, 5 mM KH_2PO_4, 10% DMSO buffer (pH 7). The excitation wavelength was 502 nm. The arrows indicate the increasing NDI concentration.

5.5 Experimental section

5.5.1 Chemistry

NDIs **1-12** were provided by prof. Mauro Freccero's group of the Department of Chemistry of University of Pavia with 95% purity as checked by ^{1}H and ^{13}C NMR.

5.5.2 G4-CPG assay

Long Chain AlkylAmine-CPG 1000 Å was functionalized with 3'-*O*-acetyl-5'-*O*-(4,4'-dimethoxytrityl)thymidine through a hexaethylene glycol spacer as previously described in section 2.4. Solid phase synthesis protocols by standard phosphoramidite chemistry on an automated Applied Biosystem 394 DNA/RNA synthesizer were used to obtain the oligonucleotide-functionalized CPG supports. In particular, using a 1 µmol-scale, "DMT-ON" protocol, the following oligonucleotides were assembled on the CPG supports: d[$(TTAGGG)_4TT$] (tel26), d[$AGGG(TTAGGG)_7$] (tel46), d(TGGGGAGGGTGGGGAGGGTGGGGAAGGTGGGGA) (cmyc), and d(CGCGAATTCGCGTTTCGCGAATTCGCG) (ds27). The coupling efficiency of each base was monitored by spectrophotometric measurements of the DMT cation, released from the support by acidic treatment with 3% TCA in CH_2Cl_2 before the subsequent coupling step. Considering the number of couplings and the average yield per cycle of 99.8%, 99.0%, 99.7%, and 99.2%, respectively for tel26, tel46, cmyc and ds27, the overall yield was determined to be 95%, 63%, 91% and 80%. Stock solutions of each tested compound were prepared by dissolving a weighed amount of the solid compound in H_2O or pure DMSO. G4-CPG binding assays were performed as described in section 3.5, using weighed amounts of functionalized CPG supports to have 100 nmol of oligonucleotide for tel26, cmyc and ds27 and 50 nmol for tel46. The UV measurements were performed on a JASCO V-550 UV-vis spectrophotometer equipped with a Peltier Thermostat JASCO ETC-505T. The UV quantification of the ligands was determined by measuring the absorbance relative to the λ_{max} characteristic of each ligand and referring it to the corresponding calibration curves. A quartz cuvette with a path length of 1 cm was used. BRACO-19, TMPyP4, TO, resveratrol and 9-Acr-COOH were purchased from Sigma-Aldrich.

5.5.3 Biological experiments

Cells and culture condition. Human fibroblasts (BJ) and human cervical cancer cells (HeLa) were obtained as previously reported. BJ-hTERT cells were obtained infecting primary BJ cells with a retrovirus carrying hTERT (Addgene plasmid #1773); BJ-EHLT derived from the transformation of BJ fibroblasts with hTERT and SV40[197] early region (BJ-EHLT). BJ-hTERT, BJ-EHLT and HeLa were grown in Dulbecco Modified Eagle Medium (DMEM, Invitrogen Carlsbad, CA, USA) supplemented with 10% Fetal Bovine Serum (FBS), 2 mM L-glutamin and antibiotics at 37°C in a 5% CO_2-95% air atmosphere.

Immunofluorescence. Cells were fixed in 2% formaldehyde and permeabilized in 0.25% Triton X-100 in phosphate buffered saline (PBS) for 5 min at r.t. For immune-labeling, cells were incubated with primary antibody for 2 h at r.t., washed twice in PBS and finally incubated with the secondary antibodies for 1 h. The following primary antibodies were used: Mouse mAb anti-γH2AX (Millipore, Billerica, MA, USA) and Rabbit pAb anti-TRF1 N19 (Santa Cruz Biotechnologies, Santa Cruz, CA, USA). The following secondary antibodies were used: Anti-Mouse IgG (H+L), $F(ab')_2$ Fragment (Alexa Fluor 488 Conjugate) (Cell Signaling) and Anti-rabbit IgG (H+L), $F(ab')_2$ Fragment (Alexa Fluor 555 Conjugate) (Cell Signaling). Nuclei were stained with 4',6-diamidino-2-phenylindole (DAPI, Sigma). Fluorescence signals were recorded by using a Leica DMIRE2 microscope equipped with a Leica DFC 350FX camera and elaborated by Leica FW4000 deconvolution software (Leica, Solms, Germany). For quantitative analysis of γH2AX positivity, 300 cells on triplicate slices were scored. For TIF analysis, a single plane was analyzed, and 30 γH2AX-positive cells were scored. Cells with at least four co-localizations (γH2AX/TRF1) were considered as TIF-positive.

Clonogenic assay. Human cervical cancer cells, HeLa, were seeded in 60 mm-Petri dishes at the clonogenic density of 500 cells/plate in DMEM medium with 10% FBS. After 24 h, cells were treated with compounds **NDI-6, NDI-8, NDI-9, NDI-3** and **NDI-4**. After 10 days, the cells were stained with 2% methylene blue in 50% ethanol and the number of colonies was counted. Surviving fractions were calculated as the ratio of absolute survival of the treated sample/absolute survival of the untreated sample.

Cell viability. BJ-hTERT fibroblasts were seeded in 60-mm Petri dishes at a density of 5×10^4 cells/plate. After 24 h from plating, cells were treated with compounds **NDI-6, NDI-8, NDI-9, NDI-3** and **NDI-4**. Cell viability (Trypan Blue dye exclusion) was determined after 6 days from treatment.

5.5.4 CD experiments

CD spectra were recorded in a quartz cuvette with a path length of 1 cm on a Jasco J-715 spectropolarimeter equipped with a Peltier-type temperature control system (model PTC-348WI). The spectra were recorded at 20 °C in the range 240-800 nm with 2 s response, 200 nm/min scanning speed, 2.0 nm bandwidth, and corrected by subtraction of the background scan with buffer. All the spectra were averaged over 3 scans. The oligonucleotides d[(TTAGGG)$_4$TT] (tel26), d[AGGG(TTAGGG)$_7$] (tel46), d(TGGGGAGGGTGGGGAGGGTGGGGAAGGTGGGGA) (cmyc) and d(CGCGAATTCGCGTTTCGCGAATTCGCG) (ds27) were synthesized by standard automated solid phase oligonucleotide synthesis on an Applied Biosystem 394 DNA/RNA synthesizer. After ammonia treatment (55 °C, 12 h), allowing both deprotection and detachment from the solid support, the crude oligonucleotides were purified by HPLC on a SAX analytical column and then dialyzed against water using a Float-A-Lyzer G2 dialysis device (MWCO 0.5-1.0 kDa, three H_2O changes over 24 h). After lyophilization, the oligonucleotides were dissolved in a 20 mM KCl, 5 mM KH_2PO_4, 10% DMSO buffer (pH 7) to obtain 2 μM solutions, then annealed by heating to 95 °C for 5 min, followed by slow cooling to room temperature. The ligand stock solution was 4 mM in DMSO. CD titrations were obtained by adding increasing amounts of the ligands (up to 6 molar equivalents, corresponding to a 12 μM solution in ligand) to tel26, tel46, cmyc and ds27. After each ligand addition, the system was allowed equilibrating before recording the spectra. For the CD-melting experiments, the ellipticity was recorded at 290 nm for tel26 and tel46, 263 and 251 nm for cmyc and ds27, respectively, with a temperature scan rate of 0.5 °C/min in the range 20-90 °C. For the CD-monitored experiments to evaluate the G-quadruplex structuring induction of **NDI-8**, 20 μM solutions of tel26 and tel46 were prepared in 10 mM Tris-HCl, 10% DMSO buffer (pH 7) and titrated with increasing amounts of NDI (up to 4 molar equivalents, corresponding to a 80 μM solution in ligand). Then the melting curves of these solutions were recorded at 290 and 293 nm, respectively for tel26/**NDI-8** and tel46/**NDI-8** 1:4 ratio mixtures, with a temperature scan rate of 0.5 °C/min in the range 20-90 °C.

5.5.5 Fluorescence experiments

Fluorescence spectra were recorded at 20 °C on HORIBA Jobin Yvon Inc. FluoroMax®-4 spectrofluorometer equipped with F-3004 Sample Heater/Cooler Peltier Thermocouple Drive, by using a quartz cuvette with a 1 cm path length. **NDI-8** was excited at 502 nm and emission

spectra were recorded between 515 and 800 nm. Both excitation and emission slits were set at 5 nm. The experiments were performed in 20 mM KCl, 5 mM KH_2PO_4, 10% DMSO buffer (pH 7). For the construction of the Job plot, the mole fraction of **NDI-8** was varied from 0 to 1 and the total molar concentration ([ligand] + [DNA]) was kept constant at 2 μM.

CHAPTER 6 - STRUCTURAL STUDIES ON THE INTERACTION OF THE DIMERIC NAPHTHALENE DIIMIDE NDI-8 WITH G-QUADRUPLEX MODELS

6.1 Selection of the G-quadruplex-forming oligonucleotide models for NMR studies

To get in-depth information on the binding mode of the dimeric naphthalene diimide **NDI-8** (Figure 87A) to different DNA G-quadruplex conformations, NMR experiments were performed with two model G-rich oligonucleotides able to fold into stable and well-characterized G-quadruplex structures, respectively a parallel and hybrid-1 type topology (Figures 87B and 87C, respectively).[189,209] This study was carried out during my research activities at the Slovenian NMR Centre, National Institute of Chemistry, Ljubljana, Slovenia under the supervision of prof. Janez Plavec.

The primary sequences of the herein used oligonucleotides, M2 d(TAGGGACGGGCGGGCAGGGT) and m-tel24 d[TTGGG(TTAGGG)$_3$A], are in line with vastly accepted consensus motif for G-quadruplex formation.[189,209] M2 G-quadruplex exhibits all strands with parallel orientation, a common feature of most G-quadruplex-forming sequences found in oncogene promoter regions.[209] On the other hand, m-tel24 corresponds to the sequence taken from human telomeric DNA and designed to favour hybrid-1 G-quadruplex topology,[189] thus reducing the high polymorphism of telomeric DNA and allowing a detailed NMR characterization.[210,211]

Both models gave high quality NMR spectra, with the predominant G4 conformation observed in solution at above 90% in the here used conditions, *i.e.* 100 mM KCl, 20 mM KH_2PO_4, pH 7.0.

6.2 NMR structures of the here studied DNA G-quadruplex models

Twelve narrow and well-resolved imino proton signals were observed in the ^{1}H NMR spectra of M2 and m-tel24, consistently, in both cases, with the formation of G-quadruplexes with three stacked G-quartets.[189,209] Under the studied conditions, M2 adopts a parallel G-quadruplex consisting of three stacked G-quartets G3:G8:G12:G17, G4:G9:G13:G18 and G5:G10:G14:G19, sandwiched between the 5'- and 3'-end overhanging residues (T_1A_2 and T_{20}, respectively), and connected by three propeller-type loops involving G5-G8, G10-G12 and G14-G17 residues (Figure 87B).[209] Our NMR study on m-tel24 was carried out at slightly higher K^+ concentration than in published articles (100 mM KCl *vs.* 70 mM KCl).[189]

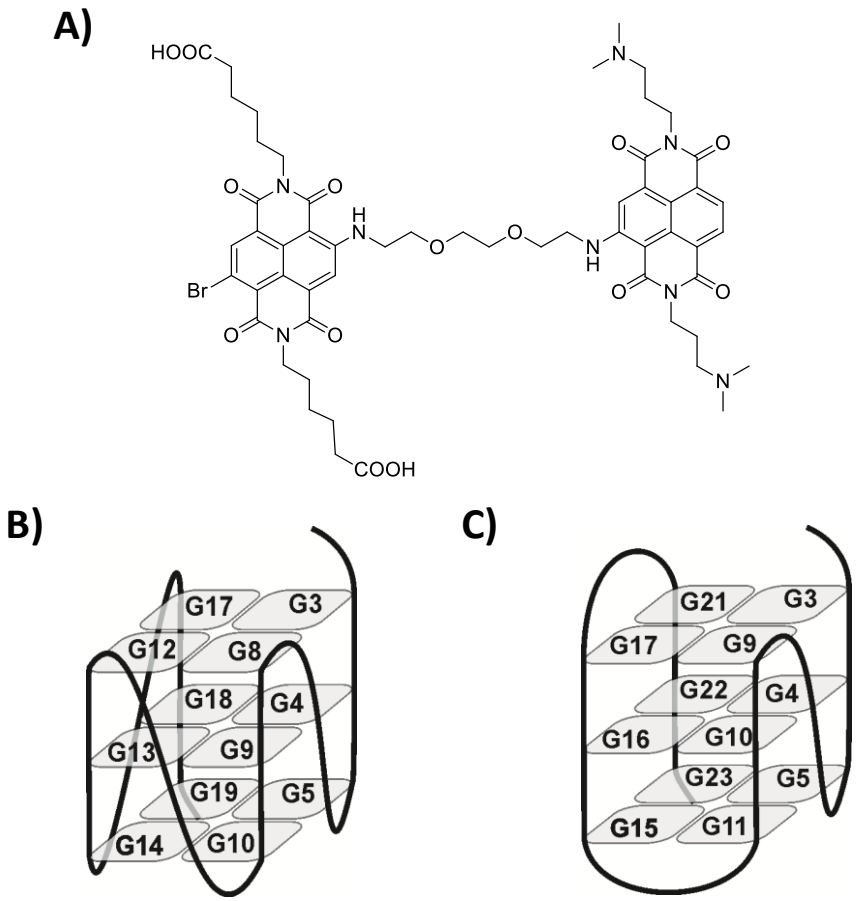

Figure 87. A) Chemical structure of the herein studied dimeric **NDI-8** and schematic representation of G-quadruplexes adopted by: B) M2 and C) m-tel24.

Hence, we used NOESY 2D NMR experiments (Figure 88) combined with ^{1}H NMR analysis of m-tel24 modified sequences containing specific thymine-to-uracil substitutions (the latter one necessary to assign the methyl groups of the different thymidines, see Figure 89) to verify that the here used conditions did not alter m-tel24 G-quadruplex structural features. The ^{1}H NMR chemical shifts of m-tel24 G-quadruplex are reported in Table 11. Further experiments (*e.g.*, HMBC) are needed to unambiguously assign A14, A20 and A24 H2 protons, which were far from other protons. Overall, our results consistently showed that under the herein used conditions, m-tel24 G-quadruplex adopts hybrid-1 type topology containing G3:G21:G17:G9, G4:G10:G16:G22, G5:G11:G15:G23 quartets, with G3, G9, G15, G16 and G21 in *syn* conformation along the *N*-glycosidic bond (Figure 87C).[189]

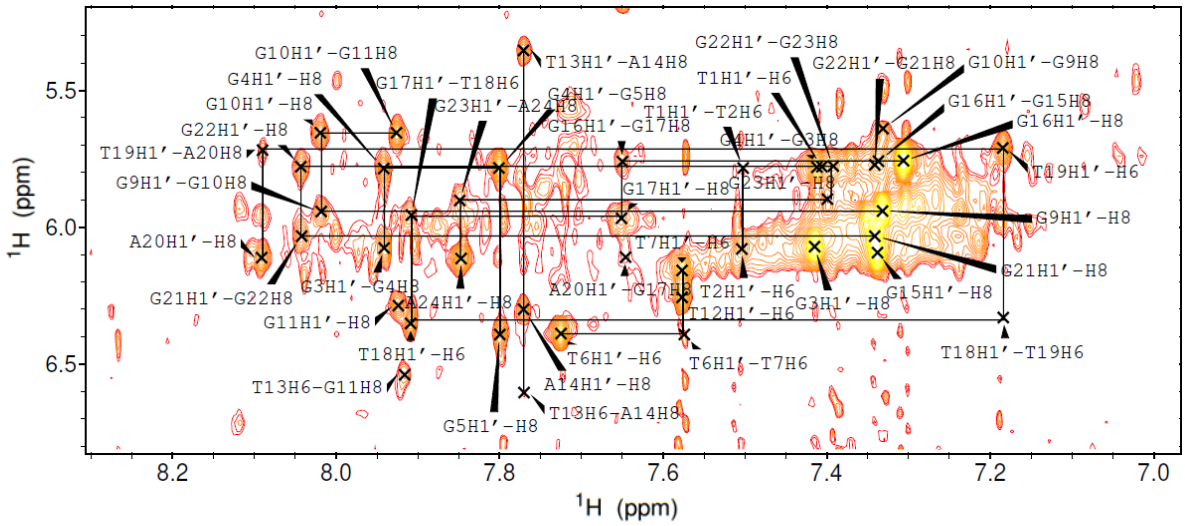

Figure 88. Anomeric-aromatic region of the NOESY spectrum of m-tel24 (at 25 °C, 0.2 mM DNA, 100 mM KCl, 20 mM KH_2PO_4, pH 7 buffer) with a mixing time of 200 ms.

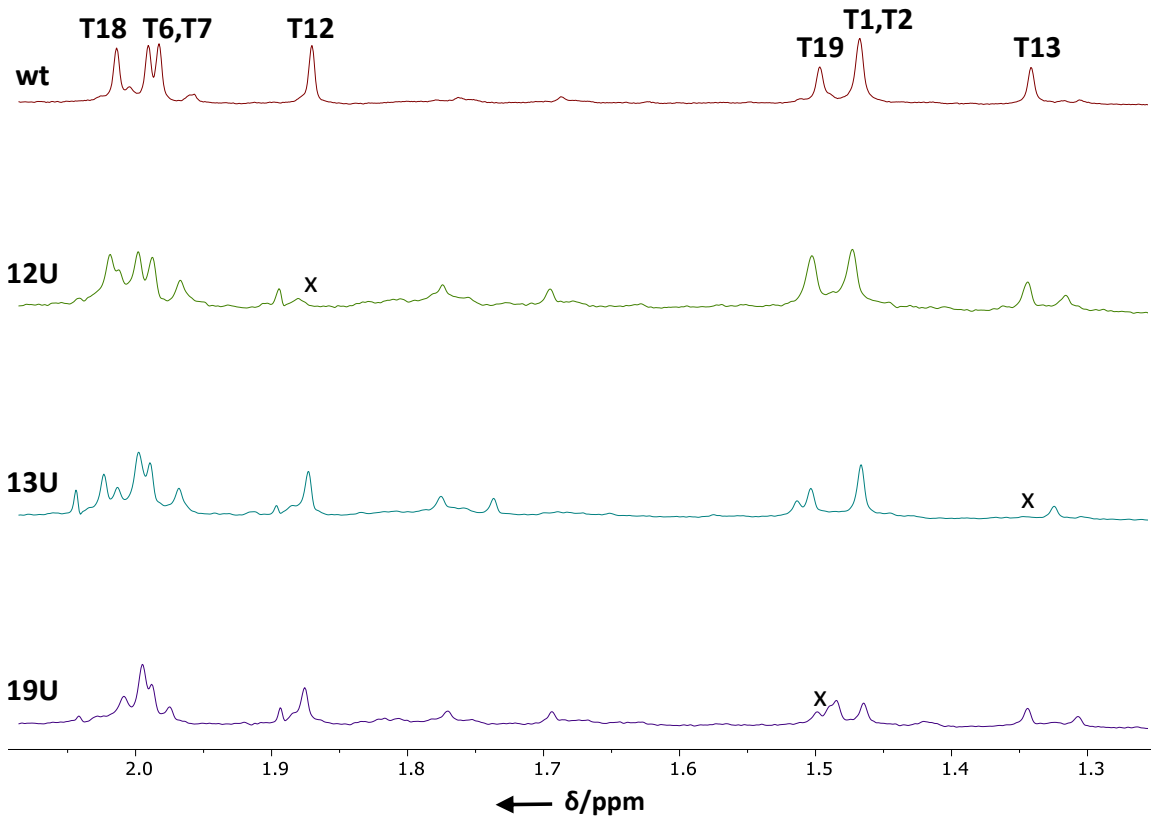

Figure 89. Methyl regions of the ^{1}H NMR spectra of the wild-type (wt) m-tel24 and its modified sequences containing T-to-U substitutions (at 25 °C, 0.2 mM DNA, 100 mM KCl, 20 mM KH_2PO_4, pH 7 buffer). Wild-type m-tel24 methyl peaks not present in the spectra of the modified sequences are marked with crosses.

Table 11. ^{1}H NMR chemical shifts of m-tel24, structured into a G-quadruplex. The chemical shifts are given in ppm and correspond to spectra recorded at 0.2 mM DNA, 100 mM KCl and 20 mM KH_2PO_4, pH 7 buffer.

Proton	**H6/H8**	**H1/Me H2/H5**	**H1'**	**H2'/H2"**	**H3'**
Residue					
T1	7.394	1.476	5.778	1.791/2.300	4.620
T2	7.503	1.474	6.072	2.095/2.326	3.742
G3	7.425	12.027	6.073	3.391/2.958	4.409
G4	7.941	11.752	5.782	2.565/2.629	5.022
G5	7.801	11.044	6.389	2.609/2.571	5.029
T6	7.725	2.014	6.389	2.529/2.475	4.869
T7	7.577	1.999	6.157	2.038/2.381	4.838
A8	8.468	8.271	6.536	2.864/3.039	5.152
G9	7.332	11.871	5.940	3.430/2.987	5.023
G10	8.019	12.175	5.650	2.636	5.067
G11	7.919	11.267	6.279	2.549/2.677	5.054
T12	7.577	1.883	6.254	2.398/2.489	4.702
T13	6.599	1.330	5.351	1.323/2.135	4.501
A14	7.771	-	6.300	2.258/2.500	4.998
G15	7.337	11.329	6.095	3.495/2.979	4.240
G16	7.302	11.206	5.756	2.521/2.460	4.990
G17	7.648	11.785	5.956	2.652/2.607	5.169
T18	7.909	2.035	6.343	2.355/2.529	4.936
T19	7.187	1.500	5.711	0.901/1.707	4.670
A20	8.090	-	6.108	2.915/2.746	4.987
G21	7.343	11.440	6.033	3.467/2.952	4.974
G22	8.042	11.641	5.776	2.668	5.059
G23	7.400	10.653	5.893	2.152/2.543	4.925
A24	7.845	-	6.104	2.668/2.412	4.684

6.3 Study on the interaction of NDI-8 with M2 and m-tel24 G-quadruplexes

Before performing the NMR experiments, we checked **NDI-8** solubility in the concentration range typically used for NMR studies by means of UV spectroscopy. Remarkably, a linear correlation between absorbance and **NDI-8** concentration was found in the 0.1-0.8 mM range (Figure 90), indicating the absence of intermolecular aggregation and/or precipitation phenomena under the studied conditions.

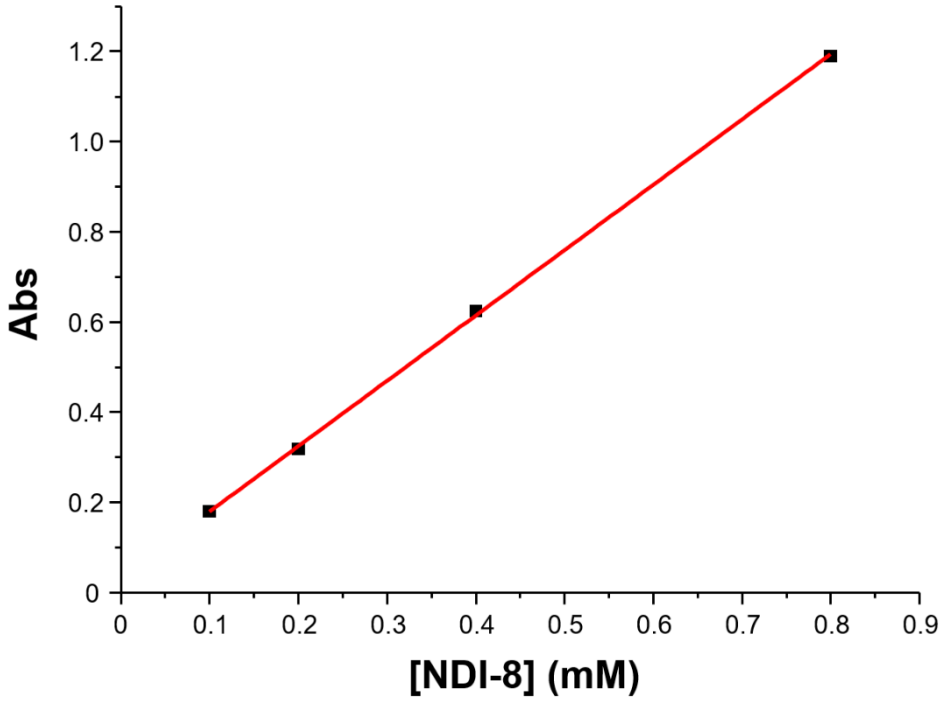

Figure 90. Absorbance *vs.* **NDI-8** concentration dependence. The samples were prepared by adding 1.8, 3.6, 7.2 and 14.4 µL of **NDI-8** dissolved at 10 mM concentration in DMSO-d_6 to the 100 mM KCl, 20 mM KH_2PO_4, pH 7.0 buffer so to reach the final volume of 180 µL. DMSO concentration was, respectively, 1%, 2%, 4%, 8% for the four samples. The absorbance was monitored at 495 nm.

Titrations of M2 and m-tel24 with **NDI-8** up to 1:4 DNA/ligand ratio were then monitored by ^{1}H NMR spectra.

As far as M2 is concerned, ^{1}H NMR imino signals corresponding to the free M2 G-quadruplex were so dramatically broadened to be practically almost undetectable from the baseline already upon addition of 0.5 molar equivalents of **NDI-8** (Figure 91). On the contrary, broad humps appeared in the region between δ 10.5 and 11.4 ppm, which became more intense and shifted slightly upfield (*ca.* 0.2 ppm) upon further addition of NDI. Aging the sample at 1:4 ratio of M2/NDI resulted in evident signals at δ 10.7, 11.0, 11.1 and 11.3 ppm, indicating slow formation of multiple complexes (Figure 91). Importantly, upon interaction with **NDI-8**, M2

retained a G-quadruplex folding, as inferred from the presence of imino ^{1}H NMR signals in the spectral region characteristic of Hoogsteen-type hydrogen bonds. Furthermore, the line broadening observed for all the imino (Figure 91) and methyl resonances as well as most of the aromatic ones (Figure 92) suggests that the ligand could explore different binding poses and/or different G4/**NDI-8** complexes could form, with fast-to-moderate rate equilibria on the ^{1}H NMR time scale.[212] In this regard, the low intensity of the ^{1}H NMR signals in the imino as well as in the other spectral regions of this system discouraged more detailed NMR studies.

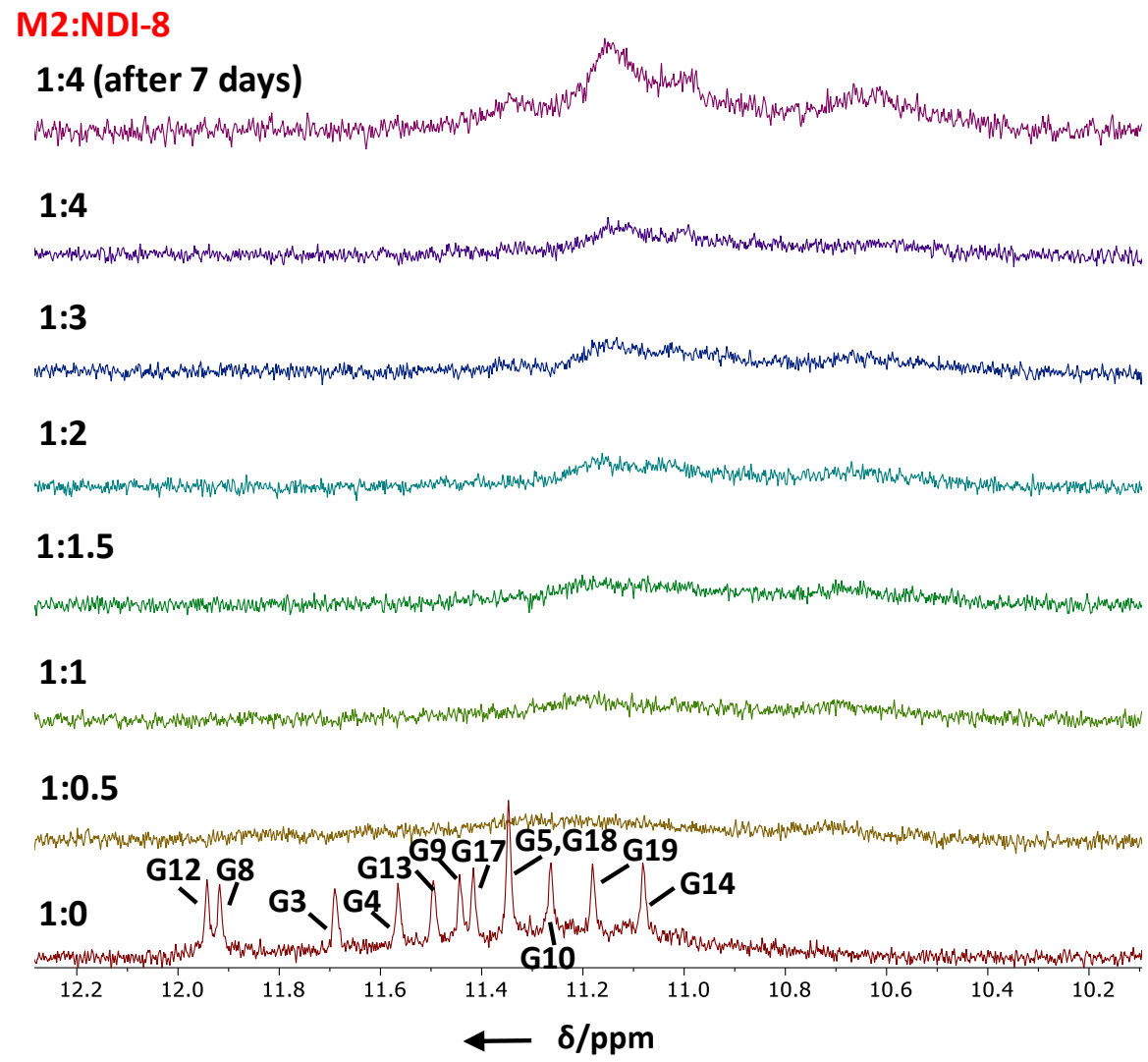

Figure 91. Imino regions of the ^{1}H NMR spectra of M2 G-quadruplex (at 25 °C, at 0.2 mM DNA, 100 mM KCl, 20 mM KH_2PO_4, pH 7 buffer) titrated with **NDI-8** (from 0.5 to 4 equivalents). Resonances are assigned according to Trajkovski *et al.*[209]

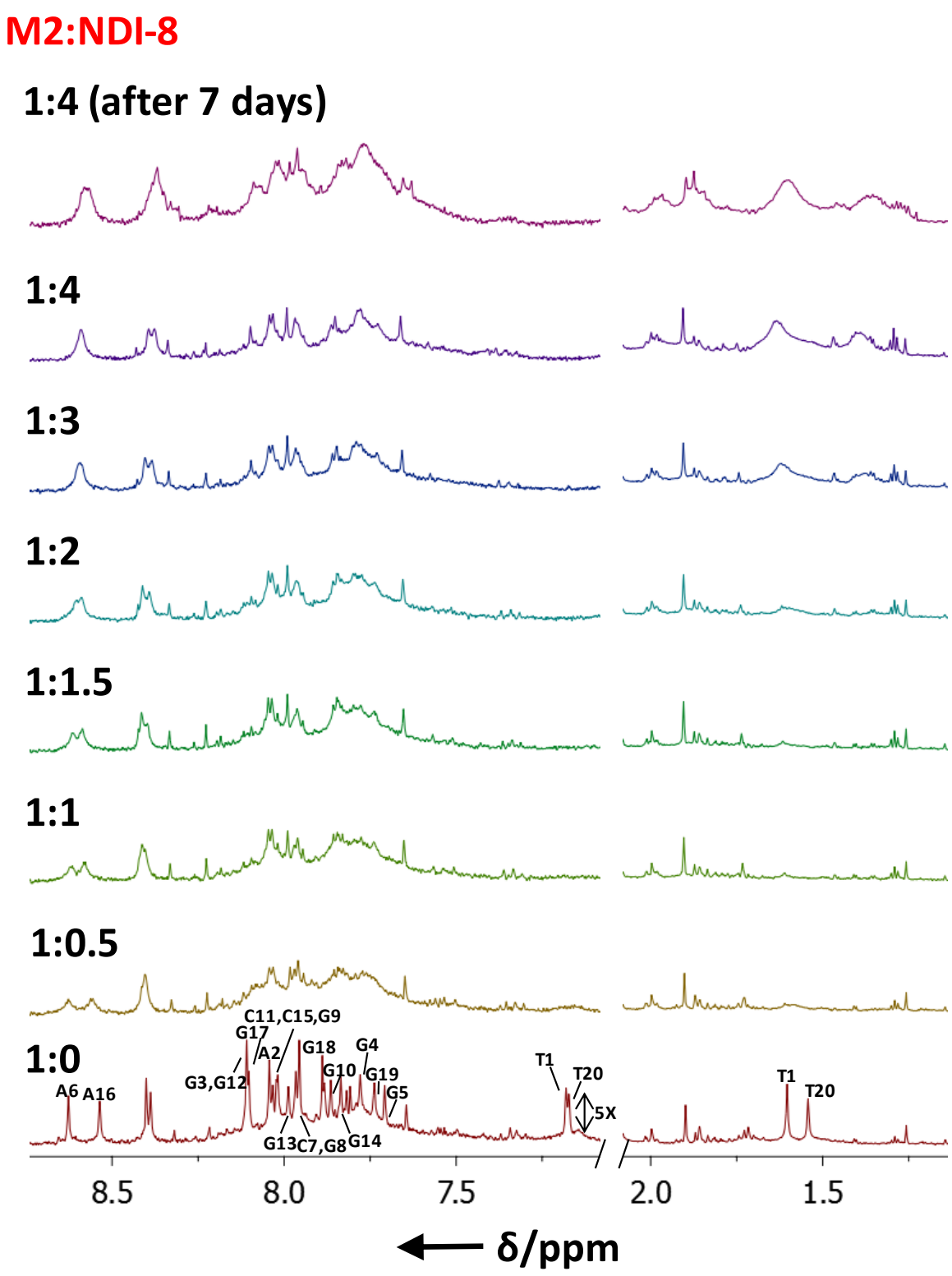

Figure 92. Aromatic and methyl regions of the ^{1}H NMR spectra of M2 G-quadruplex (recorded at 25 °C, at 0.2 mM DNA, 100 mM KCl, 20 mM KH_2PO_4, pH 7 buffer) titrated with **NDI-8** (from 0.5 to 4 equivalents). Resonances are assigned according to Trajkovski *et al.*[209]

Titration of m-tel24 G4 with **NDI-8** resulted in a stepwise broadening of the signals corresponding to the major G4 species, approaching the plateau at 1:2 DNA/NDI ratio, where imino signals were no longer observed (Figure 93).

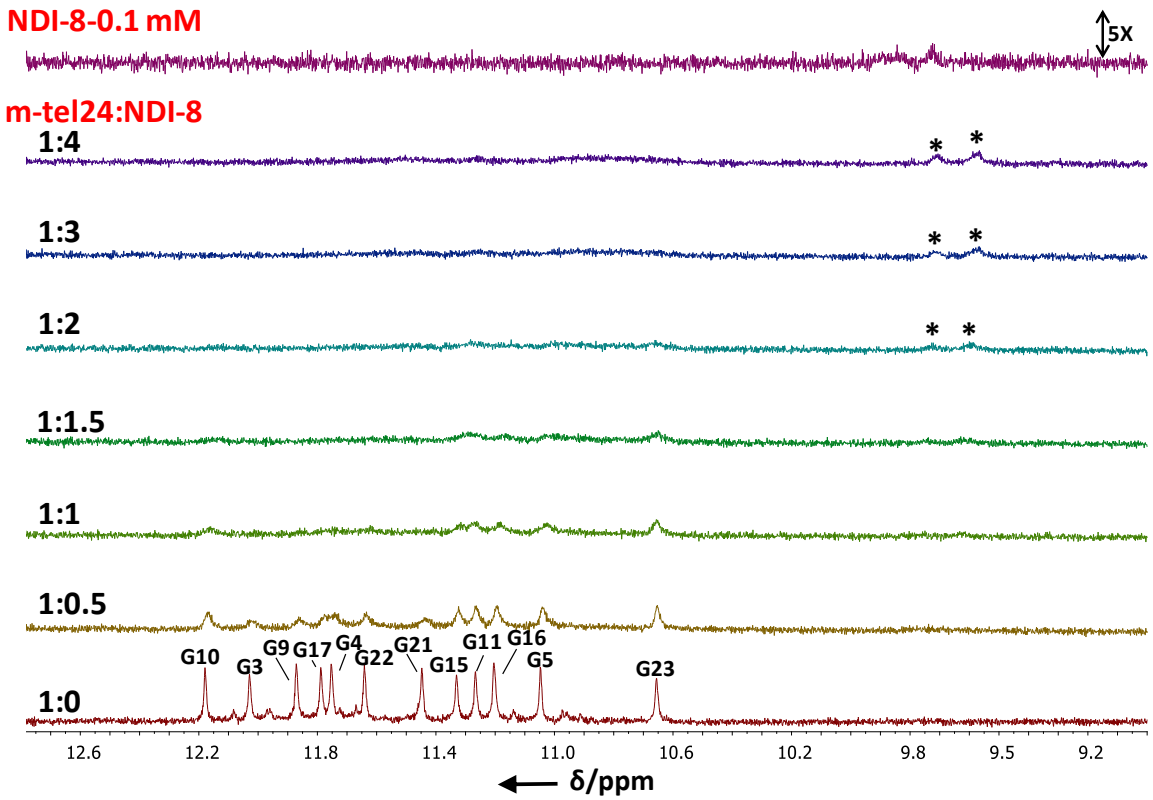

Figure 93. Imino regions of the ^{1}H NMR spectra of m-tel24 G4 (at 25 °C, 0.2 mM DNA, 100 mM KCl, 20 mM KH_2PO_4, pH 7 buffer) titrated with **NDI-8** (from 0.5 to 4 equivalents). Top: ^{1}H NMR spectrum of 0.1 mM **NDI-8** solution (at 25 °C, 100 mM KCl, 20 mM KH_2PO_4, pH 7 buffer). ^{1}H NMR signals appearing in titrated solutions corresponding to m-tel24/**NDI-8** complex(es) are labeled with stars.

The complete disappearance of the minor species ^{1}H NMR imino signals was also observed already at 1:0.5 DNA/NDI ratio. In parallel, new ^{1}H NMR signals (labelled with stars in Figures 93-95) appeared in the ^{1}H NMR spectra of the titrated solutions at δ 9.72, 9.59, 8.30, 8.06, 3.00, 2.97, 2.87, 2.79, 2.27 and 1.63 ppm. Considering that the chemical shifts of these signals did not correspond to the free NDI (Figures 93-95, top) nor to free m-tel24 G4 (Figures 93-95, bottom), we assigned them to m-tel24/**NDI-8** complex(es). On the other hand, no significant change in the chemical shifts (> 0.05 ppm) of imino, aromatic and methyl signals of m-tel24 G4 was observed up to 1:4 DNA/NDI ratio. Furthermore, no spectral change was observed at 1:4 DNA/NDI ratio after aging the sample for 7 days at room temperature. Binding of **NDI-8** to m-tel24 was also evident from dramatic line broadening – even at 0.5 molar equivalents – observed for the imino signals of G3, G4, G9, G17, G21 and G22 (Figure 93). Notably, the

guanine residues for which the line broadening was most marked are structurally related among them as they form the upper G3:G21:G17:G9 quartet and half of the consecutive middle quartet (G4 and G22). This points to a specific binding mode of **NDI-8** to m-tel24 G4. Line broadening was also evident for the aromatic protons of G17, T19, A20 and G22 and methyl group of T1, T2, T18 and T19 (Figure 94-95). Overall, these findings clearly proved the preferential binding of this NDI to the 5'-end spatially close residues and to the G3:G21:G17:G9 quartet, as schematically reported in Figure 96. Moreover, the differences in the imino ^{1}H NMR signals within the middle G4:G22:G16:G10 quartet, showing a more prominent broadening for G4 and G22 compared to G10 and G16, indicated that two structural features, *i.e.* the width of the groove and accessibility of the loop residues, seemed to be crucial for the interaction with the NDI. Indeed, among narrow and wide grooves formed by GGG tracts connected by lateral loops and two medium grooves, one loop-free and one containing a propeller loop, **NDI-8** preferred binding to the m-tel24 groove of medium width which is not covered by a loop (Figure 96).

Increasing the concentration of **NDI-8** resulted in increased line broadening at 35 °C, while no significant effects were observed at 5 and 15 °C (Figure 97). Interestingly, for a given NDI concentration, the broadening of the imino signals of the structurally related guanines was temperature-dependent: indeed, it was moderate at 25 °C, while it diminished at lower (*i.e.*, 5 °C) and increased at higher (35 °C) temperatures (Figure 97). Noteworthy, in the ^{1}H NMR spectra of the NDI alone, the signals became sharper upon heating in the 5 to 35 °C range (Figure 98). This observation, complemented by UV analysis - performed in the same buffer with the same DMSO concentration used in the NMR samples, showing absence of intermolecular interaction among NDIs at r.t. - could be explained considering that **NDI-8** indeed produced intramolecular interactions at low temperatures. In this regard, the temperature-induced broadening of imino ^{1}H NMR signals of m-tel24 G4 in the presence of **NDI-8** could be the consequence of reduced extent of NDI intramolecular interactions, which in turn favoured its binding to m-tel24 G4.

To get a deeper insight into the binding mode of **NDI-8** towards the hybrid-1 G4 model, H_2O/D_2O exchange experiments were carried out. Two samples of 0.2 mM m-tel24 in 100 mM KCl, 20 mM KH_2PO_4, 9:1 H_2O/D_2O buffer with or without 0.1 mM NDI were prepared in parallel, lyophilized and then dissolved in 99.9% D_2O. ^{1}H NMR spectra were then recorded at different times after the dissolution (Figure 99). For both samples, the slowest exchangeable protons were found to be G4, G10, G16, G21 and G22 imino protons.

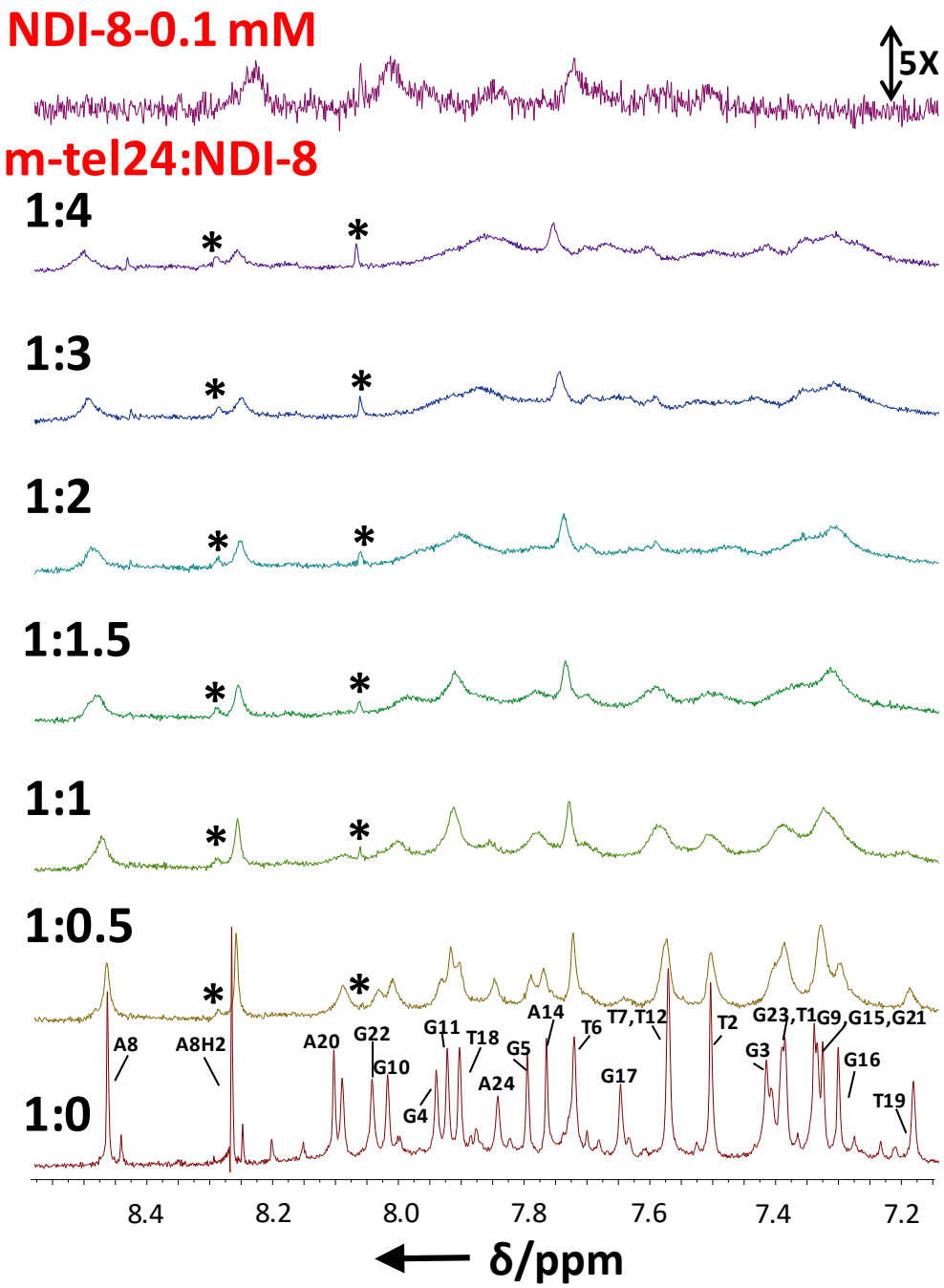

Figure 94. Aromatic regions of the ^{1}H NMR spectra of m-tel24 G4 (at 25 °C, 0.2 mM DNA, 100 mM KCl, 20 mM KH_2PO_4, pH 7 buffer) titrated with **NDI-8** (from 0.5 to 4 equivalents). Top: ^{1}H NMR spectrum of 0.1 mM **NDI-8** solution (at 25 °C, 100 mM KCl, 20 mM KH_2PO_4, pH 7 buffer). ^{1}H NMR signals appearing in titrated solutions corresponding to m-tel24/**NDI-8** complex(es) are labeled with stars.

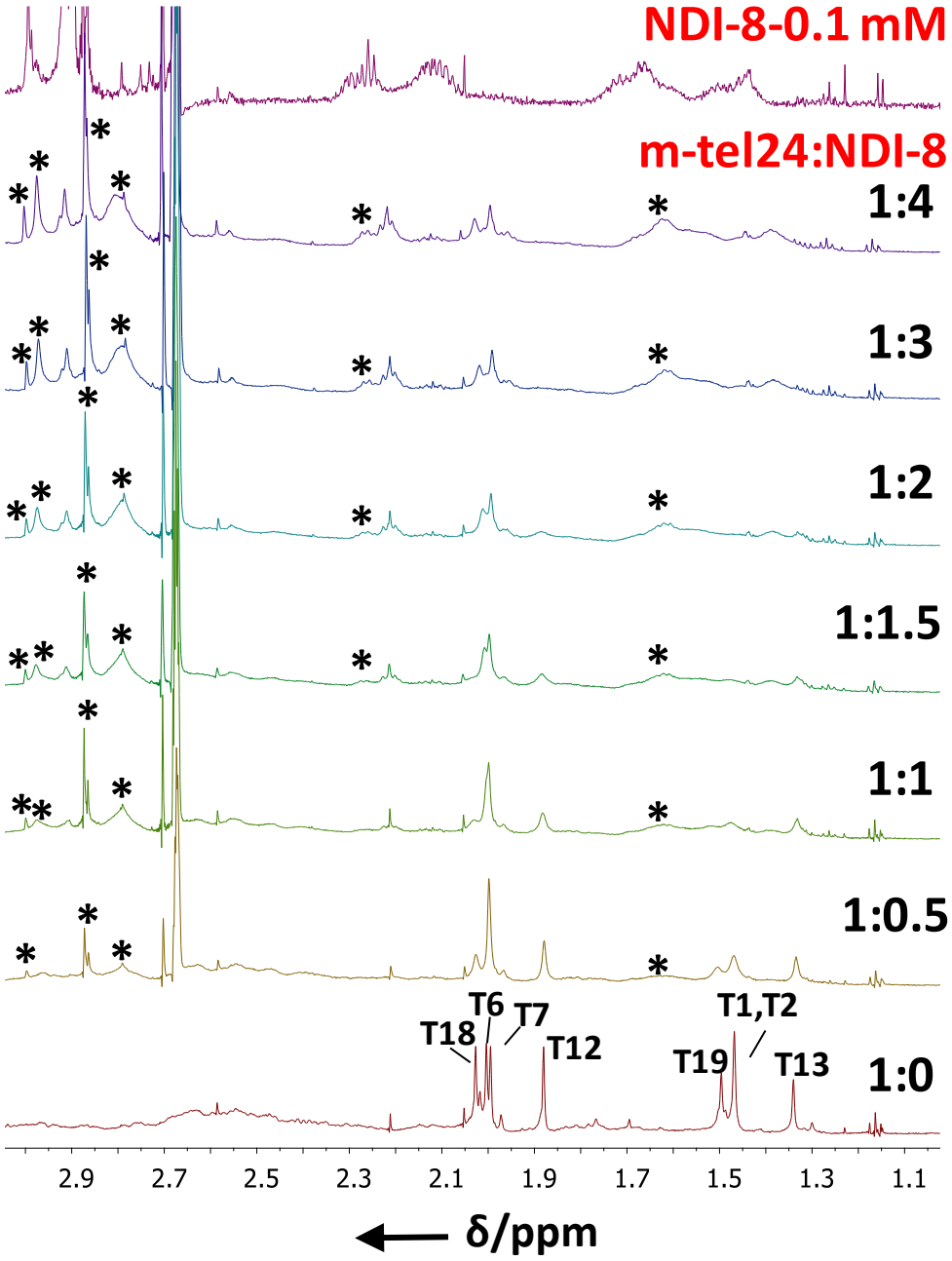

Figure 95. Methyl regions of the ^{1}H NMR spectra of m-tel24 G4 (at 25 °C, 0.2 mM DNA, 100 mM KCl, 20 mM KH_2PO_4, pH 7 buffer) titrated with **NDI-8** (from 0.5 to 4 equivalents). Top: ^{1}H NMR spectrum of 0.1 mM **NDI-8** solution (at 25 °C, 100 mM KCl, 20 mM KH_2PO_4, pH 7 buffer). ^{1}H NMR signals appearing in titrated solutions corresponding to m-tel24/**NDI-8** complex(es) are labeled with stars.

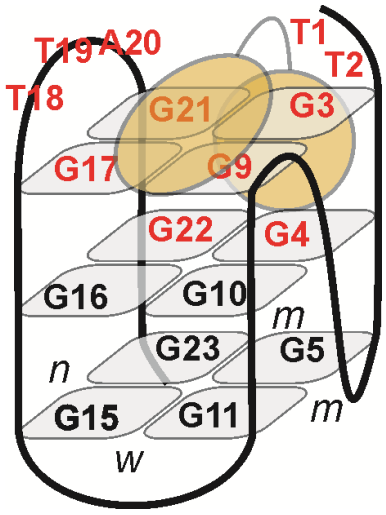

Figure 96. Schematic representation of the complex between m-tel24 and the dimeric **NDI-8** as hypothesized on the basis of the collected NMR data. Residues which showed important line broadening already at 1:0.5 G4/NDI ratio are highlighted in red.

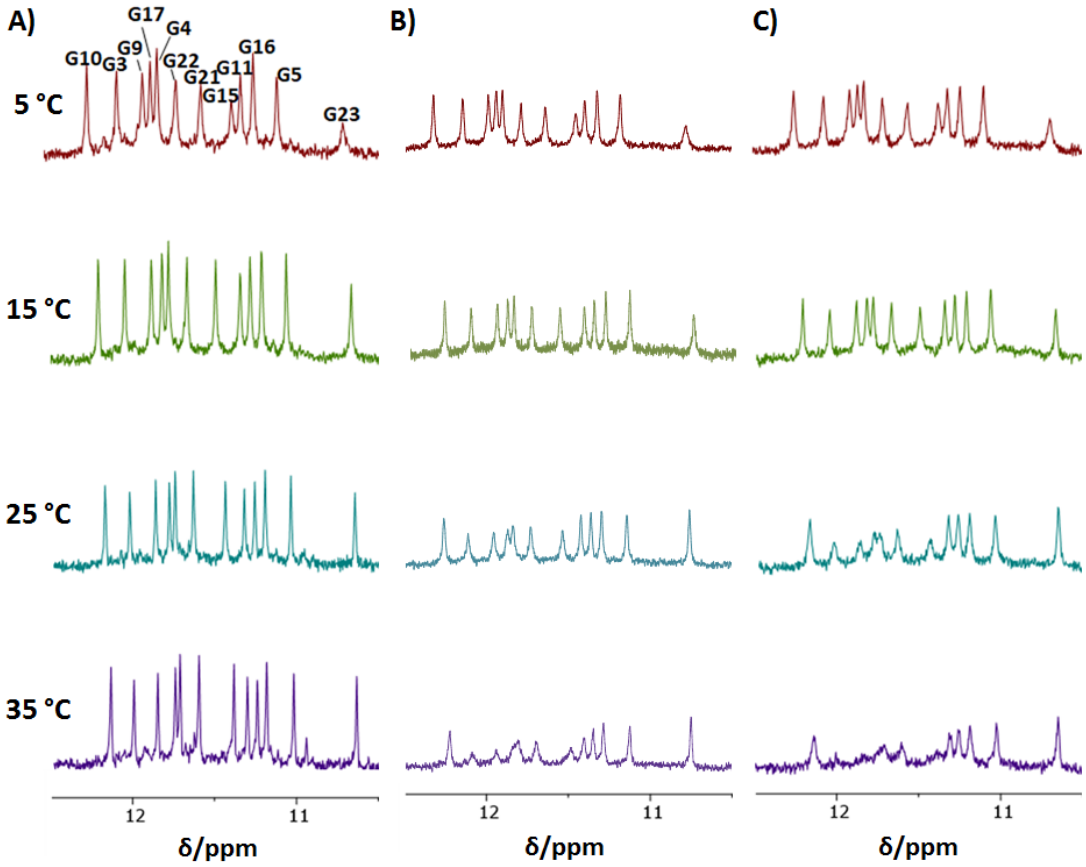

Figure 97. Imino regions of the ^{1}H NMR spectra of m-tel24 G4 (at 0.2 mM, 100 mM KCl, 20 mM KH_2PO_4, pH 7 buffer) A) in the absence of ligand, or in presence of B) 0.10 mM **NDI-8** and C) 0.15 mM **NDI-8**, recorded at different temperatures (from 5 to 35 °C).

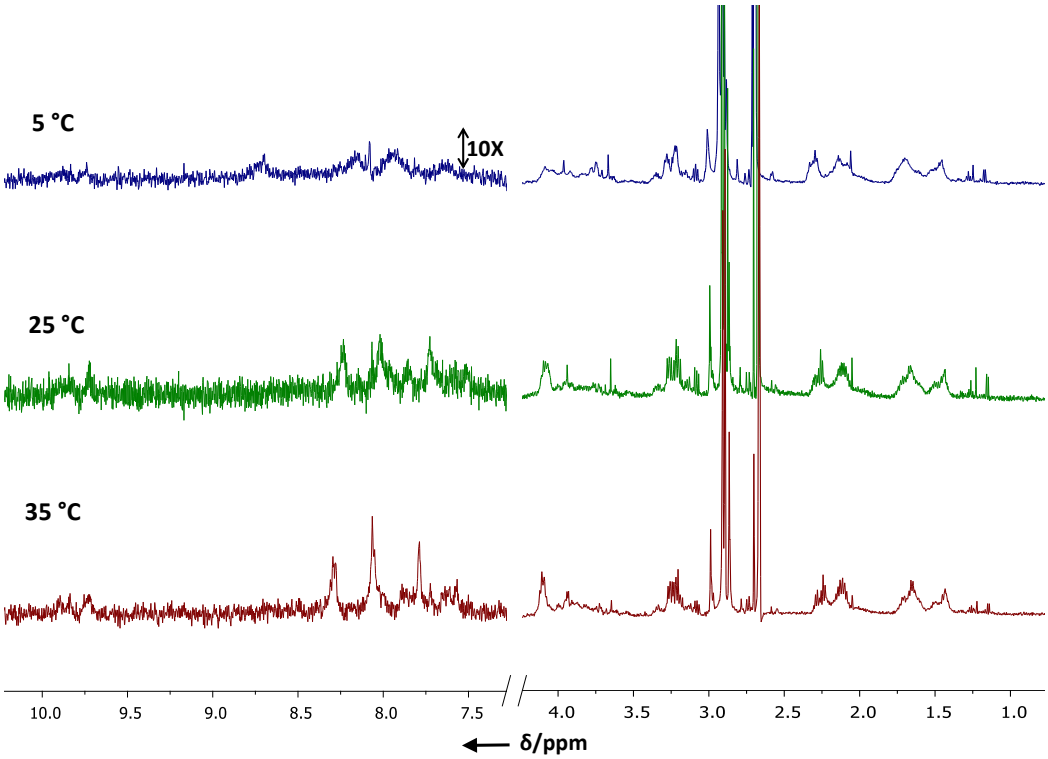

Figure 98. ^{1}H NMR spectra of 0.1 mM **NDI-8** in 100 mM KCl, 20 mM KH_2PO_4, pH 7 buffer at different temperatures.

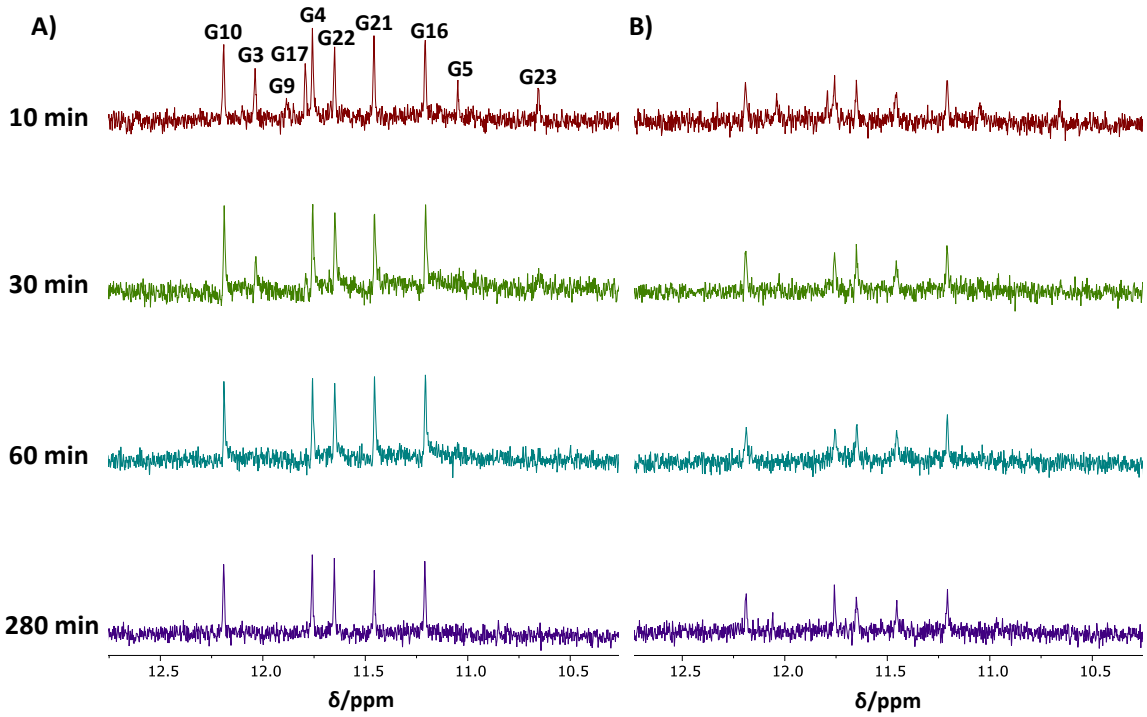

Figure 99. Imino regions of the ^{1}H NMR spectra of m-tel24 G4 (at 25 °C, 0.2 mM DNA, 100 mM KCl, 20 mM KH_2PO_4, pH 7 buffer) in: A) absence of ligand and B) presence of 0.10 mM **NDI-8** recorded at different times (from 10 to 280 min) after dissolution in 99.9% D_2O.

Different exchange rates were found for the slowest exchangeable imino protons (*i.e.*, G4, G10, G16, G21 and G22) in the absence or presence of the ligand (Figure 100), further corroborating the localization of **NDI-8** in the proximity of the upper and middle quartets of m-tel24 G-quadruplex.

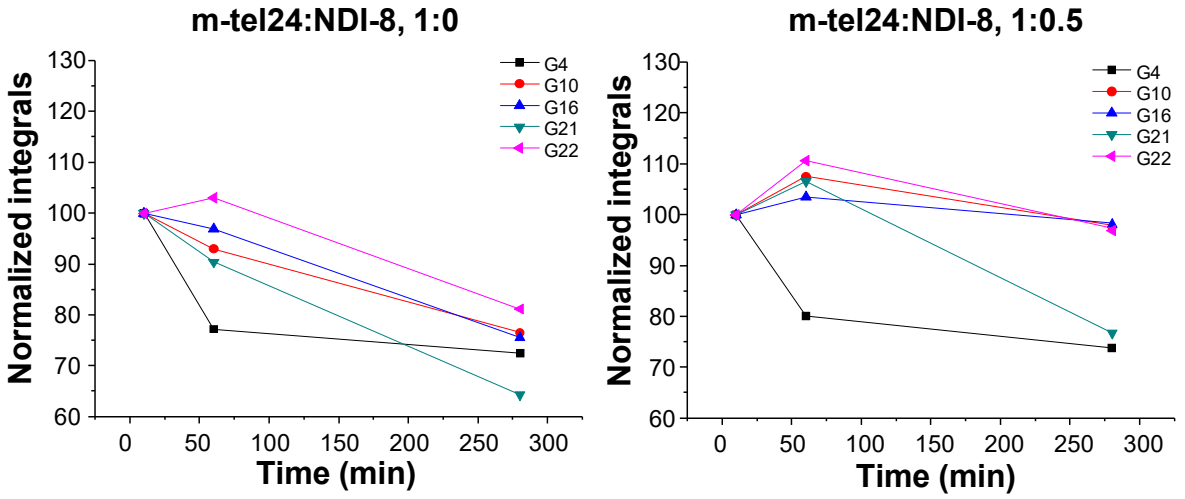

Figure 100. Normalized imino peaks integrals of m-tel24 G4 (at 25 °C, 0.2 mM DNA, 100 mM KCl, 20 mM KH_2PO_4, pH 7 buffer) in the absence (left panels) or presence (right panels) of **NDI-8** (0.10 mM) calculated for G4, G10, G16, G21 and G22 and reported as a function of different times (10, 60 and 280 min) after dissolution of the samples in 99.9% D_2O.

In order to evaluate if the translational diffusion of m-tel24 G4 is perturbed by the ligand, diffusion ordered spectroscopy (DOSY) experiments were performed in the absence and presence of 0.5 and 1 molar equivalents of **NDI-8**.[213–215] The diffusion coefficient of the G4 proved to be ~1.7 x 10^{-10} $m^2 \cdot s^{-1}$ in the absence of NDI while a coefficient of ~1.4 x 10^{-10} $m^2 \cdot s^{-1}$ was found in the presence of 0.5 and 1 molar equivalents of NDI (Figures 101 and 102). These findings indicated that in the presence of NDI the formed G4 species dispersed more slowly. Notably, the diffusion coefficients for the predominant species at 0.5 and 1.0 molar equivalents of NDI was basically the same. In this regard, it is interesting to highlight that the diffusion coefficient calculated for the system without the NDI differed by 0.3 x 10^{-10} $m^2 \cdot s^{-1}$ from the one found for the system in the presence of 0.5 or 1.0 molar equivalents NDI, which perfectly matched the difference previously reported for monomeric and dimeric G-quadruplexes.[216] Indeed, from the diffusion coefficient found for the G4 in the absence of NDI (~1.7 x 10^{-10} $m^2 \cdot s^{-1}$), calculations utilizing a spherical model[217] provided a hydrodynamic diameter of 22.4 Å (not including the hydration layer of 2 x 2.8 Å[218]), which is in reasonable agreement with the size

(~21 and ~25 Å, for the length and diameter, respectively) of monomeric m-tel24 G4 (PDB entry 2GKU).[189] A hydrodynamic diameter of 28.4 Å (not including the hydration layer of 2 x 2.8 Å[218]) was in turn derived for m-tel24 G4 in the presence of the ligand (diffusion coefficient ~1.4 x 10^{-10} $m^2 \cdot s^{-1}$), suggesting the formation of a dimeric structure. This result was fully consistent with the fluorescence data discussed in Chapter 5, showing a 2:3 stoichiometry for the DNA/NDI complex obtained by the Job plot experiments on titrating tel26. In addition, the value here obtained for m-tel24 in the presence of the NDI was in good agreement with size of ~28 Å found for previously reported dimeric G4 structures (PDB entry 2KYO and 2LED).[114,216,219] Attempts to utilize a cylindrical model in lieu of a spherical one did not result in a better representation of the hydrodynamic behaviour of the here studied G-quadruplex structures under the used conditions.[217]

Finally, peaks from minor species (labeled with stars in Figure 102), also found in the ^{1}H NMR spectrum of the G4 in the absence of NDI, were observed only in DOSY spectra of 1:0.5 and 1:1 G4/NDI samples because the severe signal broadening induced by the presence of the ligand and lower threshold required for spectra processing than in the case of 1:0 G4/NDI sample allowed them emerging.

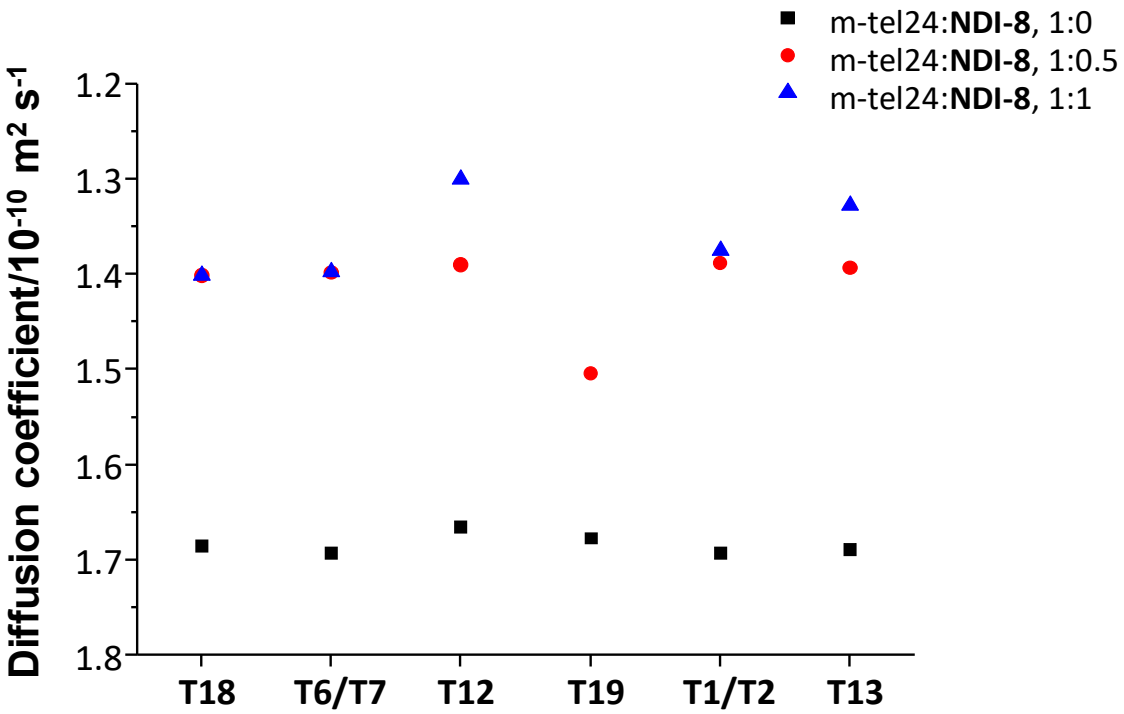

Figure 101. Diffusion coefficients for methyl ^{1}H NMR signals of m-tel24 G4 as assessed from DOSY NMR spectra (at 25 °C, 0.2 mM DNA, 100 mM KCl, 20 mM KH_2PO_4, pH 7 buffer) in the absence (black squares) or presence of 0.5 (red dots) and 1 (blue triangles) **NDI-8** equivalents.

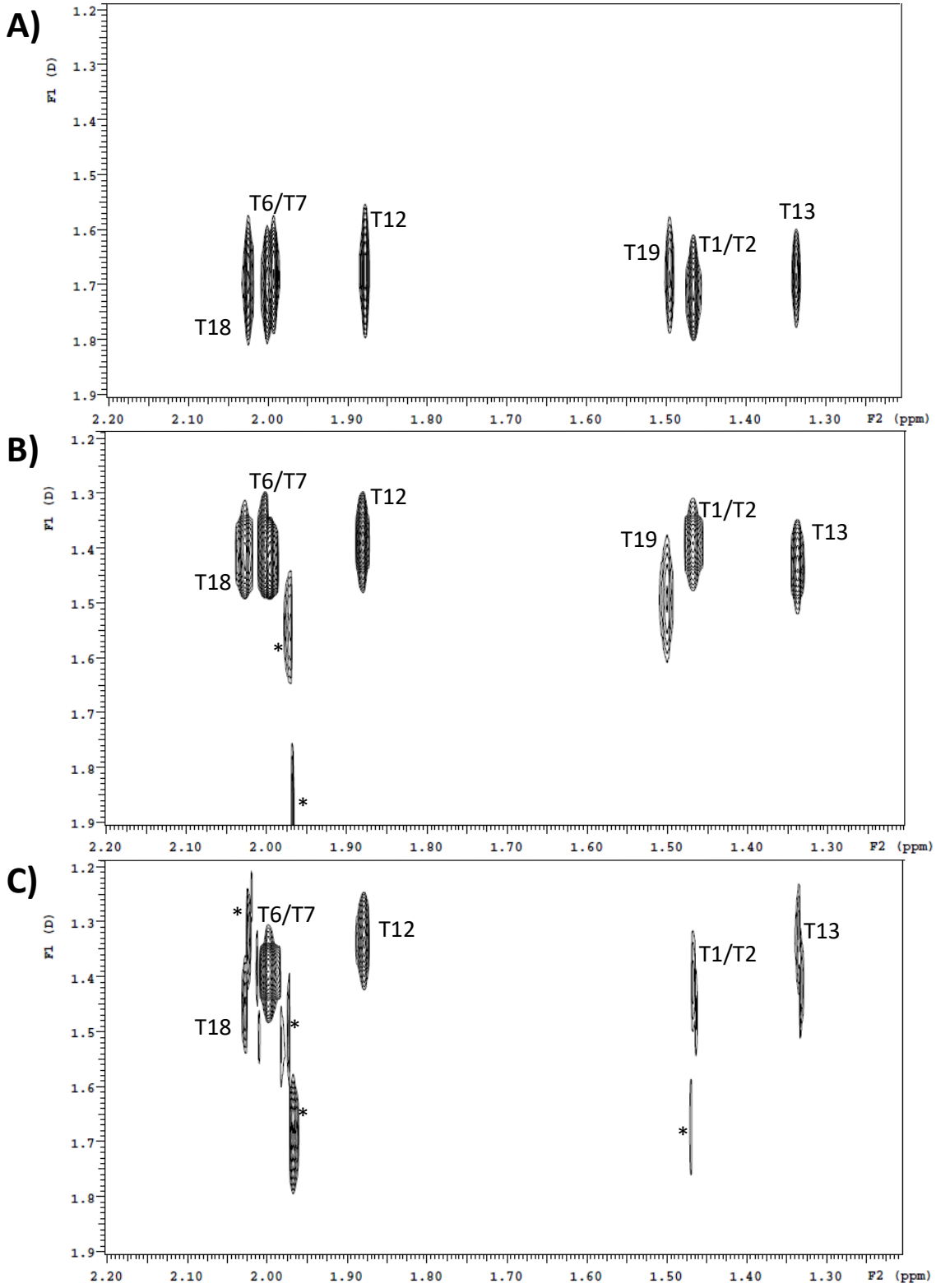

Figure 102. 2D DOSY analysis of methyl signals of m-tel24 G4 (at 25 °C, 0.2 mM DNA, 100 mM KCl, 20 mM KH_2PO_4, pH 7 buffer) A) in the absence or presence of B) 0.5 and C) 1 molar equivalents of **NDI-8**. Peaks from minor species are labeled with stars.

NOESY experiments were also carried out on a 0.2 mM m-tel24 sample in the presence of 0.1 mM **NDI-8**. Interproton distances were calculated from NOESY spectra for m-tel24 G4 in the absence or presence of 0.5 molar equivalents of NDI (Table 12), using the following equation:

$$r_{ij} = r_{ref} (a_{ref}/a_{ij})^{1/6}$$

where a_{ij} is the NOE cross-peak volume and r_{ij} is the interproton distance of the two protons i and j; cross-peak volumes and related distances between thymines H2'/H2" (1.80 Å) were used as the reference. Differences greater than 0.5 Å were found for G17H1'-T18Me and T18H2'-T19H6, located in the upper quartet and in the close lateral loop, and for G23H8-A24H8 in the 3'-flanking region (Table 12). However, no significant difference was found in other G4 regions, suggesting that the major folding was preserved even upon interaction with the NDI, as also corroborated by the fact that NOESY spectra for m-tel24 G4 in the absence or presence of NDI could be almost fully overlapped (Figure 103). Novel putative NOE peaks appeared in correspondence of the chemical shifts assigned to m-tel24/**NDI-8** complex(es) in the ^{1}H NMR spectra (see for example the aromatic-aromatic region in Figure 104), but unfortunately the weakness of these signals, not easily distinguishable from the noise, did not allow us obtaining a high-resolution model for m-tel24/**NDI-8** complex(es).

Table 12. Differences between interproton distances calculated for m-tel24 G4 (at 25 °C, 0.2 mM DNA, 100 mM KCl, 20 mM KH_2PO_4, pH 7 buffer) in the absence or presence of 0.5 molar equivalents of **NDI-8** from NOESY spectra with a mixing time of 200 ms.

Assignment	**Distance (Å) m-tel24**	**Distance (Å) m-tel24:NDI-8, 1:0.5**	**Difference**
T1H2'-H1'	2.14	2.33	0.19
T1H2'-H2''	1.79	1.68	-0.10
T1H2'-H4'	2.74	2.54	-0.20
T1H2'-H6	2.20	2.37	0.16
T1H2'-T2H6	2.63	2.89	0.26
T1H2''-H1'	1.96	1.94	-0.02
T1H2''-H6	2.58	2.61	0.03
T1H3'-H6	2.82	2.72	-0.10
T1Me-H6	1.90	2.04	0.13
T2H1'-H6	2.53	2.47	-0.05
T2H2'-H6	2.48	2.04	-0.44

T2H2''-H6	2.02	2.11	0.09
T2Me-H6	2.05	2.09	0.04
G3H2'-H1'	2.13	2.44	0.31
G3H2'-G4H8	2.04	2.14	0.10
G3H2''-H8	2.68	2.81	0.13
G3H2''-G4H8	1.94	2.13	0.19
G4H1'-H8	2.56	2.68	0.12
G4H1'-G5H8	2.35	2.55	0.20
G5H1'-H8	2.59	2.98	0.40
G5H3'-H8	2.41	2.35	-0.06
T6H1'-H6	2.19	2.20	0.00
T6Me-H1'	2.50	2.26	-0.24
T6Me-H6	1.94	1.93	-0.01
T7H1'-H6	2.56	2.31	-0.25
T7H2'-H6	1.97	1.76	-0.21
T7H2'-A8H8	2.85	2.78	-0.08
T7H2''-H1'	2.19	1.94	-0.25
T7H2''-A8H8	2.51	2.83	0.32
T7H3'-H6	2.46	2.40	-0.06
A8H1'-H8	2.33	2.49	0.17
A8H2'-H1'	1.89	1.78	-0.11
A8H2'-H8	2.29	2.25	-0.03
A8H2''-H1'	2.21	2.20	-0.01
A8H2''-H8	1.93	1.99	0.05
A8H3'-H1'	2.91	2.54	-0.38
A8H3'-H8	2.47	2.60	0.13
A8H4'-H1'	2.30	2.33	0.03
G9H1'-H8	1.77	1.88	0.11
G9H2'-G10H8	2.17	2.20	0.03
G9H2''-H1'	2.04	1.92	-0.12
G9H2''-H3'	2.21	2.77	0.56
G9H2''-G10H8	1.90	1.95	0.05
G10H1'-H8	2.64	2.61	-0.03
G10H1'-G11H8	2.43	2.30	-0.13
G10H2'/H2''-H1'	1.74	1.83	0.09

G10H2'/H2''-H8	1.78	1.77	0.00
G10H3'-H1'	2.93	2.43	-0.50
G10H4'-H1'	2.22	2.15	-0.07
G11H1-G10H1	2.67	2.94	0.27
G11H1'-H8	2.69	2.60	-0.08
G11H2'-H1'	2.02	1.72	-0.30
T12H1'-H6	2.32	2.16	-0.16
T12H2''-H1'	2.07	1.90	-0.16
T12H3'-H6	2.64	2.38	-0.27
T12Me-H6	2.06	2.08	0.02
T13H1'-H6	2.72	2.91	0.19
T13H1'-A14H8	2.55	2.65	0.11
T13H2'-H2''	1.83	1.80	-0.03
T13H2''-H1'	1.94	2.01	0.06
T13H2''-H3'	2.04	2.13	0.08
T13H2''-H6	2.45	2.45	0.00
T13H2''-A14H8	2.07	2.09	0.02
T13H3'-H6	2.59	2.87	0.28
T13H3'-A14H8	2.96	2.83	-0.13
T13H4'-H1'	2.44	2.38	-0.07
T13H4'-H3'	2.20	2.16	-0.03
T13H5'-H3'	2.49	2.46	-0.02
T13H5'-H6	2.54	2.56	0.02
T13H5''-H3'	2.25	2.17	-0.08
T13H5''-H6	2.68	2.69	0.01
T13Me-G5H1	2.70	3.12	0.42
T13Me-G11H8	2.96	2.58	-0.38
T13Me-H3'	1.94	2.01	0.07
T13Me-H6	1.78	1.85	0.07
T13Me-A14H8	2.25	2.33	0.09
A14H1'-H8	2.73	2.60	-0.13
A14H2'-H8	2.28	2.17	-0.11
G15H1'-H8	1.83	1.91	0.08
G15H2'-H1'	2.21	2.07	-0.13
G16H1'-H8	1.75	1.85	0.09

G16H2'-H1'	2.32	2.47	0.15
G16H3'-G17H8	2.52	2.74	0.22
G17H1-G10H1	2.57	2.97	0.39
G17H1'-H8	2.68	2.81	0.13
G17H2'-H3'	1.98	2.23	0.26
G17H2''-H3'	2.10	2.16	0.06
G17H3'-H8	2.43	3.01	0.57
T18H1'-H6	2.44	2.52	0.08
T18H2'-H1'	2.16	2.20	0.04
T18H2'-H6	2.11	2.03	-0.08
T18H2'-T19H6	3.39	4.22	0.84
T18H2''-T19H6	2.80	3.18	0.37
T18H3'-H6	2.76	2.69	-0.07
T18H3'-T19H6	3.49	3.29	-0.20
T18Me-G17H1'	2.46	2.98	0.53
T18Me-H6	1.95	2.00	0.05
T19H1'-H6	2.39	2.61	0.22
T19H2'-H1'	2.15	2.60	0.45
T19H2'-H2''	1.78	2.01	0.23
T19H2'-H6	1.97	2.26	0.29
T19H2'-A20H8	2.49	2.66	0.16
T19H2''-H1'	1.96	2.18	0.23
T19H2''-H6	2.32	2.44	0.12
T19H2''-A20H8	2.49	2.77	0.28
T19H3'-H6	2.31	2.70	0.39
T19H4'-H6	2.96	3.03	0.07
T19Me-H6	1.85	1.99	0.14
A20H1'-G17H8	3.32	3.50	0.19
A20H1'-H8	2.39	2.34	-0.05
A20H2'-H8	1.82	1.90	0.07
A20H2''-H8	2.05	2.06	0.01
A20H3'-H8	2.55	2.66	0.11
G21H1'-H8	1.76	1.70	-0.05
G21H1'-G22H8	2.92	2.58	-0.34
G21H2'-H1'	2.25	2.13	-0.12

G21H2'-H3'	2.65	2.94	0.29
G21H2'-G22H8	2.06	2.17	0.11
G21H2''-H1'	1.90	1.89	-0.01
G21H2''-G22H8	1.87	1.97	0.10
G21H3'-G22H8	3.08	2.65	-0.43
G22H1-G3H1	3.01	2.80	-0.21
G22H1'-H8	2.75	2.49	-0.26
G22H2'/H2''-H8	1.76	1.98	0.22
G22H3'-H8	3.05	2.77	-0.28
G22H3'-G23H8	2.98	3.04	0.06
G23H2'-H1'	2.14	2.37	0.23
G23H2'-H8	2.14	2.06	-0.08
G23H2'-A24H8	2.52	2.46	-0.06
G23H2''-H1'	1.91	1.92	0.01
G23H2''-H8	2.68	2.27	-0.41
G23H2''-A24H8	2.21	2.37	0.16
G23H3'-H8	2.83	2.71	-0.12
G23H3'-A24H8	2.96	2.69	-0.27
G23H8-A24H8	3.37	2.71	-0.65
A24H1'-H8	2.37	2.54	0.17
A24H2'-H8	2.40	2.06	-0.34
A24H2''-H1'	2.02	1.90	-0.12
A24H2''-H8	2.20	2.45	0.24
A24H3'-H8	3.01	2.68	-0.33

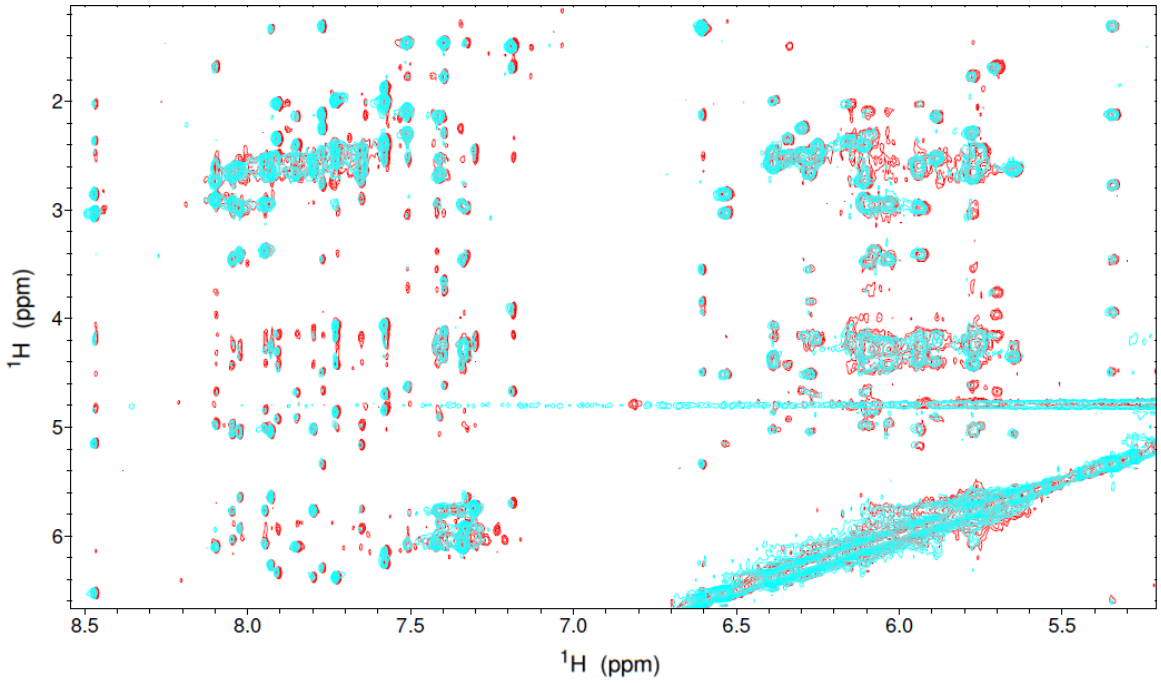

Figure 103. Overlapped NOESY spectra of m-tel24 (at 25 °C, 0.2 mM DNA, 100 mM KCl, 20 mM KH_2PO_4, pH 7 buffer) in the absence (red peaks) or presence of 0.5 molar equivalents **NDI-8** (cyan peaks) with a mixing time of 200 ms. For a better visualization, peaks assignments are not reported.

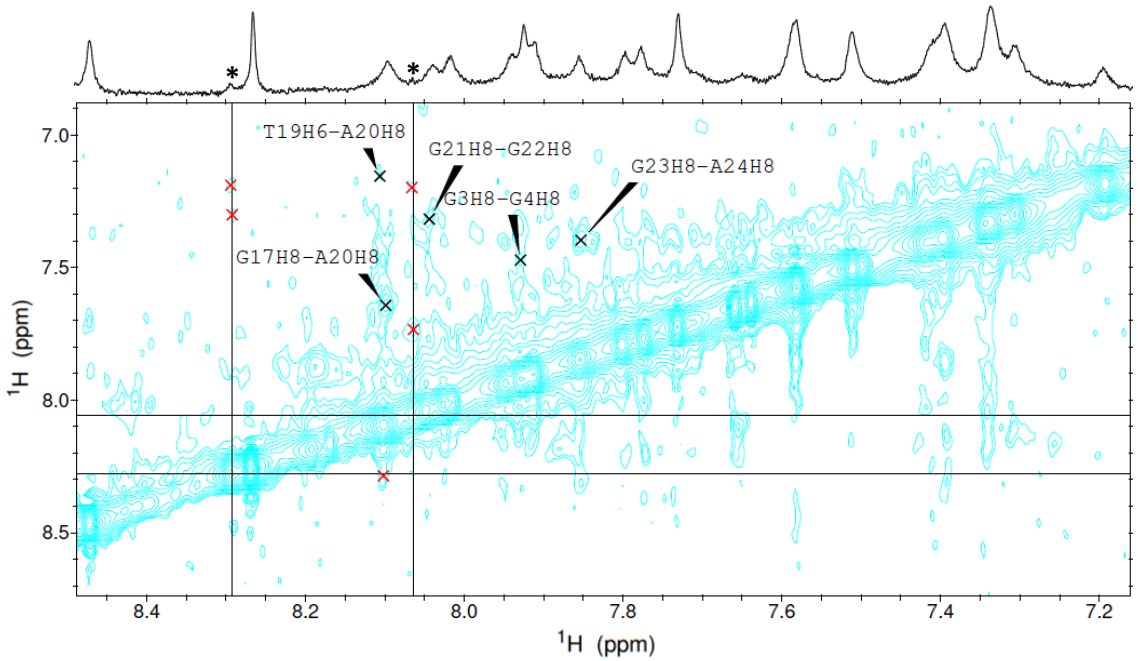

Figure 104. Aromatic-aromatic region of the NOESY spectrum of m-tel24 (at 25 °C, 0.2 mM DNA, 100 mM KCl, 20 mM KH_2PO_4, pH 7 buffer) in the presence of 0.5 molar equivalents **NDI-8** with a mixing time of 200 ms. Top: ^{1}H NMR spectrum of m-tel24/**NDI-8** 1:0.5 solution (at 25 °C, 100 mM KCl, 20 mM KH_2PO_4, pH 7 buffer). ^{1}H NMR signals corresponding to m-tel24/**NDI-8** complex(es) are labeled with stars.

6.4 PAGE experiments

To obtain further information on the binding mode of **NDI-8** to the human telomeric DNA G-quadruplexes, gel electrophoresis experiments were also carried out. The same G4-forming oligonucleotide used for NMR studies (m-tel24) was here chosen as model for telomeric DNA. Native PAGE experiments were performed analysing the oligonucleotide sample at 20 μM concentration mixed with different ligand amounts (from 1:0.5 to 1:4 m-tel24/**NDI-8** ratio, using the same ratios adopted in ^{1}H NMR titrations) in 100 mM KCl, 20 mM KH_2PO_4, pH 7 buffer (Figure 105). Furthermore, a step ladder, with 5 bp differences between adjacent DNA fragments, was used as size marker. Gels were visualized either exploiting **NDI-8** emission (Figure 105A) or by GelGreen™ staining (Figure 105B). A single band was observed for m-tel24 in the absence of the ligand (Figure 105B): considering the migration rate of the ladder, it corresponds to a monomeric G4 folding of m-tel24. Addition of **NDI-8** resulted in the appearance of a lower mobility band already at 1:0.5 m-tel24/**NDI-8** ratio (Figure 105B). By overlapping the two gels in Figure 105, this band was attributed to m-tel24 G4/**NDI-8** complex. As a control, **NDI-8** in the absence of m-tel24 was also loaded on 20% PAGE at two different concentrations (Figures 105A and 105B). **NDI-8** is neutral at pH 7 since it bears two amino and two carboxylic groups. When free in solution, **NDI-8** should not migrate on gel. However, we observed the migration of NDI bands in the same direction as DNA, probably due to the formation of negative NDI species in the here used conditions. The presence of free ligand in solution, gradually increasing with the concentration, suggested that low m-tel24/**NDI-8** ratios were not favoured, consistently with binding stoichiometries obtained by Job plot analysis for monomeric G4s. Higher DNA concentration (200 μM), previously used for the NMR experiments, resulted in worse bands resolution. Thus, native PAGE confirmed that **NDI-8** was able to interact with hybrid monomeric m-tel24 G4 and promote the formation of stable, slowly moving species, consistently with NMR and fluorescence data.

Furthermore, to evaluate the ability of **NDI-8** to induce the formation of G-quadruplex structures in the absence of cations, 20 μM solutions of m-tel24 in 10 mM Tris-HCl buffer (pH 7) were prepared and loaded on 20% PAGE with increasing amounts of the ligand (Figure 106). Noteworthy, **NDI-8** proved to be able to promote the formation of a more compact species, likely the monomeric m-tel24 G4, in perfect agreement with the CD induction experiments. Bands of lower mobility were also observed and associated to free NDI (Figure 106).

Overall, these results further validated **NDI-8** as a strong binder for G4-forming telomeric sequences.

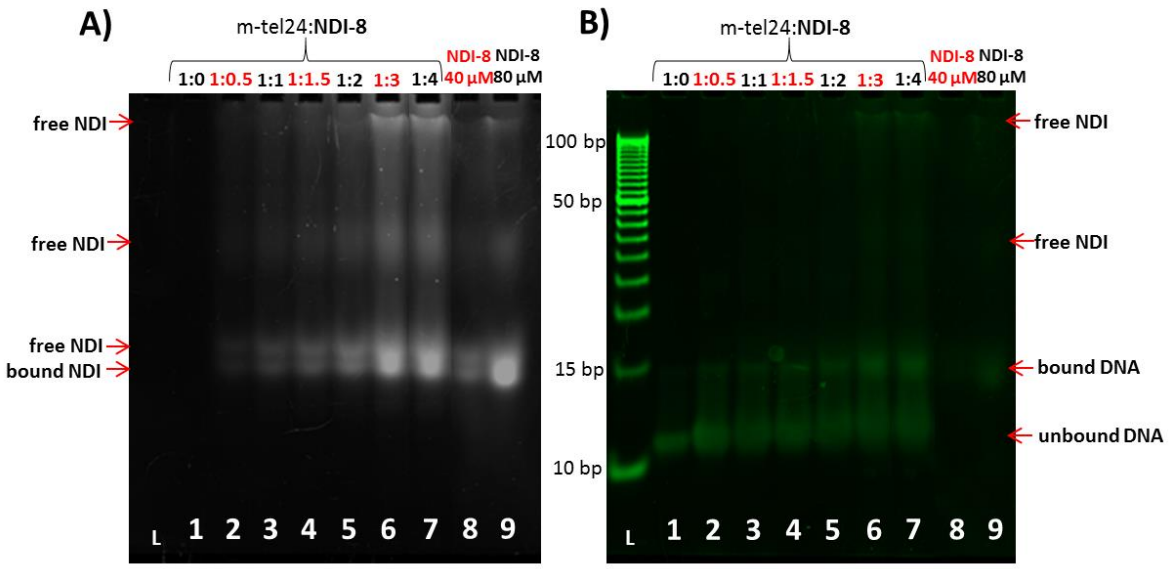

Figure 105. Native PAGE. Oligonucleotide samples were loaded at 20 µM concentration in 100 mM KCl, 20 mM KH_2PO_4, pH 7 buffer and resolved on 20% native PAGE. Lane L: 5 bp DNA ladder. Lane 1: m-tel24 (1:0). Lane 2-7: mixtures m-tel24/**NDI-8** (from 1:0.5 to 1:4). Lane 8: **NDI-8**, 40 µM in 100 mM KCl, 20 mM KH_2PO_4, pH 7 buffer. Lane 9: **NDI-8**, 80 µM in 100 mM KCl, 20 mM KH_2PO_4, pH 7 buffer. Gels were visualized exploiting **NDI-8** emission (A) or by GelGreen™ staining (B).

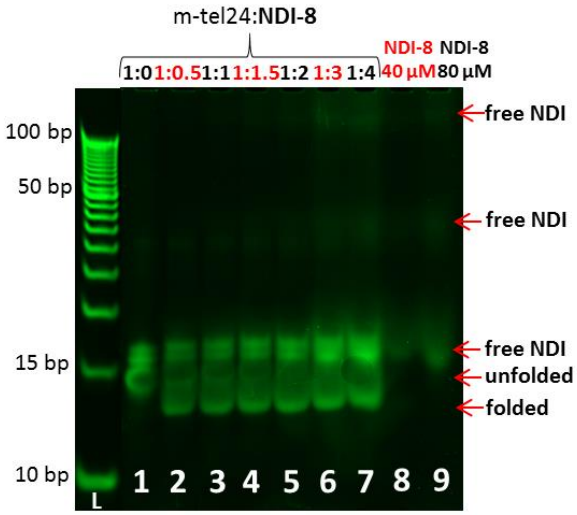

Figure 106. Native PAGE experiments. Oligonucleotide samples were loaded at 20 µM concentration in 10 mM Tris-HCl buffer (pH 7) and resolved on 20% native PAGE. Lane L: 5 bp DNA ladder. Lane 1: m-tel24 (1:0). Lane 2-7: mixtures m-tel24/**NDI-8** (from 1:0.5 to 1:4). Lane 8: **NDI-8**, 40 µM in 10 mM Tris-HCl buffer (pH 7). Lane 9: **NDI-8**, 80 µM in 10 mM Tris-HCl buffer (pH 7).

6.5 Materials and methods

6.5.1 Sample preparation

The sequences d(TAGGGACGGGCGGGCAGGGT) (M2) and d[TTGGG(TTAGGG)$_3$A] (m-tel24), as well as its modified sequences (6U, 7U, 12U, 13U, 18U and 19U), were synthesized on H-8 synthesizer (K&A LaborGerëate) with the use of standard phosphoramidite chemistry and deprotected with aqueous ammonia. Purification and desalting of DNA oligonucleotides were performed by means of: *i*) RP-HPLC using a Kromasil EternityXT-5-PhenylHexyl 21.2 × 250 mm column, then *ii*) FPLC using a HiPrep™ 26/10 Desalting 10 cm × 26 mm column, and finally *iii*) Amicon-15 centrifuge filter with 3.0 kDa MWCO. The oligonucleotide concentration was determined by measuring the absorbance at 260 nm and 90 °C, using the molar extinction coefficients calculated for the unstacked oligonucleotide.[181] Samples for NMR measurements were prepared in 100 mM aqueous KCl and 20 mM potassium phosphate buffer (pH 7). For M2, the temperature treatment of the samples included 5 min incubation at 95 °C immediately followed by cooling in an ice-water bath for 5 min. For m-tel24, the major monomeric folding was formed without annealing. The **NDI-8** stock solution was prepared by dissolving the solid compound in DMSO-d_6 at 10 mM concentration.

The samples for the calibration curve were prepared by adding 1.8, 3.6, 7.2 and 14.4 µL of **NDI-8** dissolved at 10 mM concentration in DMSO-d_6 to 100 mM KCl, 20 mM KH_2PO_4, pH 7.0 buffer to the final volume of 180 µL. DMSO concentration was, respectively, 1%, 2%, 4%, 8% for the four samples. Absorbance measurements were performed at 495 nm on a JASCO V-550 UV-vis spectrophotometer equipped with a Peltier Thermostat JASCO ETC-505T.

6.5.2 NMR spectroscopy

NMR data were collected on Varian NMR Systems 600 and 800 MHz in temperature range between 5 and 35 °C. However, most of the spectra were collected at 25 °C. NMR samples were prepared in 90%/10% H_2O/D_2O or 99.9% D_2O at 0.2 mM oligonucleotide concentration. In titration experiments, aliquots of the **NDI-8** stock solution in DMSO-d_6 were directly added to the DNA solutions inside the NMR tube; the final DMSO concentration was 8%. Control titrations were also performed by adding DMSO-d_6 alone to the DNA solutions; in all cases, no conformational change was observed for both sequences. For experiments in D_2O, H_2O was replaced with D_2O by lyophilization and dissolution in 99.9% D_2O. NMR spectra were acquired with the use of the DPFGSE solvent suppression method. NOESY spectra were acquired at mixing times between 80 and 400 ms. Twenty different gradient strengths (2.4-60.4 G/cm) were

used in diffusion NMR experiments. From diffusion coefficients obtained from DOSY experiments, hydrodynamic radius for m-tel24 in the absence or presence of the NDI was calculated by using Stokes-Einstein equation:[217]

$$D = k_bT/6\pi\eta R \rightarrow R = k_bT/6\pi\eta D$$

where R is the hydrodynamic radius, k_b is the Boltzmann constant ($1.38 \cdot 10^{-23}$ $m^2 \cdot kg \cdot K \cdot s^{-2}$), T is the temperature (298.15 K), η is the fluid viscosity for 9:1 H_2O/D_2O solution calculated as previously described (0.917 mPa·s)[220] and D is the experimentally determined diffusion coefficient.

DSS (4,4-dimethyl-4-silapentane-1-sulfonic acid) was used as a reference to calibrate the chemical shifts, assuming that DSS resonates at 0 ppm. NMR spectra were processed and analyzed with the use of VNMRJ (Varian Inc.) software and Sparky (UCSF) software.

6.5.3 Native PAGE

The mixtures m-tel24/**NDI-8** (up to 1:4 ratio), free m-tel24 G4 and **NDI-8** samples together with a O'RangeRuler™ 5 bp DNA Ladder (ThermoFisher Scientific) were loaded and resolved on native 20% polyacrylamide (19:1 acrylamide:bisacrylamide) PAGE. TBE 1X supplemented with 100 mM KCl was used as running buffer. The oligonucleotide samples loaded on gels were from 2 to 200 µM in oligonucleotide concentration per strand, in 100 mM aqueous KCl and 20 mM potassium phosphate buffer (pH 7). For induction experiments, oligonucleotide samples were prepared at 20 µM concentration in 10 mM Tris-HCl buffer (pH 7) and TBE 1X was used as running buffer. No migration marker was used. Samples were electrophoresed for 3 h at 100 V at room temperature. The bands were visualized by exploiting **NDI-8** emission or using GelGreen™ staining.

CHAPTER 7 – CONCLUSIONS AND PERSPECTIVES

The identification of selective DNA binders, able to discriminate *in vivo* non-canonical nucleic acids conformations, as G-quadruplexes, having crucial roles in tumour and/or viral diseases, is of paramount importance for the development of effective and minimally toxic anticancer and/or antiviral drugs. Taking into account that the existing therapies are always associated with heavy side effects, due to the intrinsically poor selectivity of known anticancer/antiviral drugs,[221–224] the discovery of an efficient targeted therapy, causing limited-to-null toxicity, results in a revolutionary challenge from a scientific and medical point of view.

In the last decade, increasing efforts in the G4 research field have been devoted to the search of selective G4-binders, able not only to fully discriminate G4 *vs.* duplex DNA, but also to specifically recognize different G4 topologies, thus resulting into effective ligands, and expectedly into useful anticancer/antiviral drugs with limited side effects. To reach this ambitious goal, an integrated approach is required, involving the massive production of large libraries of new putative G4 ligands, coupled with High Throughput Screening methodologies for the fast and reliable analysis of the selected compounds.

In this context, we recently described a highly reproducible affinity chromatography-based method – named G4-OAS assay – for the identification of putative G4-ligands.[159,160] Though rapid, simple and effective, a major limitation emerged when using the G4-OAS assay, resulting from the intrinsic chemical nature of the OAS support, *i.e.* unspecific binding of some lipophilic aromatic ligands on the polystyrene nude resin.[160] In this PhD thesis this crucial problem, dramatically limiting the scope of the assay, was addressed, moving from polystyrene to chemically inert CPG supports. However, all the commercially available CPG supports, typically functionalized with linkers rapidly hydrolyzed under basic conditions, were not suitable to our objectives. In fact, main requirement for our design was the attachment of the first nucleoside through a linker chemically stable to the final deprotection step, so to obtain fully deprotected oligonucleotides bound to the support on which the affinity chromatography binding assays could be performed. To solve this problem, we designed a novel functionalization for CPG supports, involving a linker – made of a flexible spacer of hexaethylene glycol attached to the first nucleoside monomer (*i.e.*, 5'-*O*-DMT-3'-*O*-acetylthymidine) through the nucleobase – being suitable for oligonucleotide elongation by standard phosphoramidite chemistry and chemically stable to the final deprotection procedure. Once synthesized the G4-forming oligonucleotides of interest on the CPG, a set of model ligands were flown through the glass supports. The molecules with high affinity for the G4s

were retained by the solid supports, while those with low affinity were eluted with a washing solution and quantified by UV measurements. The specific interaction of a given ligand with a G4 structure was confirmed by inducing its unfolding on the support by a denaturing solution, resulting in full release in solution of the captured ligand. After each binding assay, functionalized CPG supports were annealed again to allow the correct G4 refolding and reuse the same batch of support for other binding assays. Noteworthy, our results proved that the novel support had low-to-null unspecific interactions with the tested model ligands, in contrast with previously used OAS. Indeed, all the investigated ligands were generally recovered in higher amounts from nude CPG, requiring smaller volumes of the washing solution for their quantitative recovery compared to nude OAS. In addition, highly specific binding was maintained for those ligands which are well characterized G4-binders, displaying in our tests binding data with a trend respecting the order of the binding affinities determined in solution. Furthermore, for its lower unspecific binding and higher thermal stability, the same batch of functionalized CPG could be used for typically more than 50 experiments, *i.e.* about three times the number of binding assays generally carried out on the OAS resin, moreover offering much cleaner and more reliable results. Finally, compared to the other methodologies currently exploited to select G4 ligands[19,225–227] – such as FRET-based melting,[228] G4-FID,[229,230] SPR,[19] NMR,[210] ESI-MS[231] and small molecule microarray-based screenings[232] – the advantages of the G4-CPG assay consist in the possibility of attaching to the support the wild-type oligonucleotide sequence without necessarily modifying it to detect ligand-G4 binding, and of studying the ligand-G4 interaction in pseudo-physiological conditions.

Indeed, the conformational behaviour of the oligonucleotides linked to the CPG support was also studied by exploiting a water-soluble fluorescent naphthalene diimide dye, known to give different fluorescent responses upon binding to topologically different G4 structures.[184] We proved that the oligonucleotides, when anchored to CPG and left in contact with the selected buffer, adopt the same conformations they typically have in solution. This result provided a proof-of concept that our novel approach is a powerful tool to identify not only structure-selective G4-ligands, but even conformation-selective G4-ligands.

After full optimization of the G4-CPG assay, two different libraries of putative G4 ligands, based on furobenzoxazine naphthoquinone or naphthalene diimide scaffolds, were evaluated.

As far as the library of furobenzoxazine naphthoquinone derivatives is concerned, these were selected as analogs of a lead-like G-quadruplex targeting compound (**4**),[187] differing for the pendant groups on the N-atom of the oxazine ring. These molecules were tested *vs.* topologically different G4s by the G4-CPG assay. The obtained results showed that all the

compounds were able to bind several G4 structures, even though with peculiar preferences, and two of them fully discriminated G4 *vs.* duplex DNA. Biological assays proved that almost all the compounds produced effective DNA damage, also at the telomeric level, showing marked antiproliferative effects on tumour cells in the low μM range. Combined analysis of the G4-CPG binding assays and biological data led us to focus on compound **S4-5**, being less cytotoxic than the parent compound **4** on normal cells. An in-depth biophysical characterization of the binding of **S4-5** to different G4s was carried out by CD, NMR and Microscale Thermophoresis, demonstrating that the here identified ligand had higher affinity for the model G4s and higher ability to discriminate G4 *vs.* duplex DNA than **4**. Molecular docking studies, in agreement with the NMR data, suggested that **S4-5** interacted with the accessible grooves of the target G4 structures, giving clues for its increased binding selectivity. Considering that targeting the most variable regions of the G4 structures, *i.e.* the grooves and the loops, could be a successful, even though still poorly explored, approach for the specific recognition of different G4 conformations, and that very few G4-groove binders have been thus far characterized, these results are of great relevance to develop novel effective candidate anticancer drugs.

As far as the naphthalene diimide library is concerned, novel functionalized dimeric NDIs were designed, synthesized and evaluated by G4-CPG assay. Overall, all the tested compounds proved to be effective G4 ligands and stronger binders for intramolecular dimeric than monomeric G4s. In particular, **NDI-3**, **NDI-4**, **NDI-6**, **NDI-8** and **NDI-9** emerged as the most promising compounds, due to their high G4s *vs.* duplex DNA selectivity. In addition, G4-CPG assay results allowed us demonstrating that mitigating the affinity of the NDI binding core for G4s allowed the core selectivity emerging. Biological assays unambiguously designated, among the five selected NDIs, **NDI-8** as the most promising candidate due to its strong activity against cancer cells (IC_{50} = 6.6 nM) and high selectivity in killing cancer cells than normal cells. Therefore, **NDI-8** was further investigated by CD, fluorescence, NMR and gel electrophoresis analyses. By combination of CD titrations and CD-melting experiments, **NDI-8** was proved to preferentially affect G4 structures than duplex DNA. Moreover, the ability of **NDI-8** to induce G4 structure formation in the absence of cations was proved by CD and native PAGE experiments. Furthermore, fluorescence experiments revealed binding stoichiometries of 1:1 and 3:2 for complexes of **NDI-8** with telomeric G4 monomer, while binding stoichiometries of 1:1 and 5:1 were found for **NDI-8** complexes with a telomeric G4 dimer. In-depth NMR analyses showed the preferential binding of the **NDI-8** to the 5'-end spatially close residues, the upper quartet and half of the middle quartet of a G4 structure taken from the human

telomeric DNA. Finally, the remarkable ability of **NDI-8** to promote the formation of dimeric G4 species was demonstrated by DOSY experiments.

Overall, the novel developed G4-CPG method based on our newly designed CPG support allowed us identifying two promising candidate drugs for *in vivo* studies, **S4-5** and **NDI-8,** showing respectively binding preferences for parallel G4s and monomeric or higher order telomeric G-quadruplex structures, in addition to their high G4s *vs.* duplex DNA selectivity.

Our current efforts are devoted to the extension of the G4-CPG assay to biologically relevant human *i*-motif-forming[233–235] and viral G4-forming DNA sequences,[12,236,237] in order to analyze novel libraries of putative conformation-selective ligands, as well as to automate our method with the aim of speeding up the search for effective anticancer/antiviral drugs in targeted therapies.

Abbreviation

Ac, Acetyl

ACN, Acetonitrile

AD4.2, Autodock 4.2

ADP, Adenosine Diphosphate

ADT, AutoDockTools

AFM, Atomic Force Microscope

ALT, Alternative Length Telomere

AMA, Ammonium hydroxide/Methylamine

BRCA, Breast Related Cancer Antigens

CD, Circular Dichroism

c_{ex}-NDI, core extended Naphthalene Diimide

CPG, Controlled Pore Glass

CTR, Control

DAPI, 4',6-diamidino-2-phenylindole

DCC, *N*,*N*'-dicyclohexylcarbodiimide

DCM, Dichloromethane

DDR, DNA Damage Response

DEAD, Diethyl Azodicarboxylate

DMAP, 4-dimethylaminopyridine

DMEM, Dulbecco's Modified Eagle's Medium

DMF, *N*,*N*-dimethylformamide

DMSO, Dimethyl Sulfoxide

DMT, 4,4'-dimethoxytrityl

DOSY, Diffusion Ordered Spectroscopy

DPFGSE, Double Pulsed Field Gradient Spin Echo

DSS, 4,4-dimethyl-4-silapentane-1-sulfonic acid

ESI-MS, Electrospray Ionization Mass Spectrometry

ETT, 5-ethylthio-1H-tetrazole

FBS, Fetal Bovine Serum

FID, Fluorescence Intercalator Displacement

FPLC, Fast Protein Liquid Chromatography

FRET, Fluorescence Resonance Energy Transfer

G4, G-quadruplex

GALS, Genetic Algorithm Local Search

GIST, Gastrointestinal Stromal Tumours

GMP, Guanosine Monophosphate

γH2AX, phosphorylated form of histone H2AX

HOBt, 1-hydroxybenzotriazole

HPLC, High Performance Liquid Chromatography

hTERT, human Telomerase Reverse Transcriptase

hTR, human Telomerase RNA Component

HMBC, Heteronuclear Multiple Bond Correlation

HTS, High Throughput Screening

IC_{50}, Median Inhibition Concentration

IF, Immunofluorescence

IgG, Immunoglobulin G

K_d, dissociation Constant

LCAA-CPG, Long Chain AlkylAmine-CPG

M1, Mortality stage 1

M2, Mortality stage 2

MI, *N*-methylimidazole

MST, Microscale Thermophoresis

MWCO, Molecular Weight Cut-Off

NDI, Naphthalene Diimide

NHE, Nuclease Hypersensitivity Element

NMR, Nuclear Magnetic Resonance

NOESY, Nuclear Overhauser Spectroscopy

OAS, Oligo Affinity Support

PAGE, Polyacrylamide Gel Electrophoresis

PARP, Poly ADP Ribose Polymerase

PBS, Phosphate Buffered Saline

PDAC, Pancreatic Ductal Adenocarcinoma

PDB, Protein Data Bank

PDS, Pyridostatin

PIPER, *N*,*N*′-bis-(2-(1-piperidino)ethyl)-3,4,9,10-perylene tetracarboxylic acid diimide

POT1, Protection of Telomeres protein 1

PP, Polypropilene

PS, Polystyrene/polyethylene glycol

PTFE, Polytetrafluoroethylene

Py, Pyridine

RP-HPLC, Reversed-phase High-performance Liquid Chromatography

SAX, Strong Anion Exchange

S.D., Standard Deviation

Sp1, Specificity protein 1

SPR, Surface Plasmon Resonance

TBE, Tris-borate-EDTA

TEMPO, 2,2,6,6-tetramethyl-1-piperidinyloxy

TBA-Cl, Tetrabutylammonium Chloride

TCA, Trichloroacetic Acid

THF, Tetrahydrofuran

TIF, Telomere Induced Foci

TMPyP4, 5,10,15,20-tetrakis(1-methyl-4-pyridinio)porphyrin

TO, Thiazole Orange

TRF1, Telomere Repeat Factor 1

TRF2, Telomere Repeat Factor 2

References

[1] A. Rich, *Gene* **1993**, *135*, 99–109.

[2] J. D. Watson, F. H. C. Crick, *Nature* **1953**, *171*, 737–738.

[3] A. Rich, *Biochim. Biophys. Acta* **1958**, *29*, 502–509.

[4] E. Henderson, C. C. Hardin, S. K. Walk, I. Tinoco, E. H. Blackburn, *Cell* **1987**, *51*, 899–908.

[5] W. I. Sundquist, A. Klug, *Nature* **1989**, *342*, 825–829.

[6] A. Siddiqui-Jain, C. L. Grand, D. J. Bearss, L. H. Hurley, *Proc. Natl. Acad. Sci.* **2002**, *99*, 11593–11598.

[7] D. Drygin, A. Siddiqui-Jain, S. O'Brien, M. Schwaebe, A. Lin, J. Bliesath, C. B. Ho, C. Proffitt, K. Trent, J. P. Whitten, et al., *Cancer Res.* **2009**, *69*, 7653–7661.

[8] R. Hänsel-Hertsch, M. Di Antonio, S. Balasubramanian, *Nat. Rev. Mol. Cell Biol.* **2017**, *18*, 279–284.

[9] S. Balasubramanian, L. H. Hurley, S. Neidle, *Nat. Rev. Drug Discov.* **2011**, *10*, 261–275.

[10] D. Rhodes, H. J. Lipps, *Nucleic Acids Res.* **2015**, *43*, 8627–8637.

[11] S. Balasubramanian, S. Neidle, *Curr. Opin. Chem. Biol.* **2009**, *13*, 345–353.

[12] M. Metifiot, S. Amrane, S. Litvak, M. L. Andreola, *Nucleic Acids Res.* **2014**, *42*, 12352–12366.

[13] T. A. Brooks, S. Kendrick, L. Hurley, *FEBS J.* **2010**, *277*, 3459–3469.

[14] S. Neidle, *FEBS J.* **2010**, *277*, 1118–1125.

[15] G. W. Collie, G. N. Parkinson, *Chem. Soc. Rev.* **2011**, *40*, 5867–5892.

[16] S. Arnott, R. Chandrasekaran, C. M. Marttila, *Biochem. J.* **1974**, *141*, 537–543.

[17] J. Lagnado, *Biochem. Soc.* **2013**, *35*, 44–46.

[18] M. Gellert, M. N. Lipsett, D. R. Davies, *Proc. Natl. Acad. Sci.* **1962**, *48*, 2013–2018.

[19] P. Murat, Y. Singh, E. Defrancq, *Chem. Soc. Rev.* **2011**, *40*, 5293–5307.

[20] C. Platella, C. Riccardi, D. Montesarchio, G. N. Roviello, D. Musumeci, *Biochim. Biophys. Acta - Gen. Subj.* **2017**, *1861*, 1429–1447.

[21] A. Ambrus, D. Chen, J. Dai, T. Bialis, R. A. Jones, D. Yang, *Nucleic Acids Res.* **2006**, *34*, 2723–2735.

[22] R. I. Mathad, E. Hatzakis, J. Dai, D. Yang, *Nucleic Acids Res.* **2011**, *39*, 9023–9033.

[23] L. Sun, H. Jin, X. Zhao, Z. Liu, Y. Guan, Z. Yang, L. Zhang, L. Zhang, *ChemMedChem* **2014**, *9*, 993–1001.

[24] M. Marušič, J. Plavec, *Angew. Chemie - Int. Ed.* **2015**, *54*, 11716–11719.

[25] M. Webba da Silva, M. Trajkovski, Y. Sannohe, N. M. Hessari, H. Sugiyama, J. Plavec, *Angew. Chemie - Int. Ed.* **2009**, *48*, 9167–9170.

[26] X. Cang, J. Šponer, T. E. Cheatham, *Nucleic Acids Res.* **2011**, *39*, 4499–4512.

[27] Y. Wang, D. J. Patel, *J. Mol. Biol.* **1995**, *251*, 76–94.

[28] C. Kang, X. Zhang, R. Ratliff, R. Moyzis, A. Rich, *Nature* **1992**, *356*, 126–131.

[29] C. J. Lech, B. Heddi, A. T. Phan, *Nucleic Acids Res.* **2013**, *41*, 2034–2046.

[30] A. Włodarczyk, P. Grzybowski, A. Patkowski, A. Dobek, *J. Phys. Chem. B* **2005**, *109*, 3594–3605.

[31] E. Largy, A. Marchand, S. Amrane, V. Gabelica, J. L. Mergny, *J. Am. Chem. Soc.* **2016**, *138*, 2780–2792.

[32] C. C. Hardin, A. G. Perry, K. White, *Biopolymers* **2000**, *56*, 147–194.

[33] J. S. Lee, *Nucleic Acids Res.* **1990**, *20*, 6057–6060.

[34] D. Miyoshi, A. Nakao, N. Sugimoto, *Nucleic Acids Res.* **2003**, *31*, 1156–1163.

[35] T. Fujii, P. Podbevšek, J. Plavec, N. Sugimoto, *J. Inorg. Biochem.* **2017**, *166*, 190–198.

[36] D. Bhattacharyya, G. Mirihana Arachchilage, S. Basu, *Front. Chem.* **2016**, *4*, 1–14.

[37] J. L. Huppert, S. Balasubramanian, *Nucleic Acids Res.* **2005**, *33*, 2908–2916.

[38] A. Bedrat, L. Lacroix, J. L. Mergny, *Nucleic Acids Res.* **2016**, *44*, 1746–1759.

[39] O. Kikin, L. D'Antonio, P. S. Bagga, *Nucleic Acids Res.* **2006**, *34*, 676–682.

[40] J. Bidzinska, G. Cimino-Reale, N. Zaffaroni, M. Folini, *Molecules* **2013**, *18*, 12368–12395.

[41] H. Lodish, A. Berk, S. Zipursky, *Molecular Cell Biology*, *Proto-Oncogenes and Tumor-Suppressor Genes*, New York, **2000**.

[42] S. M. Bailey, J. P. Murnane, *Nucleic Acids Res.* **2006**, *34*, 2408–2417.

[43] M. A. Jafri, S. A. Ansari, M. H. Alqahtani, J. W. Shay, *Genome Med.* **2016**, *8*, 69.

[44] J. Fajkus, E. Sýkorová, A. R. Leitch, *Chromosom. Res.* **2005**, *13*, 469–479.

[45] J. D. Griffith, L. Comeau, S. Rosenfield, R. M. Stansel, A. Bianchi, H. Moss, T. De Lange, *Cell* **1999**, *97*, 503–514.

[46] Y. Cong, W. E. Wright, J. W. Shay, *Microbiol. Mol. Biol. Rev.* **2002**, *66*, 407.

[47] K. Jäger, M. Walter, *Genes (Basel).* **2016**, *7*, 1–24.

[48] A. T. Phan, J. L. Mergny, *Nucleic Acids Res.* **2002**, *30*, 4618–4625.

[49] V. Sekaran, J. Soares, M. B. Jarstfer, *J. Med. Chem.* **2014**, *57*, 521–538.

[50] G. Biffi, M. Di Antonio, D. Tannahill, S. Balasubramanian, *Nat. Chem.* **2014**, *6*, 75–80.

[51] G. Biffi, D. Tannahill, J. McCafferty, S. Balasubramanian, *Nat. Chem.* **2013**, *5*, 182–186.

[52] A. Henderson, Y. Wu, Y. C. Huang, E. A. Chavez, J. Platt, F. B. Johnson, R. M. Brosh, D. Sen, P. M. Lansdorp, *Nucleic Acids Res.* **2014**, *42*, 860–869.

[53] A. Laguerre, K. Hukezalie, P. Winckler, F. Katranji, G. Chanteloup, M. Pirrotta, J. M.

Perrier-Cornet, J. M. Y. Wong, D. Monchaud, *J. Am. Chem. Soc.* **2015**, *137*, 8521–8525.

[54] D. L. Ma, Z. Zhang, M. Wang, L. Lu, H. J. Zhong, C. H. Leung, *Chem. Biol.* **2015**, *22*, 812–828.

[55] Y. C. Chan, J. W. Chen, S. Y. Su, C. C. Chang, *Biosens. Bioelectron.* **2013**, *47*, 566–573.

[56] H. Y. Liu, Q. Zhao, T. P. Zhang, Y. Wu, Y. X. Xiong, S. K. Wang, Y. L. Ge, J. H. He, P. Lv, T. M. Ou, et al., *Cell Chem. Biol.* **2016**, *23*, 1261–1270.

[57] L. Maestroni, S. Matmati, S. Coulon, *Genes (Basel)* **2017**, *8*, 1–16.

[58] E. M. Rezler, D. J. Bearss, L. H. Hurley, *Curr. Opin. Pharmacol.* **2002**, *2*, 415–423.

[59] D. E. Shippen, *Curr. Opin. Genet. Dev.* **1993**, *3*, 759–763.

[60] J. D. Watson, T. A. Baker, S. P. Bell, A. Gann, M. Levine, R. Losich, *Molecular Biology of the Gene*, **2004**.

[61] E. Demkovicova, L. Bauer, P. Krafcìkovà, K. Tluckova, P. Tóthova, A. Halaganová, E. Valušová, V. Víglaský, *J. Nucl. Sci. Technol.* **2017**, *2017*, 1–14.

[62] Y. Xu, *Chem. Soc. Rev.* **2011**, *40*, 2719–2740.

[63] Y. Xu, H. Sato, Y. Sannohe, K. I. Shinohara, H. Sugiyama, *J. Am. Chem. Soc.* **2008**, *130*, 16470–16471.

[64] P. Baumann, T. R. Cech, *Science* **2001**, *292*, 1171–1175.

[65] D. Liu, A. Safari, M. S. O'Connor, D. W. Chan, A. Laegeler, Q. Jun, S. Y. Zho, *Nat. Cell Biol.* **2004**, *6*, 673–680.

[66] A. J. Zaug, E. R. Podell, T. R. Cech, *Proc. Natl. Acad. Sci. U. S. A.* **2005**, *102*, 10864–10869.

[67] R. Giraldo, M. Suzuki, L. Chapman, D. Rhodes, *Proc. Natl. Acad. Sci. U. S. A.* **1994**, *91*, 7658–7662.

[68] Y. Xu, A. Goldkorn, *Genes (Basel)* **2016**, *7*, 1–22.

[69] A. L. Wolfe, K. Singh, Y. Zhong, P. Drewe, V. K. Rajasekhar, V. R. Sanghvi, K. J. Mavrakis, M. Jiang, J. E. Roderick, J. Van Der Meulen, et al., *Nucleic Acids Res.* **2009**, *18*, 764–7.

[70] J. Dai, M. Carver, D. Yang, *Biochimie* **2008**, *90*, 1172–1183.

[71] G. N. Parkinson, M. P. H. Lee, S. Neidle, *Nature* **2002**, *417*, 876–880.

[72] J. Dai, M. Carver, C. Punchihewa, R. A. Jones, D. Yang, *Nucleic Acids Res.* **2007**, *35*, 4927–4940.

[73] A. T. Phan, K. N. Luu, D. J. Patel, *Nucleic Acids Res.* **2006**, *34*, 5715–5719.

[74] V. Víglaský, L. Bauer, K. Tluckova, P. Javorsky, *J. Nucleic Acids* **2010**, *2010*, 1–8.

[75] J. Dai, C. Punchihewa, A. Ambrus, D. Chen, R. A. Jones, D. Yang, *Nucleic Acids Res.* **2007**, *35*, 2440–2450.

[76] V. Víglaský, L. Bauer, K. Tluckovà, *Biochemistry* **2010**, *49*, 2110–2120.

[77] A. I. Karsisiotis, N. M. A. Hessari, E. Novellino, G. P. Spada, A. Randazzo, M. Webba Da Silva, *Angew. Chemie - Int. Ed.* **2011**, *50*, 10645–10648.

[78] P. Tòthovà, P. Krafcìkovà, V. Víglaský, *Biochemistry* **2014**, *53*, 7013–7027.

[79] R. del Villar-Guerra, J. O. Trent, J. B. Chaires, *Angew. Chemie - Int. Ed.* **2018**, *57*, 7171–7175.

[80] L. G. Palmer, M. M. Civan, *J. Membr. Biol* **1977**, *33*, 41–61.

[81] L. Petraccone, *Top Curr. Chem.* **2013**, *330*, 23–46.

[82] L. Petraccone, C. Spink, J. O. Trent, N. C. Garbett, C. S. Mekmaysy, C. Giancola, J. B. Chaires, *J. Am. Chem. Soc.* **2011**, *133*, 20951–20961.

[83] L. Petraccone, C. Spink, J. O. Trent, N. C. Garbett, C. S. Mekmaysy, C. Giancola, J. B. Chaires, *J. Am. Chem. Soc.* **2011**, *133*, 20951–20961.

[84] Y. Xu, T. Ishizuka, K. Kurabayashi, M. Komiyama, *Angew. Chemie - Int. Ed.* **2009**, *48*, 7833–7836.

[85] L. Petraccone, A. Malafronte, J. Amato, C. Giancola, *J. Phys. Chem. B* **2012**, *116*, 2294–2305.

[86] L. Petraccone, N. Garbett, J. B. Chaires, J. O. Trent, *Biopolymers* **2010**, *93*, 533–548.

[87] M. H. Hu, S. Bin Chen, B. Wang, T. M. Ou, L. Q. Gu, J. H. Tan, Z. S. Huang, *Nucleic Acids Res.* **2017**, *45*, 1606–1618.

[88] A. Cummaro, I. Fotticchia, M. Franceschin, C. Giancola, L. Petraccone, *Biochimie* **2011**, *93*, 1392–1400.

[89] T. Wahlström, M. Arsenian Henriksson, *Biochim. Biophys. Acta - Gene Regul. Mech.* **2015**, *1849*, 563–569.

[90] B. J. Chen, Y. L. Wu, Y. Tanaka, W. Zhang, *Int. J. Biol. Sci.* **2014**, *10*, 1084–1096.

[91] M. K. Ramlee, J. Wang, W. X. Toh, S. Li, *Genes (Basel)* **2016**, *7*, 1–43.

[92] T. A. Brooks, L. H. Hurley, *Genes Cancer* **2010**, *1*, 641–649.

[93] E. Desjardins, N. Hay, *Mol. Cell. Biol.* **1993**, *13*, 5710–5724.

[94] L. C. Showe, R. C. Moore, J. Erikson, C. M. Croce, *Proc. Natl. Acad. Sci. U. S. A.* **1987**, *84*, 2824–8.

[95] O. Sakatsume, H. Tsutsui, H. Gao, X. Tang, T. Murata, K. Itakura, K. K. Yokoyama, *J. Biol. Chem.* **1996**, *271*, 31322–31333.

[96] T. Simonsson, M. Pribylova, M. Vorlickova, *Biochem. Biophys. Res. Commun.* **2000**, *278*, 158–166.

[97] A. T. Phan, Y. S. Modi, D. J. Patel, *J. Am. Chem. Soc.* **2004**, *126*, 8710–8716.

[98] M. A. Islam, S. D. Thomas, V. V. Murty, K. J. Sedoris, D. M. Miller, *J. Biol. Chem.* **2014**, *289*, 8521–8531.

[99] J. Seenisamy, E. M. Rezler, T. J. Powell, D. Tye, V. Gokhale, C. S. Joshi, A. Siddiqui-Jain, L. H. Hurley, *J. Am. Chem. Soc.* **2004**, *126*, 8702–8709.

[100] H. You, J. Wu, F. Shao, J. Yan, *J. Am. Chem. Soc.* **2015**, *137*, 2424–2427.

[101] S. D. H. LH, *J. Med. Chem.* **2009**, *52*, 2863–2874.

[102] Y. Yarden, W. J. Kuang, T. Yang-Feng, L. Coussens, S. Munemitsu, T. J. Dull, E. Chen, J. Schlessinger, U. Francke, A. Ullrich, *EMBO J.* **1987**, *6*, 3341–3351.

[103] J. Yang, X. Du, A. J. Lazar, R. Pollock, K. Hunt, K. Chen, X. Hao, J. Trent, W. Zhang, *Cancer* **2008**, *113*, 1532–1543.

[104] R. J. Roskoski, *Biochem. Biophys. Res. Commun.* **2005**, *338*, 1307–1315.

[105] A. Hoeben, P. Schoffski, M. Debiec-Rychter, *Br. J. Cancer.* **2008**, *98*, 684–688.

[106] D. A. Tuveson, N. A. Willis, T. Jacks, J. D. Griffin, S. Singer, C. D. Fletcher, J. A. Fletcher, G. D. Demetri, *Oncogene* **2001**, *20*, 5054–5058.

[107] M. J. Zhu, W. B. Ou, C. D. Fletcher, P. S. Cohen, G. D. Demetri, J. A. Fletcher, *Oncogene* **2007**, *26*, 6386–6395.

[108] C. D. Mol, D. R. Dougan, T. R. Schneider, R. J. Skene, M. L. Kraus, D. N. Scheibe, G. P. Snel, H. Zou, B. C. Sang, K. P. Wilson, *J. Biol. Chem.* **2004**, *279*, 31655–31663.

[109] H. Fernando, A. P. Reszka, J. Huppert, S. Ladame, S. Rankin, A. R. Venkitaraman, S. Neidle, S. Balasubramanian, *Biochemistry* **2006**, *45*, 7854–7860.

[110] A. T. Phan, V. Kuryavyi, S. Burge, S. Neidle, D. J. Patel, *J. Am. Chem. Soc.* **2007**, *129*, 4386–4392.

[111] A. K. Todd, S. M. Haider, G. N. Parkinson, S. Neidle, *Nucleic Acids Res.* **2007**, *35*, 5799–5808.

[112] D. Wei, G. N. Parkinson, A. P. Reszka, S. Neidle, *Nucleic Acids Res.* **2012**, *40*, 4691–4700.

[113] D. Wei, J. Husby, S. Neidle, *Nucleic Acids Res.* **2015**, *43*, 629–644.

[114] V. Kuryavyi, A. T. Phan, D. J. Patel, *Nucleic Acids Res.* **2010**, *38*, 6757–6773.

[115] M. Daniel, G. W. Peek, T. O. Tollefsbol, *Gene* **2012**, *498*, 135–146.

[116] M. Ruden, N. Puri, *Cancer Treat. Rev.* **2013**, *39*, 444–456.

[117] S. M. L. Palumbo, S. W. Ebbinghaus, L. H. Hurley, *J. Am. Chem. Soc.* **2009**, *131*, 10878–10891.

[118] J. B. Chaires, J. O. Trent, R. D. Gray, W. L. Dean, R. Buscaglia, S. D. Thomas, D. M. Miller, *PLoS One* **2014**, *9*, 1–13.

[119] K. W. Lim, L. Lacroix, D. J. E. Yue, J. K. C. Lim, J. M. W. Lim, A. T. Phan, *J. Am. Chem. Soc.* **2010**, *132*, 12331–12342.

[120] L. Strekowski, B. Wilson, *Mutat. Res. - Fundam. Mol. Mech. Mutagen.* **2007**, *623*, 3–13.

[121] E. Gavathiotis, R. A. Heald, M. F. G. Stevens, M. S. Searle, *J. Mol. Biol.* **2003**, *334*, 25–36.

[122] E. Salvati, C. Leonetti, A. Rizzo, M. Scarsella, M. Mottolese, R. Galati, I. Sperduti, M.

F. G. Stevens, M. D'Incalci, M. Blasco, et al., *J. Clin. Invest.* **2007**, *117*, 3236–3247.

[123] N. H. Campbell, G. N. Parkinson, A. P. Reszka, S. Neidle, *J. Am. Chem. Soc.* **2008**, *130*, 6722–6724.

[124] M. Read, R. J. Harrison, B. Romagnoli, F. A. Tanious, S. H. Gowan, A. P. Reszka, W. D. Wilson, L. R. Kelland, S. Neidle, *Proc. Natl. Acad. Sci. U. S. A.* **2001**, *98*, 4844–4849.

[125] A. M. Burger, F. Dai, C. M. Schultes, A. P. Reszka, M. J. Moore, J. A. Double, S. Neidle, *Cancer Res.* **2005**, *665*, 1489–1496.

[126] Y. Du, X. Zhou, *Chem. Rec.* **2013**, *13*, 371–384.

[127] G. N. Parkinson, R. Ghosh, S. Neidle, *Biochemistry* **2007**, *46*, 2390–2397.

[128] A. T. Phan, V. Kuryavyi, H. Y. Gaw, D. J. Patel, *Nat. Chem. Biol.* **2005**, *1*, 167–173.

[129] C. L. Grand, H. Han, R. M. Muñoz, S. Weitman, D. D. Von Hoff, L. H. Hurley, D. J. Bearss, *Mol. Cancer Ther.* **2002**, *1*, 565–573.

[130] K. Shin-ya, K. Wierzba, K. Matsuo, T. Ohtani, Y. Yamada, K. Furihata, Y. Hayakawa, H. Seto, *J. Am. Chem. Soc.* **2001**, *123*, 1262–1263.

[131] Y. X. Xiong, Z. S. Huang, J. H. Tan, *Eur. J. Med. Chem.* **2015**, *97*, 538–551.

[132] M. Y. Kim, M. Gleason-Guzman, E. Izbicka, D. Nishioka, L. H. Hurley, *Cancer Res.* **2003**, *63*, 3247–3256.

[133] W. J. Chung, B. Heddi, M. Tera, K. Iida, K. Nagasawa, A. T. Phan, *J. Am. Chem. Soc.* **2013**, *135*, 13495–13501.

[134] T. Tauchi, K. Shin-Ya, G. Sashida, M. Sumi, S. Okabe, J. H. Ohyashiki, K. Ohyashiki, *Oncogene* **2006**, *25*, 5719–5725.

[135] C. Hounsou, L. Guittat, D. Monchaud, M. Jourdan, N. Saettel, J. L. Mergny, M. P. Teulade-Fichou, *ChemMedChem* **2007**, *2*, 655–666.

[136] S. M. Kerwin, G. Chen, J. T. Kern, P. W. Thomas, *Bioorg. Med. Chem. Lett.* **2002**, *12*, 447–450.

[137] T. Taka, L. Huang, A. Wongnoppavich, S. W. Tam-Chang, T. R. Lee, W. Tuntiwechapikul, *Bioorg. Med. Chem.* **2013**, *21*, 883–890.

[138] E. Micheli, M. Martufi, S. Cacchione, P. De Santis, M. Savino, *Biophys. Chem.* **2010**, *153*, 43–53.

[139] F. Doria, M. Nadai, G. Sattin, L. Pasotti, S. N. Richter, M. Freccero, *Org. Biomol. Chem.* **2012**, *10*, 3830–3840.

[140] R. Perrone, F. Doria, E. Butovskaya, I. Frasson, S. Botti, M. Scalabrin, S. Lago, V. Grande, M. Nadai, M. Freccero, et al., *J. Med. Chem.* **2015**, *58*, 9639–9652.

[141] F. Cuenca, O. Greciano, M. Gunaratnam, S. Haider, D. Munnur, R. Nanjunda, W. D. Wilson, S. Neidle, *Bioorg. Med. Chem. Lett.* **2008**, *18*, 1668–1673.

[142] M. Arévalo-Ruiz, F. Doria, E. Belmonte-Reche, A. De Rache, J. Campos-Salinas, R. Lucas, E. Falomir, M. Carda, J. M. Pérez-Victoria, J. L. Mergny, et al., *Chem. Eur. J.* **2017**, *23*, 2157–2164.

[143] G. W. Collie, R. Promontorio, S. M. Hampel, M. Micco, S. Neidle, G. N. Parkinson, *J. Am. Chem. Soc.* **2012**, *134*, 2723–2731.

[144] M. Nadai, G. Cimino-Reale, G. Sattin, F. Doria, E. Butovskaya, N. Zaffaroni, M. Freccero, M. Palumbo, S. N. Richter, M. Folini, *Int. J. Oncol.* **2015**, *46*, 369–380.

[145] C. Marchetti, K. G. Zyner, S. A. Ohnmacht, M. Robson, S. M. Haider, J. P. Morton, G. Marsico, T. Vo, S. Laughlin-Toth, A. A. Ahmed, et al., *J. Med. Chem.* **2018**, *61*, 2500–2517.

[146] M. J. B. Moore, F. Cuenca, M. Searcey, S. Neidle, *Org. Biomol. Chem.* **2006**, *4*, 3479–3488.

[147] S. Cosconati, L. Marinelli, R. Trotta, A. Virno, S. De Tito, R. Romagnoli, B. Pagano, V. Limongelli, C. Giancola, P. G. Baraldi, et al., *J. Am. Chem. Soc.* **2010**, *132*, 6425–6433.

[148] A. K. Jain, S. Bhattacharya, *Bioconjug. Chem.* **2011**, *22*, 2355–2368.

[149] J. Ren, J. B. Chaires, *Biochemistry* **1999**, *38*, 16067–75.

[150] B. Pagano, A. Virno, C. A. Mattia, L. Mayol, A. Randazzo, C. Giancola, *Biochimie* **2008**, *90*, 1224–1232.

[151] L. Martino, A. Virno, B. Pagano, A. Virgilio, S. Di Micco, A. Galeone, C. Giancola, G. Bifulco, L. Mayol, A. Randazzo, *J. Am. Chem. Soc.* **2007**, *129*, 16048–16056.

[152] B. Pagano, I. Fotticchia, S. De Tito, C. A. Mattia, L. Mayol, E. Novellino, A. Randazzo, C. Giancola, *J. Nucleic Acids* **2010**, *2010*, 1–7.

[153] A. Rizzo, S. Iachettini, P. Zizza, C. Cingolani, M. Porru, S. Artuso, M. Stevens, M. Hummersone, A. Biroccio, E. Salvati, et al., *J. Exp. Clin. Cancer Res.* **2014**, *33*, 1–8.

[154] A. Ali, S. Bhattacharya, *Bioorganic Med. Chem.* **2014**, *22*, 4506–4521.

[155] C. E. Kaiser, V. Gokhale, D. Yang, L. H. Hurley, *Top Curr. Chem.* **2013**, *330*, 1–21.

[156] S. Balasubramanian, L. H. Hurley, S. Neidle, *Nat. Rev. Drug Discov.* **2011**, *10*, 261–275.

[157] H. Xu, M. Di Antonio, S. McKinney, V. Mathew, B. Ho, N. J. O'Neil, N. Dos Santos, J. Silvester, V. Wei, J. Garcia, et al., *Nat. Commun.* **2017**, *8*, 14432.

[158] D. Drygin, A. Lin, J. Bliesath, C. B. Ho, S. E. O'Brien, C. Proffitt, M. Omori, M. Haddach, M. K. Schwaebe, A. Siddiqui-Jain, et al., *Cancer Res.* **2011**, *71*, 1418–1430.

[159] D. Musumeci, J. Amato, A. Randazzo, E. Novellino, C. Giancola, D. Montesarchio, B. Pagano, *Anal. Chem.* **2014**, *86*, 4126–4130.

[160] D. Musumeci, J. Amato, P. Zizza, C. Platella, S. Cosconati, C. Cingolani, A. Biroccio, E. Novellino, A. Randazzo, C. Giancola, et al., *Biochim. Biophys. Acta - Gen. Subj.* **2017**, *1861*, 1341–1352.

[161] *http://www.glenresearch.com/Technical/TB_OAS.pdf*

[162] C. Platella, D. Musumeci, A. Arciello, F. Doria, M. Freccero, A. Randazzo, J. Amato, B. Pagano, D. Montesarchio, *Anal. Chim. Acta* **2018**, *1030*, 133–141.

[163] a) C. Platella, D. Musumeci, J. Amato, A. Randazzo, B. Pagano, D. Montesarchio, *Method for the preparation of a low unspecific binding-support for affinity chromatography and/or on-line synthesis of oligonucleotides.* The content is object of

the European Patent Application Number EP18161706.9 filed on March 14, **2018**; b) C. Platella, D. Musumeci, J. Amato, A. Randazzo, B. Pagano, D. Montesarchio, *Metodo per la preparazione di un supporto a basso legame aspecifico per cromatografia di affinità e/o sintesi diretta di oligonucleotidi.* The content is object of the Italian Patent Application Number 102017000030473 filed on March 20, **2017**.

[164] *http://www.linktech.co.uk/products/dna_solid_supports*

[165] U. Maskos, E. M. Southern, *Nucleic Acids Res.* **1992**, *20*, 1679–1684.

[166] E. Quezada, D. Viña, G. Delogu, F. Borges, L. Santana, E. Uriarte, *Helv. Chim. Acta* **2010**, *93*, 309–313.

[167] L. Wang, B. E. Hingerty, A. R. Srinivasan, W. K. Olson, S. Broyde, *Biophys. J.* **2002**, *83*, 382–406.

[168] H. R. Drew, R. M. Wing, T. Takano, C. Broka, S. Tanaka, K. Itakura, R. E. Dickerson, *Proc. Natl. Acad. Sci.* **1981**, *78*, 2179–2183.

[169] P. D. Dans, L. Danilane, I. Ivani, T. Drsata, F. Lankas, A. Hospital, J. Walther, R. I. Pujagut, F. Battistini, J. L. Gelpi, et al., *Nucleic Acids Res.* **2016**, *44*, 4052–4066.

[170] L. E. Xodo, G. Manzini, F. Quadrifoglio, G. Van Der Marel, J. van Boom, *Nucleic Acids Res.* **1991**, *19*, 1505–1511.

[171] S. N. Volkov, E. V. Paramonova, A. V. Yakubovich, A. V. Solovyov, *J. Phys. Condens. Matter* **2012**, *24*, 1–6.

[172] Y. Niibori, M. Kunita, O. Tochiyama, T. Chida, *J. Nucl. Sci. Technol.* **2000**, *37*, 349–357.

[173] *http://www.glenresearch.com/Technical/Deprotection.pdf*

[174] D. Monchaud, C. Allain, H. Bertrand, N. Smargiasso, F. Rosu, V. Gabelica, A. De Cian, J. L. Mergny, M. P. Teulade-Fichou, *Biochimie* **2008**, *90*, 1207–1223.

[175] C. Platella, S. Guida, L. Bonmassar, A. Aquino, E. Bonmassar, G. Ravagnan, D. Montesarchio, G. N. Roviello, D. Musumeci, M. P. Fuggetta, *Biochim. Biophys. Acta - Gen. Subj.* **2017**, *1861*, 2843–2851.

[176] M. Cheng, C. Modi, J. C. Cookson, I. Hutchinson, R. A. Heald, A. J. Mccarroll, S. Missailidis, F. Tanious, W. D. Wilson, J. Mergny, et al., *J. Med. Chem.* **2008**, *51*, 963–975.

[177] R. Ferreira, A. Aviñó, S. Mazzini, R. Eritja, *Molecules* **2012**, *17*, 7067–7082.

[178] J. L. Mergny, J. Li, L. Lacroix, S. Amrane, J. B. Chaires, *Nucleic Acids Res.* **2005**, *33*, 1–6.

[179] J. L. Mergny, L. Lacroix, *Curr. Protoc. Nucleic Acid Chem.* **2009**, *17*, 1–15.

[180] J. Kypr, I. Kejnovská, D. Renčiuk, M. Vorlíčková, *Nucleic Acids Res.* **2009**, *37*, 1713–1725.

[181] M. J. Cavaluzzi, *Nucleic Acids Res.* **2004**, *32*, e13.

[182] B. Ward, R. Rehfuss, J. Goodisman, J. C. Dabrowiak, *Biochemistry* **1988**, *27*, 1198–1205.

[183] L. A. Marky, K. J. Breslauer, *Proc. Natl. Acad. Sci. U. S. A.* **1987**, *84*, 4359–63.

[184] M. Zuffo, F. Doria, S. Botti, G. Bergamaschi, M. Freccero, *Biochim. Biophys. Acta - Gen. Subj.* **2017**, *1861*, 1303–1311.

[185] D. L. Ma, V. P. Y. Ma, D. S. H. Chan, K. H. Leung, H. J. Zhong, C. H. Leung, *Methods* **2012**, *57*, 106–114.

[186] S. Cosconati, L. Marinelli, R. Trotta, A. Virno, L. Mayol, E. Novellino, A. J. Olson, A. Randazzo, *J. Am. Chem. Soc.* **2009**, *131*, 16336–16337.

[187] B. Pagano, J. Amato, N. Iaccarino, C. Cingolani, P. Zizza, A. Biroccio, E. Novellino, A. Randazzo, *ChemMedChem* **2015**, *10*, 640–649.

[188] J. Amato, C. Platella, S. Iachettini, P. Zizza, D. Musumeci, S. Cosconati, A. Pagano, E. Novellino, A. Biroccio, A. Randazzo, et al., *Eur. J. Med. Chem.* **2019**, *163*, 295–306.

[189] K. N. Luu, A. Tu, V. Kuryavyi, L. Lacroix, D. J. Patel, *J. Am. Chem. Soc.* **2006**, *128*, 9963–9970.

[190] A. Ambrus, D. Chen, J. Dai, R. A. Jones, D. Yang, *Biochemistry* **2005**, *44*, 2048–2058.

[191] J. W. Jaroszewski, V. Clausen, J. S. Cohen, O. Dahl, *Nucleic Acids Res.* **1996**, *24*, 829–834.

[192] C. Entzian, T. Schubert, *Methods* **2016**, *97*, 27–34.

[193] S. Cosconati, S. Forli, A. L. Perryman, R. Harris, D. S. Goodsell, A. J. Olson, *Expert Opin. Drug Discov.* **2010**, *5*, 597–607.

[194] A. Rizzo, E. Salvati, A. Biroccio, *Methods* **2012**, *57*, 93–99.

[195] C. Thiriet, J. J. Hayes, *Mol. Cell* **2005**, *18*, 617–622.

[196] H. Takai, A. Smogorzewska, T. De Lange, *Curr. Biol.* **2003**, *13*, 1549–1556.

[197] W. Chen, W. C. Hahn, *Histol. Histopathol.* **2003**, *18*, 541–550.

[198] F. Doria, M. Nadai, G. Costa, G. Sattin, C. Gallati, G. Bergamaschi, F. Moraca, S. Alcaro, M. Freccero, S. N. Richter, *European J. Org. Chem.* **2016**, *2016*, 4824–4833.

[199] M. Nadai, F. Doria, M. Di Antonio, G. Sattin, L. Germani, C. Percivalle, M. Palumbo, S. N. Richter, M. Freccero, *Biochimie* **2011**, *93*, 1328–1340.

[200] F. Doria, M. Nadai, M. Zuffo, R. Perrone, M. Freccero, S. N. Richter, *Chem. Commun.* **2017**, *53*, 2268–2271.

[201] S. T. G. Street, D. N. Chin, G. J. Hollingworth, M. Berry, J. C. Morales, M. C. Galan, *Chem. Eur. J.* **2017**, *23*, 6953–6958.

[202] E. Salvati, F. Doria, F. Manoli, C. D'Angelo, A. Biroccio, M. Freccero, I. Manet, *Org. Biomol. Chem.* **2016**, *14*, 7238–7249.

[203] F. Doria, I. Manet, V. Grande, S. Monti, M. Freccero, *J. Org. Chem.* **2013**, *78*, 8065–8073.

[204] F. Doria, A. Oppi, F. Manoli, S. Botti, N. Kandoth, V. Grande, I. Manet, M. Freccero, *Chem. Commun.* **2015**, *51*, 9105–9108.

[205] M. Zuffo, A. Guedin, E. Leriche, F. Doria, V. Pirota, V. Gabelica, J. L. Mergny, M. Freccero, *Nucleic Acids Res.* **2018**, *46*, e115.

[206] C. Q. Zhou, T. C. Liao, Z. Q. Li, J. Gonzalez-Garcia, M. Reynolds, M. Zou, R. Vilar, *Chem. Eur. J.* **2017**, *23*, 4713–4722.

[207] C. Q. Zhou, J. W. Yang, C. Dong, Y. M. Wang, B. Sun, J. X. Chen, Y. S. Xu, W. H. Chen, *Org. Biomol. Chem.* **2015**, *14*, 191–197.

[208] L. Martino, B. Pagano, I. Fotticchia, S. Neidle, C. Giancola, *J. Phys. Chem. B* **2009**, *113*, 14779–14786.

[209] M. Trajkovski, T. Endoh, H. Tateishi-Karimata, T. Ohyama, S. Tanaka, J. Plavec, N. Sugimoto, *Nucleic Acids Res.* **2018**, *46*, 4301–4315.

[210] M. Adrian, B. Heddi, A. T. Phan, *Methods* **2012**, *57*, 11–24.

[211] M. Webba da Silva, *Methods* **2007**, *43*, 264–277.

[212] M. Trajkovski, E. Morel, F. Hamon, S. Bombard, M. P. Teulade-Fichou, J. Plavec, *Chem. Eur. J.* **2015**, *21*, 7798–7807.

[213] H. T. Le, W. L. Dean, R. Buscaglia, J. B. Chaires, J. O. Trent, *J. Phys. Chem. B* **2014**, *118*, 5390–5405.

[214] H. T. Le, R. Buscaglia, W. L. Dean, J. B. Chaires, J. O. Trent, *Top Curr. Chem.* **2013**, *330*, 98–101.

[215] A. Ambrus, D. Yang, *Anal. Biochem.* **2007**, *367*, 56–67.

[216] M. Trajkovski, M. Webba Da Silva, J. Plavec, *J. Am. Chem. Soc.* **2012**, *134*, 4132–4141.

[217] P. Atkins, J. De Paula, *Physical Chemistry*, Oxford: Oxford UP, **2006**.

[218] Y. Huang, X. Zhang, Z. Ma, W. Li, Y. Zhou, J. Zhou, W. Zheng, C. Q. Sun, *Sci. Rep.* **2013**, *3*, 1–5.

[219] P. Šket, J. Plavec, *J. Am. Chem. Soc.* **2010**, *132*, 12724–12732.

[220] J. Lapham, J. P. Rife, P. B. Moore, D. M. Crothers, *J. Biomol. NMR* **1997**, *10*, 255–262.

[221] D. Musumeci, C. Platella, C. Riccardi, A. Merlino, T. Marzo, L. Massai, L. Messori, D. Montesarchio, *Dalt. Trans.* **2016**, *45*, 8587–8600.

[222] Z. Liu, B. Delavan, R. Roberts, W. Tong, *Trends Pharmacol. Sci.* **2017**, *38*, 852–872.

[223] N. J. Wheate, S. Walker, G. E. Craig, R. Oun, *Dalt. Trans.* **2010**, *39*, 8113–8127.

[224] J. P. Martinez, F. Sasse, M. Brönstrup, J. Diez, A. Meyerhans, *Nat. Prod. Rep.* **2015**, *32*, 29–48.

[225] B. Pagano, S. Cosconati, V. Gabelica, L. Petraccone, S. De Tito, L. Marinelli, V. La Pietra, F. S. di Leva, I. Lauri, R. Trotta, et al., *Curr. Pharm. Des.* **2012**, *18*, 1880–99.

[226] J. Jaumot, R. Gargallo, *Curr. Pharm. Des.* **2012**, *18*, 1900–1916.

[227] C. Giancola, B. Pagano, *Top Curr. Chem.* **2013**, *330*, 211–242.

[228] T. Simonsson, R. Sjöback, *J. Biol. Chem.* **1999**, *274*, 17379–17383.

[229] D. Monchaud, C. Allain, M. P. Teulade-Fichou, *Bioorg. Med. Chem. Lett.* **2006**, *16*, 4842–4845.

[230] P. L. T. Tran, E. Largy, F. Hamon, M. P. Teulade-Fichou, J. L. Mergny, *Biochimie* **2011**, *93*, 1288–1296.

[231] G. Yuan, Q. Zhang, J. Zhou, H. Li, *Mass Spectromery Rev.* **2011**, *30*, 1121–1142.

[232] K. M. Felsenstein, L. B. Saunders, J. K. Simmons, E. Leon, D. R. Calabrese, S. Zhang, A. Michalowski, P. Gareiss, B. A. Mock, J. S. Schneekloth, *ACS Chem. Biol.* **2016**, *11*, 138–148.

[233] S. Benabou, A. Aviñó, R. Eritja, C. González, R. Gargallo, *RSC Adv.* **2014**, *4*, 26956–26980.

[234] M. Zeraati, D. B. Langley, P. Schofield, A. L. Moye, R. Rouet, W. E. Hughes, T. M. Bryan, M. E. Dinger, D. Christ, *Nat. Chem.* **2018**, *10*, 631–637.

[235] H. A. Day, P. Pavlou, Z. A. E. Waller, *Bioorg. Med. Chem.* **2014**, *22*, 4407–4418.

[236] R. Perrone, M. Nadai, I. Frasson, J. A. Poe, E. Butovskaya, T. E. Smithgall, M. Palumbo, G. Palù, S. N. Richter, *J. Med. Chem.* **2013**, *56*, 6521–6530.

[237] B. De Nicola, C. J. Lech, B. Heddi, S. Regmi, I. Frasson, R. Perrone, S. N. Richter, A. T. Phan, *Nucleic Acids Res.* **2016**, *44*, 6442–6451.

List of publications and patents

PUBLICATIONS:

1. D. Musumeci, **C. Platella**, C. Riccardi, A. Merlino, T. Marzo, L. Massai, L. Messori, D. Montesarchio*
   A first-in-class and a fished out anticancer platinum compound: cis-[$PtCl_2(NH_3)_2$] and cis-[$PtI_2(NH_3)_2$] compared for their reactivity towards DNA model systems
   Dalton Transactions, **2016**, 45: 8587-8600, DOI: 10.1039/c6dt00294c

   Abstract
   Contrary to what was believed for many years, *cis*-$PtI_2(NH_3)_2$, the diiodido analogue of cisplatin, displays high *in vitro* antiproliferative activity toward a set of tumour cell lines, overcoming resistance to cisplatin in a platinum-resistant cancer cell line. In the context of a general reappraisal of iodinated Pt(II) derivatives, aiming at a more systematic evaluation of their chemical and biological profiles, here we report on the reactivity of *cis*-$PtI_2(NH_3)_2$ with selected DNA model systems, in single, double strand or G-quadruplex form, using cisplatin as a control. A combined approach has been exploited in this study, including circular dichroism (CD), UV-visible spectroscopy and electrospray mass spectrometry (ESI-MS) analyses. The data reveal that *cis*-$PtI_2(NH_3)_2$ shows an overall reactivity towards the investigated oligonucleotides significantly higher than cisplatin.

2. **C. Platella**, C. Riccardi, D. Montesarchio, G.N. Roviello, D. Musumeci*
   G-quadruplex-based aptamers against protein targets in therapy and diagnostics
   Biochimica et Biophysica Acta – General Subjects, **2017**, 1861: 1429-1447, DOI: 10.1016/j.bbagen.2016.11.027

   Abstract
   Nucleic acid aptamers are single-stranded DNA or RNA molecules identified to recognize with high affinity specific targets including proteins, small molecules, ions, whole cells and even entire organisms, such as viruses or bacteria. They can be identified from combinatorial libraries of DNA or RNA oligonucleotides by SELEX technology, an in vitro iterative selection procedure consisting of binding (capture), partitioning and amplification steps. Remarkably, many of the aptamers selected against biologically relevant protein targets are G-rich sequences that can fold into stable G-quadruplex (G4) structures. Aiming at disseminating novel inspiring ideas within the scientific community in the field of G4-structures, the emphasis of this review is placed on: 1) recent advancements in SELEX technology for the efficient and rapid identification of new candidate aptamers (introduction of microfluidic systems and next generation sequencing); 2) recurrence of G4 structures in aptamers selected by SELEX against biologically relevant protein targets; 3) discovery of several G4-forming motifs in important regulatory regions of the human or viral genome bound by endogenous proteins, which per se can result into potential aptamers; 4) an updated overview of G4-based aptamers with therapeutic potential and 5) a discussion on the most attractive G4-based aptamers for diagnostic applications.

3. D. Musumeci, J. Amato, P. Zizza, **C. Platella**, S. Cosconati, C. Cingolani, A. Biroccio, E. Novellino, A. Randazzo, C. Giancola, B. Pagano*, D. Montesarchio*
Tandem application of ligand-based virtual screening and G4-OAS assay to identify novel G-quadruplex-targeting chemotypes
Biochimica et Biophysica Acta – General Subjects, **2017**, 1861: 1341-1352, DOI: 10.1016/j.bbagen.2017.01.024

Abstract
BACKGROUND:
G-quadruplex (G4) structures are key elements in the regulation of cancer cell proliferation and their targeting is deemed to be a promising strategy in anticancer therapy.
METHODS:
A tandem application of ligand-based virtual screening (VS) calculations together with the experimental G-quadruplex on Oligo Affinity Support (G4-OAS) assay was employed to discover novel G4-targeting compounds. The interaction of the selected compounds with the investigated G4 in solution was analysed through a series of biophysical techniques and their biological activity investigated by immunofluorescence and MTT assays.
RESULTS:
A focused library of 60 small molecules, designed as putative G4 groove binders, was identified through the VS. The G4-OAS experimental screening led to the selection of 7 ligands effectively interacting with the G4-forming human telomeric DNA. Evaluation of the biological activity of the selected compounds showed that 3 ligands of this sub-library induced a marked telomere-localized DNA damage response in human tumour cells.
CONCLUSIONS:
The combined application of virtual and experimental screening tools proved to be a successful strategy to identify new bioactive chemotypes able to target the telomeric G4 DNA. These compounds may represent useful leads for the development of more potent and selective G4 ligands.
GENERAL SIGNIFICANCE:
Expanding the repertoire of the available G4-targeting chemotypes with improved physico-chemical features, in particular aiming at the discovery of novel, selective G4 telomeric ligands, can help in developing effective anti-cancer drugs with fewer side effects.

4. **C. Platella**, S. Guida, L. Bonmassar, A. Aquino, E. Bonmassar, G. Ravagnan, D. Montesarchio, G.N. Roviello*, D. Musumeci*, M.P. Fuggetta*
Antitumour activity of resveratrol on human melanoma cells: a possible mechanism related to its interaction with malignant cell telomerase
Biochimica et Biophysica Acta – General Subjects, **2017**, 1861: 2843-2851, DOI: 10.1016/j.bbagen.2017.08.001

Abstract
BACKGROUND:
trans-Resveratrol (tRES) is a polyphenolic stilbene found in plant products which has attracted great attention because of its antioxidant, anti-inflammatory and anticancer properties.
METHODS:
The possible correlation between tRES-induced suppression of melanoma cell growth and its influence on telomerase expression has been investigated by biological assays. Moreover, in order to gain new knowledge about possible mechanisms of action of tRES as antineoplastic agent, its interaction with biologically relevant secondary structure-forming DNA sequences, its aggregation

properties and copper-binding activity have been studied by CD, UV and fluorescence spectroscopies.
RESULTS:
Biological assays have confirmed that growth inhibitory properties of tRES well correlate with the reduction of telomerase activity and hTERT gene transcript levels in human melanoma cells. Biophysical studies in solution have proved that tRES binds all the studied DNA model systems with low affinity, however showing high ability to discriminate G-quadruplex vs. duplex DNA. In addition, tRES has shown no propensity to form aggregates in the explored concentration range and has been found able to bind Cu^{2+} ions with a 2:1 stoichiometry.
CONCLUSIONS:
From these biological and biophysical analyses it has emerged that tRES produces cytotoxic effects on human melanoma cells and, at a molecular level, is able to bind Cu^{2+} and cancer-involved G-quadruplexes, suggesting that multiple mechanisms of action could be involved in its antineoplastic activity.
GENERAL SIGNIFICANCE:
Expanding the knowledge on the putative mechanisms of action of tRES as antitumour agent can help to develop novel, effective tRES-based anticancer drugs.

5. D. Musumeci, **C. Platella**, C. Riccardi, F. Moccia, D. Montesarchio*
Fluorescence sensing using DNA aptamers in cancer research and clinical diagnostics
Cancers, **2017**, 9: 174-217, DOI:10.3390/cancers9120174

Abstract
Among the various advantages of aptamers over antibodies, remarkable is their ability to tolerate a large number of chemical modifications within their backbone or at the termini without losing significant activity. Indeed, aptamers can be easily equipped with a wide variety of reporter groups or coupled to different carriers, nanoparticles, or other biomolecules, thus producing valuable molecular recognition tools effective for diagnostic and therapeutic purposes. This review reports an updated overview on fluorescent DNA aptamers, designed to recognize significant cancer biomarkers both in soluble or membrane-bound form. In many examples, the aptamer secondary structure switches induced by target recognition are suitably translated in a detectable fluorescent signal using either fluorescently-labelled or label-free aptamers. The fluorescence emission changes, producing an enhancement ("signal-on") or a quenching ("signal-off") effect, directly reflect the extent of the binding, thereby allowing for quantitative determination of the target in bioanalytical assays. Furthermore, several aptamers conjugated to fluorescent probes proved to be effective for applications in tumour diagnosis and intraoperative surgery, producing tumour-type specific, non-invasive in vivo imaging tools for cancer pre- and post-treatment assessment.

6. **C. Platella**, D. Musumeci, A. Arciello, F. Doria, M. Freccero, A. Randazzo, J. Amato, B. Pagano, D. Montesarchio*
Controlled Pore Glass-based oligonucleotide affinity support: towards High Throughput Screening methods for the identification of conformation-selective G-quadruplex ligands
Analytica Chimica Acta, **2018**, 1030: 133-141, DOI: 10.1016/j.aca.2018.04.071

Abstract
Target selectivity is one of the main challenges in the search for small molecules able to act as effective and non-toxic anticancer and/or antiviral drugs. To achieve this goal, handy, rapid and reliable High Throughput Screening methodologies are needed. We here describe a novel

functionalization for the solid phase synthesis of oligonucleotides on Controlled Pore Glass, including a flexible hexaethylene glycol spacer linking the first nucleoside through the nucleobase via a covalent bond stable to the final deprotection step. This allowed us preparing fully deprotected oligonucleotides still covalently attached to their supports. In detail, on this support we performed both the on-line synthesis of different secondary structure-forming oligonucleotides and the affinity chromatography-based screenings of conformation-selective G-quadruplex ligands. By using a fluorescent core-extended naphthalene diimide with different emitting response upon binding to sequences folding into G-quadruplexes of different topologies, we have been able to discriminate not only G-quadruplex vs. duplex DNA structures, but also different G-quadruplex conformations on the glass beads by confocal microscopy.

7. J. Amato, **C. Platella**, S. Iachettini, P. Zizza, D. Musumeci, S. Cosconati, A. Pagano, E. Novellino, A. Biroccio, A. Randazzo, B. Pagano,* D. Montesarchio*
Tailoring a lead-like compound targeting multiple G-quadruplex structures
European Journal of Medicinal Chemistry, **2019**, 163: 295-306, DOI: 10.1016/j.ejmech.2018.11.058.

Abstract
A focused library of analogs of a lead-like G-quadruplex (G4) targeting compound (**4**), sharing a furobenzoxazine naphthoquinone core and differing for the pendant groups on the N-atom of the oxazine ring, has been here analyzed with the aim of developing more potent and selective ligands. These molecules have been tested vs. topologically different G4s by the G4-CPG assay, an affinity chromatography-based method for screening putative G4 ligands. The obtained results showed that all these compounds were able to bind several G4 structures, both telomeric and extra-telomeric, thus behaving as multi-target ligands, and two of them fully discriminated G4 vs. duplex DNA. Biological assays proved that almost all the compounds produced effective DNA damage, showing marked antiproliferative effects on tumor cells in the low μM range. Combined analysis of the G4-CPG binding assays and biological data led us to focus on compound **S4-5**, proved to be less cytotoxic than the parent compound **4** on normal cells. An in-depth biophysical characterization of the binding of **S4-5** to different G4s showed that the here identified ligand has higher affinity for the G4s and higher ability to discriminate G4 vs. duplex DNA than **4**. Molecular docking studies, in agreement with the NMR data, suggest that **S4-5** interacts with the accessible grooves of the target G4 structures, giving clues for its increased G4 vs. duplex selectivity.

PATENTS:

1. **C. Platella**, D. Musumeci, J. Amato, A. Randazzo, B. Pagano, D. Montesarchio
Metodo per la preparazione di un supporto a basso legame aspecifico per cromatografia di affinità e/o sintesi diretta di oligonucleotidi
The Content Is Object of the Italian Patent Application Number 102017000030473 Filed on March 20, **2017**.

Abstract
È presentato un metodo per preparare supporti solidi funzionalizzati da utilizzarsi in cromatografia di affinità e/o per la sintesi diretta di oligonucleotidi legati al supporto, completamente deprotetti formanti strutture secondarie.

2. **C. Platella**, D. Musumeci, J. Amato, A. Randazzo, B. Pagano, D. Montesarchio
Method for the preparation of a low unspecific binding-support for affinity chromatography and/or on-line synthesis of oligonucleotides
The Content Is Object of the European Patent Application Number EP18161706.9 Filed on March 14, **2018**.

Abstract
A method for preparing functionalized solid supports to be used in the on-line synthesis of support-bound, fully deprotected secondary structure-forming oligonucleotides and/or for low unspecific binding affinity chromatography is disclosed.

List of oral communications and posters presented to conferences and schools

ORAL COMMUNICATIONS:

1. **C. Platella***, D. Musumeci, J. Amato, S. Cosconati, E. Novellino, A. Randazzo, C. Giancola, B. Pagano, D. Montesarchio
   G4-OAS assay: A helpful tool in anticancer drug discovery
   XXXVII Convegno Nazionale della Divisione di Chimica Organica, Venice, Italy, September 18-22, **2016**

2. **C. Platella***, D. Montesarchio, D. Musumeci, G.N. Roviello, S. Guida, A. Aquino, L. Bonmassar, M.P. Fuggetta
   Resveratrol: a novel ligand for cancer-involved G-quadruplexes?
   II International Summer School on Natural Products, Naples, Italy, July 3-7, **2017**

3. **C. Platella***, D. Musumeci, A. Arciello, F. Doria, M. Freccero, A. Randazzo, J. Amato, B. Pagano, Daniela Montesarchio
   Controlled Pore Glass-based Oligonucleotide Affinity Support: developing High Throughput Screening methods for the identification of conformation-selective G-quadruplex ligands
   17th Edition "Giornate Scientifiche Borsisti CINMPIS", Cagliari, Italy, December 15-16, **2017**

FLASH COMMUNICATIONS:

1. **C. Platella***, D. Musumeci, J. Amato, A. Randazzo, B. Pagano, D. Montesarchio
   Towards High Throughput Screening method to identify G4-selective ligands
   6th International Meeting on Quadruplex Nucleic Acids, Prague, Czech Republic, May 31-June 3, **2017**

POSTER PRESENTATIONS:

1. **C. Platella***, D. Musumeci, J. Amato, A. Randazzo, B. Pagano, D. Montesarchio
   Synthesis of a novel oligonucleotide affinity support for the screening of DNA-targeting therapeutic agents
   XLI International Summer School on Organic Synthesis "A. Corbella", Gargnano (BS), Italy, June 12-17, **2016**

2. **C. Platella***, D. Musumeci, J. Amato, A. Randazzo, B. Pagano, D. Montesarchio
   CPG-based Oligonucleotide Affinity Supports: Developing HTS methods to identify anticancer G-quadruplex-selective ligands
   XXII International Roundtable on Nucleosides, Nucleotides and Nucleic Acids, Paris, France, July 18-22, **2016**

3. **C. Platella***, D. Musumeci, J. Amato, A. Randazzo, B. Pagano, D. Montesarchio
   Towards High Throughput Screening method to identify G4-selective ligands
   6th International Meeting on Quadruplex Nucleic Acids, Prague, Czech Republic, May 31-June 3, **2017**

4. **C. Platella***, D. Musumeci, A. Arciello, F. Doria, M. Freccero, A. Randazzo, J. Amato, B. Pagano, D. Montesarchio
   Conformation-sensitive detection of secondary structure-forming oligonucleotides on nanoporous glass beads
   9th International Symposium on Nano and Supramolecular Chemistry, Naples, Italy, September 4-7, **2017**

5. **C. Platella***, D. Musumeci, J. Amato, B. Pagano, A. Randazzo, A. Biroccio, D. Montesarchio*
   Evidence for selectivity improvement in G-quadruplex-targeting chemotype analogs by G4-CPG binding assay, biological and biophysical evaluation
   Biology of non-canonical nucleic acids: from humans to pathogens, International Symposium, Padua, Italy, September 26-28, **2018**